

Synthesis, Characterization and Application of New Functional Gels

Dissertation

Zur Erlangung des Doktorgrades der Naturwissenschaften

Dr. rer. nat.

an der Fakultät für Chemie und Pharmazie
der Universität Regensburg



vorgelegt von

Marleen Häring

aus Ebersberg

Regensburg 2018

Die Arbeit wurde angeleitet von:

Prof. Dr. David Díaz Díaz

Promotionsgesuch eingereicht am:

09. Juli 2018

Der experimentelle Teil der vorliegenden Arbeit wurde in der Zeit von Januar 2015 bis Mai 2018 unter der Leitung von Prof. Dr. David Díaz Díaz am Lehrstuhl für Organische Chemie der Universität Regensburg angefertigt. Zusätzliche Betreuer waren Dr. Françoise Quignard von März bis Mai 2016 am Institut Charles Gerhardt Montpellier (ICGM) in Montpellier (Frankreich) und Dr. Raul Pérez-Ruiz im Oktober 2017 am IMDEA Energy Institute in Mostóles/Madrid (Spanien).

Besonderen Dank gilt Herrn Prof. Dr. David Díaz Díaz für die Überlassung der äußerst interessanten Themen und Projekte, sowie für die vorbildliche Betreuung, Unterstützung und Förderung.

dedicated to my family

“The only true wisdom is in knowing you know nothing” - Sokrates

Table of Contents

1. Summary.....	1
2. Introduction	5
2.1. Definition of Gels.....	5
2.2. Supramolecular Gels.....	6
2.3. Smart Gels	7
2.4. Gels for Biomedical Applications	9
2.5. Gels as Nanoreactors	10
2.6. References.....	11
3. Main part.....	13
3.1. Keratin Catalyzed Nitroaldol (Henry) Reaction and Comparison with other Biopolymers.....	13
3.1.1. Abstract.....	14
3.1.2. Introduction	15
3.1.3. Results and Discussion.....	17
3.1.3.1. Solvent Screening.....	17
3.1.3.2. Substrate Scope	18
3.1.3.3. Recycling Experiments.....	24
3.1.3.4. Kinetic Analysis.....	25
3.1.4. Conclusion and Outlook	27
3.1.5. Experimental Part	28
3.1.5.1. Materials and Methods.....	28
3.1.5.2. General Procedure for Keratin-Catalyzed Nitroaldol (Henry) Reaction	28
3.1.5.3. Typical Recycling Procedure.....	29
3.1.5.4. Kinetic Studies	29
3.1.6. References	30
3.2. Alginate-Phenylboronic Acid Based Hydrogels.....	33

3.2.1.	Abstract	34
3.2.2.	Introduction.....	35
3.2.3.	Results and Discussion.....	38
3.2.3.1.	Synthesis of Alginate-Phenylboronic Acid (Alg-PBA)	38
3.2.3.2.	Preparation of Alg-PBA Hydrogels	40
3.2.3.3.	Characterization of Hydrogels.....	41
3.2.3.4.	Self-healing Behavior.....	43
3.2.3.5.	Stress-Strain Behavior	46
3.2.3.6.	Biological Studies and Drug Release Experiments	53
3.2.4.	Conclusion and Outlook.....	56
3.2.5.	Experimental Part	58
3.2.5.1.	Materials and Methods.....	58
3.2.5.2.	Synthesis of Alg-PBA.....	59
3.2.5.3.	Determination of Acid Dissociation Constant (pK_a).....	59
3.2.5.4.	Preparation of Alg-PBA hydrogels.....	59
3.2.5.5.	Biological Studies	59
3.2.6.	References	62
3.3.	Topology-Controlled Self-Healing Properties of Ionene Polymer Hydrogels	65
3.3.1.	Abstract	66
3.3.2.	Introduction.....	67
3.3.3.	Results and Discussion.....	69
3.3.3.1.	Synthesis of Ionene Polymers and Hydrogel Preparation	69
3.3.3.2.	Self-Healing Experiments of Hydrogels.....	69
3.3.3.3.	Load-bearing Experiments.....	73
3.3.4.	Conclusion and Outlook.....	76
3.3.5.	Experimental Part	77
3.3.5.1.	Materials and Methods.....	77

3.3.5.2.	Synthesis of Monomers.....	77
3.3.5.3.	Synthesis of Polymers.....	78
3.3.5.4.	Preparation of Hydrogels	78
3.3.6.	References	79
3.4.	Isosteric Substitution for Tuning Self-Assembly of Soft Supramolecular Materials.	81
3.4.1.	Abstract.....	82
3.4.2.	Introduction	83
3.4.3.	Results and Discussion.....	86
3.4.3.1.	Synthesis of TIA Derivatives	86
3.4.3.2.	Hydrogelation Ability of Click-TIA	87
3.4.3.3.	Characterization of Hydrogels	87
3.4.3.4.	<i>In Vitro</i> Cytotoxicity Evaluation of Click-TIA and 5-TIA	93
3.4.3.5.	OXT Encapsulation and Release <i>in Vitro</i>	94
3.4.3.6.	Metal-Induced Gelation Ability of Click-TIA	97
3.4.3.7.	Characterization of Metallogels	100
3.4.4.	Conclusion and Outlook	104
3.4.5.	Experimental Part	106
3.4.5.1.	Materials and Methods.....	106
3.4.5.2.	Synthesis of 5-(1 <i>H</i> -1,2,3-triazol-5-yl)isophthalic acid (click-TIA).....	106
3.4.5.3.	Synthesis of 5-TIA	108
3.4.5.4.	Preparation of Hydrogels	109
3.4.5.5.	Cell Viability Studies.....	109
3.4.5.6.	Procedure for Preparation of Drug-Loaded Hydrogels and <i>in Vitro</i> Drug Release Experiments.....	110
3.4.5.7.	Preparation of Metallogels.....	110
3.4.6.	References	112

3.5. Photoreduction of Aryl Halides by TTA-UC Under Aerobic Conditions in Gel Medium	115
3.5.1. Abstract	116
3.5.2. Introduction	117
3.5.3. Results and Discussion	120
3.5.3.1. Synthesis of LMW gelators	120
3.5.3.2. TTA-UC Systeme	121
3.5.3.3. Intragel Photoreduction	121
3.5.3.4. Mechanistic Investigation	125
3.5.4. Conclusion and Outlook	127
3.5.5. Experimental Part	128
3.5.5.1. Materials and Methods	128
3.5.5.2. Synthesis of LMW Gelator	129
3.5.5.3. General Procedure for Photocatalytic Dehalogenation Reaction	130
3.5.6. References	131
3.6. Air-Sensitive Photoredox Catalysis Performed under Aerobic Conditions in Gel Networks	134
3.6.1. Abstract	135
3.6.2. Introduction	136
3.6.3. Results and Discussion	137
3.6.3.1. Synthesis of LMW Gelator	137
3.6.3.2. Photocatalytic Arylation Reaction	137
3.6.3.3. Photocatalytic Trifluoromethylation Reaction	144
3.6.3.4. Mechanistic Investigation	146
3.6.4. Conclusion and Outlook	149
3.6.5. Experimental Part	150
3.6.5.1. Materials and Methods	150

3.6.5.2.	Synthesis of LMW Gelators.....	152
3.6.5.3.	General Procedure for Photocatalytic Arylation Reaction	153
3.6.5.4.	General Procedure for Photocatalytic Trifluoromethylation Reaction.....	160
3.6.6.	References	164
4.	List of Abbreviations.....	166
5.	Curriculum Vitae.....	170
6.	Acknowledgements	175
7.	Declaration.....	178

1. Summary

This thesis comprises six chapters which deal with the synthesis, characterization and application of new functional gels or polymers.

The introduction gives a brief overview of the definition and classification of gels. Supramolecular gels are more closely described, including their versatile properties and potential application possibilities.

The first chapter describes the first investigation of keratin, a ubiquitous biopolymer extracted from wool, as “green” catalyst for C-C bond forming reactions. The nitroaldol (Henry) reaction was chosen as a model reaction which was performed in the presence of keratin in its powder form. Both, DMSO and water were tested as solvent since the background reaction could be neglected. The reaction in DMSO displayed complete conversion after 24 h whereas in water a phase-transfer catalyst, here TBAB, was additionally necessary and the double amount of reaction time was required. Aromatic and heteroaromatic aldehydes with strong or moderate electron-withdrawing groups as substrates lead to good conversion. The catalyst could be recovered and reused for further catalytic cycles. However, there was a gradual deactivation of the catalyst which was higher in DMSO than in water. Finally, the kinetic of the keratin-catalyzed Henry reaction was compared to other biopolymers.

The second chapter deals with the synthesis of phenylboronic acid-modified alginate (Alg-PBA) which is able to form hydrogels under basic pH. Different hydrogel formulations could be prepared by changing the polymer concentration and the added amount of NaOH. Especially, two hydrogel formulations, the **3-75** (*i.e.*, 3% w/v Alg-PBA + 75 μ L NaOH per mL Alg-PBA solution) and the **7-35** (*i.e.*, 7% Alg-PBA + 35 μ L NaOH per mL Alg-PBA solution) were characterized and compared regarding their self-healing ability and stretchability (*i.e.*, stress-strain behavior). Although both formulations were self-healable and stretchable, both properties were superior for the **7-35** hydrogel. Both formulations display a multi-stimuli responsiveness and are biocompatible, injectable materials which could be used as carrier for drug release experiments of oxytetracycline hydrochloride.

The third chapter deals with the self-healing ability of ionene polymers which are cationic polyelectrolytes. Three different topomers were obtained which were all able to form hydrogels. The self-healing properties were compared with respect to the polymer topology which was found to play a crucial role. Specifically, the *ortho*-isomer showed superior shape persistent, self-standing and self-healing properties compared to its *meta*- and *para*-

analogues. Additional experiments such as load-bearing and injectability, as well as further investigations such as FE-SEM were performed with the most promising polymer, *i.e.* the *ortho*-ionene polymer.

The fourth chapter describes the isosteric substitution of the 1,2,4-triazole moiety of **5-TIA**, a metallogelator in the presence of $\text{Ca}(\text{OAc})_2$, by a 1,2,3-triazole affording **click-TIA**, a versatile gelator with the ability to form hydrogels and metallogels. The first part of this chapter deals with the hydrogelation ability of **click-TIA**, as well as the ability of forming a hybrid gel together with **5-TIA** (molar ratio **click-TIA**:**5-TIA** 1:0.2). These gels were compared and characterized regarding their rheological properties, thermal properties, mechanical stability and morphology. Interestingly, neither **click-TIA** nor **5-TIA** displayed cytotoxic effects which allowed the encapsulation and *in vitro* release studies with oxytetracycline hydrochloride. Different pH values lead to different release kinetics which were fitted following a first-order kinetic. The second part of this chapter describes the metallogelation ability of **click-TIA** in the presence of $\text{Cu}(\text{OAc})_2$. Several metallogels could be obtained at different concentrations, ratios and solvents (*i.e.* DMF, DMA and pyridine). Three metallogel formulations were chosen to be further investigated and characterized with respect to their rheological behavior, thermal stability, spectroscopic properties and their morphology.

The last two chapters are about photochemical reactions which are performed under aerobic conditions with a gel medium as nanoreactor.

The fifth chapter describes a proof-of-concept which demonstrated for the first time the possibility of photocatalytic reduction of aryl halides by TTA-UC of a proper donor/acceptor pair embedded in a physical gel. The gel network provides a protecting microenvironment which allows the reaction under aerobic conditions at RT. The photocatalytic reduction of 4-bromoacetophenone as substrate with PtOEP and DPA as donor/acceptor pair in DMF was used as a model reaction which was performed in two different gels. Initial control and optimization reactions were conducted. Good conversions and excellent mass balances were also observed with several aryl halides. The gel properties and morphology was investigated and compared before and after irradiation.

The last chapter is an extension of the fifth chapter which demonstrates that also C-C bond forming photocatalytic reactions can be performed in air using a gel medium. Two reactions, the arylation of aryl halides and the trifluoromethylation of arenes were investigated. The arylation reaction was described more in detail, whereas a summary was given for the

trifluoromethylation reaction. For the arylation reaction, 2-bromobenzonitrile and *N*-methylpyrrole in DMSO with Rh-6G as catalyst and DIPEA as electron donor embedded in a gel medium were used as model reaction. Initial control and optimization reactions were performed. Several different aryl or hetero aryl halides with different trapping agents could be converted into the desired product in good yields. Chromoselective as well as subsequential reactions could be performed within the gel medium under aerobic conditions. The gel properties and morphology was investigated and compared before and after irradiation. In addition, the mechanism behind the protection was further investigated by spectroscopic experiments.

2. Introduction

2.1. Definition of Gels

Gels are ubiquitous in our daily life since they have a broad range of applications in food, medicines, biomaterials, cosmetics, *etc.*¹ In general, gels are viscoelastic solid-like materials consisting of a hierarchical 3D cross-linked network entrapping a large amount of solvent which does not flow after inverting the test tube.² These materials can be classified depending on their origin, constitution, the type of cross-linking and the entrapped medium (Figure 1).³ Naturally occurred gels are usually based on macromolecules forming a gel through physical cross-linking. If they are of artificial origin, they can be based on either supramolecular or macromolecular origin forming gels through chemical or physical interactions whereas supramolecular gels are solely based on physical interactions, *i.e.* H-bonding, π - π interactions, van der Waals forces, donor-acceptor interactions, metal coordinations and solvophobic forces, among others. Depending on the solvent, gels can be classified as organogels (*i.e.* organic solvents), hydrogels (*i.e.* water) or aero-/xerogels if the solvent is exchanged by air.

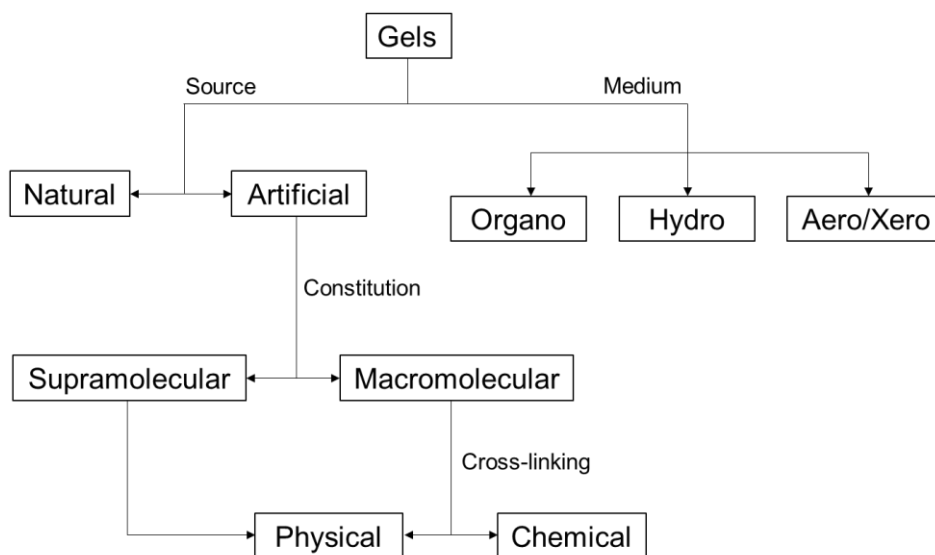


Figure 1. Classification of gels. Adapted from ref. 3 with permission of The Royal Society of Chemistry.

2.2. Supramolecular Gels

Many well-known products in fields ranging from food, cosmetics or biomedical applications were based on polymer gels but since the last two decades, more supramolecular gels, especially based on LMW compounds, were discovered and gained increasing attention due to their versatility which opens up multiple potential applications.³

As mentioned above (chapter 2.1.), supramolecular gels consisting of LMW gelators, are able to self-assemble in an appropriate solvent into a 1D nano- or micro-scale structures, such as rods, fibers, ribbons, tapes, tubes, helices, sheets and spheres. 3D architectures are obtained through intermolecular non-covalent interactions between the 1D structures which immobilized a large amount of solvent molecules, defining an unique gel morphology (Figure 2).^{3,4}

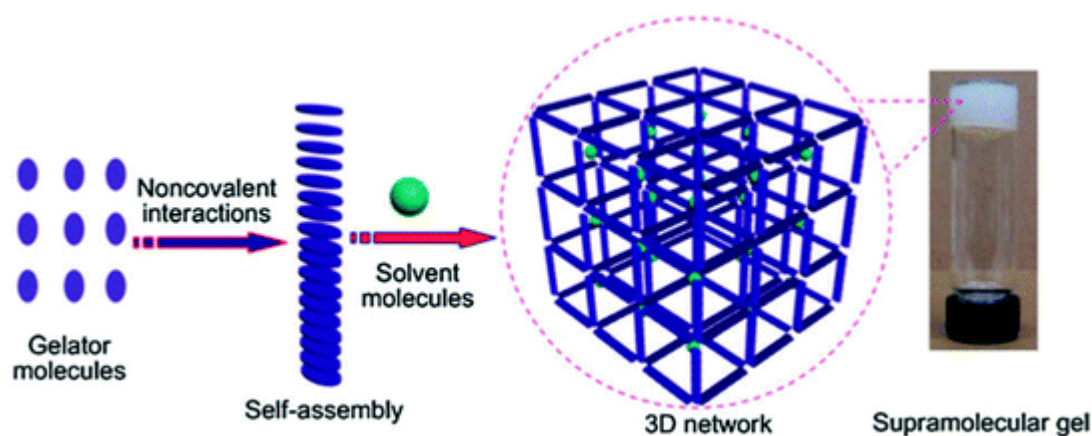


Figure 2. Schematic representation of the formation of a supramolecular gel. Reprinted from ref. 4 with permission of The Royal Society of Chemistry.

In the beginning of the research area of LMW gels, their discovery was mainly based on serendipity. Nowadays, the design of new gelator molecules is getting more predictable by incorporation specific features, e.g. H-bonding motifs such as amides, ureas and saccharides, and different approaches facilitate the design of new gelator molecules, however, the whole gelation process is not fully understood yet.⁵

The molecular modification of the gelator molecules has a huge impact on the nano-scale assembly of the gel and, therefore, on the gel properties, allowing the control over specific material functions.⁶

2.3. Smart Gels

Due to the non-covalent interactions, that hold the supramolecular gel network together, the gels exhibit a reversible *gel-to-sol* phase transition in response to external stimuli such as heat, mechanical stress, pH, light, redox reactions, electrical field or magnetic field (Figure 3).⁷ These functional gels are called “smart” gels and are widely used in multiple applications in fields, such as regenerative medicine, drug-delivery, sensors, actuators, cosmetic, foods, environmental remediation, and nanoelectronic, among others.^{6,8}

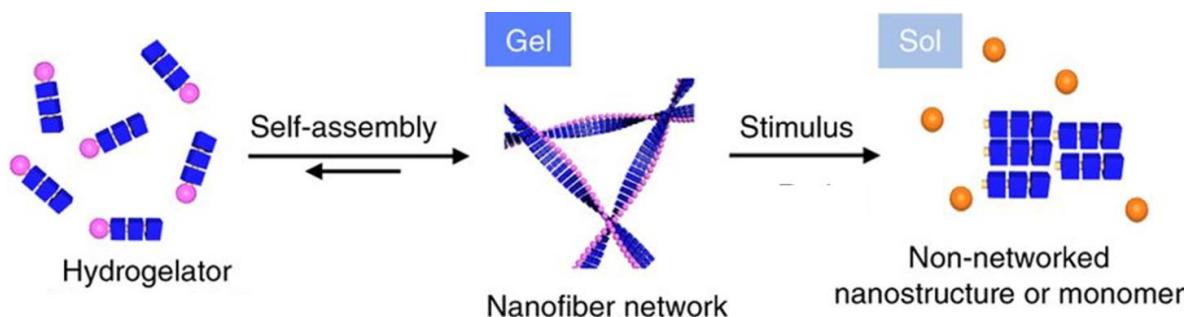


Figure 3. General scheme of a stimuli-induced *gel-to-sol* transition. Adapted from ref. 9 with permission from Springer Nature, Copyright 2016.

Supramolecular gels can be used for thermosensing applications if they respond to heat. Light-sensitive gels can be obtained by incorporating spectroscopically active units to the gelator compound, e.g. photoisomerizable groups such as azobenzene or anthracene.¹⁰ *Gel-to-sol* transitions are then reversibly induced by the irradiation with light due to the gelator isomerization. Such gels are promising materials in optical technologies. A chemical response can be obtained by introducing a receptor unit into the gelator molecule. If the receptor recognizes its ligand, the gel structure undergoes a change which could be useful for applications, such as sensors or actuators. Acidic or basic moieties in the gel structure are sensitive to pH changes, leading to reversible *gel-to-sol* transitions. Thermochromic gels that display different colors in the sol and in the gel states could be obtained with the addition of chromophores to the gelator, e.g. the addition of a pH sensitive dye.¹¹ The color change can be explained with different preferred interactions between the chromophore and the gelator molecules either in gel or sol phase. Metallogels are gels that contain gelators and metal ions, where the metal ion can either act as inert substitute, cross-linker or as functional component of the gel and can impart structural rigidity or novel photophysical, magnetic or redox properties to the gel.¹² Metallogels are ideal candidates for luminescence-based technologies, photovoltaics, and photocatalysis.⁶

Besides gels with response to one stimulus, there are also many examples of gels which respond to multiple stimuli (*i.e.* multi-stimuli responsiveness).¹³

More recently, novel smart gels have been developed with self-healing properties to obtain materials with increased lifetime and enhanced reliability, maintenance and durability.¹⁴ After mechanical stress, *e.g.* scratching traditional gels, they are losing their gel integrity and functionality.¹⁵ Many self-healing strategies are based on dynamic covalent and non-covalent chemistry underlying reversible molecular interactions. Reversibility allows the breaking and re-formation of bonds, the key to a self-healing behavior.¹⁶ Non-covalent interactions are based on hydrophobic interactions, host-guest interactions, hydrogen bonds, crystallization, polymer-nanocomposite interaction and/or multiple intermolecular interactions.¹⁵ Dynamic covalent bonds are mainly based on phenylboronate esters, disulfides, imines, acylhydrazones, reversible radical reactions and reversible Diels-Alder cycloadditions (Figure 3).¹⁵

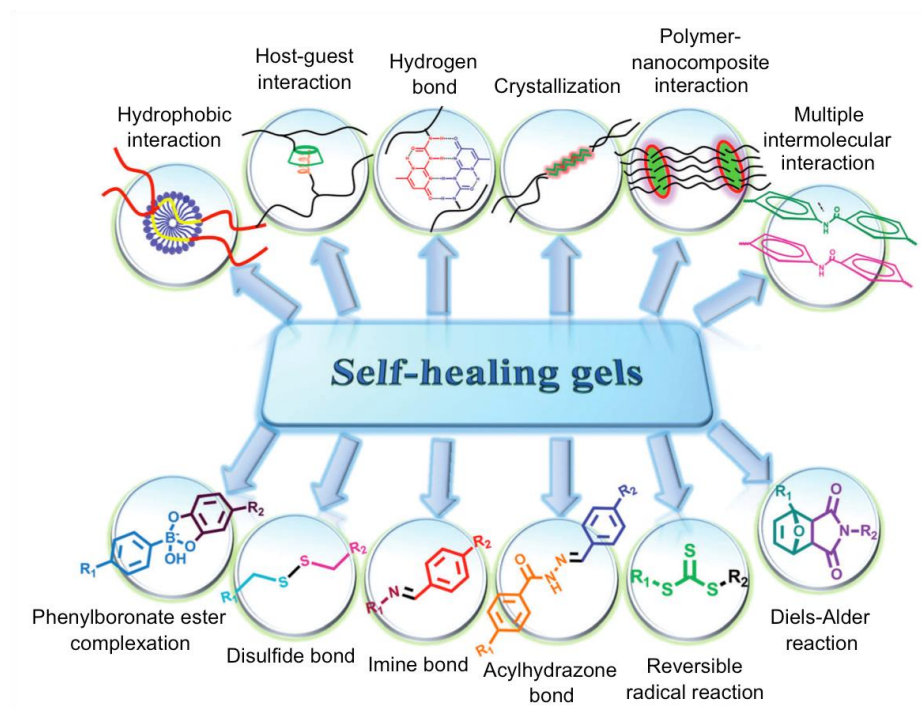


Figure 3. Various strategies to synthesize physical and chemical self-healing gels. Adapted from ref. 15 with permission of The Royal Society of Chemistry.

Self-healing gels need to have an excellent flowability in order to generate a “mobile phase” after a damage, *i.e.* filling and bridging the damaged area which allows the self-healing process.^{15,17} In addition, self-healing gels are either non-automatically or automatically self-healable materials depending if they need an external stimulus (*e.g.* heat, light, pH, *etc.*) or if they are able to self-heal without any stimulus.¹⁵

2.4. Gels for Biomedical Applications

It has been widely demonstrated that supramolecular hydrogels, which are biocompatible and therefore biodegradable and non-toxic, are ideal candidates for biomedical applications, e.g. for drug delivery systems.¹⁸ Many pharmaceutical drugs have a low solubility in water which leads to a reduced membrane permeability and, therefore, low therapeutic efficiency.¹⁹ To overcome this problem and to avoid side effects, caused by long drug routes from administration to the target side, controlled drug delivery systems are desired.²⁰ Supramolecular gels are a promising alternative for the encapsulation and delivery of drug molecules since they are able to deliver low water soluble drugs and create a drug depot within the gel which is released by applying a stimulus (Figure 4).²¹

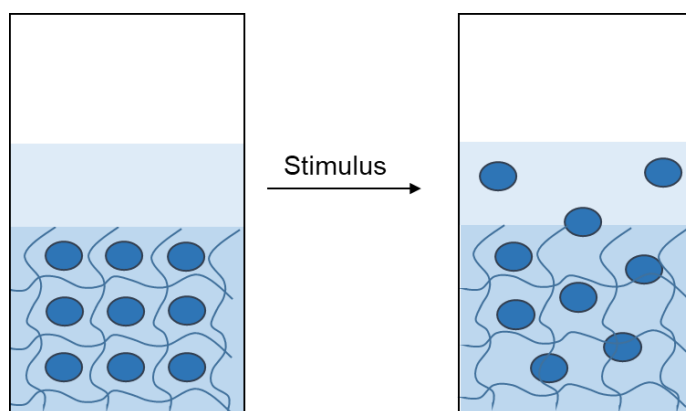


Figure 4. Vials containing supramolecular hydrogels loaded with drug molecules, overlaid with a buffer (left), followed by a stimulus-induced controlled release of the drug molecules (right).

In addition, it allows site specific administration which reduces side effects. Many physical gels can be obtained from cheap materials and are easy to prepare and due to their tunable properties, such as pore size or stimuli-responsiveness among others, they display many advantages in comparison to traditional polymer gels.²¹

2.5. Gels as Nanoreactors

Confined environments have always been the preferred medium of Nature's reaction, ranging from nanometer-sized systems, such as enzymes, to micrometer-sized complexes, such as cells.²² This led to the development of artificial micro- and nanoreactors by scientists.²³ Heterogeneous and organized media are able to improve the selectivity of chemical reactions as well as open up new reaction pathways.²⁴ In general, confined media have the advantage that they have large active reaction areas, adjustable functionalities, they can decrease overheating and overconcentration effects and, in addition, they can be recycled and reused for more reactions.²⁴

Furthermore, it has been shown that supramolecular aggregation is important in many different catalytic processes.^{25a} Due to the versatility and the porous nature of supramolecular gels, they are promising candidates as selective nanoreactors and/or heterogeneous recyclable catalyst.²⁵ The advantages of gels in comparison to solutions are a high specific surface area, remarkable diffusion properties and their reversibility which makes them stimuli-sensitive. During the last decade, it has been demonstrated that physical gels are able to enhance the selectivity of many processes due to specific interactions between the reactants inside the confined media.^{25b}

Many photocatalytic reactions have been beneficial in confined media such as mesoporous inorganic materials,²⁶ micelles,²⁷ liquid foams,²⁸ among others.²⁹ Properties such as light absorption, generation of reactive intermediates, lifetime of excited species and many more are influenced by the reaction environment.³⁰ However, there are only some examples of photochemical and photophysical processes inside gel matrices but the research area attracted increasing interest and is continuously growing.²⁵

Soft gels have been already acted as reaction vessels and nanoreactors for photochemical processes, including photodimerizations,³¹ photosensitized isomerizations,³² and photooxidations.³³ The gel provides spatially confined micro- and nanoreactors to improve reaction kinetics, selectivity and processability in comparison to homogeneous solutions.

In future, photo-induced processes inside gel medium have possible applications in areas like photovoltaics, photocatalysis and phototherapy. However, more studies for a better understanding between the interactions reactants and the confined media are important in order to predict the outcome of the photochemical and – physical processes.

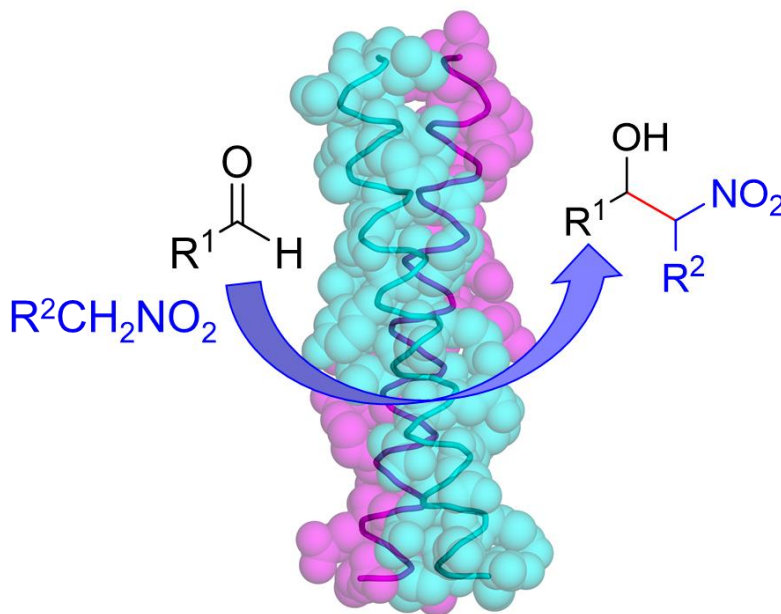
2.6. References

- [1] a) Polymer gels: Fundamentals and Biomedical Applications (Eds.: D. De Rossi, K. Kajiwara, Y. Osada, A. Yamauchi), Plenum Press, New York, **1991**; b) Hydrogels in Medicine and Pharmacy; vol. III: Properties and Applications (Ed.: N. A. Peppas), CRC Press, Boca Raton, **1987**.
- [2] K. Almdal, *Polym. Gels Networks*, **1993**, 1, 5-17.
- [3] N. M. Sangeetha, U. Maitra, *Chem. Soc. Rev.*, **2005**, 34, 821-836.
- [4] G. Y. X. Yan, C. Han, F. Huang, *Chem. Soc. Rev.*, **2013**, 42, 6697.
- [5] P. Dastidar, *Chem. Soc. Rev.*, **2008**, 37, 2699-2715.
- [6] A. R. Hirst, B. Escuder, J. F. Miravet, D. K. Smith, *Angew. Chem., Int. Ed.*, **2008**, 47, 8002.
- [7] Y. Osada, S. B. Ross-Murphy, *Sci. Am.* **1993**, 42-47.
- [8] N. Fujita, P. Mukhopadhyay, S. Shinkai, *Annu. Rev. Nano Res.*, **2006**, 1, 385.
- [9] H. Shigemitsu, T. Fujisaku, S. Onogi, T. Yoshii, M. Ikeda, I. Hamachi, *Nat. Protoc.* **2016**, 11, 1744-1756.
- [10] K. Murata, M. Aoki, T. Nishi, A. Ikeda, S. Shinkai, *J. Chem. Soc., Chem. Commun.*, **1991**, 1715.
- [11] U. Maitra, S. Mukhopadhyay, A. Sarkar, P. Rao, S. S. Indi, *Angew. Chem. Int. Ed.*, **2001**, 40, 2281.
- [12] J. W. Steed, *Chem. Commun.*, **2011**, 47, 1379-1383.
- [13] S. A. Ahmed, X. Sallenave, F. Fages, G. Mieden-Gundert, W. M. Müller, F. Vögtle, J.-L. Pozzo, *Langmuir*, **2002**, 18, 7096.
- [14] T.-P. Huynh, P. Sonar, H. Haick, *Adv. Mater.* **2017**, 29, 1604973.
- [15] Z. Wei, J. H. Yang, J. Zhou, F. Xu, M. Zrinyi, P. H. Dussault, Y. Osada, Y. M. Chen, *Chem. Soc. Rev.*, **2014**, 43, 8114-8131.
- [16] a) C. R. South, C. Burd, M. Weck, *Acc. Chem. Res.*, **2007**, 40, 63; b) S. J. Rowan, S. J. Cantrill, G. R. Cousins, J. K. Sanders, J. F. Stoddart, *Angew. Chem., Int. Ed.*, **2002**, 41, 898; c) S. K. M. Nalluri, C. Berdugo, N. Javid, P. W. J. M. Frederix, R. V. Ulijn, *Angew. Chem., Int. Ed.*, **2014**, 53, 5882; d) S. K. M. Nalluri, R. V. Ulijn, *Chem. Sci.*, **2013**, 4, 3699.
- [17] R. P. Wool, *Soft Matter*, **2008**, 4, 400.
- [18] S. Banerjee, R. K. Das, U. Maitra, *J. Mater. Chem.*, **2009**, 19, 6649-6687.
- [19] a) S. Song, B. Tian, F. Chen, W. Zhang, Y. Pan, Q. Zhang, X. Yang, W. Pan, *Drug Dev. Ind. Pharm.*, **2015**, 41, 51-62; b) M. Z. Ahmad, A. A. Mohammed, M. M. Ibrahim,

- Pharm, Dev. Technol.*, **2016**, 7450, 1-10; c) M. Z. Ahmad, S. Akhter, N. Mohsin, B. A. Abdel-Wahab, J. Ahmad, M. H. Warsi, M. Rahman, N. Mallick, F. J. Ahmad, *Curr. Drug Discovery Technol.*, **2014**, 11, 197-213.
- [20] a) J. A. Hubbell, A. Chilkoti, *Science*, **2012**, 337, 303-305; b) R. Lin, H. Cui, *Curr. Opin. Chem. Eng.*, **2015**, 7, 75-83.
- [21] J. Mayr, C. Saldías, D. D. Díaz, *Chem. Soc. Rev.*, **2018**, 47, 1484-1515.
- [22] M. Vriezema, M. C. Aragonès, J. A. A. W. Elemans, J. J. L. M. Cornelissen, A. E. Rowan, R. J. M. Nolte, *Chem. Rev.*, **2005**, 105, 1445-1489.
- [23] Z. V. Todres, *Organic chemistry in confined media*, Springer International Publishing, Switzerland, **2013**.
- [24] a) D. G. Blackmond, M. Klusmann, *Chem. Commun.*, **2007**, 3990; b) L. Schiaffino, G. Ercolani, *Angew. Chem., Int. Ed.*, **2008**, 47, 6832.
- [25] a) D. Kühbeck, R. J. Koopmans, D. D. Díaz, *Chem. Soc. Rev.*, **2011**, 40, 427-448; b) R. Pérez-Ruiz, D. D. Díaz, *Soft Matter*, **2015**, 11, 5180-5187.
- [26] M. Antonietti, G. A. Ozin, *Chem.-Eur. J.*, **2004**, 10, 28-41.
- [27] C. Harris, P. V. Kamat, *ACS Nano*, **2009**, 3, 682-690.
- [28] D. G. Shchukin, E. A. Ustinovich, A. I. Kulak, D. V. Sviridov, *Photochem. Photobiol. Sci.*, **2004**, 3, 157-159.
- [29] a) J. H. Fendler, *Chem. Rev.*, **1987**, 87, 877-899; b) J. G. Riess, *Chem. Rev.*, **2001**, 101, 2797-2920; c) O. V. Vasil'tsova, V. N. Parmon, *Kinet. Catal.*, **1999**, 40, 62-70; d) K. Uekama, F. Hirayama, T. Irie, *Chem. Rev.*, **1998**, 98, 2045-2076.
- [30] a) G. Palmisano, V. Augugliaro, M. Pagliaro, L. Palmisano, *Chem. Commun.*, **2007**, 3425-3437; b) M. Pagliaro, R. Ciriminna, G. Palmisano, *Chem. Soc. Rev.*, **2007**, 36, 932-940.
- [31] a) A. Dawn, N. Fujita, S. Haraguchi, K. Sada, S. Shinkai, *Chem. Commun.*, **2009**, 2100-2102; b) A. Dawn, N. Fujita, S. Haraguchi, K. Sada, S.-I. Tamaru, S. Shinkai, *Org. Biomol. Chem.*, **2009**, 7, 4378-4385; c) A. Dawn, T. Shiraki, S. Haraguchi, H. Sato, K. Sada, S. Shinkai, *Chem.-Eur. J.*, **2010**, 16, 3676-3689; d) S. Bhat, U. Maitra, *Molecules*, **2007**, 12, 2181-2189; e) Rajkamal, D. Chatterjee, A. Paul, S. Banerjee, S. Yadav, *Chem. Commun.*, **2014**, 50, 12131-12134.
- [32] X. Wei, W. Liang, W. Wu, C. Yang, F. Trotta, F. Caldera, A. Mele, T. Nishimoto, Y. Inoue, *Org. Biomol. Chem.*, **2015**, 13, 2905-2912.
- [33] J. Bachl, A. Hohenleutner, B. B. Dhar, C. Cativiela, U. Maitra, B. König, D. D. Díaz, *J. Mater. Chem. A*, **2013**, 1, 4577-4588.

3. Main part

3.1. Keratin Catalyzed Nitroaldol (Henry) Reaction and Comparison with other Biopolymers



This chapter has been published in:

M. Häring, A. Pettignano, F. Quignard, N. Tanchoux, D. D. Díaz, 'Keratin protein-catalyzed nitroaldol (Henry) reaction and comparison with other biopolymers', *Molecules* **2016**, 21, 1122. – Reproduced with permission from *Molecules* **2016**, 21, 1122. Copyright © 2016, MDPI.

Author contribution:

MH did the experiments for Table 2-5, the recycling experiments and the kinetics for keratin. AP performed the experiments shown in Table 1. The kinetic data used for comparison were published by the group in previous publications (see references). All authors contributed to the scientific discussion of the results.

3.1.1. Abstract

This chapter describes the preliminary investigations on the ability of natural keratin as green organocatalyst for the nitroaldol (Henry) reaction between aldehydes and nitroalkanes as a model reaction in both DMSO or water in the presence of tetra-*n*-butylammonium bromide (TBAB) as a phase-transfer catalyst (PTC). Negligible background reactions were observed in these solvent systems. Both aromatic and heteroaromatic aldehydes bearing strong or moderate electron-withdrawing groups were converted into the corresponding β -nitroalcohol products. Aromatic aldehydes bearing electron-donating groups and aliphatic aldehydes showed poor or no conversion, respectively. In general, the reactions in water/TBAB required twice the amount of time than in DMSO to achieve similar conversions. Additionally, kinetics of the nitroaldol (Henry) reaction catalyzed by keratin in both solvent systems were compared with other biopolymers as catalysts.

3.1.2. Introduction

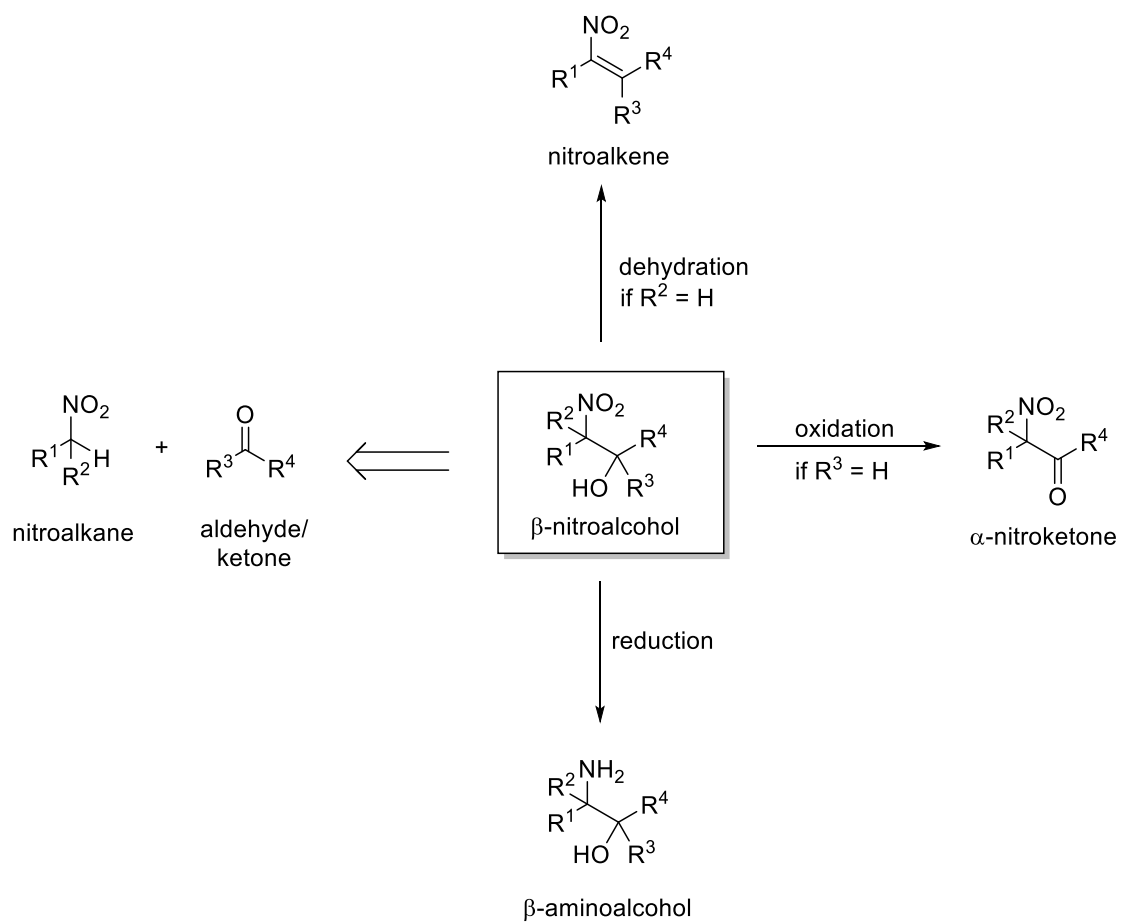
Due to the growing concern for our environment on the one hand and stricter environmental regulations by governments on the other, the utilization of environmentally friendly and sustainable resources and processes is highly demanded.¹ Recently, biopolymers have gained increasing attention due to their unique properties, such as biodegradability and biocompatibility. In addition, the cheap and easy availability of products, derived from naturally occurring materials, has become more common for many high-tech applications.²

During the last decade, keratinous materials have become an important source of renewable biomaterials, especially since keratin wastes have been estimated to be more than 5 million tons per year.³ Keratin has been used after degradation for different applications including scaffolds for tissue engineering^{4,5} and support matrices for catalytic metal nanoparticles,⁶ among others.^{7,8}

Keratin is one of the most abundant non-food proteins and represents a group of insoluble, cysteine-rich and stable filament-forming materials derived primarily from wool, hair, feathers, beaks, hooves, horns and nails.⁹ Depending on their sulfur content, keratins can be classified as soft or hard keratins. Soft keratins, with a cysteine content up to 2% and found in outer layers of the epidermis and hair core, have a weaker mechanical and chemical stability. Hard keratins with a cysteine content of 10%-14% in hair, wool and skin, exhibit a higher resistance to thermal and chemical influences due to the higher content of disulfide bridges.¹⁰ Keratins contain a central ~ 310 residue domain with four segments in an α -helical conformation that are separated by three short linker segments in β -turn conformation.¹¹ The complete amino acid sequence of keratins obtained from different sources has been reported in several publications,¹²⁻¹⁵ making the protein a suitable candidate to be tested as a catalyst.

In addition, the nitroaldol (Henry) reaction is a highly versatile C-C bond-forming reaction between aldehydes or ketones and nitroalkanes to yield β -nitroalcohols, which are valuable building blocks that can be transformed into β -aminoalcohols, β -nitroketones, nitroalkenes and are used among other important intermediates for synthesizing insecticide, fungicides, antibiotics and some useful natural compounds (Scheme 1).¹⁶⁻¹⁸

Scheme 1. A general overview of β -nitroalcohols as versatile building blocks.



3.1.3. Results and Discussion

3.1.3.1. Solvent Screening

The nitroaldol (Henry) reaction between 4-nitrobenzaldehyde (**1a**, 0.1 mmol) and nitromethane (**2a**, 1.0 mmol) was chosen as a model reaction to demonstrate the potential ability of keratin to promote C-C bond formation under mild conditions. In preliminary experiments, the Henry reaction was performed in different solvents in the presence of 10 mg keratin. No formation of the desired β -nitroalcohol **3a** could be observed in toluene, THF or CH₃CN (Table 1, entries 1-3), and very low yields of **3a** (approx. 10%) were obtained in DCM, CHCl₃ or H₂O (Table 1, entries 4,5 and 7). However, DMSO and water containing tetra-*n*-butylammonium bromide (TBAB) as PTC were found to be appropriate solvents allowing the selective formation of **3a** in modest yields at room temperature with no or very low background reaction (Table 1, entry 6 and entry 8). The keratin loading could be reduced to 2 mg without detriment in the product yield. However, 10 mg was used in most experiments for practical reasons. In addition, the reaction can be scaled up (*i.e.*, 1 mmol of **1a**) without detracting from the product yield.

Table 1. Initial solvent screening for the nitroaldol (Henry) reaction between **1a** and **2a**.^a

Entry	Solvent	Yield of 3 (%) ^c
1	Toluene	0
2	THF	0
3	CH ₃ CN	0
4	DCM	11
5	CHCl ₃	10
6	DMSO	66 (0) ^d
7	H ₂ O	11
8	H ₂ O/TBAB ^b	57 (3) ^d

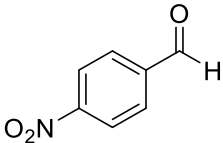
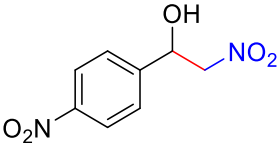
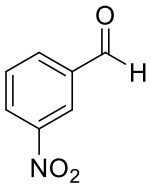
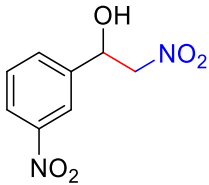
^a Reaction conditions: **1a** (0.1 mmol), **2a** (1.0 mmol), keratin (10 mg), solvent (0.5 mL), RT, orbital shaking (150 rpm), 24 h; ^b TBAB (0.1 mmol). The addition of the phase-transfer catalyst did not change the pH of the solution; ^c ¹H-NMR yields of crude product obtained in the presence of dimethyl acetamide (DMA) as internal standard; ^d Background reaction without keratin.

3.1.3.2. Substrate Scope

With these preliminary results in hand, the substrate scope of the reaction was examined using different aldehydes in combination with nitromethane or nitroethane in either DMSO (Table 2 and 3) or H₂O/TBAB (Table 4 and 5) at room temperature.

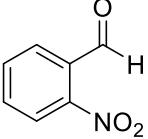
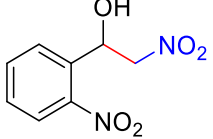
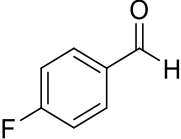
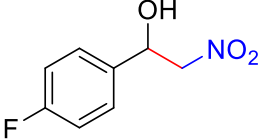
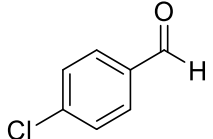
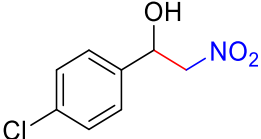
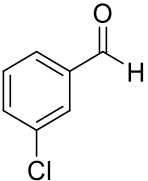
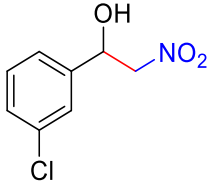
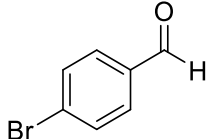
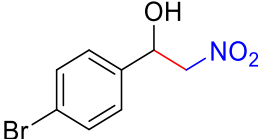
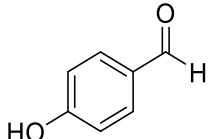
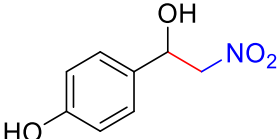
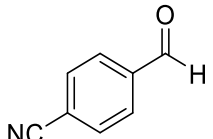
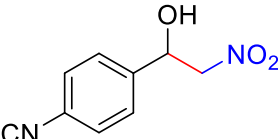
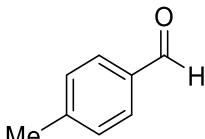
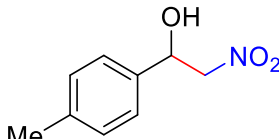
Aromatic aldehydes bearing strong electron-withdrawing substituents, such as –NO₂, were easily converted in DMSO into the corresponding β-nitroalcohols **3a-c** in excellent yields regardless the position of the substituent (*ortho*-, *meta*-, *para*-) (Table 2, entries 1-3). Weaker acceptor substituents afforded the corresponding product in moderate yields (Table 2, entries 4, 5, 7, 9, 12). Interestingly, the *meta*-position of the substituent (Table 2, entry 6) seemed to be more favored here, giving rise to **3f** in good yield and twice as much than the *para*-substituted substrate (Table 2, entry 5). In contrast, benzaldehyde or aromatic aldehydes bearing electron-donating substituents yielded only trace amounts of the expected product (Table 2, entries 8, 10, 11). Heteroaromatic aldehydes such as 2-pyridinecarboxaldehyde (Table 2, entry 13) lead to the desired product in excellent yield, whereas furfural and 1-naphthaldehyde (Table 2, entries 14 and 15) proceeded only with low yields. It is also worth mentioning that aliphatic aldehydes such as isobutyraldehyde were not converted. Moreover, despite the α-helical chiral structure of keratin, HPLC analysis of the reaction mixtures showed no enantioselectivity, which has been observed with other biocatalysts in the same reaction.¹⁸⁻²⁰

Table 2. Keratin-catalyzed nitroaldol (Henry) reaction between different aldehydes and nitromethane in DMSO.^a

$\text{R}-\overset{\text{O}}{\parallel}{\text{C}}-\text{H} + \text{CH}_3\text{NO}_2 \xrightarrow[\text{RT, 24 h}]{\text{Keratin, DMSO}} \text{R}-\text{CH}(\text{OH})-\text{CH}_2\text{NO}_2$			
1a-o	2a		3a-o
Entry	Aldehyde	Product	Yield of 3 (%) ^b
1	 1a	 3a	84
2	 1b	 3b	93

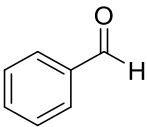
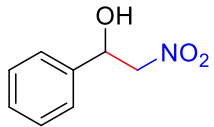
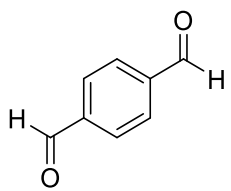
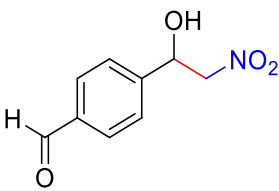
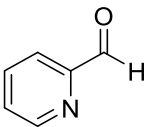
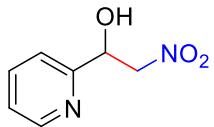
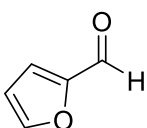
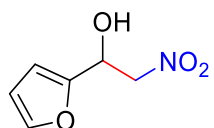
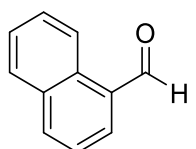
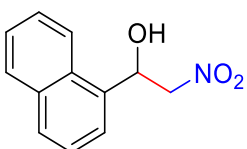
continued next page

Continuation of Table 2

Entry	Aldehyde	Product	Yield of 3 (%) ^b
3		1c 	3c 94
4		1d 	3d 10
5		1e 	3e 25
6		1f 	3f 48
7		1g 	3g 25
8		1h 	3h 5
9		1i 	3i 30
10		1j 	3j 7

continued next page

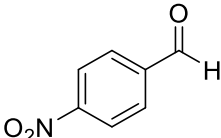
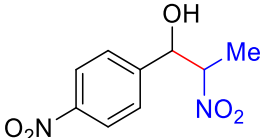
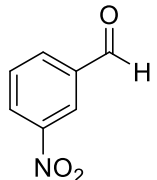
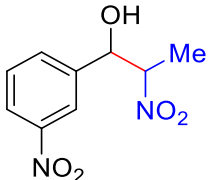
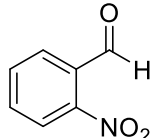
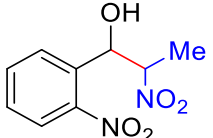
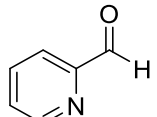
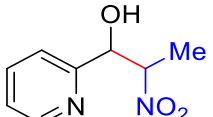
Continuation of Table 2

Entry	Aldehyde		Product		Yield of 3 (%) ^b
11		1k		3k	9
12		1l		3l	65 ^c
13		1m		3m	90
14		1n		3n	3
15		1o		3o	13

^a Reaction conditions: **1** (0.1 mmol), **2a** (1.0 mmol), keratin (10 mg), DMSO (0.5 mL), RT, orbital shaking (150 rpm), 24 h; ^b Yield determined by ¹H-NMR in the presence of DMA as internal standard; ^c Yield of monosubstituted β -nitroalcohol.

Regarding the nature of the nucleophile, the use of nitroethane instead of nitromethane provided slightly higher yields of the desired product albeit with no or little diastereoselectivity favoring the *syn* diastereomer (Table 3, entries 1, 3 and 4). Slight *anti* diastereoselectivity was observed only with 3-nitrobenzaldehyde (Table 3, entry 2). Relative configurations were assigned by comparison with ¹H-NMR data reported in the literature.¹⁸⁻²² These results are similar to those obtained with other biopolymers such as gelatin and suggest that the acidity of the nitroalkane (nitroethane pK_a = 8.6; nitromethane pK_a = 10.2) constitutes, in most cases, a more important factor than steric effects.²³

Table 3. Keratin-catalyzed nitroaldol (Henry) reaction between different aldehydes and nitroethane in DMSO.^a

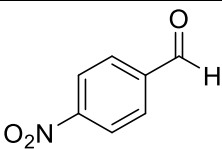
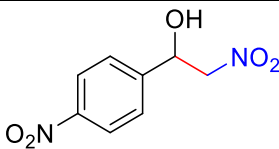
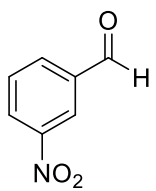
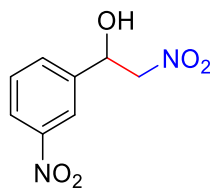
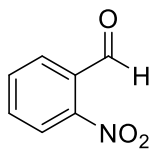
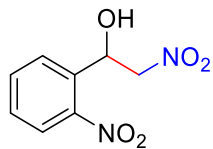
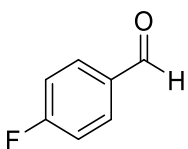
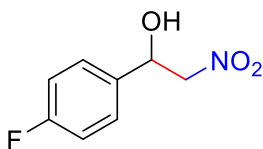
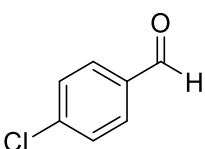
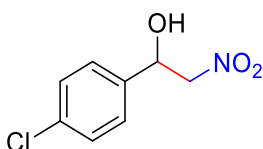
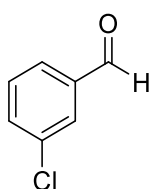
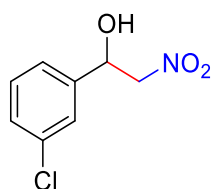
$\text{R}-\text{CHO} + \text{EtNO}_2 \xrightarrow[\text{RT, 24 h}]{\text{keratin, DMSO}} \text{R}-\text{CH}(\text{OH})-\text{CH}(\text{Me})\text{NO}_2 + \text{R}-\text{CH}(\text{OH})-\text{CH}(\text{Me})\text{NO}_2$		<i>anti</i> - 4	<i>syn</i> - 4
1a-m	2b		
Entry	Aldehyde	Product	Yield of 4 (%) ^b
1	 1a	 4a	96 (1:1) ^c
2	 1b	 4b	98 (1:0.8) ^c
3	 1c	 4c	96 (1:1.3) ^c
4	 1m	 4m	96 (1:1.7) ^c

^a Reaction conditions: **1** (0.1 mmol), **2b** (1.0 mmol), keratin (10 mg), DMSO (0.5 mL), RT, orbital shaking (150 rpm), 24 h; ^b Yield determined by ¹H-NMR in the presence of DMA as internal standard; ^c Diastereomeric ratio *anti/syn* determined by ¹H-NMR analyses.

As demonstrated in the preliminary solvent screening (Table 1), water in the presence of TBAB constitutes an appropriate solvent for the keratin-catalyzed nitroaldol reaction between 4-nitrobenzaldehyde **1a** and nitromethane **2a**. In the following, the substrate scope was expanded in H₂O/TBAB, however, the reactions took two times longer than in DMSO to achieve similar conversions. In H₂O/TBAB the substituent position in the aldehyde **1** was found to have higher influence than in DMSO. For example, strong electron-withdrawing substituents in *ortho*- and *para*-position favored the reaction (Table 4, entries 1 and 3), whereas a significant decrease of the yield was observed with the same substituent placed in *meta*-position (Table 4, entry 2). The reasons for the differences observed in H₂O/TBAB and DMSO may be related to the solubilization of the reactants and/or involve important variations in the mechanistic pathways, which remain unclear and need to be investigated in future research. Furthermore, the expected products were obtained in good yields also with

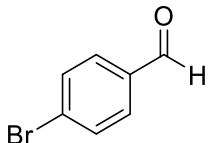
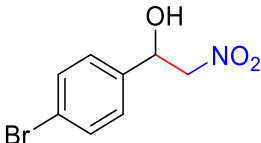
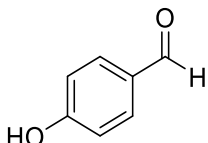
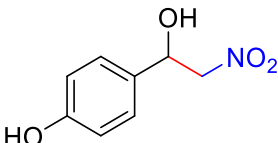
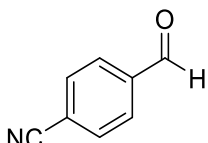
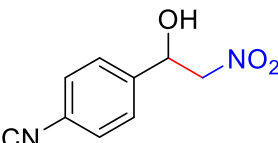
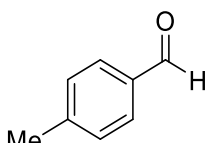
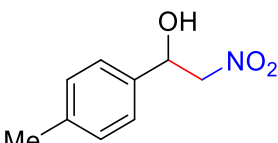
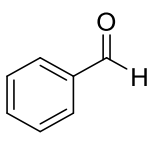
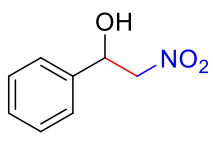
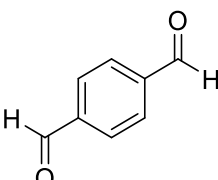
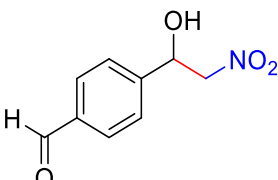
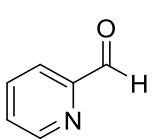
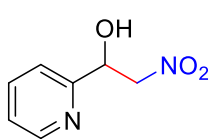
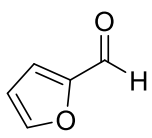
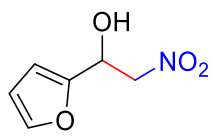
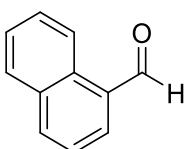
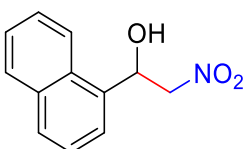
4-cyanobenzaldehyde (Table 4, entry 9) and 2-pyridine carboxaldehyde (table 4, entry 13). Other aldehydes were converted less efficiently. It is worth mentioning that the replacement of TBAB by other ionic materials such as 1-butyl-3-methylimidazolium hexafluorophosphate (BMIM-PF₆) afforded the desired compound albeit in lower yield even at longer reaction time (Table 4, entry 1).

Table 4. Keratin-catalyzed nitroaldol (Henry) reaction between different aldehydes and nitromethane in H₂O/TBAB.^a

$\text{R}-\overset{\text{O}}{\parallel}{\text{C}}-\text{H} + \text{CH}_3\text{NO}_2 \xrightarrow[\text{RT, 48 h}]{\text{keratin, H}_2\text{O/TBAB}} \text{R}-\overset{\text{OH}}{\underset{\text{NO}_2}{\text{C}}}-\text{H}$			
1a-o	2a		3a-o
Entry	Aldehyde	Product	Yield of 3 (%) ^b
1			73 (50) ^c
2			21
3			70
4			9
5			18
6			34

continued next page

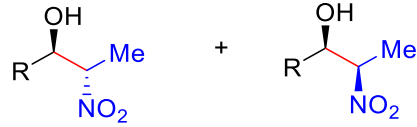
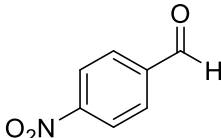
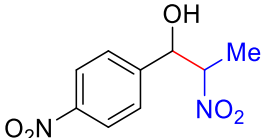
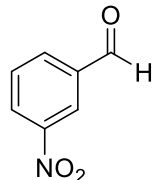
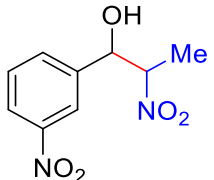
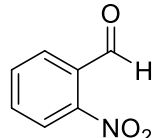
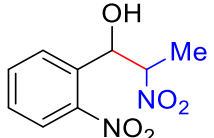
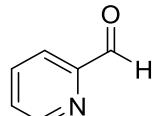
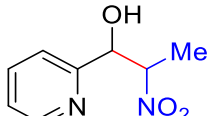
Continuation of Table 4

Entry	Aldehyde		Product		Yield of 3 (%) ^b
7		1g		3g	14
8		1h		3h	1
9		1i		3i	66
10		1j		3j	4
11		1k		3k	8
12		1l		3l	19 ^d
13		1m		3m	72
14		1n		3n	11
15		1o		3o	0

^a Reaction conditions: **1** (0.1 mmol), **2a** (1.0 mmol), TBAB (0.1 mmol), keratin (10 mg), H₂O (0.5 mL), RT, orbital shaking (150 rpm), 48 h; ^b Yield determined by ¹H-NMR in the presence of DMA as internal standard; ^c Yield of the reaction carried out in the presence of BMIM-PF₆ (0.1 mmol) instead of TBAB. Reaction time = 72 h; ^d Yield of monosubstituted β-nitroalcohol.

Furthermore, the use of nitroethane instead of nitromethane provided significant higher yields (>85%) of the desired product (Table 5) albeit with almost negligible diastereoselectivity (Table 5, entries 2 and 4). Interestingly, using nitroethane instead of nitromethane, lead to the formation of the desired product in higher yields, *i.e.* an increase of at least 13%. It is worth mentioning, that the substrate **1b** showed an increase of 77% (Table 5, entry 2 in comparison to Table 4, entry 2) which seems that using a different nucleophile could be favored for some substrates.

Table 5. Keratin-catalyzed nitroaldol (Henry) reaction between different aldehydes and nitroethane in H₂O/TBAB.^a

$\text{R}-\text{CHO} + \text{EtNO}_2 \xrightarrow[\text{RT, 24 h}]{\text{keratin, H}_2\text{O/TBAB}}$			
1a-m	2b	<i>anti</i> - 4	<i>syn</i> - 4
Entry	Aldehyde	Product	Yield of 4 (%) ^b
1	 1a	 4a	94 (n.d.) ^c
2	 1b	 4b	98 (1:0.8) ^c
3	 1c	 4c	89 (n.d.) ^c
4	 1m	 4m	85 (1:0.9) ^c

^a Reaction conditions: **1** (0.1 mmol), **2b** (1.0 mmol), TBAB (0.1 mmol), keratin (10 mg), H₂O (0.5 mL), RT, orbital shaking (150 rpm), 48 h; ^b Yield determined by ¹H-NMR in the presence of DMA as internal standard;

^c Diastereomeric ratio *anti/syn* determined by ¹H-NMR analyses, n.d. = not detectable.

3.1.3.3. Recycling Experiments

The heterogeneous nature of the protein catalyst allowed its recovery from the reaction mixture and its reuse for further cycles. However, a gradual deactivation of the catalyst could

be observed in both organic and aqueous media, although the reduction of the catalytic activity was clearly more pronounced in DMSO (Figure 1).

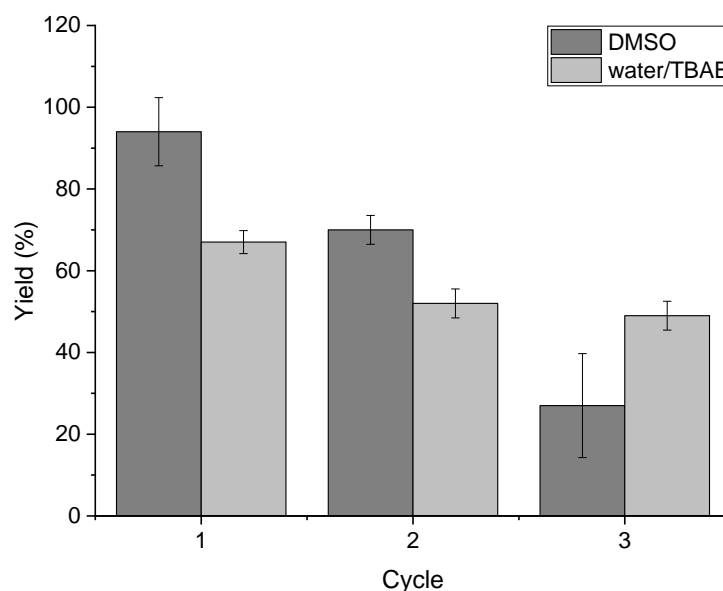


Figure 1. Typical recycling experiments for keratin-catalyzed nitroaldol (Henry) reaction in DMSO and H₂O/TBAB. Reaction conditions: 4-nitrobenzaldehyde (**1a**, 15.1 mg, 0.1 mmol), nitromethane (**2a**, 54 μ L, 1.0 mmol), solvent (0.5 mL), keratin powder (10 mg), room temperature, 24-48 h. Yields correspond to ¹H-NMR values obtained from at least two experiments. The values represent the average of two measurements. For the experiments in H₂O/TBAB, the addition of new TBAB after each cycle (*i.e.* 32.2 mg, 0.1 mmol) was necessary to ensure a constant concentration during the reactions as confirmed by NMR analyses of the reaction mixtures.

Such behavior has also been observed with other biopolymers and could be associated to loss of catalyst loading (*e.g.*, inefficient isolation by filtration) after each cycle and/or formation of intermediate linear or cyclic aminals that could block catalytic sites of the protein.¹⁸⁻²¹ These potential competitive processes are somehow more critical in DMSO than in aqueous solution; however, the reasons behind these differences need to be further investigated.

3.1.3.4. Kinetic Analysis

At this point, kinetic analyses of the model reaction between **1a** and **2a** were carried out catalyzed by keratin in both DMSO and H₂O/TBAB under the described conditions. The results were compared with the performance of other biopolymers as biocatalysts for the same reaction that have been previously studied (*i.e.*, alginate,¹⁸ silk fibroin,¹⁹ gelatin,²⁰ collagen,²⁰ bovine serum albumin (BSA),^{20,24} and chitosan²¹) under optimized conditions. Figure 2 shows the first-order kinetics corresponding to each biopolymer within the first hours of reaction. In general, powdered keratin displayed rate constants in the range of aerogel calcium alginate and significantly below the other biopolymers demonstrating the possibility of fine-tuning the

kinetics of the nitroaldol (Henry) reaction by appropriate selection of the biopolymer and solvent system. It is worth mentioning that although these biopolymers are not superior to standard base catalysts such as tetramethylethylenediamine (TMEDA), the former avoided the formation of byproducts and allowed to work under ecofriendly and heterogeneous conditions. However, far beyond the interest of these materials as a standard catalyst, their mechanism of action to promote C-C bond formation reactions may be more relevant within the context of biological evolution.

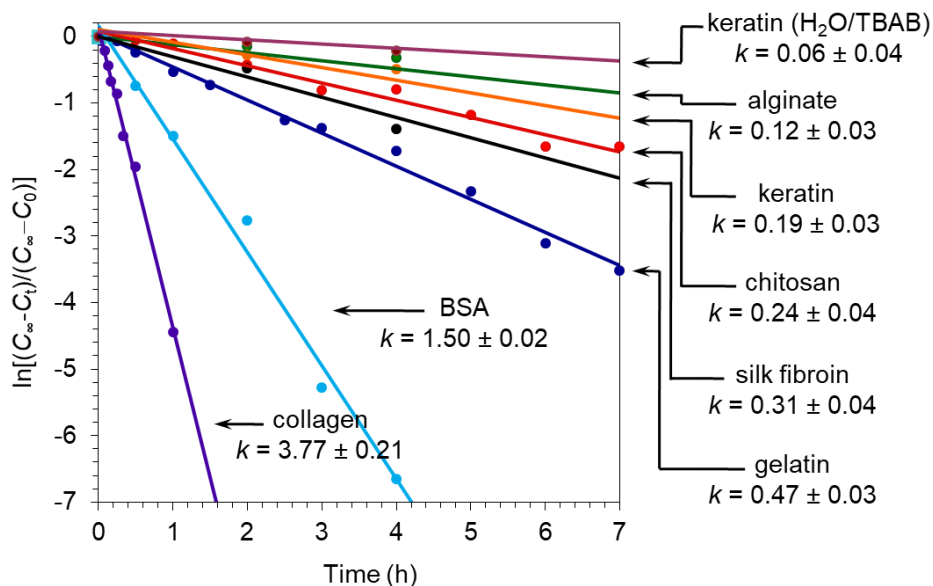


Figure 2. First-order kinetics plots for the nitroaldol (Henry) reaction between **1a** and **2a** catalyzed by different biopolymers in powder form. Unless otherwise indicated, reactions were made in DMSO as described in the text and experimental section. Apparent rate constants are given in units of h^{-1} . Each data point represents the average of at least two independent measurements. C_∞ = final concentration at infinite time; C_t = concentration at given time t ; C_0 = initial concentration at $t = \text{zero time}$.

3.1.4. Conclusion and Outlook

In conclusion, we have demonstrated that keratin proteins are able to promote C-C bond formation via the nitroaldol (Henry) reaction between various aldehydes and nitroalkanes. Appropriate control experiments demonstrated the intrinsic catalytic activity of the keratin. Both aromatic and heteroaromatic aldehydes having strong or moderate electron-withdrawing groups were converted exclusively into the corresponding β -nitroalcohol products in both DMSO and in water in the presence of TBAB as phase transfer catalyst. In contrast, aromatic aldehydes bearing electron-donating groups and aliphatic aldehydes showed poor or no conversion, respectively. In general, the reactions in water/TBAB required twice the amount of reaction time than in DMSO to achieve similar conversions. Although the heterogeneous nature of the reaction allowed for the recovery and reuse of the keratin, a gradual deactivation of the catalyst was observed after each cycle. Comparative kinetic studies with other biopolymers revealed that the rate of the nitroaldol (Henry) reaction strongly depends on the nature of the biopolymer.

The effect of different forms of keratins (e.g. hydrogels, aerogels, xerogels) on the ability to catalyze the nitroaldol (Henry) reaction and on other C-C bond forming reactions in both organic and aqueous media, including different ionic liquids, could give more insight into the catalytic potential of keratin and the underlying reaction mechanism.

3.1.5. Experimental Part

3.1.5.1. Materials and Methods

Unless otherwise indicated, analytical grade solvents and reactants were commercially available and used as received without further purification. Deionized water was used for experiments in aqueous solutions. Aldehydes (purity by GC > 98%) were purchased from TCI Europe (TCI Europe, Zwijndrecht, Belgium). Keratin extracted from wool (CAS 6943036-0, Cat. Nr. AB 250197) was purchased from ABCR. Tetrabutylammonium bromide (CAS 1643-19-2, Cat. Nr. 86860) was purchased from Fluka (Fluka Chemical Corp., Milwaukee, WI, USA). 1-Buthyl-3-methylimidazolium hexafluorophosphate (BMIM-PF₆) was purchased from TCI Europe (CAS 174501-64-5, Cat. Nr. B2320).

¹H-NMR spectra were recorded on Avance 300 or Avance 400 spectrometers (Bruker, Billerica, MA, USA) at 25 °C. Chemical shifts for ¹H were reported as δ , parts per million (ppm), relative to the signal of the residual solvent (CHCl₃ = 7.26 ppm). Coupling constants (J) are given in Hertz (Hz). The following notations indicate the multiplicity of the signals: s = singlet, br s = broad singlet, d = doublet, t = triplet, q = quartet, dd = doublet of doublets, m = multiplet. Estimated error of reported values: 0.01 ppm (δ , ¹H NMR), 0.1 Hz (J, coupling constant). Yields were determined by ¹H-NMR analyses of the crude product in CDCl₃ using dimethyl acetamide (0.1 mmol, 9.2 μ L) as internal standard after complete work-up of the reaction. Enantiomeric excess was evaluated by chiral HPLC (Agilent Technologies, Santa Clara, CA, USA) (column: Phenomenex (Phenomenex, Aschaffenburg, Germany) Lux Cellulose-1, 4.6 mm x 250 mm, 5 μ m, eluents: *n*-heptane, *i*-propanol 70:30, flow: 0.5 mL min⁻¹). Relative configurations were assigned by comparison with ¹H-NMR data reported in the literature.¹⁸⁻²² For example, in the model reaction between **1a** and **2a**, the *anti* diastereomer was identified by a doublet at 4.85 ppm (J = 8.3 Hz), whereas the *syn* diastereomer showed the doublet at 5.41 ppm (J = 2.4 Hz). For kinetics calculations, the ¹H-NMR analyses of the reaction mixtures were performed in the presence of an internal standard as above indicated. In general, given yield values correspond to the average of at least two independent measurements with STDV \pm 2%-4%. Among various kinetic models, the straight lines shown in the kinetics plots correspond to the best fit of the first-order model (*e.g.*, (nitromethane) \geq (aldehyde)).

3.1.5.2. General Procedure for Keratin-Catalyzed Nitroaldol (Henry) Reaction

Keratin (10 mg) was added in one portion to a mixture of aldehyde (0.1 mmol), nitroalkane (1.0 mmol), TBAB (0.1 mmol, if water is the solvent) and solvent (0.5 mL) placed into a 4-mL

screw-capped vial. The resulting reaction mixture was gently shaken in an orbital shaker (150 rpm) for the appropriate time at room temperature. After completion, water (1 mL) was added. The reaction mixture was extracted with EtOAc (4 x 1.5 mL), dried over anhydrous sodium sulfate, filtrated and evaporated under reduced pressure. The yield was determined by $^1\text{H-NMR}$ of the crude product in CDCl_3 using dimethyl acetamide (9.2 μL , 0.1 mmol) as an internal standard. All β -nitroalcohol products are known and the spectroscopic data obtained from NMR analysis of the reaction mixtures were in agreement with those reported in the literature.¹⁸⁻²²

3.1.5.3. Typical Recycling Procedure

After reaction and extraction with EtOAc, the aqueous phase with the remaining catalyst was freeze-dried prior addition of the reaction substrates and solvent for the next run.

3.1.5.4. Kinetic Studies

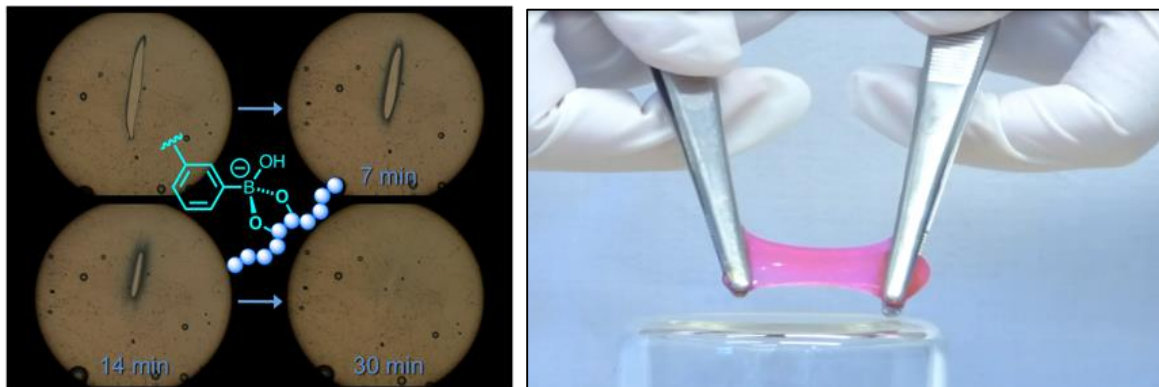
Reaction conversions were unequivocally calculated by $^1\text{H-NMR}$ analysis for the reaction mixtures according to the integration of characteristic signals of the species in the reaction mixture in the presence of a suitable internal standard. Each experiment point represents the average of at least two experiments. Among various kinetic models, lines presented in the kinetic plots show best-fits of the first-order model for each case (*i.e.*, $(\text{NO}_2\text{R}) \geq (\text{aldehyde})$). Due to the fact that not all reactions reached 100% yield, data fitting was made according to the variation of $\ln((C_t - C_\infty)/(C_\infty - C_0))$ with time, where C_t is the concentration at a given time t ; C_∞ the final concentration (at infinite time) and C_0 the initial concentration (at $t = \text{zero time}$). For reaction conversions close to 100%, plots of $\ln(C_t/C_0)$ versus time provided consistent results ($C_\infty = 0$). Under these considerations, minor differences were observed between the exponential and linear fits. All errors reported for the rate constants k were calculated by graphical analysis. Kinetics data for other biopolymers have been previously reported by us and were used for comparison: calcium alginate aerogel,¹⁸ freeze-dried silk fibroin,¹⁹ gelatin,²⁰ collagen,²⁰ BSA,^{20,24} and chitosan.²¹ Sample preparation and details of the reactions can be found in the corresponding references.

3.1.6. References

- [1] R. Höfer, J. Bigorra, *Green Chem.* **2007**, 9, 203-212.
- [2] M. Elnashar (ed.), *Biopolymers*, InTech, **2010**.
- [3] C. Tonin, A. Aluigi, M. Zoccola, *J. Mol. Struct.* **2009**, 938, 35-40.
- [4] P. Sierpinski, J. Garrett, J. Ma, P. Apel, D. Klorig, T. Smith, L.A. Koman, A. Atala, M. Van Dyke, *Biomaterials* **2008**, 29, 118-128.
- [5] J. M. Saul, M. D. Ellenburg, R. C. de Guzman, M. van Dyke, *J. Biomed. Mater. Res. A* **2011**, 98A, 544-553.
- [6] M. Hengchang, B. Zhikang, H. Guobin, Y. Ningning, X. Yufei, Y. Zengming, C. Wei, M. Yuan, *Chin. J. Catal.* **2013**, 52, 578-584
- [7] R. Karthikeyan, S. Balaji, P. K. Sehgal, *J. Sci. Ind. Res.* **2007**, 52, 710-715.
- [8] S. J. McNeil, M. R. Sunderland, S. J. Leighs, *Appl. Catal., A*, **2017**, doi:10.1016/j.apcata.2017.04.021.
- [8] J. G. Rouse, M. E. van Dyke, *Materials* **2010**, 3, 999-1014.
- [9] T. Kornilowics-Kowalska, J. Bohacz, *Waste Manag.* **2011**, 31, 1689-1701
- [10] C. H. Lee, M. S. Kim, B. M. Chung, D. J. Leahy, *Nat. Struct. Mol. Biol.* **2012**, 19, 707-715
- [11] X. M. Zhou, W. W. Idler, A. C. Steven, D. R. Roop, P. M. Steinert, *J. Biol. Chem.* **1988**, 263, 15584-15589.
- [12] J. O'Donnell, *Aust. J. Bioi. Sci.* **1973**, 26, 415-437.
- [13] K. M. Arai, R. Takahashi, Y. Yokote, K. Akahane, *Eur. J. Biochem.* **1983**, 132, 501-507.
- [14] P. M. Steinert, R. H. Rice, D. R. Roop, B. L. Trus, A. C. Steven, *Nature* **1983**, 302, 794-800.
- [15] F. A. Luzzio, *Tetrahedron* **2001**, 57, 915-945.
- [16] R. Ballini, S. Gabrielli, A. Palmieri, M. Petrini, *Curr. Org. Chem.* **2011**, 15, 1482-1506.
- [17] *Industrial Biocatalysis*, page 506, by Peter Grunwald, CRC Press, Taylor & Francis Group, LLC, **2015**
- [18] D. Kühbeck, J. Mayr, M. Häring, M. Hofmann, F. Quignard, D. D. Díaz, *New J. Chem.*, **2015**, 39, 2306-2315.
- [19] D. Kühbeck, M. Gosh, S. S. Gupta, D. D. Díaz, *ACS Sustain. Chem. Eng.* **2014**, 2, 1510-1517.
- [20] D. Kühbeck, B. B. Dhar, E.-M. Schön, C. Cativiela, V. Gotor-Fernández, D. D. Díaz, *Beilstein J. Org. Chem.* **2013**, 9, 1111-1118.

- [21] D. Kühbeck, G. Saidulu, K. R. Reddy, D. D. Díaz, *Green Chem.* **2012**, *14*, 378-392.
- [22] a) P. Li, Y. Liu, L. Wang, M. Tao, W. Zhang, *J. Appl. Polym. Sci.* **2018**, *135*, 45992; b) S. S. Ganesan, A. Ganesan, J. Kothandapani, *Synlett* **2014**, *25*, 1847-1850.
- [23] K. Akutu, H. Kabashima, T. Seki, H. Hattori, *Appl. Catal. A* **2003**, *247*, 65-74.
- [24] E. Busto, V. Gotor-Fernández, V. Gotor, *Org. Process Res. Dev.* **2011**, *15*, 236-240.

3.2. Alginate-Phenylboronic Acid Based Hydrogels



This chapter has been published in:

A. Pettignano, S. Grijalvo, M. Häring, R. Eritja, N. Tanchoux, F. Quignard, D. D. Díaz, '*Boronic acid-modified alginate enables direct formation of injectable, self-healing and multistimuli-responsive hydrogel*', *Chem. Commun.* **2017**, 53, 3350-3353. – Reproduced with permission of The Royal Society of Chemistry.

K. Suresh, M. Häring, G. Kumaraswamy, D. Díaz, '*Self-healing alginate gels that do not fail on stretching to 16000%*'. – submitted.

Author contribution:

AP did the self-healing experiments with **3-75**. SG did the biocompatibility tests, MH worked on the self-healing and drug release experiments with **7-35** and worked together with KS on the stretching experiments. All authors contributed to the scientific discussion of the results.

3.2.1. Abstract

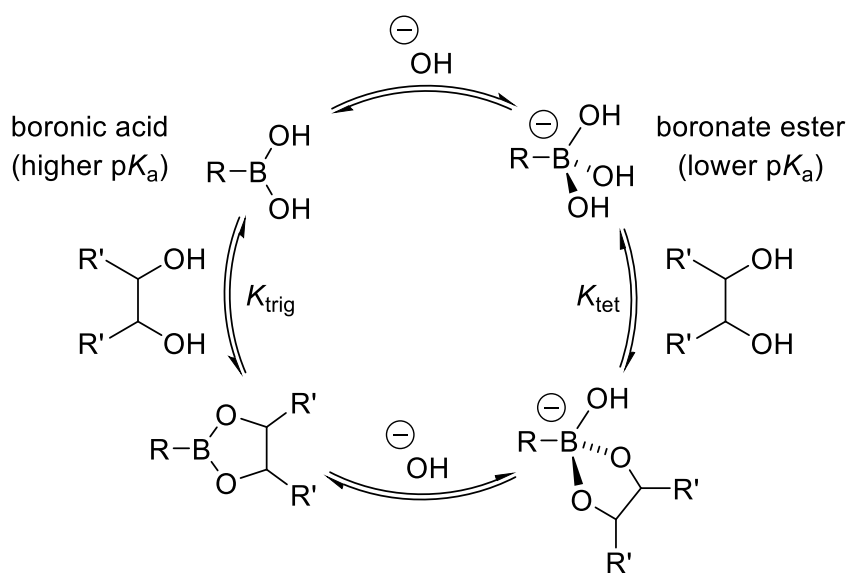
One-step functionalization of alginate with boronic acid groups allowed spontaneous formation of biocompatible hydrogels under basic conditions without additional complementary molecules or crosslinking agents. The dynamics of boronate ester bond formation can be tuned by changing the content of phenylboronic acid-modified alginate (Alg-PBA) and the added amount of NaOH. Two different hydrogel formulations, the **3-75** (*i.e.* 3% w/v Alg-PBA + 75 μ L NaOH per mL Alg-PBA solution) and the **7-35** (*i.e.* 7% Alg-PBA + 35 μ L NaOH per mL Alg-PBA solution) were chosen to be further investigated and compared regarding their gel properties, self-healing and stretching behavior. Both formulations show a multi-stimuli behavior toward changes in pH or in the presence of a sugar like fructose. Although both hydrogels display self-healing properties, the **7-35** is superior to the kinetics of self-healing. In addition, the **7-35** hydrogel exhibits an extraordinary stretchability without breaking, even when exceeded over 16000% whereas the **3-75** hydrogel fails at relatively low stretch ratios. All hydrogels are biocompatible and injectable and can be used for drug delivery which was tested with an antibiotic, oxytetracycline (OXT), as a model drug. It was demonstrated that Alg-PBA hydrogels release their cargo in different kinetics depending on the pH of the medium which can be used for controlled drug delivery.

3.2.2. Introduction

During the last years, studies to optimize the properties and applicability of hydrogels have increasingly become the focal point of soft material scientists. Specifically, hydrogels that simultaneously possess self-healing ability and stretchability have attracted great interest due to promising applications in areas ranging from packaging to surface engineering, energy harvesting and stretchable electronics. A number of different strategies have been developed to obtain hydrogels with good mechanical stretchability (Table S1).

One strategy to obtain hydrogels with superior properties is the introduction of dynamic bonds,¹ e.g. with boronic acids which have been extensively studied due to their excellent ability to form reversibly boronate esters with diols. The most common interaction occurs with 1,2- and 1,3-diols, forming five and six membered rings, respectively, with a binding affinity following the order *cis*-1,2-diol > 1,3-diol >> *trans*-1,2-diol.² The formation and dissociation of the boronic ester derivatives can occur both in aqueous and organic media and depend significantly on pH, as well as on the pK_a of the boronic acid-diol pair. Previous studies have demonstrated that the reaction kinetics are fastest in aqueous basic media, where boron is present in its anionic form. The tetrahedral boronate anion, in fact, presents a higher reactivity than its neutral trigonal form with differences in the rate of 10^4 .³ Nevertheless, even if significantly slower, the reactivity of the neutral boronic acids with diols should not be ignored and the overall equilibria can be illustrated as a cycle (Scheme 1).

Scheme 1. Equilibria involved in the pH-dependent boronate ester formation.



More in detail, K_{tet} describes the diol-boronate anion complex and K_{trig} the diol-boronic acid complex formation, with $K_{\text{tet}} > K_{\text{trig}}$. Taking this into account, the binding affinity of boronic acid with diols is highly dependent on the pH of the medium, with pH values above the pK_a of the boronic acid, favoring the formation of boronate ester. Conversely, the diol-boronic acid interaction is not favored near the physiological pH and is completely cleaved under highly acidic conditions.⁴

This high reactivity between boronic acids and diols has led to intensive studies of boronic acid-containing polymers as therapeutic agents, self-regulated drug delivery systems, nucleotide adsorbents, and sensors for a number of biologically important species, including saccharides, glycoproteins and neurotransmitters such as dopamine.⁵ Moreover, the use of boronic acid-based polymers for biomedical applications is not only possible but largely encouraged by the lack of apparent toxicity or *in vivo* instability issues of these compounds.⁶ Furthermore, the dynamic nature of the boronate ester bonds has enabled the development of different self-healing systems, mainly based on the interaction between synthetic polymers bearing pending diols and boronic acid groups.⁷

Hydrogels based on natural occurring polymers have several advantages since such polymers are biocompatible, non-toxic, inexpensive, and easy to obtain from renewable resources. Within this context, one of the most famous natural polymers used in materials synthesis is alginate, an anionic polysaccharide typically obtained from the cell walls of brown algae, which has already been widely applied in a broad range of biomedical applications.⁸ Alginate is a linear, unbranched copolymer with homopolymeric blocks of (1-4)-linked β -D-mannuronate and α -L-guluronate residues, covalently linked together in different sequences. Alginate can easily form strong hydrogels upon metal exchange of its monovalent metal with divalent or multivalent cations, especially Ca^{2+} , which builds a so-called “egg-box” model where each calcium atom is coordinated to the carboxylates and hydroxyl groups of four guluronate monomers from two adjacent chains of the polymer (Figure 1).⁹

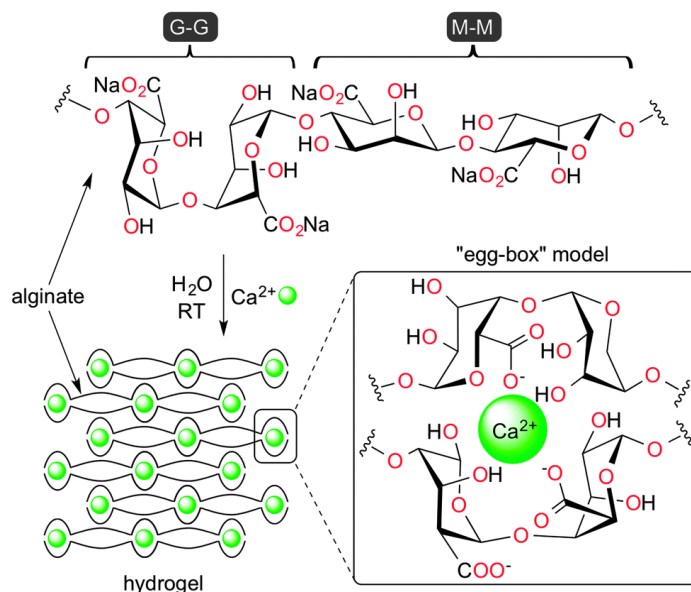


Figure 1. Structure of the repeating units of sodium alginate and formation of the hydrogel by coordination of Ca^{2+} cations between adjacent alginate chains as per the "egg-box" model. Reproduced of ref. 10 with permission of The Royal Society of Chemistry.

Phenylboronic acid-modified alginate polymers have been already reported in the literature.¹¹⁻¹⁴ In all cases, they have been used in combination with other diol-containing polymers, e.g. dopamine-grafted alginate,¹¹ poly(vinyl alcohol) (PVA),^{12,13} or hyaluronate.¹⁴ Due to the dynamic nature of the PBA-diol ester bond, the obtained materials display self-healing properties^{11,13} and/or a shape memory,¹¹⁻¹³ response to pH and diols (such as glucose or fructose).¹² Due to their properties and lack of toxicity, they are promising candidates for biomedical applications.¹⁴

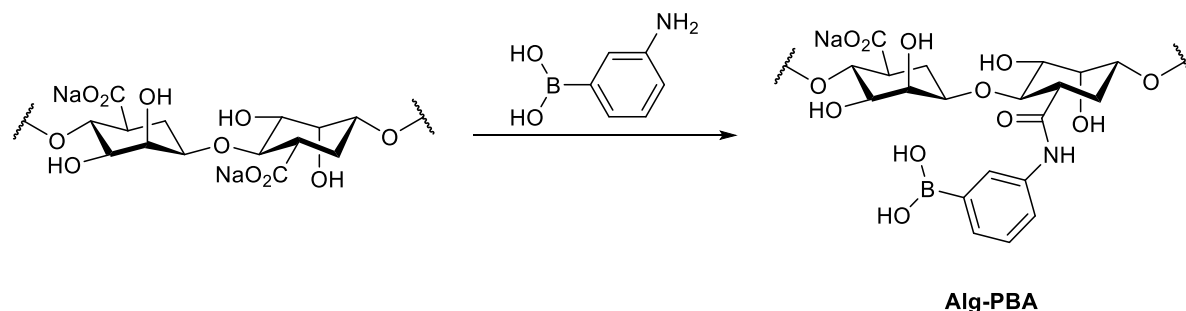
The boronic acid-modification could be a powerful tool to obtain hydrogels with advanced properties with promising applications in a wide range of different fields.

3.2.3. Results and Discussion

3.2.3.1. Synthesis of Alginate-Phenylboronic Acid (Alg-PBA)

Alginate was modified with 3-aminophenylboronic acid by one-step functionalization. Therefore, the carboxylic acid sodium salt of alginate was activated with 1-(3-dimethylaminopropyl)-2-ethylcarbodiimide hydrochloride (EDC) to build an amide bond between alginate and the phenylboronic acid derivative. The reaction was followed as described in the literature with slight modifications (Scheme 2).¹³

Scheme 2. Overview of the synthesis of Alg-PBA.



The successful modification was confirmed by ^1H NMR, showing the typical phenyl group signals around 7.5 ppm. The alginate degree of substitution (DS), *i.e.* the molar ratio of phenylboronic acid unit to the carboxylate groups of alginate, was calculated from the ratio between the integration values of the phenylboronic acid unit those from alginate and taking into account the number of hydrogens responsible for the integrated area (*i.e.* 5H alginate integrated around DHO peak and 4H for the phenyl group). Although the complex interpretation of the polysaccharide signals in these conditions impedes an exact determination of the DS, the calculated value (25%) is in very good agreement with the previously reported one.⁹ Moreover, ^1H NMR analysis of the material through a pH gradient (*i.e.* acidic, neutral and basic pH) showed a gradual chemical shift of signals in the 7-8 ppm region, which is consistent with the boronate ester formation at basic pH (Figure S1). The modified biopolymer, Alg-PBA, was further characterized by FTIR showing the expected small band at 1450 cm^{-1} associated to the C-B vibration (Figure 2). A slight broadening of the alginate signals at ~ 1410 and $\sim 1300\text{ cm}^{-1}$ (corresponding, respectively, to the O-C-O symmetric vibration and C-C-H and O-C-H deformation of the pyranose rings)¹⁵ can also be noticed and associated to the B-O vibrations, which normally are present around 1350 and 1300 cm^{-1} .¹⁶

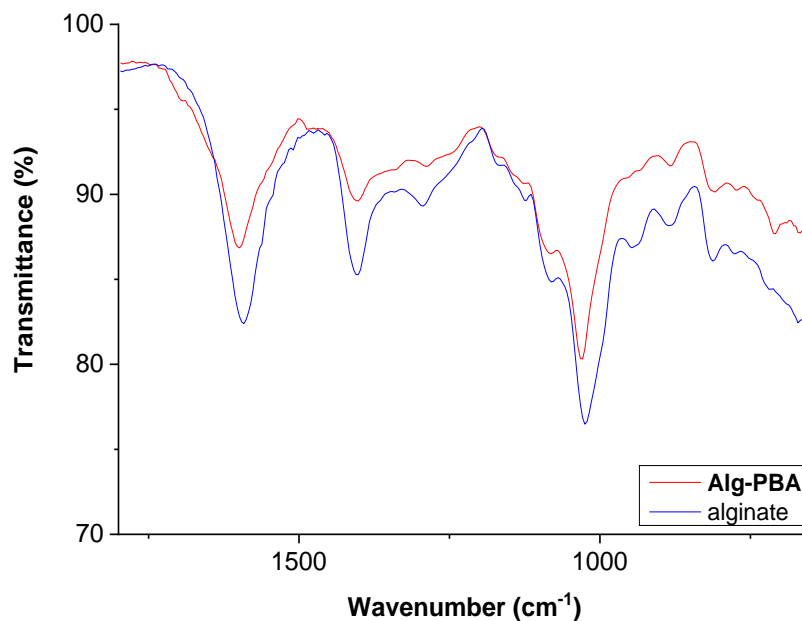


Figure 2. FT-IR of Alg-PBA (red) and unmodified alginate (blue). The complete spectrum can be found in the ESI. Determination of the pK_a of the conjugate and native alginate was carried out by acid-base titration at constant ionic strength.¹⁷ As expected, acid-base titration of both Alg-PBA and native alginate revealed the presence of carboxylic groups with a pK_a of ~ 3.3 (as observed in native alginate) as well as a more basic group with a pK_a of ~ 9.5 ascribed to the boronic acid moiety (Figure 3).

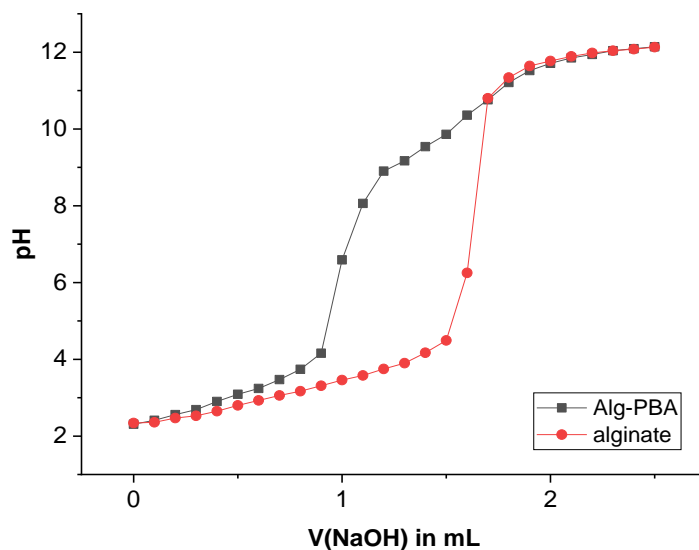


Figure 3. Determination of the pK_a of Alg-PBA (black) in comparison to unmodified alginate (red) by acid-base titration.

3.2.3.2. Preparation of Alg-PBA Hydrogels

As hypothesized, in a basic environment the boronic acid pending groups of Alg-PBA could reasonably interact with the vicinal diols present on alginate pyranose rings, leading to the formation of cross-linked alginate bearing reversible boronic ester linkages (note that the involvement of hydroxyl groups from different alginate chains in the complexation of boronic units, at least to some extent, should also be considered). Under this scenario, the straightforward synthesis of metal-free alginate hydrogels could be achieved without the need for any external diol source and/or divalent cations to ionically crosslink the alginate through the well-known egg-model.^{7e} The addition of 1 M NaOH to Alg-PBA aqueous solutions in 0.1 M PBS led to immediate gelation (Figure 4).

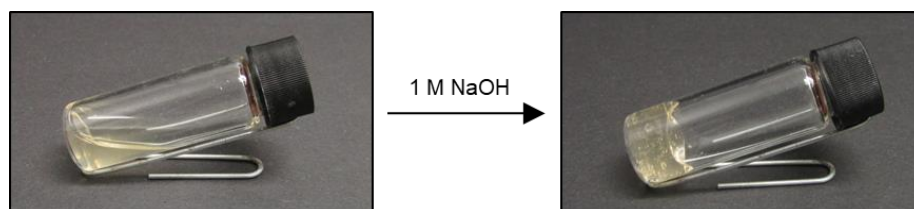


Figure 4. Gelation of **Alg-PBA** solution upon crosslinking by increasing the pH.

Stable hydrogels could be prepared at different Alg-PBA concentrations and varying amounts of 1 M NaOH per mL Alg-PBA solution (Table 1). Two different hydrogel formulations, the **3-75** (*i.e.* 3% w/v Alg-PBA + 75 μ L NaOH per mL Alg-PBA solution) and the **7-35** (*i.e.* 7% Alg-PBA + 35 μ L NaOH per mL Alg-PBA solution) were chosen to be further investigated and compared regarding their properties which will be discussed in the next chapters.

Table 1. Hydrogel screening by varying the Alg-PBA concentration and the added amount of NaOH.^a

Alg-PBA (% w/v)	Addition of 1 M NaOH per mL Alg-PBA solution (μ L)				
	15	25	35	50	75
3	L	G	G	G	G
5	L	G	G	G	G
7	L	G	G	G	G
10	n.t.	n.t.	G	G	n.t.

^a First, Alg-PBA solutions were prepared then the corresponding amount of 1 M NaOH was added. Mixtures were left overnight for equilibration before characterization. Used abbreviations: G = gel, L = liquid, n.t. = not tested.

It is worth mentioning that the hydrogel can be lyophilized (freeze-drying), giving a free-flowing powder, which can be subsequently used to reform the hydrogel upon simple addition of water (*i.e.*, an equivalent amount to that removed). This allows convenient storage of the gel precursor formulation for long periods of time while not in use.

3.2.3.3. Characterization of Hydrogels

Oscillatory rheological experiments were performed in order to confirm the viscoelastic gel state and to examine the qualitative difference between the **3-75** and **7-35** gels. First, the storage modulus G' and the loss modulus G'' were measured as a function of shear strain (dynamic strain sweep experiments, DSS) and angular frequency ω (dynamic frequency sweep experiments, DFS) to determine the linear viscoelastic regime (Figure 5).

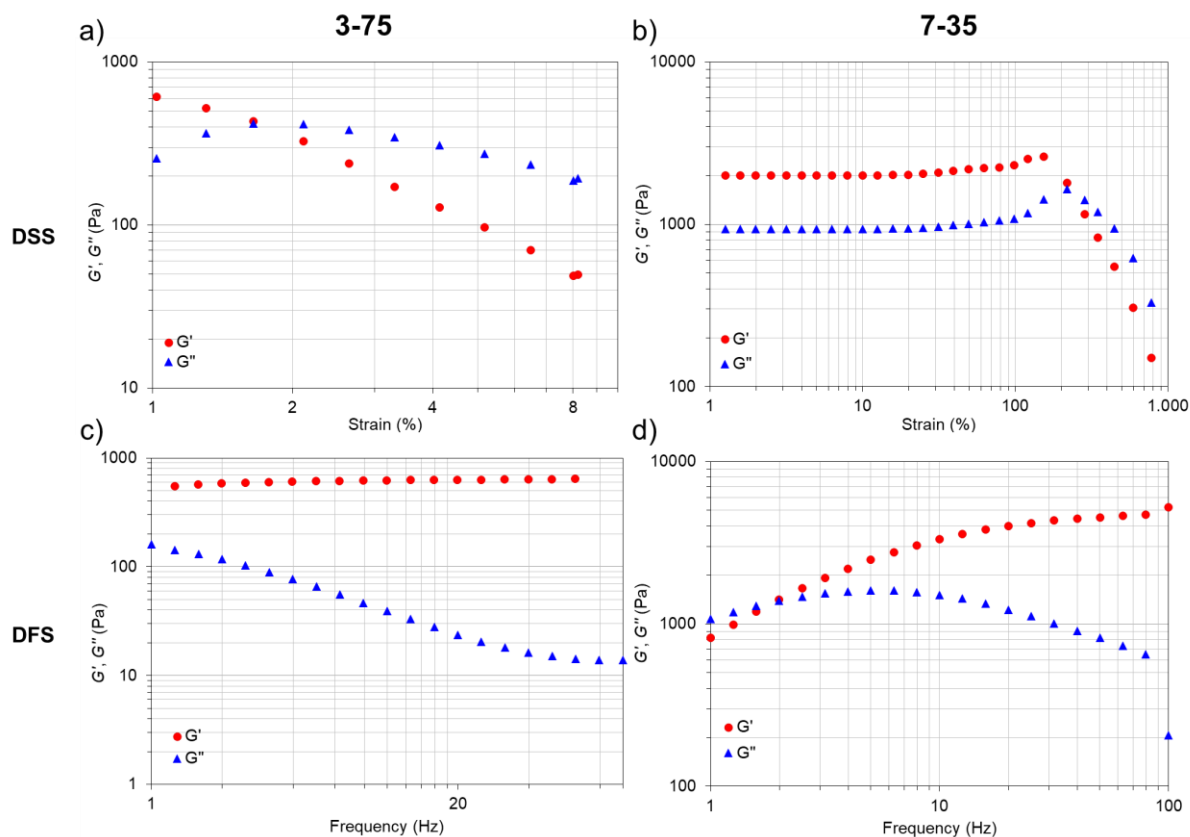


Figure 5. Oscillatory rheological measurements: DSS of a) **3-75** at 1 Hz and b) **7-35** at 10 Hz; DFS of c) **3-75** at 0.05% strain and d) **7-35** at 5% strain.

Within the linearity limits of deformation, G' of **3-75** (about 630 Pa) was one order of magnitude higher than the loss modulus G'' (about 40 Pa). At quite low strain values (*i.e.* 1.8%) the gel turns into a liquid with a cross-over modulus at 300 Pa (Figure 5a). In comparison, G' of **7-35** (about 4000 Pa) was only twice as G'' (about 2000 Pa). The cross-over of G' and G'' was observed at higher strain values (*i.e.* 110%) with a cross over modulus of 3500 Pa (Figure 5b). The dynamic frequency sweep experiments were measured at 0.05% and 5% strain for **3-75** and **7-35**, respectively. When the frequency was increased, the storage modulus of **3-75** was constant over the entire range of frequencies (Figure 5c). Interestingly, with **7-35**, G'' is higher

than G' at small frequency values. A cross-over could be observed at about 2 Hz and G' increases with increasing frequency whereas G'' decreases (Figure 5d).

In order to gain a visual insight into the morphology of the two hydrogel formulations, **3-75** and **7-35**, scanning electron microscopy (SEM) was conducted of the corresponding xerogels prepared by freeze-drying of the as-prepared hydrogels (Figure 6). A dense globular like structure composed of particles around 0.5 μm in diameter was characteristic for the xerogel of **3-75** (Figure 6a and 6b). In comparison, the microstructure of the corresponding xerogel of **7-35** displays a microporous structure with pore diameters of several microns (Figure 6c and 6d).

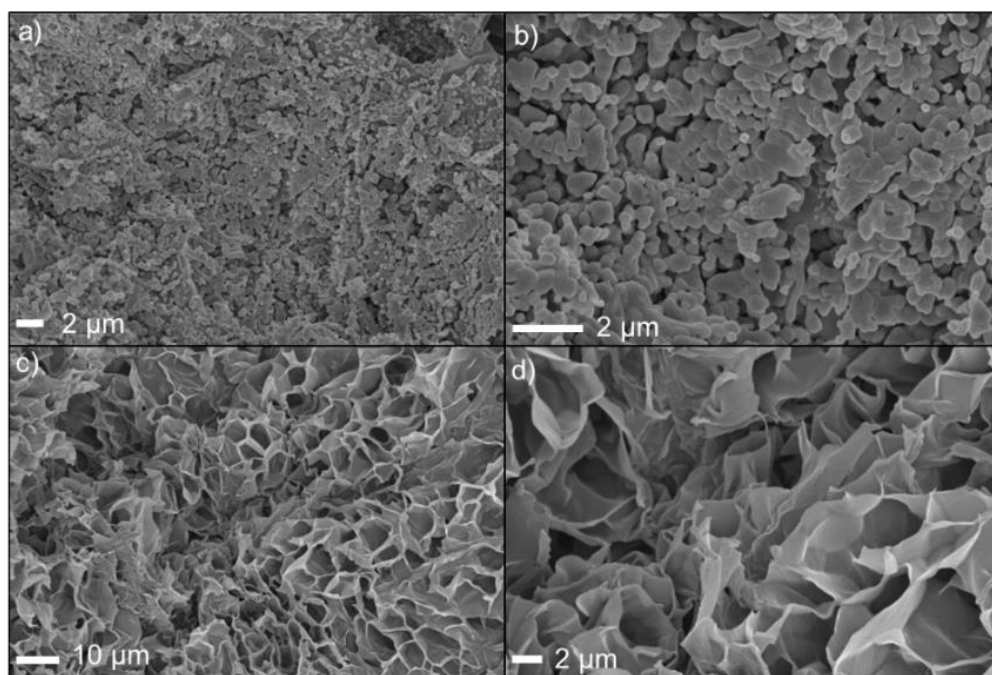


Figure 6. SEM images of the xerogels of a)-b) **3-75** and c)-d) **7-35**.

The response of Alg-PBA hydrogels to various stimuli was also studied. After obtaining the hydrogels under basic conditions, the medium pH was lowered by adding 200 μL of acetate buffer (pH 5). This led to the collapse of the gel due to the dissociation of the pH dependent boronate bonds between the polymeric chains. After raising the pH again by adding 100 μL of 1 M NaOH (pH 10), the stable gel was reformed (Figure 7a). The complexation of boronic units with hydroxyl groups of alginate (about 5% of the available hydroxyl groups) has been previously investigated.¹⁸ Moreover, the stability of the gel network could also be controlled upon addition of competitive saccharide molecules at basic pH. For this experiment, fructose was chosen due to its elevated binding affinity towards boronic acids.¹⁹ 200 μL of a 10 mM fructose solution was added to the gel. After a few minutes, the gel started to flow and shortly

turned into a free-flowing liquid due to the strong interactions between the monosaccharide and the boronic acid crosslinker moieties, leading to the progressive disintegration of the gel network (Figure 7b).

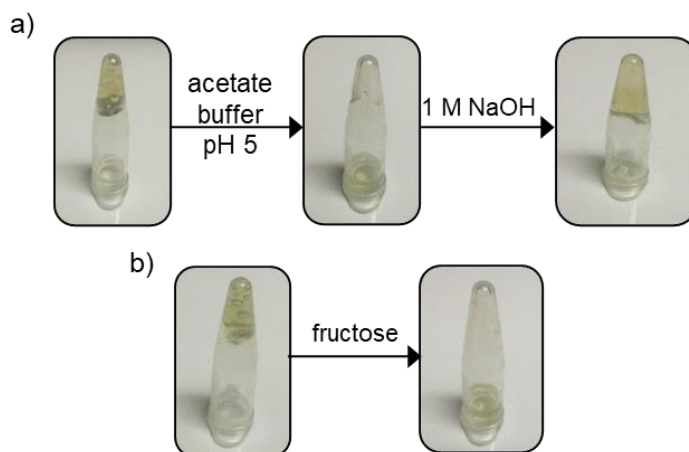


Figure 7. Stimuli-responsiveness of **3-75** hydrogels, a) response to pH, b) response to fructose. Stimuli-responsiveness of **7-35** can be found in the ESI.

It is worth mentioning, that this multi-stimuli behavior could be observed with **3-75** as well as with **7-35** with no visible difference.

3.2.3.4. Self-healing Behavior

Interestingly, hydrogels prepared with different Alg-PBA concentrations and varying amounts of NaOH (e.g. **3-75** or **7-35**) display different properties, revealing a delicate balance between elasticity and stretchability, accompanied with gel stability and self-healing properties, respectively. The self-healing behavior of the hydrogel **3-75** and **7-35** were investigated and compared. Interestingly, both formulations lead to hydrogels with self-healing properties but with different healing times. A bulk gel of either **3-75** or **7-35** was cut into two pieces and placed back in contact with each other. The interfaces between the different pieces visually disappeared during the healing process. The healing time for **3-75** was 10 min, whereas the **7-35** gel was completely self-healed within one minute (Figure 8).

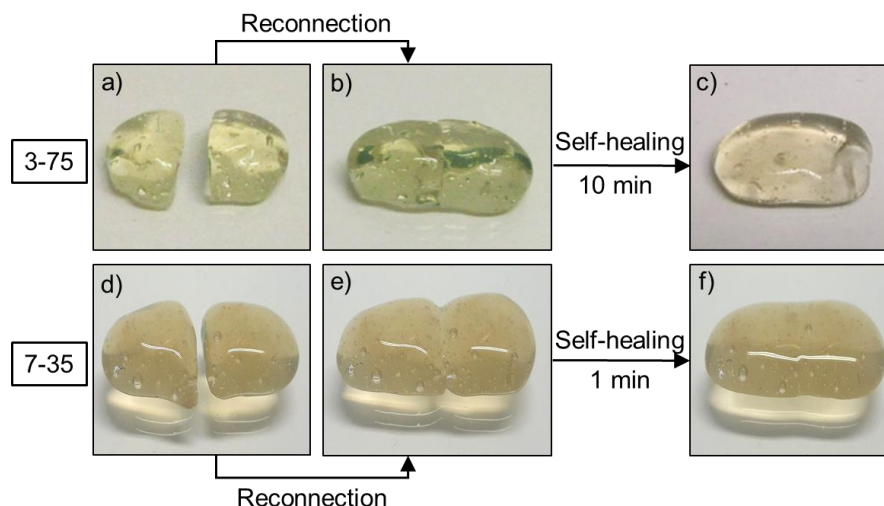


Figure 8. Self-healing behavior of bulk Alg-PBA hydrogels of different formulations, a)-c) **3-75** and d)-f) **7-35**.

For a better visualization of the self-healing properties and to demonstrate the efficient fusion of non-complementary interfaces (*i.e.* two gel bodies prepared independently) hydrogel pieces of dyed and non-dyed bulk gels were alternately connected (Figure 9). For both hydrogel formulations (*i.e.* **3-75** and **7-35**) the free diffusion of the dye through the gel interfaces could be observed.

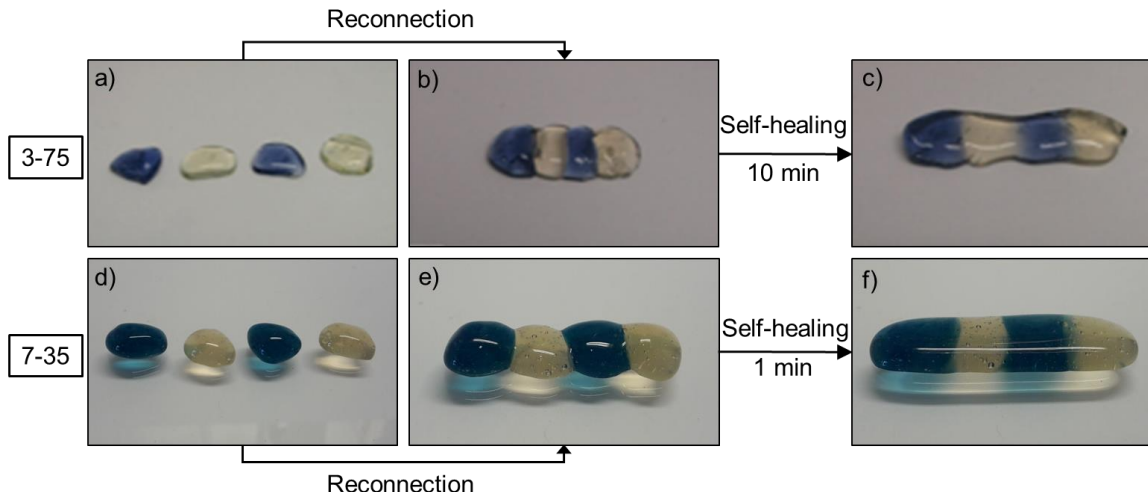


Figure 9. Self-healing process of dyed and non-dyed pieces of Alg-PBA hydrogels made of a)-c) **3-75** and d) - f) **7-35**. The used dye was Direct Blue 1.

The self-healing ability of the Alg-PBA hydrogels was further examined by punching a 0.5 cm hole in the middle of a gel body of either **3-75** or **7-35** (Figure 10) which demonstrate that the hydrogels are not only able to self-heal after connecting two pieces through fusion but also to heal themselves without being in contact to the interface of the other side.

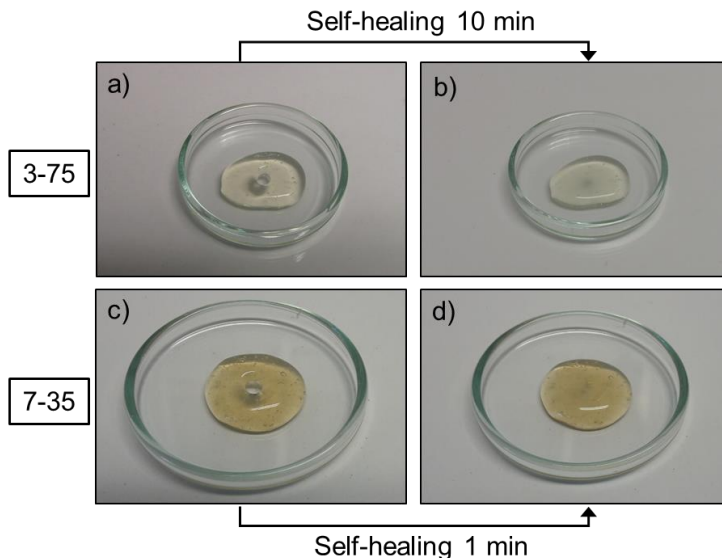


Figure 10. Self-healing behavior after punching a ca. 0.5 cm hole into the Alg-PBA hydrogel made of a)-b) **3-75** and c)-d) **7-35**.

In both cases, the hole underwent a gradual instant reduction in size until its complete disappearance. As in the previous observations, the hydrogel **3-75** needed ~ 10 min until complete self-healing, whereas the **7-35** healed itself within one minute.

For a better insight, the progressive self-healing of a scratch made on an Alg-PBA gel film was monitored by optical microscopy. After cutting **3-75**, the scratch displays a clear decrease of its size after 7 min and a totally repaired surface within 30 min (Figure 11). Remarkably, the self-healing ability of **7-35** after scratching it, could not be monitored due to extremely fast self-healing, *i.e.* the scratch disappeared immediately after cutting (video available on the ESI).

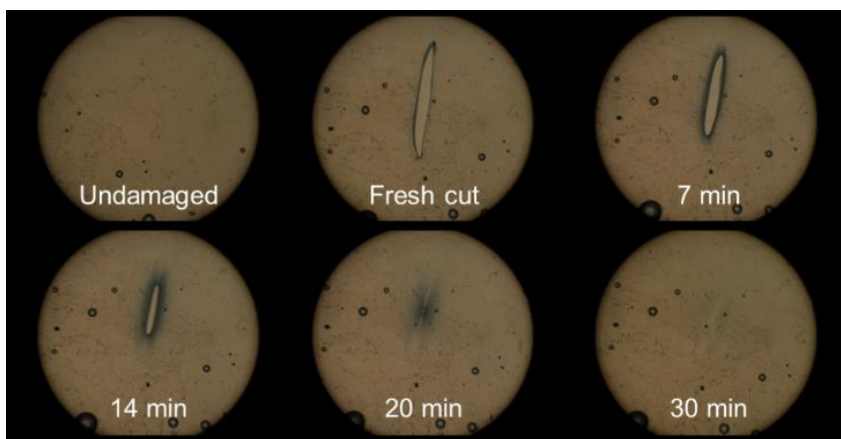


Figure 11. Microscopic images of self-healing process of Alg-PBA hydrogel **3-75**. The process could not be monitored for **7-35** due to its immediate healing.

Besides the observed macroscopic self-healing property of the bulk gels, the thixotropic behavior of **3-75** and **7-35** was also confirmed by a three-step rheological loop test. In the first step, a low shear strain (*i.e.* 5% at 1 Hz for **3-75** and 10 Hz for **7-35**) was applied for 5 min. Here, the sample remained in the gel state, *i.e.* $G' > G''$. Then, in the second step, the shear strain was increased to 500% and maintained for 2 min to ensure the rupture of the gel ($G' < G''$). In the last step, the shear strain was reduced to the initial value for 10 min to stabilize the recovered gel network ($G' > G''$). The loop was repeated three times and revealed the full recovery of the gel strength within a few minutes after each cycle (Figure 12).

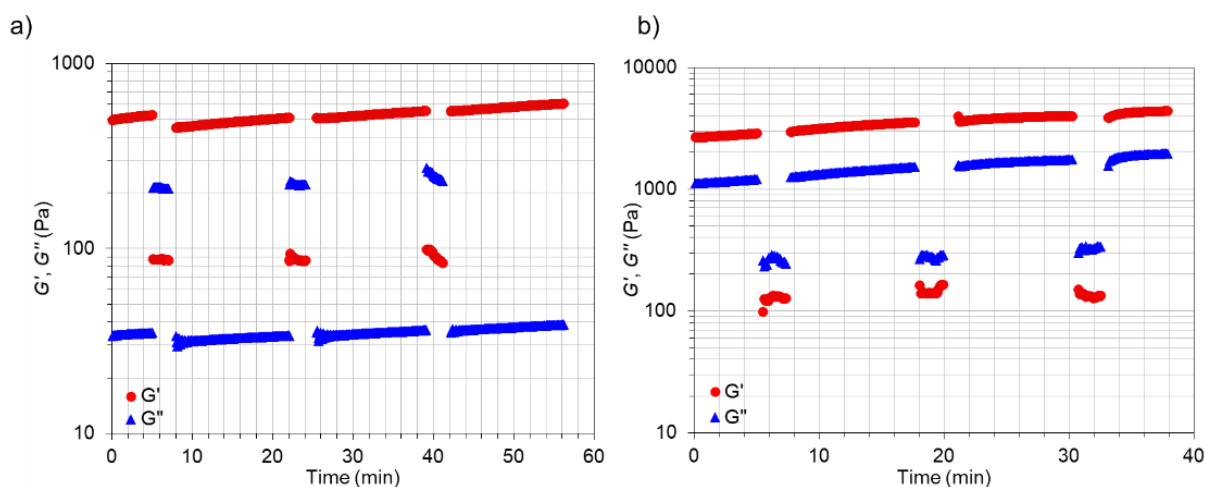


Figure 12. Rheological loop test for a) **3-75** and b) **7-35** hydrogel.

Oscillatory rheological experiments showed the restoration of the mechanical strength and damping properties of the material after the self-healing process (*vide infra*). It is also important to emphasize that the macroscopic self-healing process could be repeated many times without any detriment to the functional properties of the material.

3.2.3.5. Stress-Strain Behavior

The dynamics of the boronate ester bond formation do not only lead to self-healing properties but also, depending on the concentration, to hydrogels with extraordinary stretchability

The mechanical properties of the hydrogel are controlled by both, the polymer content and the NaOH concentration. Thus, varying the polymer content and NaOH concentration afforded control over the stretchability, elastic recoil and moldability of the gels. In general, the decrease of the NaOH concentration renders the gel less stiff, and the gels transform into liquids at acidic pH. For example, **3-75** gives a high modulus gel that rigidly “sets” into shape after about 15 minutes of mixing. When the amount of NaOH is changed from 75 to 35 μL per mL of an Alg-PBA solution, the hydrogel rigidity decreases and bounces elastically when

impinged against a surface. Additionally, these gels do not set as rigidly as **3-75** and can be readily remolded. The hydrogel stiffness is also a strong function of polymer content. Gels are less stiff and deform much more readily depending on the polymer concentration. As an example, the **3-75** gel is sufficiently stiff, therefore, it can be clamped in a rectangular geometry for stretching measurements. In comparison, the **7-35** deforms on the application of small loads, so it cannot be clamped in the same manner. Visual observation of different prepared compositions indicates that the **7-35** gel has optimal mechanical properties, with a balance between stiffness and stretchability. In the following, the stretching properties of two gel compositions, **3-75** and **7-35**, were examined and compared.

The **3-75** and **7-35** gels were stretched in the RSA-III DMA. When the **3-75** gel is stretched, it exhibited uniform elongation with no necking until it fails abruptly (Figure 13). The failure is observed at relatively low stretch ratios λ (see equation 1) by the sudden formation of a crack midway along the sample length, in a direction perpendicular to the stretching direction.

$$\text{stretch ratio: } \lambda = \frac{l_t}{l_0} \quad (\text{eq. 1})$$

(l_t and l_0 are the sample gauge lengths at time t and 0)

Gels stretched at 0.1 mm s^{-1} fail at $\lambda = 2.4$. When the stretching rate is increased to 1 mm s^{-1} , the gels even fail at lower $\lambda = 1.08$. Since the sample does not exhibit significant necking, the true stress σ_t could be obtained by equation 2:

$$\text{true stress: } \sigma_t = \frac{F}{A_0} \lambda, \quad (\text{eq. 2})$$

(F is the measured normal force, A_0 is the cross-sectional area of the sample at the beginning of the stretching experiment)

$$\text{true strain: } \varepsilon_t = \ln \lambda \quad (\text{eq. 3})^{20}$$

The true stress increases linearly with ε_t for low true strain values. Hence, the Young's modulus of the gel can be obtained from this linear response region (Figure 13, inset). For a stretching rate of 1 mm s^{-1} , the Young's modulus of the **3-75** gel is 60 kPa. σ_t increases monotonically with λ , until $\sigma_t \approx 6 \text{ kPa}$, after which a crack forms and the gel ruptures. For a lower stretching rate (*i.e.* 0.1 mm s^{-1}), the modulus was 12 kPa. After the initial linear increase of σ_t with the strain, the gel yields after which the rate of increase of σ_t decreases. Again, no necking was visible before the gel fails at $\lambda = 2.4$ (Figure 13). A similar stretching rate dependence of gel modulus and failure strain has been previously reported.²¹

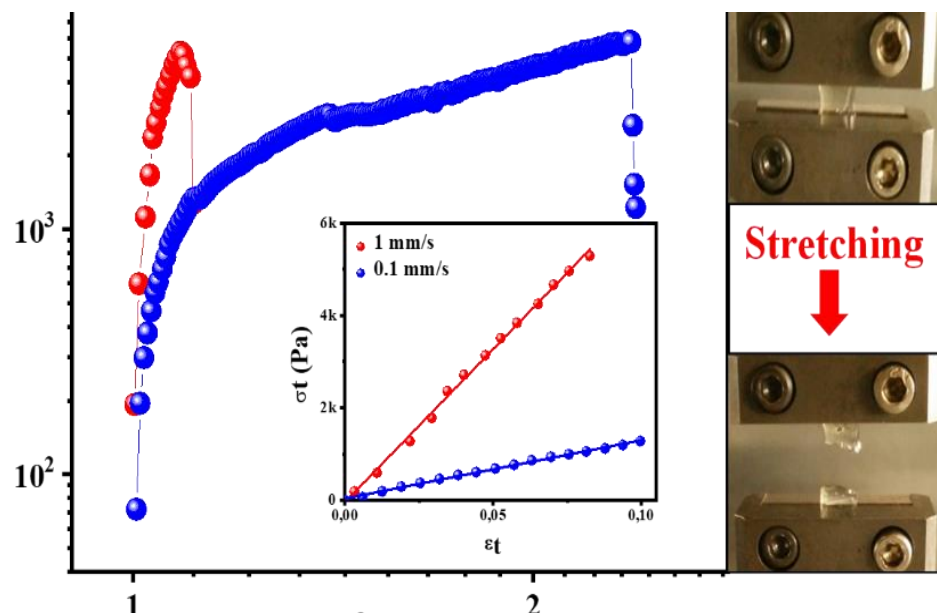


Figure 13. Tensile testing of **3-75** at two different strain rates. Photographs of the sample during tensile testing are shown on the right. Inset: Young's modulus from the linear response region.

In comparison, the **7-35** gel shows remarkable differences in mechanical response. Interestingly, the **7-35** gels exhibited remarkable adhesion to metal, therefore, the prepared samples could be molded in forms of cylinders where the flat ends adhered to the plates of the tensile tester (Figure 14, inset or Figure S7). During the measurements, the gel adhered properly to the plates and, remarkably, did not even fail on stretching to the limit of the device (*i.e.* over 160-fold its original length) (Figure 14).

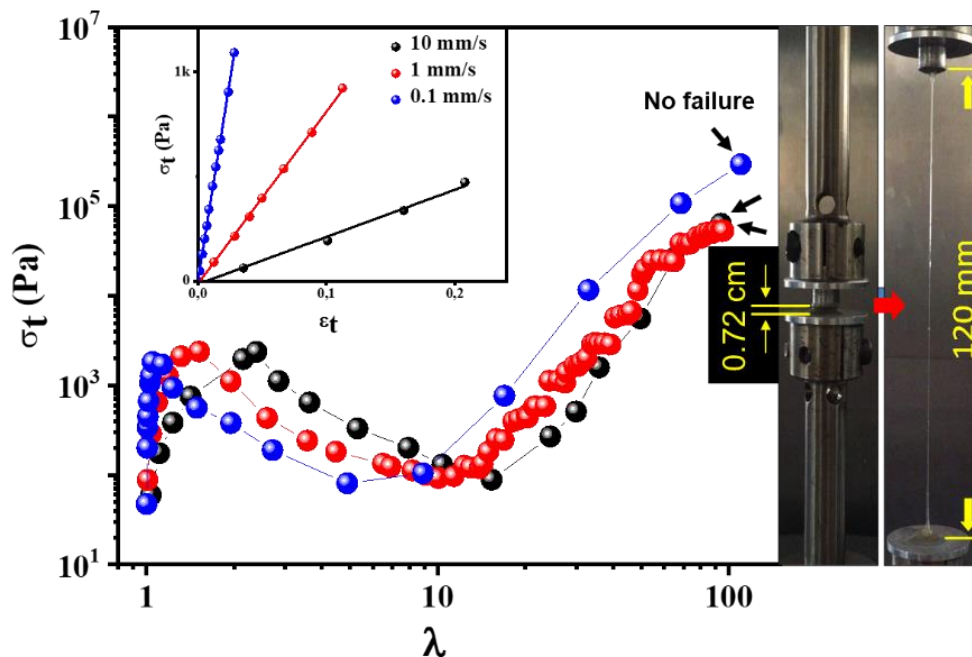


Figure 14. Tensile testing of **7-35** at three different strain rates. Photographs of the sample during tensile testing are shown on the right. The gel did not fail even at this stretch ratio. The initial fixture gap is 0.72 mm and final fixture gap is 120 mm yielding $\lambda \approx 167$. Inset: Young's modulus from the linear response region.

As the **7-35** gel is stretched, it deforms non-uniformly along its length. The true stress was calculated at the midpoint of the sample by dividing the measured normal force by the instantaneous cross-sectional area of the gel strand at its midpoint. The Young's modulus could be obtained from the initial linear regime (Figure 14, inset). In contrast to the **3-75** gel, Young's modulus of the **7-35** gel modulus decreases from 38 kPa to 10 kPa and 2 kPa, by increasing the stretching rate from 0.1 mm s⁻¹ to 1 mm s⁻¹ and 10 mm s⁻¹, respectively. Thus, while visual observation suggests that the **3-75** gel is more rigid than **7-35**, Young's moduli for these gels are strongly stretching rate dependent. The modulus increases with the rate for **3-75** and unusually decreases for **7-35**. Further stretching of **7-35**, lead to an increase of σ_t to about 2 kPa, then the gel starts to neck, forming a thin strand. Subsequently, the stress decreases for all stretching rates. At the point of necking, there is a rapid decrease in the normal force (Figure 15a).

While the cross-sectional area of the sample decreases on the formation of the thin strand, the even more rapid decrease in normal force results in a decrease in σ_t until about 80 Pa after which σ_t increases again. The **7-35** hydrogel shows the same qualitative behavior for all stretching rates. The values of λ where σ_t starts decreasing (λ_{yield}) and then subsequently starts increasing (λ_{draw}), increase with the stretching rate. It was termed $\lambda_{\text{yield}} < \lambda < \lambda_{\text{draw}}$ as the softening regime, and $\lambda > \lambda_{\text{draw}}$ as the hardening regime. At λ_{yield} , the **7-35** gel starts to yield at

a single location at the center of the stretched sample and forms a “neck” which thins with an increase in λ . Drawing the gel above λ_{draw} necessitates an increase in σ_t . For $\lambda > \lambda_{\text{draw}}$, the “neck” continues to thin down as the material is drawn outwards from the initial yield location. This decrease in the cross-sectional area results in an increase in σ_t . Remarkably, over the entire range of stretching rates investigated, there was no failure observable of the **7-35** gel, even for $\lambda = 167$.

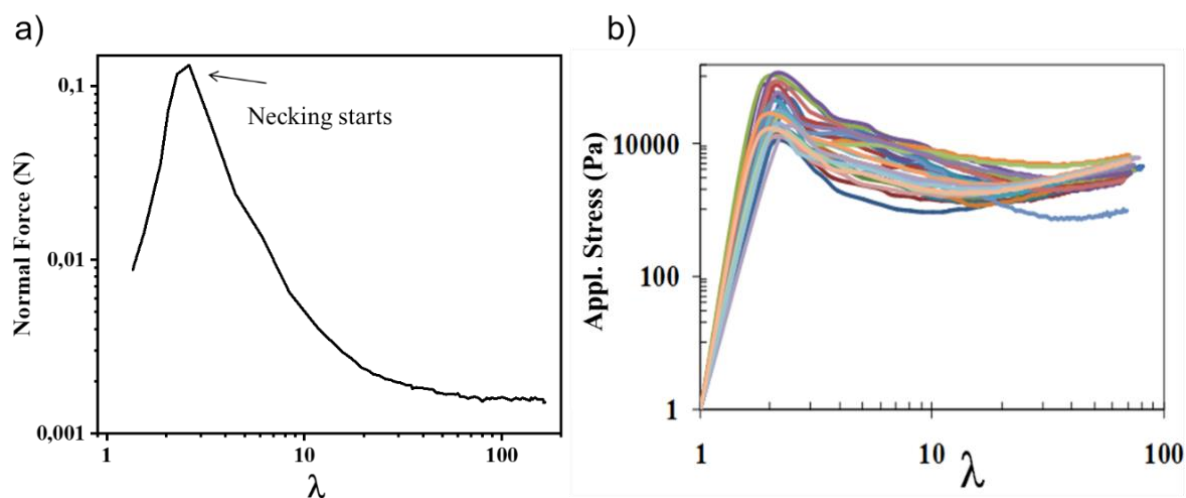


Figure 15. a) Normal force as a function of extension ratio of the **7-35** hydrogel. Normal force decreases rapidly when the sample necking starts; b) Cyclic study on the **7-35** hydrogel. The apparent stress (σ_{app}) was calculated from the engineering stress (σ_{eng}) using the equation $\sigma_{\text{app}} = \sigma_{\text{eng}} (1 + \epsilon_{\text{eng}})$ that assumes volume conservation and uniform deformation along the sample length.²⁰ Note, the engineering stress is calculated as the normal force divided by the original cross-sectional area of the sample before stretching. After the sample is stretched to $\lambda = 100$, it is remolded and stretched again. No systematic change in the data over 30 cycles was observed. All experiments were performed at a strain rate of 5 mm s^{-1} .

Repetitive stretching experiments confirmed that the increase in σ_t is not a consequence of drying of the thin thread as the neck is drawn. These experiments were performed to $\lambda = 100$ on the **7-35** gel at 5 mm s^{-1} . After each stretching cycle, the stretched gel was molded back to the original cylindrical shape and the experiment was repeated on this sample. There was no systematic variation in the stress-strain curve for up to 30 repeated cycles of stretching (Figure 15b), suggesting that there is no drying of the sample during the stretching experiment.

The Considère construction shows a distinct difference between the behavior of **3-75** and **7-35** gels (Figure 13 and 14, respectively), in terms of the number of tangent points for a secant line. The σ_t - λ plot for **3-75** is concave down, with only one tangent point. Stretching at 1 mm s^{-1} results in failure of the gel sample just after the yield point while the gel stretched at 0.1 mm s^{-1} deforms after yield before it finally fails. In contrast to **3-75**, the **7-35** gel shows a sigmoidal

σ_t - λ plot with two tangents. The two tangents in the sigmoidal plot for the **7-35** gel correspond to the softening and hardening regimes.

Small amplitude oscillatory shear rheology was used to investigate the origin of the qualitative difference in the response of **3-75** and **7-35**. As previously described, rheological measurements were performed within the linear viscoelastic (LVE) response of the gels. At low frequencies, the loss modulus G'' exceeds the storage modulus G' which is the case for all gel samples (Figure 5 and Figure S12). Above a cross-over frequency, ω_c , G' becomes larger than G'' . ω_c is a function of both, the polymer and the NaOH concentration. The inverse of ω_c represents the time scale that characterizes the gel relaxation (Table S13a).

Thus, going from **3-75** to **7-35** results in a 60-fold decrease in the gel relaxation time which is consistent with the visual observation of the flowability of the gels.

Overlap of the LVE data from the different gels and fitting to a universal Maxwell form (Figure S13b) indicates qualitative similarities in the small strain response of the gels and, therefore, the equilibrium structure of the gels is governed by association-dissociation equilibrium of the NaOH-mediated boronic ester bonds between the alginate polymers. It is surprising that the large strain behavior of these gels in the stretching experiments are so remarkably different, although their equilibrium structure is similar. It is suggested that the differences in the large strain behavior arise from differences in the dynamic bonding in these gels. By increasing the polymer concentration from 3 wt.% to 7 wt.%, the corresponding concentration of anionic groups, available for bonding, is also increasing. The increased availability of the alginate polymer and decreased NaOH concentration allows for rapid association-dissociation equilibration times, leading to the 60-fold decrease in gel relaxation time. Hence, the **3-75** gel is characterized by a sparse network of long-living bonds, in comparison to a denser network of short-living bonds for the **7-35** gel (Figure 16).

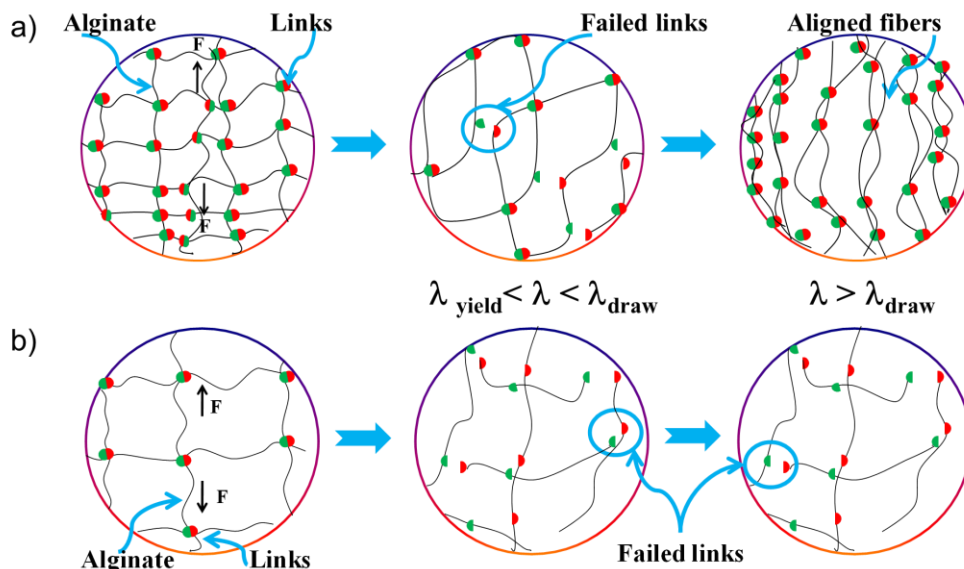


Figure 16. Dynamic association/dissociation kinetics of the boronate ester bonds as a plausible explanation for the mechanical properties for a) stretchability of **7-35** due to fast kinetics and the b) the lack of stretchability of **3-75** due to slow kinetics.

There is a 60-fold increase in the time scale for bond association-dissociation kinetics for **3-75** relative to **7-35**, resulting in the observed qualitative differences in behavior of the **7-35**. When **7-35** is stretched, there is stress-induced bond breakage and rapid re-equilibration of the bonding network due to the rapid dynamics of bond association-dissociation. At slower stretching rates, it is possible that alignment of the alginate chains decreases the kinetic barrier to bonding and results in the formation of a higher concentration of bonds. Thus, a higher modulus for the gel at lower stretch rates was observed. This rapid bond equilibration is due to the higher polymer chain content (resulting in a higher local concentration of available anionic groups) and the lower NaOH concentration (that decreases the propensity to form bonds, decreasing the bond lifetime). Above $\sigma_i \approx 2$ kPa, there is debonding/disentanglement of the network, resulting in the sample yielding. There is considerable chain alignment of the disentangled network and after further stretching it results in rapid formation of bonds between the alginate chains – thus, the sample strain hardens. Therefore, the remarkable mechanical properties of the **7-35** hydrogel arise from optimally tuning the gel composition by adjusting the polymer and NaOH concentration. At this optimal composition, the alginate bond association-dissociation kinetics are optimized such that the gel network can restructure during stretching preventing rupture and allowing the gel to be stretched to over $\lambda = 160$.

3.2.3.6. Biological Studies and Drug Release Experiments

Hydrogels are widely used for biomedical applications.²² A fundamental requirement constitutes the injectability of the hydrogels, which was tested and confirmed by immediate re-gelation after flowing the gel without clogging through a 21-gauge needle (Figure 17a).

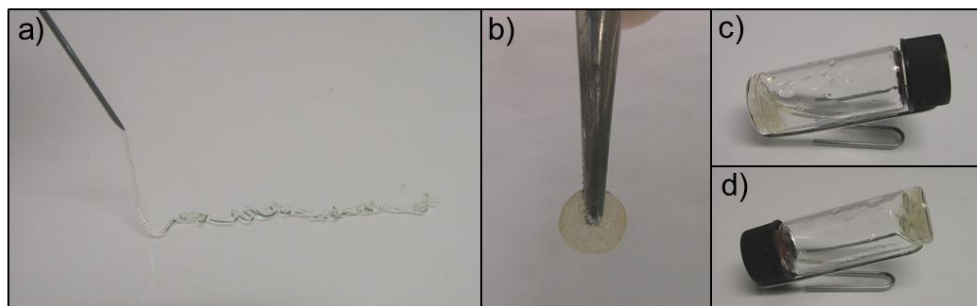


Figure 17. a) Injectability property of **3-75**, b) reshape of the extruded hydrogel into a disc, c) and d) reformation of the hydrogel upon injection into a vial containing buffer solution (pH 7.4).

As expected from the previous experiments, the extruded gel could also be remolded into any desired shape by gently pressing it for less than 5 min (Figure 17b). When the injection of the gel was performed into 1 mL of pH 7.4 buffer, the gel successfully reformed at the bottom of the vial and remained stable upon inversion of the vial (Figure 17c-d).

Furthermore, in order to assess the potential of the injectable Alg-PBA hydrogel for biomedical applications, the cellular viability and cell release properties were explored (Figure 18).²³ For this purpose, the 3D encapsulation of HeLa cells was carried out during the gelation. The results from MTT assays showed excellent biocompatibilities with cell viabilities greater than 90% until 72 h incubation when compared to non-encapsulated cells (positive control). No significant differences were observed between 24 and 72 h incubation time. These results also confirmed the ability of HeLa cells to proliferate after being released through the alginate network. Gradual degradation of the hydrogel during incubation at 37 °C (pH 7) allowed cells to be released through the polymeric network without affecting their morphology (Figure 18b-d) After successful cell encapsulation, injection studies of cell-encapsulated hydrogels were carried out through a needle and the subsequent cell release of the restored hydrogel were evaluated.²⁴ *In vitro* MTT studies showed that a significant proportion of cells were able to bear the large stress generated by the injection and self-healing processes (*i.e.*, 63% cell viability), indicating preservation of the biocompatible character of the hydrogel (Figure 19d).

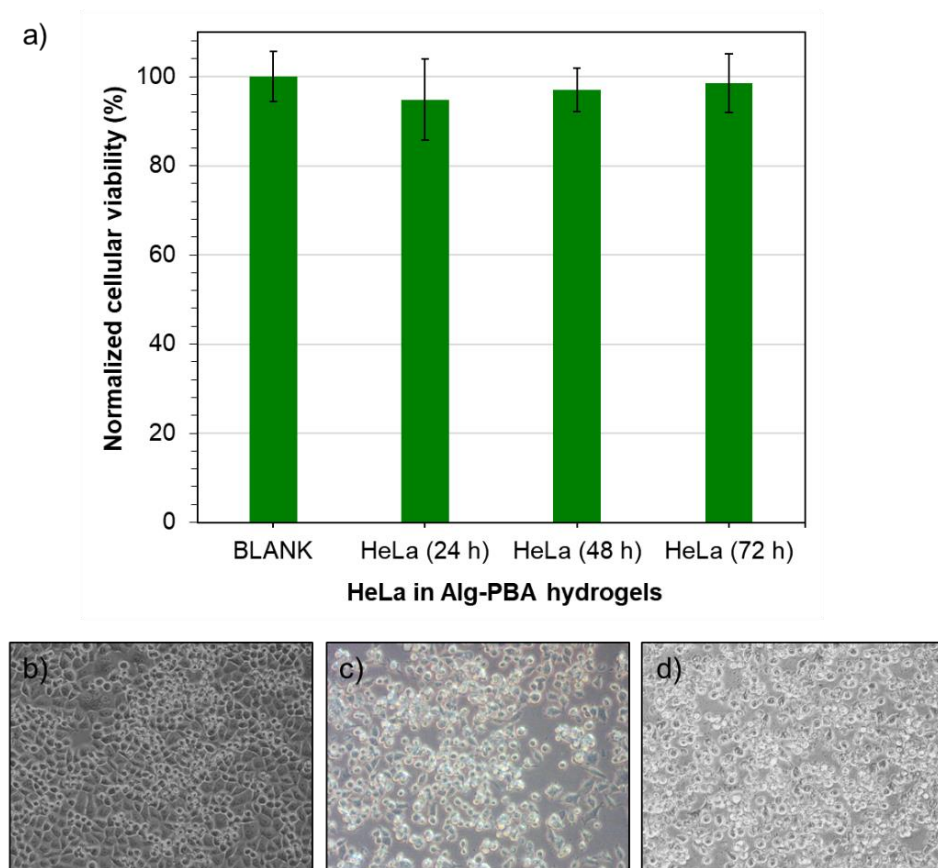


Figure 18. a) *In vitro* MTT-based cytotoxicity for **Alg-PBA** hydrogels cultured with HeLa cells at 24, 48 and 72 h of incubation, b) non-encapsulated HeLa cells used as a control, c) release of encapsulated HeLa cells after 72 h of incubation, d) release of HeLa cells after being encapsulated and extruded into a 24-well cell culture plate (24 h of incubation).

Due to the injectability and biocompatibility, Alg-PBA hydrogels were preliminarily evaluated as drug carriers for tuning the kinetics of the drug release. Oxytetracycline (OXY), a broad-spectrum antibiotic, was used as a hydrophilic model drug to be entrapped in Alg-PBA hydrogels (initial drug concentration = 0.8 g L^{-1}). The release kinetics were investigated at different pH values. Figure 19a displays the cumulative drug release profiles using the **7-35** hydrogel at pH 1.2, 7.4 and 10. At low pH the release plateau was reached at 40% after 17 h, whereas the plateau at basic pH was below 30% after 17 h. Interestingly, at pH 7.4 there was no plateau within 24 h. In general, a first-order release model fitted very well all release curves and displayed an almost perfect linear regression with correlation coefficients >98 , indicating a dependence of the release rate with the drug concentration (Figure 19b-d).

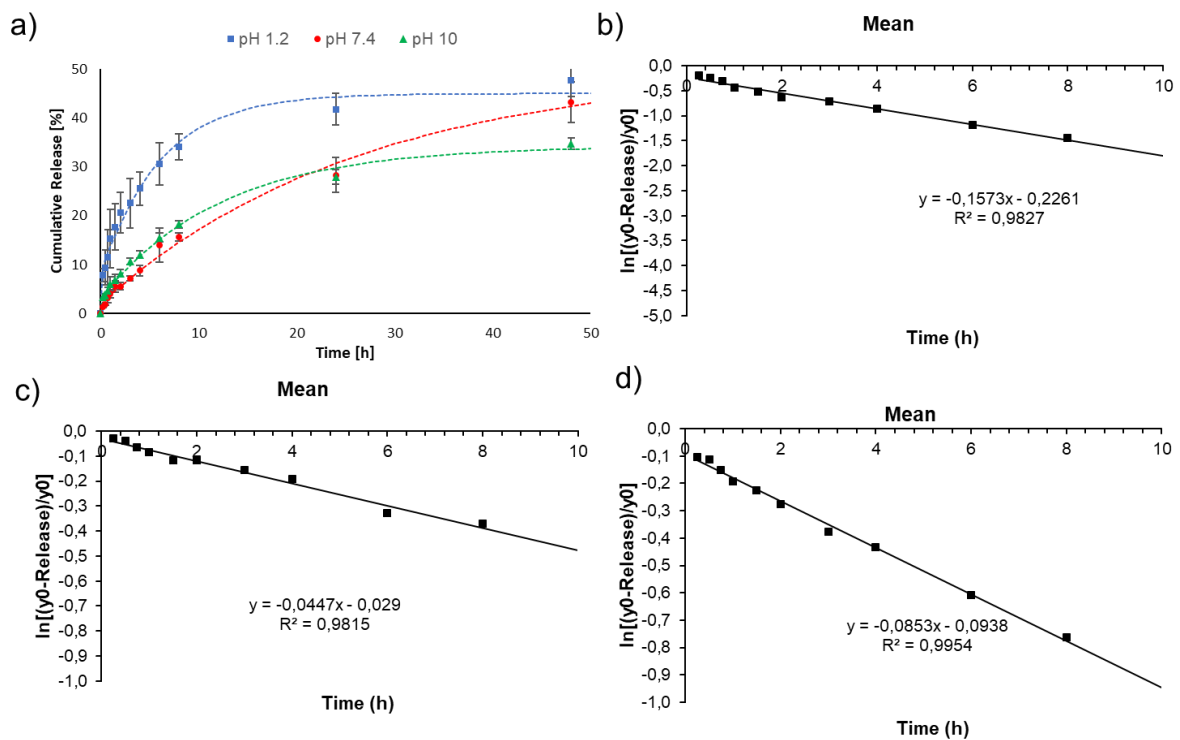


Figure 19. a) Drug release experiments of OXY from Alg-PBA hydrogels at different pH values and the corresponding first-order release model fitting at b) pH 1.2, c) pH 7.4 and d) pH 10.

These results show that Alg-PBA hydrogels are promising candidates for biomedical applications, e.g. as drug delivery carrier for controlled drug release due to their biocompatibility and the pH-dependent release of their cargo.

3.2.4. Conclusion and Outlook

In summary, straightforward functionalization of alginate with boronic acid moieties allowed spontaneous formation of a versatile hydrogel under basic conditions. The reaction between the boronic acid groups and vicinal diols present on the pyranose rings of the biopolymer afforded a crosslinked hydrogel without the need for additional complementary molecules. Extraordinary self-healing, injectability and multi-stimuli responsive properties were demonstrated for this material. Undistinguished interfaces were observed after the rapid self-healing of a damaged gel or after the fusion of two gels prepared independently. The self-healing kinetics was superior for **7-35** which was about one order of magnitude faster than **3-75**. The dynamic nature of boronate ester bonds permitted the control of the molecular assembly/disassembly by either change in the pH or addition of a competitive monosaccharide.

In addition, it was demonstrated that subtle variations in Alg-PBA and NaOH concentrations give rise to qualitative differences in the mechanical response of Alg-PBA hydrogels. Gels prepared at low alginate concentration and high NaOH concentration (**3-75**) are stretchable and self-healable. However, there is a dramatic difference when the polymer concentration is increased while decreasing the NaOH concentration (**7-35**). These gels do not fail on stretching to over 16000% (in comparison with ~ 100% for **3-75**) and gel pieces held together, self-healing to their original strength rapidly, within a minute. This extension ratio is significantly higher than that reported for gels in the literature (Table S1). Therefore, the **7-35** gel formulation represents a super stretchable gel.

These remarkable properties appear to arise from an optimization of the dynamic association/dissociation kinetics of the boronate ester bonds. The rapid time scales that characterize these kinetics at low NaOH concentrations, with the ready availability of alginate polymers distinguishes the **7-35** gel from the **3-75** gel. Remarkably, this qualitative difference in the high strain behavior is not apparent from low amplitude oscillatory studies that both gels show Maxwell-like behavior with only quantitative differences in the crossover modulus and frequency.

In addition, the hydrogel showed good biocompatibility upon encapsulation of HeLa cells, of which a significant proportion of cells survived after consecutive gel injection and self-healing processes. The foregoing results indicate that the material could be useful for different biomedical applications.

In the future, it could be interesting to investigate different phenylboronic acid-modified biopolymers (e.g. chitosan, gelatin, dextran, among others), regarding the gel formation and gel properties. In addition, different structures of boronic acid-containing units could give a better insight into the self-healing behavior and stretchability or impart other interesting gel properties. There are many possibilities to create new hydrogels and to investigate their features which could be useful for different applications, e.g. as (glucose) sensor or different biomedical uses.

3.2.5. Experimental Part

3.2.5.1. Materials and Methods

Unless otherwise indicated, analytical grade solvents and reactants were commercially available and used as received without further purification. Alginic acid sodium salt (low viscosity, 15-20 cP for 1% in H₂O) and dialysis tubing cellulose membranes (MWCO 14000, LOT 3110) were purchased from Sigma Aldrich. 1-Ethyl-3-(3-dimethylaminopropyl)carbodiimide (EDC) was purchased from Carl Roth. 3-Aminophenylboronic acid monohydrate was purchased from Alfa Aesar.

¹H-NMR spectra were recorded on a Bruker Avance 300 spectrometer at 25 °C. Chemical shifts for ¹H were reported as δ , parts per million (ppm), relative to the signal of the residual solvent (CHCl₃ = 7.26 ppm). Coupling constants (J) are given in Hertz (Hz). The following notations indicate the multiplicity of the signals: s = singlet, br s = broad singlet, d = doublet, t = triplet, q = quartet, dd = doublet of doublets, m = multiplet. Estimated error of reported values: 0.01 ppm (δ , ¹H NMR), 0.1 Hz (J, coupling constant). UV-Vis spectroscopy was recorded with Ocean Optics DH-2000-BAL UV-vis/NIR spectrophotometer. FT-IR spectra were recorded with an Agilent Technologies Cary 630 FTIR spectrometer equipped with a Golden Gate Diamond ATR (attenuated total reflection). Oscillatory rheology was performed with a TA-ARES G2 strain-controlled rheometer equipped with a normal force transducer. A 1000 μ m gap setting and 25 °C were used for the measurements in a plain-plate (40 mm, stainless steel). Rheological measurements involved dynamic strain sweep (DSS), dynamic frequency sweep and dynamic time sweep. The self-healing behavior of model gels was investigated by several cycles of a 3-steps loop experiment involving: application of (1) low shear strain (5 min, 5% strain, 1 Hz for **3-75** and 10 Hz for **7-35**), G' (storage modulus) > G'' (loss modulus); (2) increase of the shear strain until the gel fractures (2 min, 500% strain, 1 Hz for **3-75**, 10 Hz for **7-35**), viscous material, $G' > G''$, and (3) return at the same rate to the initial strain % value (10 min, 5% strain, 1 Hz for **3-75** and 10 Hz for **7-35**), recovered gel phase, $G' > G''$). Tensile testing was performed on a TA Instruments dynamic mechanical analyzer (DMA, RSA-III). Stretching experiments were performed with rectangular tension geometry for **3-75**. As-prepared hydrogels were cut into rectangular shapes and vertically clamped into the geometry and stretched at a constant rate (0.1, 1 or 10 mm s⁻¹). In contrast, **7-35** thin rapidly on clamping in the rectangular geometries. Therefore, as-prepared samples were molded in form of cylinders and due to their remarkable adhesion to metal, 8.4 mm diameter

parallel plate geometries could be used to fix the gels for the stretching experiments. All measurements were repeated several times (at least 5 times) to confirm the reproducibility.

3.2.5.2. Synthesis of Alg-PBA

Alg-PBA was prepared by grafting 3-aminophenylboronic acid onto alginate in the presence of 1-ethyl-3-(3-dimethylaminopropyl)carbodiimide (EDC) following a previously reported procedure¹³ with slight modifications. Sodium alginate (5 g, 25 mmol based on monomer unit) was dissolved in deionized water (500 mL) to which EDC (4.8 g, 25 mmol) and 3-aminophenylboronic acid (1.95 g, 12.5 mmol) were added. The mixture was stirred at room temperature for 24 h and then dialyzed against distilled water for 1 week, replacing water at least 7 times, and lyophilized.

3.2.5.3. Determination of Acid Dissociation Constant (pK_a)

Determination of the pK_a of the conjugate and native alginate was carried out by acid-base titration at constant ionic strength.¹⁷ Specifically, the corresponding alginate material (1% w/v) was dissolved in 4 mL of 50 mM KCl and the pH was reduced to pH 2.3 by adding 0.1 M HCl. Then, the pH was increased by gradually adding 0.1 M NaOH until pH 12 was reached. The changes in pH during the titration experiment were monitored potentiometrically.

3.2.5.4. Preparation of Alg-PBA hydrogels

The desired amount of Alg-PBA was dissolved in 0.1 M PBS aqueous solution to obtain a final concentration of 3-10 % w/v. The addition of a certain amount of 1 M NaOH per mL of solution led to the immediate formation of the gel.

The response of Alg-PBA hydrogel to pH change: After obtaining an Alg-PBA hydrogel under basic conditions, the pH of the medium was lowered by addition of 200 μ L $\text{CH}_3\text{COONa}/\text{CH}_3\text{COOH}$ buffer (pH = 5) on top of the gel. The drastic pH change led to the collapse of the gel due to the dissociation of the pH dependent boronate bonds between the polymeric chains. After raising the pH again by addition of 100 μ L NaOH, a stable gel was reformed, due to the reversible formation of cyclic boronate esters. The response of **3-75** and **7-35** toward pH changes was similar and without a visible difference.

3.2.5.5. Biological Studies

Cell Culture and Materials

HeLa cells were maintained in a humidified atmosphere (5% CO_2) at 37 °C and cultured in Dulbecco's modified Eagle's medium (DMEM), which was supplemented with fetal bovine

serum (FBS, 10%), streptomycin ($100 \mu\text{g mL}^{-1}$) and penicillin (100 U mL^{-1}). DMEM, phosphate-buffered saline (pH 7.4) and trypsin-EDTA (0.05%) phenol red were purchased from Gibco. 3-(4,5-Dimethylthiazol-2-yl)-2,5-diphenyltetrasolium bromide was purchased from Sigma Aldrich.

Cell Encapsulation

To explore the cellular viability and cell release of Alg-PBA hydrogels, the 3D encapsulation of HeLa cells was carried out: HeLa cells were regularly passaged to maintain an exponential growth. Cells were incubating with Trypsin-EDTA (2 mL) for 5 min at 37°C to detach cells from the flask surface. DMEM was added (8 mL) and the mixture was put in a 15 mL centrifuge tube. Cells were centrifuged for 5 min at 1300 rpm. Cells (10×10^6 and 2×10^6) were re-suspended in Alg-PBA solution (15 mg in 500 μL of PBS), respectively. 80 μL of the solution were placed in three molds and 1 M NaOH (6 μL) was added. The final mixture was slightly stirred. The 3D encapsulation of cells within alginate hydrogels took place in less than 2 min. Monoliths containing cells were incubated in DMEM (1 mL) supplemented with FBS (10 %) without antibiotics at 37°C in a 24-well and 6-well cell culture plates.

Injection Experiment

HeLa cells at a concentration of 18×10^6 were suspended in Alg-PBA solution (32 mg in 1 mL of PBS) following the same procedure described above. 1 M NaOH (160 μL) was added and the resultant solution was slightly stirred. Once Alg-PBA hydrogels (x 2) containing cells were formed, they were extruded through a 21-gauge needle directly into a 24-well cell culture plate. Gels were incubated in DMEM (1 mL) supplemented with FBS (10%) for 24 h.

Cytotoxicity Studies

The MTT assay²⁵ was used to confirm the safety and compatibility of Alg-PBA hydrogels by evaluating the mitochondrial function of cultured cells and evaluating the formazan production in cells: After 24 h of hydrogel incubation (encapsulated and extruded hydrogels, respectively), DMEM was removed and cells were washed with PBS (400 μL). Trypsin-EDTA (150 μL) was added and incubated for 5 min at 37°C . After adding DMEM (850 μL), cell suspensions were centrifuged ((3 rcf x 3 min), 8 min). Then, cells were seeded in a 96-well plate at a density of 5000 cells/well in complete DMEM supplemented with 10% FBS (200 μL). Cells were incubated 24, 48 and 72 h. MTT dye solution (25 μL ; 5 mg mL^{-1}) were added at appropriate times and cells were incubated for additional 4 h at 37°C . The medium was removed and DMSO (100 μL) was added in order to dissolve formazan crystals. The plate was read at 570 nm in a Promega Glomax Multidetecion System instrument. Six replicates

were used for each sample and results are shown as the mean \pm standard deviation (SD). Cell viability is reported as the percentage of non-encapsulated compared to encapsulated cells.

Drug Release Experiments

A weighted amount of Alg-PBA (7% w/v) and 1 mL of an aqueous stock solution of oxytetracycline hydrochloride (OXT) (0.8 g L^{-1}) were placed in a screw-capped glass vial and stirred until Alg-PBA was completely dissolved. After addition of 35 μL 1 M NaOH, immediate formation of the gel was observed which were allowed to equilibrate at RT for 16 h. After this time, the gels were overlaid with PBS buffer (1 mL, pH 1-10)²⁶ corresponding to time = 0 of the release studies. At selected points of time, aliquots (100 μL) were removed from the supernatant and diluted with PBS to reach 1 mL of total volume. Then fresh PBS buffer (100 μL) was added over the gel to maintain infinite sink conditions. Drug concentrations were determined by UV-vis spectroscopy after proper calibration using the maximum absorbance of OXT at $\lambda_{\text{max}} = 353 \text{ nm}$. Each experiment was performed at least in triplicate. The data obtained from the *in vitro* release experiments were fitted according to four drug release mathematical models, namely first-order release,²⁷ Higuchi,²⁸ Korsmeyer-Peppas,²⁹ and Weibull,³⁰ although the first-order release model matched the best with coefficients $R^2 > 0.98$.

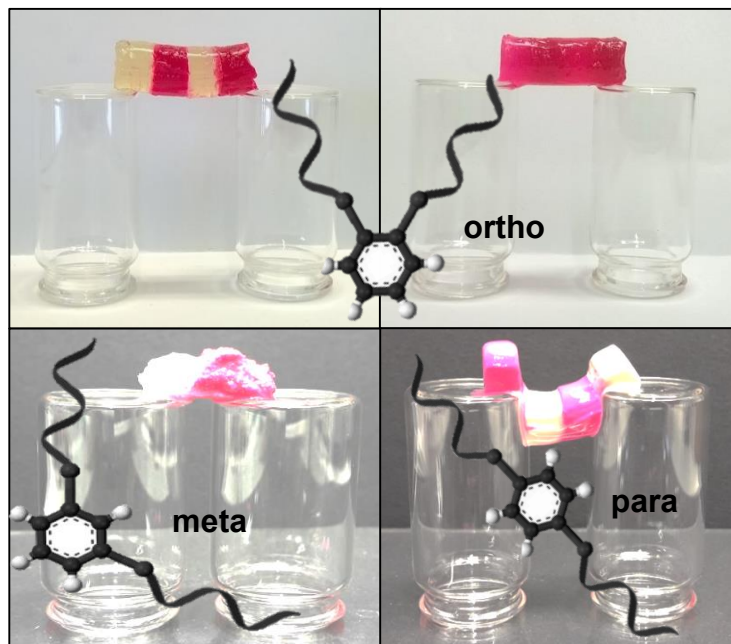
→ Additional information on gel characterization and additional stretching experiments can be found in the ESI on the enclosed CD.

3.2.6. References

- [1] a) X. Le, W. Lu, J. Zheng, D. Tong, N. Zhao, C. Ma, H. Xiao, J. Zhang, Y. Huang, T. Chen, *Chem. Sci.* **2016**, 7, 6715-6720; b) F. Tao, L. Qin, Z. Wang, Q. Pan, *ACS Appl. Mater. Interfaces* **2017**, 9, 15541-15548; c) J. P. Chaudhary, F. Kholiya, N. Vadodariya, V. M. Budheliya, A. Gogda, R. Meena, *Arab. J. Chem.* **2017** doi: 10.1016/j.arabjc.2017.12.034; d) Y. Chen, W. Qian, R. Chen, H. Zhang, X. Li, D. Shi, W. Dong, M. Chen, Y. Zhao, *ACS Macro Lett.* **2017**, 6, 1129-1133.
- [2] D. Horton, *Adv. Carbohydr. Chem. Biochem.*, Elsevier Academic Press, Amsterdam and San Diego, **2012**, ch. 1, vol. 68, pp. 1–58.
- [3] a) D. T. James, M. D. Phillips, S. Shinkai, Boronic acids in saccharide recognition, *Royal Society of Chemistry*, Cambridge, **2006**; b) L. I. Bosch, T. M. Fyles, T. D. James, *Tetrahedron*, **2004**, 60, 11175–11190.
- [4] C. C. Deng, W. L. Brooks, K. A. Abboud, B. S. Sumerlin, *ACS Macro Lett.*, **2015**, 4, 220–224.
- [5] J. N. Cambre, B. S. Sumerlin, *Polymer*, **2011**, 52, 4631–4643.
- [6] a) D. G. Hall, Boronic acids: preparation, applications in organicsynthesis and medicine, John Wiley & Sons, Weinheim, **2006**; b) L. He, D. E. Fullenkamp, J. G. Rivera, P. B. Messersmith, *Chem. Commun.*, **2011**, 47, 7497–7499.
- [7] a) M. Nakahata, S. Mori, Y. Takashima, A. Hashidzume, H. Yamaguchi, A. Harada, *ACS Macro Lett.*, **2014**, 3, 337–340; b) H. Meng, P. Xiao, J. Gu, X. Wen, J. Xu, C. Zhao, J. Zhang, T. Chen, *Chem. Commun.*, **2014**, 50, 12277–12280; c) M. Piest, X. Zhang, J. Trinidad, J. F. Engbersen, *Soft Matter*, **2011**, 7, 11111–11118; d) A. E. Ivanov, H. Larsson, I. Y. Galaev, B. Mattiasson, *Polymer*, **2004**, 45, 2495–2505; e) Lee, K. Y.; Mooney, D. J., *Prog. Polym. Sci.* **2012**, 37, 106-126.
- [8] M. Pérez-Madrigal, J. Torras, J. Casanovas, M. Häring, C. Aleman, D. D. Díaz, *Biomacromolecules* **2017**, 18, 2967–2979.
- [9] D. Ruiz-Molina, F. Novio, C. Roscini, Bio- and Bioinspired Nanomaterials, John Wiley & Sons, Weinheim, **2014**.
- [10] D. Kühbeck, J. Mayr, M. Häring, M. Hofmann, F. Quignard, D. D. Díaz, *New J. Chem.*, **2015**, 39, 2306-2315.
- [11] Z. Li, W. Lu, T. Ngai, X. Le, J. Zheng, N. Zhao, Y. Huang, X. Wen, J. Zhang, T. Chen, *Polym. Chem.*, **2016**, 7, 5343-5346.
- [12] H. Meng, J. Zheng, X. Wen, Z. Cai, J. Zhang, T. Chen, *Macromol. Rapid. Commun.* **2015**, 36, 533-537.

- [13] H. Meng, P. Xiao, J. Gu, X. Wen, J. Xu, C. Zhao, J. Zhang, T. Chen, *Chem. Commun.*, **2014**, 50, 12277-12280.
- [14] W. Yu, G. Jiang, Y. Zhang, D. Liu, B. Xu, J. Zhou, *Mater. Sci. Eng., C*, **2017**, 80, 187-196.
- [15] S. K. Papageorgiou, E. P. Kouvelos, E. P. Favvas, A. A. Sapalidis, G. E. Romanos, F. K. Katsaros, *Carbohydr. Res.*, **2010**, 345, 469-473.
- [16] Z. Sebestyén, K. Máthé, Á. Buvári-Barcza, E. Vass, F. Ruff, J. Szemán, L. Barcza, *Carbohydr. Res.*, **2011**, 346, 833-838.
- [17] O. Prodanovic, D. Spasojevic, M. Prokopijevic, K. Radotic, N. Markovic, M. Blazic, R. Prodanovic, *React. Funct. Polym.* **2015**, 93, 77-83.
- [18] M. Chtchigrovsky, Y. Lin, K. Ouchaou, M. Chaumontet, M. Robitzer, F. Quignard, F. Taran, *Chem. Mater.*, **2012**, 24, 1505-1510.
- [19] L. P. Lorand, J. O. Edwards, *J. Org. Chem.*, **1959**, 24, 769-774.
- [20] D. Roylance, *Stress-Strain Curves*. MIT Press; Cambridge, MA, **2001**.
- [21] K. Mayumi, A. Marcellan, G. Ducouret, C. Creton, T. Narita, *ACS Macro Lett.* **2013**, 2, 1065-1068.
- [22] a) Y. Li, J. Rodrigues, H. Tomás, *Chem. Soc. Rev.*, **2012**, 41, 2193-2221; b) K. H. Bae, L.-S. Wang, M. Kurisawa, *J. Mater. Chem. B.*, **2013**, 1, 5371-5388; c) Q. V. Nguyen, D. P. Huynh, J. H. Park, D. S. Lee, *Eur. Polym. J.*, **2015**, 72, 602-619; d) I. Yu, J. Ding, *Chem. Soc. Rev.*, **2008**, 37, 1473-1481.
- [23] M. Kurisawa, J. E. Chung, Y. Y. Yang, S. J. Gao, H. Uyama, *Chem. Commun.*, **2005**, 4312-4314.
- [24] B. Yang, Y. Zhang, X. Zhang, L. Tao, S. Li, Y. Wei, *Polym. Chem.*, **2012**, 3, 3235-3238.
- [25] a) T. Miao, S. L. Fenn, P. N. Charron, R. A. Oldinski, *Biomacromolecules*, **2015**, 16, 3740-3750; b) K. Cai, J. Zhang, L. H. Deng, L. Yang, Y. Hu, C. Chen, L. Xue, L. Wang, *Adv. Eng. Mat.*, **2007**, 9, 1082-1088.
- [26] H. Zhang, Y. Dong, L. Wang, G. Wang, J. Wu, Y. Zheng, H. Yang, S. Zhu, *J. Mater. Chem.* **2011**, 21, 13530-13537.
- [27] E. Mathiowitz, *Encyclopedia of Controlled Drug Delivery*; 1st ed.; Wiley, **1999**; Vol. II, pp 698-729.
- [28] T. Higuchi, *J. Pharm. Sci.* **1963**, 52, 1145-1149.
- [29] P. L. Ritger, N. A. Peppas, *J. Controlled Release* **1987**, 5, 37-42.
- [30] W. Weibull, *J. Appl. Mech.* **1951**, 18, 293-297.

3.3. Topology-Controlled Self-Healing Properties of Ionene Polymer Hydrogels



3.3.1. Abstract

Ionenes are cationic polyelectrolytes with a positively charged heteroatom which is part of the backbone. Here, the ionene polymer consists of a disubstituted phenylene dibenzamide core connected with DABCO. The so-obtained polymers are able to form hydrogels. The polymer topology controlled by the disubstitution pattern of the aromatic core of these ionene polymers has been found to play a crucial role on the self-healing properties of the hydrogels. Specifically, the *ortho*-isomer showed very superior shape persistent, self-standing and self-healing properties compared to its *meta*- and *para*-analogues.

3.3.2. Introduction

Natural self-healing processes are one of the most impressive properties in living organisms and have inspired researchers worldwide to develop self-healable synthetic materials to reduce replacement costs while improving their lifetime and safety.¹ In general, these materials are based on either irreversible (e.g., encapsulation of healing agents) or reversible approaches (e.g., dynamic covalent bonds and non-covalent bonds).^{2,3} Among a number of materials with potential self-healing properties, viscoelastic (soft) materials such as polyelectrolyte hydrogels are very promising for biomedical applications due to their biocompatibility and similar mechanical properties to those of natural tissues.⁴ In addition, polyelectrolytes have also attracted increasing attention in recent years as self-healable coatings with anticorrosion properties.⁵ In most cases, the healing process of polyelectrolyte-containing materials is based on ionic interactions between oppositely charged polymers.⁶⁻⁹

In previous studies,¹⁰ the synthesis of a series of isomeric ionene polyelectrolytes **1-3** (Figure 1) and their intriguing self-assembly properties in aqueous medium was described.^{10,11} In general, ionenes are synthetic polycations bearing quaternary ammonium functions distributed along the backbone. In the case of ionenes **1-3**, the positive charges are provided by the use of 1,4-diazabicyclo[2.2.2]octane (DABCO) linker, whereas an *N,N'*-(*ortho*-/*meta*-/*para*-phenylene)dibenzamide core enabled the preparation of the three different topomers.

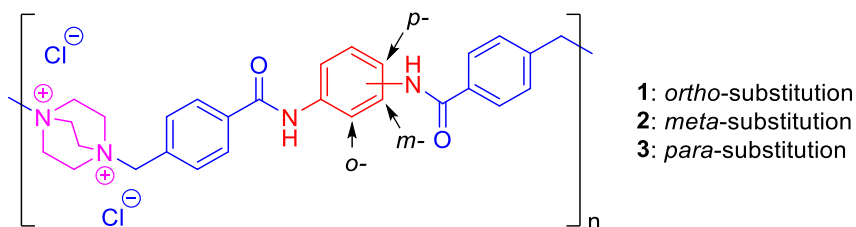


Figure 1. Structures of isomeric ionene polymers **1-3**.

Previously, a combined computational-experimental approach was developed to improve the hydrogelation and to understand the gelation mechanism behind the three topomers **1-3**.¹⁰ Molecular dynamic simulations of **1-3** with explicit water molecules were performed. The results demonstrated a significant difference in the assembly of each polymer. For the polymers **1** and **2**, polymer-water interactions, as well as polymer-polymer interactions, were evident, whereas polymer-water interactions are the only intermolecular interactions in **3**. These observations were confirmed by the corresponding radial distribution functions. The theoretical approach was in good agreement with the experimental results where **1** constitutes

the best hydrogelation ability with the lowest CGC, the highest thermal stability, superior optical properties and the best gelation kinetics.

These versatile polymers have shown potential for antimicrobial applications,¹² gene transfection,¹³ dye removal,¹⁴ and phase transfer catalysis.¹⁵ Moreover, ionenes **1-3** form hydrogels when dissolved either in neutral¹⁰ or acidic aqueous media.¹¹

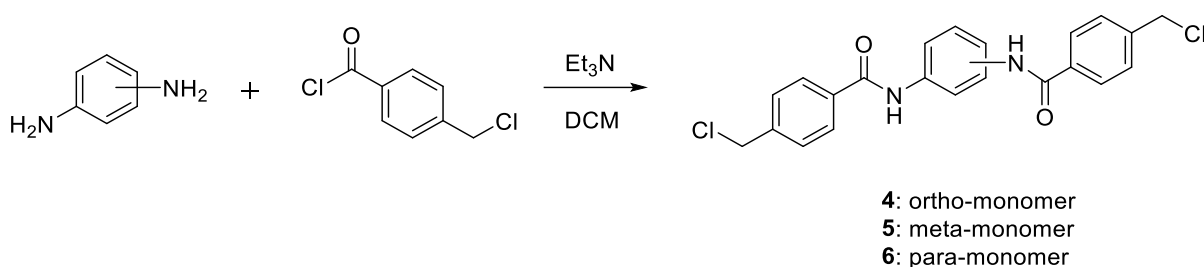
Motivated by the previous results, macroscopic self-standing and self-healing properties of their corresponding hydrogels were investigated and compared with respect to their topological influence.

3.3.3. Results and Discussion

3.3.3.1. Synthesis of Ionene Polymers and Hydrogel Preparation

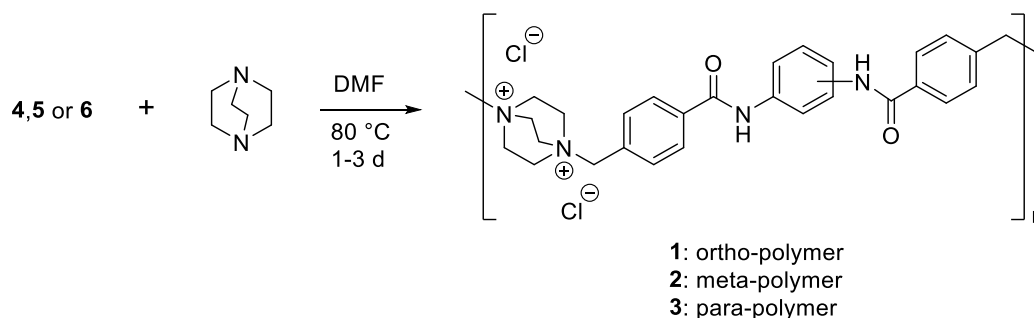
As previously reported,¹⁰ ionenes **1-3** are easily synthesized via a two-step reaction sequence, starting with the amidation of isomeric phenylenediamines with 4-(chloromethyl)benzoyl chloride in the presence of Et₃N in CH₂Cl₂ which afforded the corresponding ionene monomers **4-6** in good yields (87 – 96%) upon recrystallization (Scheme 1).

Scheme 1. Synthesis of ionene monomers **4-6**.



The subsequent step-growth copolymerization of so-formed ionene monomers **4-6** with DABCO under equimolar conditions in DMF at 80 °C gave the desired ionene polymers **1-3** as white precipitates within 1-3 days in good yields (69 – 98%) after simple filtration, washing and drying protocol (Scheme 2).

Scheme 2. Synthesis of ionene polymers **1-3**.



Hydrogels were prepared by cooling an isotropic solution of the ionene polymers to RT, above the critical gelation concentration (CGC) of 2.5%, 10%, and 5% (w/v) for **1**, **2**, and **3**, respectively.

3.3.3.2. Self-Healing Experiments of Hydrogels

In order to perform macroscopic self-healing studies, the free-standing ability of hydrogel bars was investigated first. Self-standing monolithic gels (*i.e.*, gels that support their own weight

when suspended between two vials) could be obtained for **1** at concentrations $\geq 7.5\%$ (w/v), **2** at $\geq 10\%$ (w/v), and **3** at $\geq 13\%$ (w/v) (Figure 2).

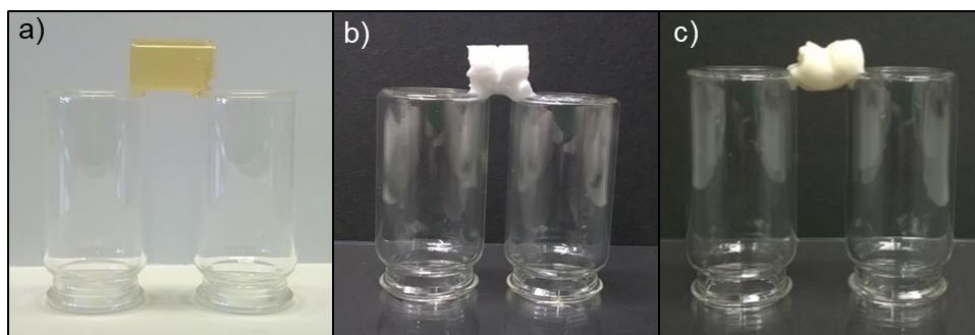


Figure 2. Self-standing ionene polymer hydrogels of a) **1** at 7.5% (w/v), b) **2** at 13% (w/v) and c) **3** at 10% (w/v).

Among these polymers, *ortho*-ionene **1** afforded gel bars with superior shape-persistent properties allowing, for instance, the formation of stable gel bridges of 2.7 cm and 4 cm in length (total volume = 2 mL and 5 mL, respectively). Remarkably, only the hydrogel made of *ortho*-ionene **1** ($\geq 7.5\%$ w/v) showed macroscopic self-standing and self-healing properties. It is worth mentioning that, in contrast to other polyelectrolytes,⁶⁻⁹ the combination of **1** with an oppositely charged polymer was not necessary for the material to display self-healing properties. Figure 3 illustrates the self-healing ability of hydrogels made of *ortho*-ionene **1** (7.5% w/v) in conventional gel block fusion experiments.

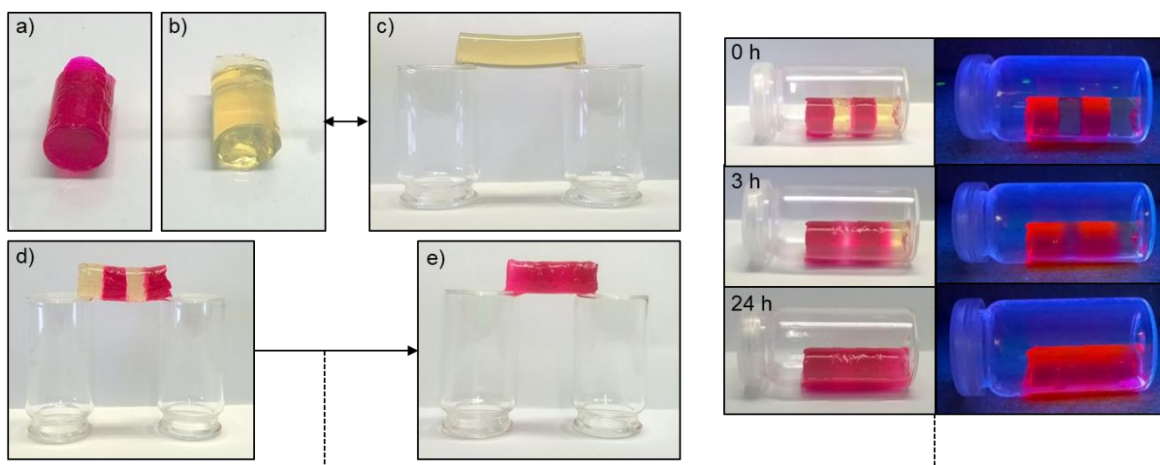


Figure 3. Ionene-based hydrogels made of **1** (7.5% w/v): a) dye-doped, and b) undoped monolithic gel blocks; c) undoped gel block supporting its own weight suspended between two vials; d) gel bridge made by fusing dye-doped and undoped gel blocks in an alternating manner (picture was taken immediately after fusion); e) aspect of the gel bridge after 24 h. Pictures showing temporal dye diffusion through the entire self-healed gel are given. Photographs were also taken under UV light (365 nm) for better visualization of dye diffusion.

For a better visualization of the self-healing process, one of the gel blocks was dye-doped by adding a dye (*i.e.*, rhodamine B, $c = 0.5 \text{ g L}^{-1}$) into the polymer solution prior gelation (Figure 3a). The dye-doped and undoped gel blocks were cut into 0.5 cm pieces and

alternatingly rearranged to each other. Gel blocks underwent immediate fusion upon contact and afforded the formation of stable gel bridges without external stimuli (Figure 3d). The cut interfaces gradually disappeared over time with a concurrent diffusion of the dye through the gel body affording homogeneous self-healed gel sample within 24 h. This process could be nicely observed either by the naked eye or under UV-light irradiation (Figure 3d-e). On the other hand, when gel blocks were prepared at 9% w/v, cut and re-joined, several hours of interface contact were necessary to obtain a stable gel bridge, and the reconnected gel pieces were less uniform at the blocking interfaces in comparison to the self-healed gel bridge made at 7.5% w/v. Nevertheless, in both cases, the dye was distributed through the entire gel body over time, indicating a good restoration of the diffusion properties at the interfaces between the cut gel pieces. It is worth mentioning that the incorporation of different dyes did not affect the self-healing property of the bulk material, although the diffusion kinetics of the dye depended on the dye structure presumably due to their different interactions with the polyelectrolyte gel network (Figure 4).

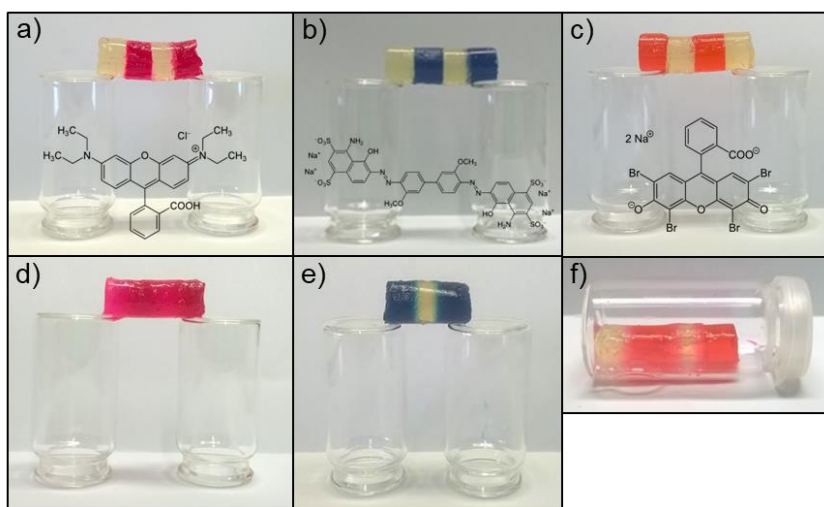


Figure 4. Self-healing bridge experiments of **1** with different dyes; dye-doped with a) rhodamine B, b) Direct Blue 1, c) eosin Y. Diffusion of dyes are dye structure dependent: d) complete diffusion after 24 h, e) and f) partial diffusion after 1 week and 24 h, respectively.

Considering just a balance between self-healing time and uniformity of the self-healed bulk gel, it was focused on further experiments mainly on the gel prepared at 7.5% w/v. Interestingly, the self-healing process takes place even when an acidic solution (1 N HCl) is spread over the cut surfaces before rejoining them, which is in concordance with the ability of **1** to form also a gel with aqueous acidic solutions.¹¹

Besides the macroscopic self-healing ability of hydrogels made of **1**, oscillatory rheological measurements showed a thixotropic response against mechanical stress caused by large-

amplitude oscillations.¹⁰ Taking advantages of these properties, the injectability of the hydrogel by placing it into a plastic disposable syringe and continuously ejecting it through a 21-gauge needle was demonstrated (Figure 5a). Reformation of a stable gel took place immediately after injection acquiring the shape of the container that served as a mold (Figures 5b-c). The gel could also be shaped in any desired form, which persisted over time (Figures 5d-f).

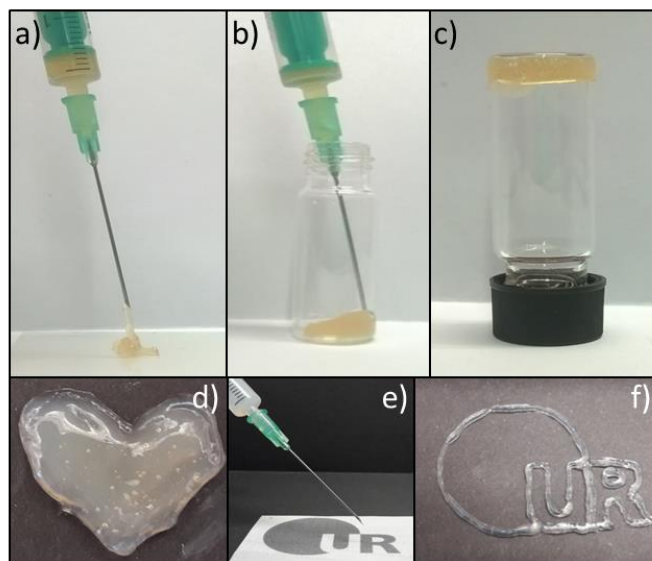


Figure 5. a-b) Injectability property of the hydrogel made of **1** (7.5% w/v) through a 21-gauge needle, c) upside-down vial showing the reconstituted hydrogel after injection, d-f) gel samples prepared with different shapes.

The injectability of hydrogels made of non-toxic polymers, such as *ortho*-ionene **1**,¹³ together with a rapid restoration of the gel phase constitutes a very important property for numerous biomedical applications.¹⁶⁻¹⁸

Field emission scanning electron microscopy (FE-SEM) images of the xerogel prepared from the undamaged hydrogel revealed overlapped laminar structures consisting of large and homogeneous sheets (Figure 6a). The same bulk morphology of a thin gel film was observed after cutting damage and spontaneous self-healing (Figure 6b). Moreover, optical microscopy imaging confirmed a gradual microscopic healing of a cut gel surface, although the damaged area was still slightly visible under the microscope after 24 h (Figure 6c-d).

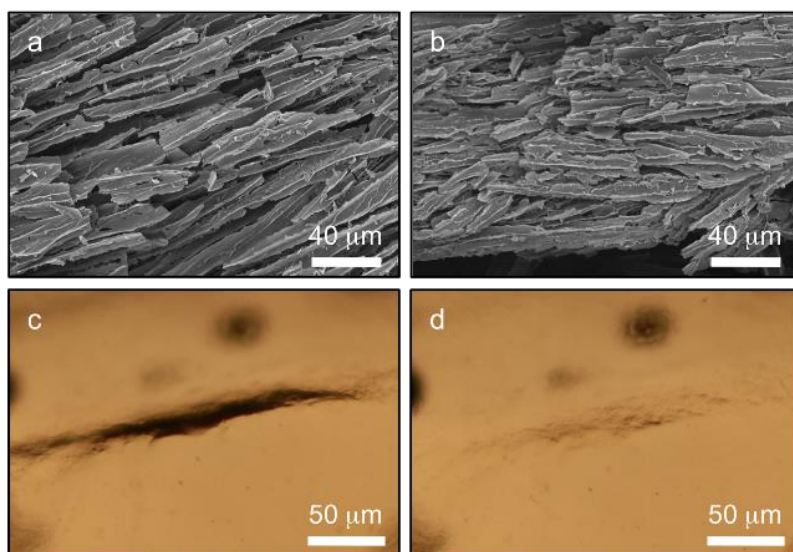


Figure 6. a) FE-SEM image of the xerogel obtained by freeze-drying the pristine hydrogel made of **1** (7.5% w/v), b) FE-SEM image of the xerogel prepared from the previous hydrogel after the destruction and spontaneous regeneration, c) optical microscopy image of a film hydrogel immediately after cutting the surface, d) optical microscopy image of the film 24 h after the damage.

3.3.3.3. Load-bearing Experiments

Furthermore, the load-bearing capacity of hydrogels is also a desired property for biomedical applications.^{19,20} In this context, although hydrogels made of **1** at a concentration of 9% w/v showed relatively slower self-healing in comparison to those prepared at 7.5% w/v, they displayed the highest load-bearing capacity. As shown in Figure 7, a gel body made of **1** at 9% w/v could support at least 26-times its own weight before it collapsed and broke into pieces. This corresponded to a weight 1.7-times higher than the maximum load supported by the gel prepared at 7.5% w/v. It should be noted that although no load-bearing experiments at concentrations higher than 9% w/v was performed, *ortho*-ionene **1** also enables the preparation of hydrogels at exceptionally high concentrations (> 100% w/v), being accompanied by a significant increase in the stability of the bulk gel,¹⁰ albeit with a certain detriment in the self-healing capacity (*vide supra*). Therefore, much higher load-bearing values might be possible, in principle, working with hydrogels made of **1** at much higher concentrations. A proper balance between load-bearing and self-healing properties of these gels should be considered in order to meet specific requirements for potential applications.

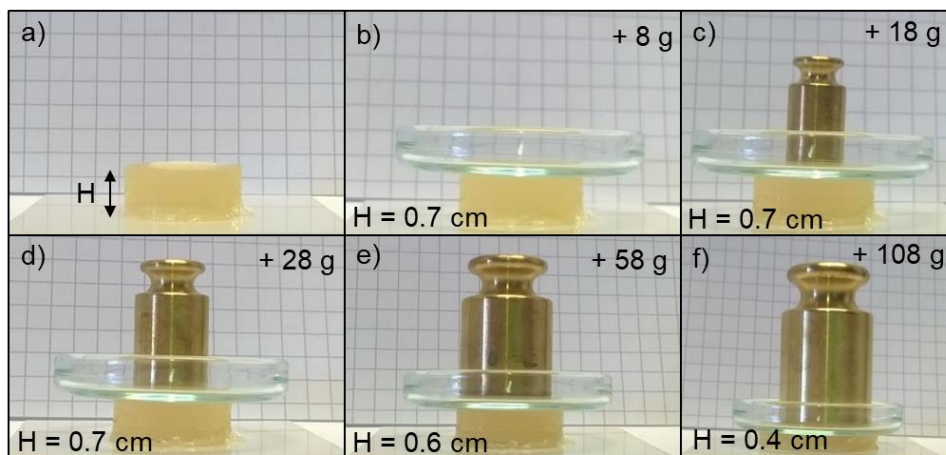


Figure 7. The load-bearing capacity of the hydrogel made of **1** (9% w/v). The applied load and the height of the monolith (H) are indicated on the top-right corner and below each picture, respectively. Total gel volume = 2 mL.

A different load-bearing experiment was carried out by hanging a calibration weight connected to a metal wire from a gel bridge (Figure 8). When a 2 g-weight was hanged from the 7.5% w/v hydrogel, the metal wire cut the surface and the load moved down due to gravity. Interestingly, the cut occurred until the middle of the gel where the weight remained suspended without further moving (Figure 8a-b). Remarkably, when the load was increased to 5 g, the metal wire weight crossed the entire gel body without destabilizing the bridge (Figure 8c-d).

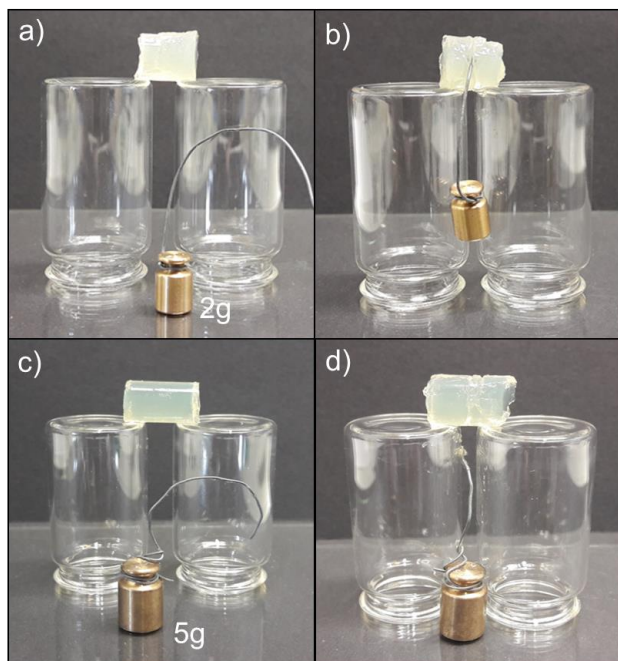


Figure 8. Load-bearing experiments of hydrogel bridge made of ionene **1** (7.5% w/v) with a-b) 2 g load, and c-d) 5 g load. In this case, the load was suspended from the top of the gel cylinder using a metal wire. Images a) and c) are before the experiment, and images b) and d) are after the experiment, respectively.

A close inspection of the gel sample showed a self-healing of the damaged area caused by the wire, albeit a tiny scar was still visible in the translucent gel. A similar behavior was observed with gels prepared at different concentrations between 7-9% w/v. The process could be repeated at least three times on the self-healed bridge without rest period obtaining comparable results.

3.3.4. Conclusion and Outlook

In conclusion, the polymer topology of DABCO-containing ionene hydrogelators **1-3**, defined by the disubstitution pattern of a phenylene dibenzamide core, was found to be critical for the macroscopic self-healing capacity of the corresponding hydrogels. In particular, the *ortho*-isomeric ionene **1** displayed superior shape persistent, self-standing, load-bearing and self-healing properties compared to its *meta*- and *para*-analogues. Interestingly, the healing process occurred without the need of involving oppositely charged species. Along with this line, the potential effect of counterions and the incorporation of polyanions on both the gelation ability and the self-healing properties of the hydrogels, as well as their use for biomedical applications, will be a focus of future research in our laboratory.

In cooperation with Prof. Carlos Aléman from the Universitat Politècnica de Catalunya (UPC) in Barcelona (Spain), computational calculations will be performed in order to gain a better understanding of the involved self-healing mechanism of the three different topomers. The results will be published together with the self-healing experiments.

3.3.5. Experimental Part

3.3.5.1. Materials and Methods

All chemicals were of analytical grade and used as received without any further purification. Deionized water was used for preparing the hydrogels. Synthesis of monomers and corresponding ionene polymers **1-3** and characterization, such as elemental analysis (EA), size-exclusion chromatography (SEC), thermal gravimetric analysis (TGA), differential scanning calorimetry (DSC), differential thermal analysis (DTA), Fourier-transform infra-red (FT-IR), UV-Vis-NIR, T_{gel} , oscillatory rheology, polarized optical microscopy (POM), TEM/FE-SEM were previously reported.¹⁰

^1H -NMR spectra were recorded on Avance 300 or Avance 400 spectrometers (Bruker, Billerica, MA, USA) at 25 °C. Chemical shifts for ^1H were reported as δ , parts per million (ppm), relative to the signal of the residual solvent (DMSO = 2.50 ppm, H_2O = 4.79 ppm). Coupling constants (J) are given in Hertz (Hz). The following notations indicate the multiplicity of the signals: s = singlet, bs = broad singlet, d = doublet, t = triplet, q = quartet, dd = doublet of doublets, m = multiplet. Estimated error of reported values: 0.01 ppm (δ , ^1H NMR), 0.1 Hz (J, coupling constant).

3.3.5.2. Synthesis of Monomers

To a stirred solution of the corresponding diaminobenzene (500 mg, 4.55 mmol) and Et_3N (1.6 mL, 11.4 mmol) in DCM (20 mL) at 0 °C was added dropwise a solution of 4-(chloromethyl)benzoyl chloride (1.75 g, 9.09 mmol) in DCM (20 mL) via a pressure-compensated addition funnel. The reaction mixture was allowed to warm to RT and stirred for 0.5-2 h after which time TLC analysis showed full conversion of the starting materials. The organic phase was washed with H_2O (2x 15 mL) and brine (2x 15 mL), dried over anhydrous Na_2SO_4 , filtered, and concentrated via a rotary evaporator. The solid residue thus obtained was recrystallized from DCM/pentane, affording the desired bifunctional monomers as crystalline solids. Ortho-monomer: 96% yield (1.81 g, 4.37 mmol), white crystalline solid. Meta-monomer: 87% (1.64 g, 3.96 mmol), white slight brownish solid. Para-monomer: 91% (1.71 g, 4.14 mmol), off-white solid. The corresponding spectroscopic data matched those reported in the literature.¹⁰

^1H -NMR (DMSO- d_6 , 300 MHz) for **4**: δ (ppm) = 10.08 (s, 2H), 7.96 (d, J = 8.2 Hz, 4H), 7.67 (dd, J = 6.0, 3.6 Hz, 2H), 7.58 (d, J = 8.3 Hz, 4H), 7.30 (dd, J = 6.0, 3.5 Hz, 2H), 4.83 (s, 4H).

$^1\text{H-NMR}$ (DMSO-d_6 , 300 MHz) for **5**: δ (ppm) = 10.36 (s, 2H), 8.33 (t, J = 1.9 Hz, 1H), 7.98 (d, J = 8.3 Hz, 4H), 7.59 (d, J = 8.3 Hz, 4H), 7.51 (dd), 4.80 (s, 4H).

$^1\text{H-NMR}$ (DMSO-d_6 , 300 MHz) for **6**: δ (ppm) = 10.28 (s, 2H), 7.97 (d, J = 8.3 Hz, 4H), 7.76 (s, 4H), 7.59 (d, J = 8.4 Hz, 4H), 4.85 (s, 4H).

3.3.5.3. Synthesis of Polymers

To a stirred solution of the corresponding monomers (0.82 g, 2.00 mmol) in DMF (15, 45 or 25 mL, respectively) at 80 °C was added 1,4-diazabicyclo[2.2.2]octane (DABCO) (0.22 g, 2.00 mmol) in one portion. The reaction mixture was stirred at 80 °C for 2-3 days, after which time TLC analysis showed full conversion of the starting materials. The mixture was cooled down to RT and the precipitated polymers (**1**, **2** or **3**, respectively) thus obtained were isolated by filtration, washed subsequently with DMF, DCM and CH_2Cl_2 , and finally dried under vacuum. Ionene **1**: 98% yield (1.15 g, 1.96 mmol), white solid. Ionene **2**: 69% yield (0.81 g, 1.38 mmol), off-white slight brownish solid. Ionene **3**: 90% yield (1.08 g, 1.80 mmol), off-white solid. Spectroscopic data matched those reported in the literature.¹⁰

$^1\text{H-NMR}$ (D_2O , 300 MHz) for **1**: δ (ppm) = 7.86 – 7.26 (m, 6H), 4.54 – 4.18 (m, J = 6.7 Hz, 1H), 3.93 – 3.66 (m, J = 28.2, 12.4 Hz, 4H), 3.42 – 3.18 (m, J = 15.8, 6.9 Hz, 2H), 3.13 – 2.94 (m, J = 12.7, 6.7 Hz, 2H).

$^1\text{H-NMR}$ (D_2O , 300 MHz) for **2**: δ (ppm) = 8.00 – 7.18 (m, 6H), 4.44 (s, 1H), 3.91 (s, 4H), 3.34 (d, J = 6.6 Hz, 2H), 3.05 (d, J = 6.2 Hz, 2H).

$^1\text{H-NMR}$ (D_2O , 300 MHz) for **3**: δ (ppm) = 7.88 (s, 2 H), 7.72 – 7.39 (m, 4H), 4.67 – 4.23 (m, 1H), 3.82 (bs, 4H), 3.33 (bs, 2H), 3.05 (bs, 2H).

3.3.5.4. Preparation of Hydrogels

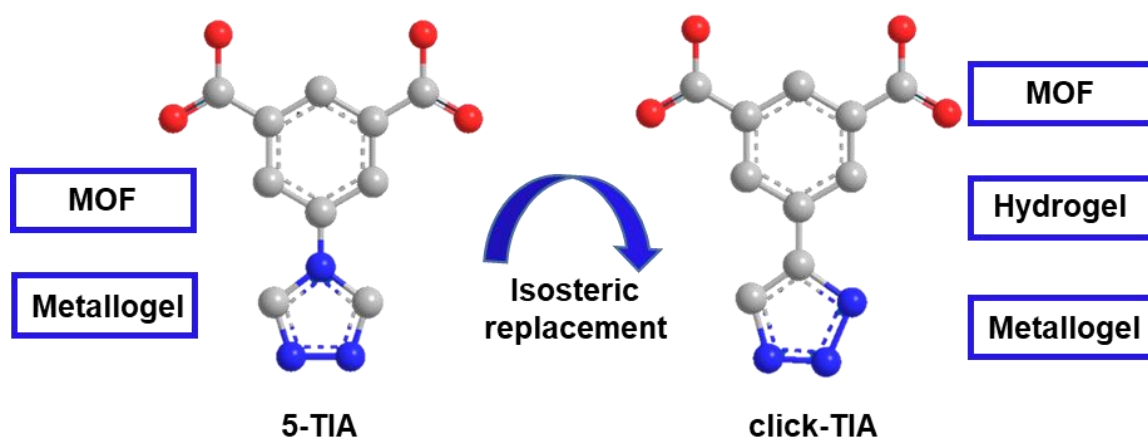
Typically, a weighted amount of the corresponding polymer **1**, **2** or **3** was placed into a screw-capped glass vial (4 mL volume) and after addition of deionized water, the mixture was gently heated with a heat gun until the solid material was completely dissolved. The resulting isotropic solution was then spontaneously cooled down to RT. No control over temperature rate during the heating-cooling process was applied. The material was preliminarily classified as “gel” if it did not exhibit gravitational flow upon turning the vial upside-down at RT.

3.3.6. References

- [1] S. Van der Zwaag, Self-healing materials: An Alternative Approach to 20 Centuries of Materials Science, Springer, Dordrecht, **2007**.
- [2] J. M. Lehn, *Prog. Polym. Sci.*, **2005**, *30*, 814–831.
- [3] Z. Qi, C. A. Schalley, *Acc. Chem. Res.*, **2014**, *47*, 2222–2233.
- [4] A. Phadke, C. Zhang, B. Arman, C.-C. Hsu, R. A. Mashelkar, A. K. Lele, M. J. Tauber, G. Arya, S. Varghese, *Proc. Natl. Acad. Sci.*, **2012**, *109*, 4383–4388.
- [5] H. Wei, Y. Wang, J. Guo, N. Z. Shen, D. Jiang, X. Zhang, X. Yan, J. Zhu, Q. Wang, L. Shao, H. Lin, S. Wei, Z. Guo, *J. Mater. Chem. A*, **2015**, *3*, 469–480.
- [6] F. Luo, T. L. Sun, T. Nakajima, T. Kurokawa, A. Bin Ihsan, X. Li, H. Guo, J. P. Gong, *ACS Macro Lett.*, **2015**, *4*, 961–964.
- [7] F. Luo, T. L. Sun, T. Nakajima, T. Kurokawa, Y. Zhao, K. Sato, A. Bin Ihsan, X. Li, H. Guo, J. P. Gong, *Adv. Mater.*, **2015**, *27*, 2722–2727.
- [8] A. Bin Ihsan, T. L. Sun, T. Kurokawa, S. N. Karobi, T. Nakajima, T. Nonoyama, C. K. Roy, F. Luo, J. P. Gong, *Macromolecules*, **2016**, *49*, 4245–4252.
- [9] Y. Huang, P. G. Lawrence, Y. Lapitsky, *Langmuir*, **2014**, *30*, 7771–7777.
- [10] J. Bachl, D. Zanuy, D. E. López-Pérez, G. Revilla-López, C. Cativiela, C. Alemán, D. D. Díaz, *Adv. Funct. Mater.*, **2014**, *24*, 4893–4904.
- [11] J. Bachl, O. Bertran, J. Mayr, C. Alemán, D. D. Díaz, *Soft Matter*, **2017**, *13*, 3031–3041.
- [12] J. Mayr, J. Bachl, J. Schlossmann, D. D. Díaz, *Int. J. Mol. Sci.*, **2017**, *18*, 303.
- [13] J. Mayr, S. Grijalvo, J. Bachl, R. Pons, R. Eritja, D. D. Díaz, *Int. J. Mol. Sci.*, **2017**, *18*, 1139.
- [14] E. S. Dragan, J. Mayr, M. Häring, A. Irina, D. D. Díaz, *ACS Appl. Mater. Interfaces*, **2016**, *8*, 30908–30919.
- [15] M. Tiffner, K. Zielke, J. Mayr, M. Häring, D. D. Díaz, M. Waser, *ChemistrySelect*, **2016**, *1*, 4030–4033.
- [16] Y. Li, J. Rodrigues, H. Tomás, *Chem. Soc. Rev.*, **2012**, *41*, 2193–2221.
- [17] P. J. Kondiah, Y. E. Choonara, P. P. D. Kondiah, T. Marimuthu, P. Kumar, L. C. du Toit, V. Pillay, *Molecules*, **2016**, *21*, 1580.
- [18] M. Liu, X. Zeng, C. Ma, H. Yi, Z. Ali, Z. Mou, S. Li, Y. Deng, N. He, *Bone Res.*, **2017**, *5*, 17014.
- [19] G. Tozzi, A. De Mori, A. Oliveira, M. Roldo, *Materials*, **2016**, *9*, 267.

- [20] M. Mehrali, A. Thakus, C. P. Pennisi, S. Talebian, A. Arpanaei, M. Nikkhah, A. Dolatshahi-Pirouz, *Adv. Mater.*, **2017**, 29, 1603612.

3.4. Isosteric Substitution of 4*H*-1,2,4-Triazole by 1*H*-1,2,3-Triazole in Isophthalic Derivative for Tuning Self-Assembly of Soft Supramolecular Materials



The first part of this chapter has been published in:

M. Häring, J. Rodríguez-López, S. Grijalvo, M. Tautz, R. Eritja, V. S. Martín, D. D. Díaz, 'Isosteric substitution of 4*H*-1,2,4-triazole in isophthalic derivative enabled hydrogel formation for controlled drug release', *Mol. Pharm.* **2018**, doi: 10.1021/acs.molpharmaceut.7b01049. – Reprinted with permission from *Mol. Pharm.* **2018**, doi: 10.1021/acs.molpharmaceut.7b01049. Copyright © 2018 American Chemical Society.

Author contribution:

MH prepared and characterized the gels and performed drug release experiments. JRL synthesized **click-TIA**. MT synthesized **5-TIA**. SG did the toxicity tests. All authors contributed to the scientific discussion of the results.

3.4.1. Abstract

In this chapter, the simple substitution of the 1,2,4-triazole moiety in 5-(4*H*-1,2,4-triazol-4-yl)isophthalic acid (**5-TIA**) by the 1*H*-1,2,3-triazol-5-yl unit, affording its isostere **click-TIA**, is described and the different gelation behavior is investigated.

The first part deals with the observation that the **click-TIA** undergoes self-assembly in water upon sonication, in sharp contrast to its isostere **5-TIA**, leading to the formation of stable supramolecular viscoelastic hydrogels. Hydrogels made of **click-TIA** as well as hybrid hydrogels made of the mixture **click-TIA** and **5-TIA** (molar ratio 1:0.2) were used to compare different properties of the materials (*i.e.* rheological properties, thermal properties, mechanical stability, morphology). In terms of toxicity, neither **click-TIA** nor **5-TIA** showed cytotoxic effects on the cellular viability of HeLa cells when compared to untreated cells incubated with DMSO. This allowed using the hydrogels for the encapsulation and *in vitro* controlled release experiments of oxytetracycline (OXT) that followed first-order kinetics. The drug release was investigated in different delivery systems at different pH values, ranging between pH 1.2 and pH 10, which demonstrated a pH-dependant release behavior of the hybrid system.

The second part describes the investigation of **click-TIA** to form metallogels in the presence of Cu(OAc)₂·H₂O (CuA) whereas **5-TIA** forms only metallogels in the presence of Ca(OAc)₂. The gel formation between **click-TIA** and CuA could be obtained at different concentrations, ratios and solvents (*i.e.* DMF, DMA and pyridine), wherefore three metallogel formulations in DMF (metallogel-1, -2 and -3 with **click-TIA**:CuA ratio 0.2 M:0.1 M, 0.2 M:0.2 M, and 0.2 M:0.3 M, respectively) and the corresponding xerogels were further investigated and characterized with respect to rheological behavior, thermal stability, spectroscopic properties and morphology.

3.4.2. Introduction

Supramolecular gels have gained great attention due to their potential applications in diverse fields including, among others, biomedicine,¹ sensors,² catalysis,³ environmental remediation,⁴ and material synthesis.⁵ These gel materials are made by self-assembly of either low-molecular weight (LMW) gelators or polymers, via non-covalent interactions (e.g., hydrogen-bonding, van der Waals, π - π stacking, charge-transfer, coordination interactions, etc).⁶ The solid-like appearance of these materials and their rheological properties are the result of the immobilization of the liquid phase (major component) in the interstices of an entangled self-assembled solid matrix usually by capillary forces.⁷

The design of new functional gels is difficult due to the lack of information about the molecular self-assembly process and many systems have been discovered by serendipity. Nevertheless, there are some strategies to obtain a more rational design route toward new gels, which are based on either a molecular engineering approach or on structure-property correlation.⁸

A few years ago, our group demonstrated that the isosteric replacement,⁹ a well-established paradigm in medicinal chemistry could be successfully applied to the synthesis of new supramolecular gels with tailored functionality.¹⁰ Isosters¹¹ have been defined by Burger as compounds or groups that possess near-equal molecular shapes and volumes, approximately the same distribution of electrons, with similar physical properties.¹² As a proof-of-concept, the gelation ability of *N*-stearyl-L-glutamic acid (**C₁₈-Glu**) was compared to its isostere namely **click-Glu**, where the 1,4-disubstituted 1,2,3-triazole unit replaced the amide moiety in **C₁₈-Glu** (Figure 1).¹⁰

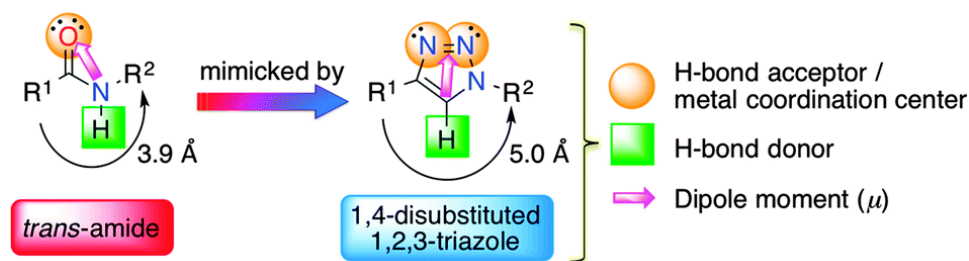


Figure 1. Main structural features of disubstituted *trans*-amides and 1,2,3-triazoles for their consideration as bioisosteres. Reproduced from ref. 10 with permission of The Royal Society of Chemistry.

The results showed that **click-Glu** displayed superior features with respect to CGC, *gel*-to-*sol* transition temperature (T_{gel}) and mechanical stabilities in polar protic solvents, whereas **C₁₈-Glu** exhibited improved properties in nonpolar solvents. Furthermore, co-assembly of both

isosteres was proved to be a useful approach for fine-tuning the release of the antibiotic vancomycin. In addition, it should not be underestimated that triazole nucleus is one of the most well-known and important heterocycles which constitute a core structural component in a large variety of natural and medicinal products. Indeed, the broad and potent activity of triazoles and their derivatives has established them as pharmacologically significant scaffolds.

More recently, the use of 5-(4*H*-1,2,4-triazol-4-yl)isophthalic acid (**5-TIA**) was reported for the preparation of unprecedented 3D porous, crystalline metal-organic framework (MOF) and metallo-organogels using Ca^{2+} as metal ion (Figure 2, top).¹³

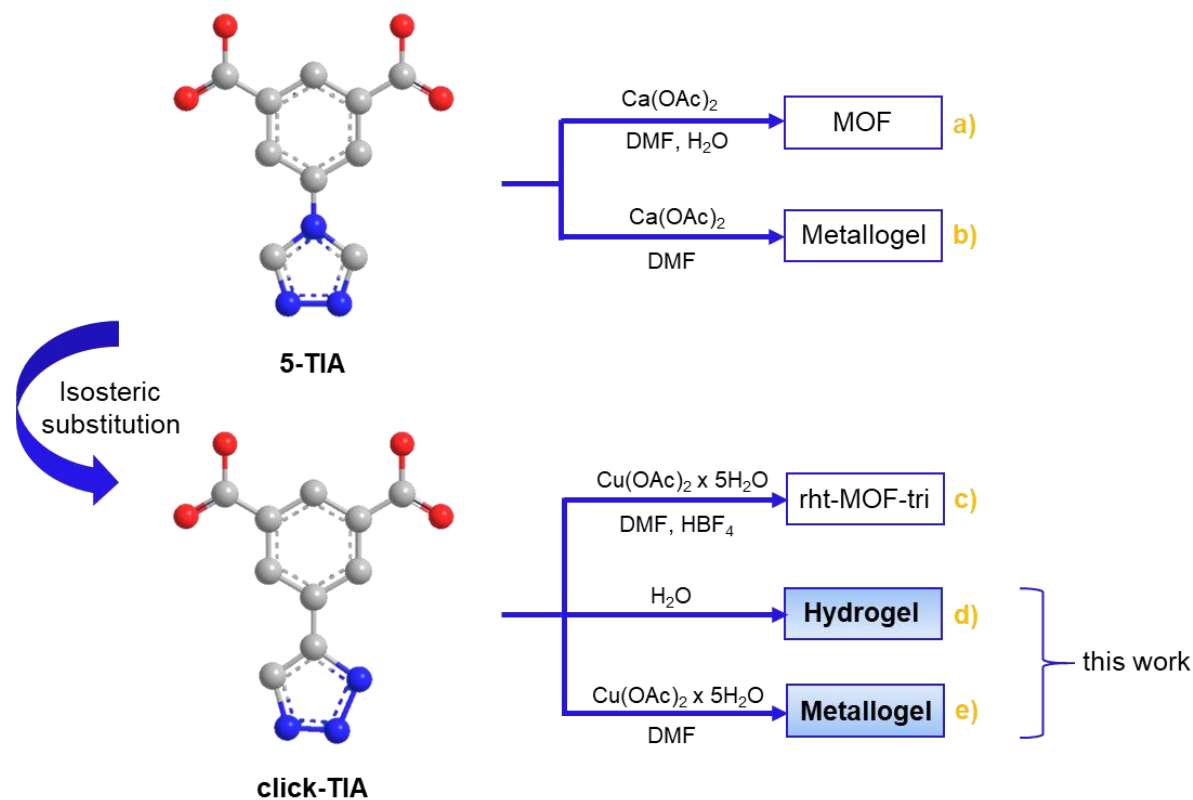


Figure 2. Relevant uses of a) **5-TIA** and c) **click-TIA** as building blocks for the preparation of MOFs; and b), d-e) gel-based materials.

In good agreement with the delicate balance existing between gelation and crystallization,¹⁴ the only presence of water in the solvent system was found to favor the formation of crystalline Ca-MOF (space group *Cmca*) (Figure 2a), whereas pure organic solvent induces gelation (Figure 2b). Interestingly, the xerogel obtained by freeze-drying the corresponding metallo-organogel showed 20% higher CO_2 -uptake than the crystalline MOF at 1 atm and 298 K. The use of 5-(1*H*-1,2,3-triazol-5-yl)isophthalic acid (**click-TIA**), which can be considered as an isostere of **5-TIA**, yielded rht-MOF-tri (space group *Fm3m*) (Figure 2c).¹⁵

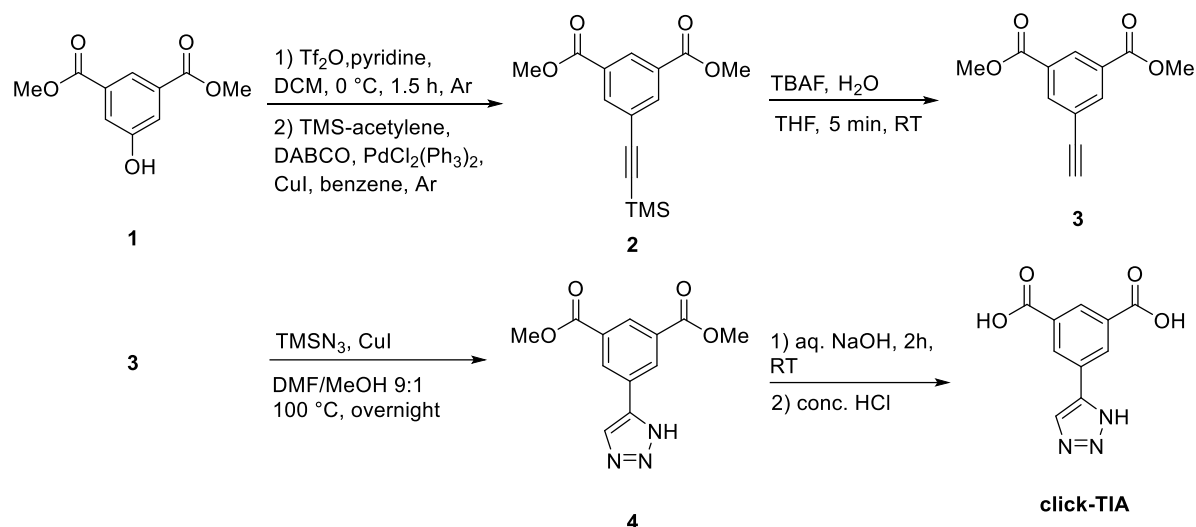
In the following, the synthesis and the intrinsic gelation ability of **click-TIA** as hydro- and metallogelator will be discussed and the obtained gels characterized.

3.4.3. Results and Discussion

3.4.3.1. Synthesis of TIA Derivatives

Click-TIA was synthesized in four steps starting from commercially available dimethyl 5-hydroxyisophthalate (**1**, Scheme 1).

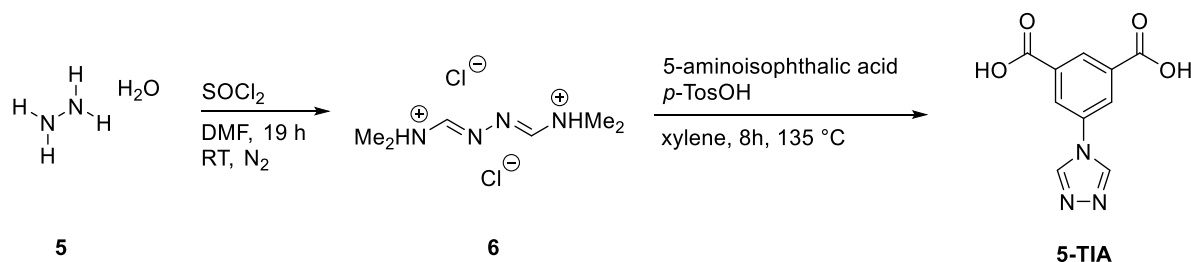
Scheme 1. The synthetic route for the preparation of **click-TIA**.



The alkyne unit was nearly quantitatively introduced into the aromatic ring by a classical Sonogashira cross-coupling reaction using trimethylsilylacetylene yielding the corresponding aromatic trifluoromethanesulfonate derivative **2**. Deprotection of trimethylsilyl (TMS) group of the alkyne with tetra-*n*-butylammonium fluoride (TBAF), and subsequent copper(I)-catalyzed azide-alkyne cycloaddition using azidotrimethylsilane as azide source afforded the expected 5-substituted-1*H*-1,2,3-triazole derivative **4** in excellent overall yield. Finally, alkaline hydrolysis of the ester groups yielded the desired **click-TIA** in nearly quantitative yield.

5-TIA was obtained as a white solid in two steps following a reported procedure with slight modifications (Scheme 2).¹³

Scheme 2. The synthetic route for the preparation of **5-TIA**.



The process involved the formation of an *N,N*-dimethylformohydrazoneamide derivative intermediate **6** from the reaction between hydrazine (**5**) and DMF, followed by cyclization reaction in the presence of 5-aminoisophthalic acid in hot xylene, affording **5-TIA**.

3.4.3.2. Hydrogelation Ability of Click-TIA

The gelation ability of **5-TIA** was previously demonstrated in some organic solvents (*i.e.*, DMF, DMSO, DMA, quinoline, DEF) in combination with calcium acetate.¹³ Interestingly, the replacement of the 4*H*-1,2,4-triazole moiety by 1*H*-1,2,3-triazole afforded the isostere **click-TIA** which allowed the formation of stable hydrogels upon simple sonication of the mixture for ~ 2-3 min at RT, with a critical gelation concentration of 6 g L⁻¹ (0.026 mM) (Figure 3).

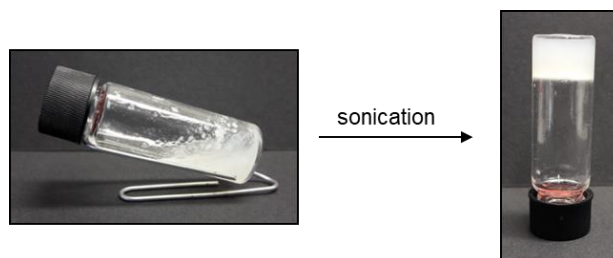


Figure 3. Gelation of **click-TIA** ($c = 6 \text{ g L}^{-1}$) in water upon sonication.

This value indicated the immobilization of ~ 2150 molecules of water per molecule of gelator, which is a common ratio among many known LMW gelators.¹⁶ The gelation time at concentrations $6 \leq c \text{ (g L}^{-1}\text{)} < 18$ varied between 30 and 60 min, whereas at $c > 18 \text{ g L}^{-1}$, hydrogels were formed immediately. In previous reports, sonication-induced gelation has been associated with the solvent cavitation.¹⁷ Because of the low water solubility of the gelator, it forms aggregated particles on water upon mixing at room temperature which could be associated to the entropic/hydrophobic effect. It is possible that the mechanical energy provided by ultrasound may help to destroy the initial assemblies and facilitate a new supramolecular organization through the entire sample leading to the formation of the gel network.

3.4.3.3. Characterization of Hydrogels

The visual appearance of so-formed hydrogels was white opaque, suggesting the formation of aggregates larger than the wavelength of visible light (about 380-780 nm), which was further confirmed by electron microscopy imaging (see below).

Moreover, the hydrogels did not show gravitational flow upon turning the vials upside-down and the gel nature was later confirmed by oscillatory rheological measurements. These gels

were observed to remain stable for at least one month under steady neutral or acidic conditions, but they also responded to several stimuli (Figure 4).

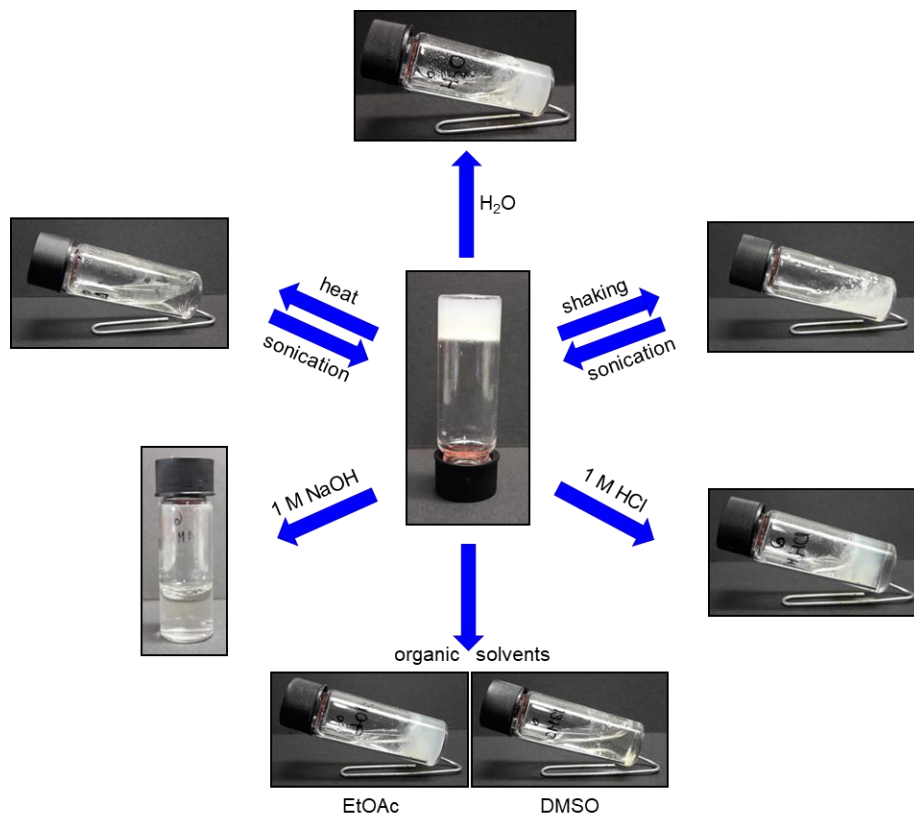


Figure 4. The response of the hydrogel made of click-TIA in H_2O ($c = 6 \text{ g L}^{-1}$) to various stimuli as described in the main text. Note: T_d of the freshly prepared gel was found to be the same than the reformed gel after thermal *gel-to-sol* transition and subsequent ultrasound treatment. Therefore, the thermal properties of the gel do not seem to be affected by the sonication process.

However, the addition of aqueous NaOH solution (1.0 M) caused the dissolution of the hydrogels within minutes leading to homogeneous clear solutions. In addition, the irreversible *gel-to-sol* transition was induced by the addition of DMSO on top of the hydrogel, whereas overlying other solvents such as EtOAc, EtOH, *i*-PrOH, and *n*-hexane did not cause gel disruption overnight. Gels at concentrations below 12 g L^{-1} , could form isotropic solutions upon heating and sonication induces gelation almost instantaneously even at the CGC (6 g L^{-1}), whereas gel formation by only sonication usually takes $\sim 3 \text{ h}$. In previous work, the beneficial effect of combining heating and sonication on the gelation kinetics of supramolecular gels was reported.¹⁷ In general, the gel phase destroyed either by heating or vigorous mechanical agitation could be easily restored by application of ultrasound.

Moreover, a good thermal stability up to 65°C was observed for the hydrogel prepared at the CGC (6 g L^{-1}). However, the bulk gel material did not show the typical *gel-to-sol*

thermoreversibility associated with most physical (or supramolecular) gels upon a heating-cooling cycle.¹⁸ For this reason, and to avoid confusion, the above temperature was defined as destruction temperature (T_d) instead of the classical *gel-to-sol* transition temperature (T_{gel}). Thus, T_d represents here the temperature when the entire bulk gel was no longer stable after inversion of the vial regardless of the fate of the phase (e.g., precipitate, solution). Preliminary results suggest an irreversible thermal transition to a stable crystalline phase. Interestingly, although no thermoreversibility (*i.e.*, *gel-to-sol* and subsequent *sol-to-gel* transition) was achieved with these materials upon a classical heating-cooling cycle, reversible transitions were achieved by heating hydrogels made of **click-TIA** at concentrations below 12 g L^{-1} (*i.e.*, *gel-to-sol* phase transition) and subsequent sonication of the obtained isotropic solutions for $\sim 2\text{-}3 \text{ min}$ (*i.e.*, *sol-to-gel* phase transition) (Figure 5).

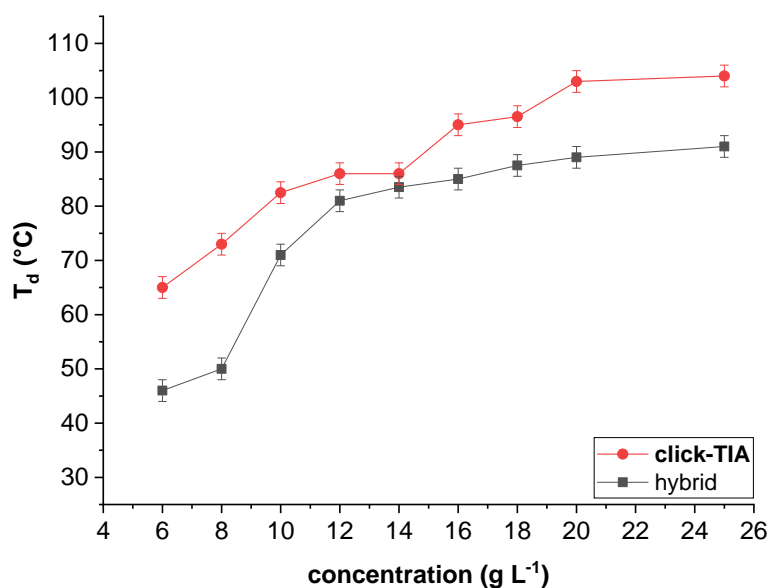


Figure 5. Evolution of T_d with gelator concentration for the gels made of **click-TIA** and **click-TIA + 5-TIA** (molar ratio 1:0.2).

As observed with other gels made of LMW compounds,^{18,19} the transition temperature gradually increased with the gelator concentration (Figure 5). Astonishingly, T_d reached a value of $104 \text{ }^{\circ}\text{C}$, slightly above the boiling point of water, when the concentration of **click-TIA** was adjusted to 25 g L^{-1} . Concentrations above this value were not evaluated in this work. In a previous report, the use of a supramolecular co-assembly strategy for fine-tuning the properties of hydrogels could be successfully used for drug delivery applications.²⁰ With this in mind, stable gels could also be made of **click-TIA/5-TIA** mixtures at different molar ratios, with **click-TIA** always being the major component. The incorporation of **5-TIA** into the gel formulation (*i.e.*, **click-TIA/5-TIA** = 1:0.2) caused a decrease of the transition temperature in

~ 20 °C at low concentrations, whereas this difference was reduced to ~ 10 °C at higher concentrations, allowing to reach a T_d as high as 90 °C at 25 g L⁻¹.

FT-IR spectroscopy was measured of the solid gelators and xerogels, obtained by freeze-drying the corresponding hydrogels (Figure 6).

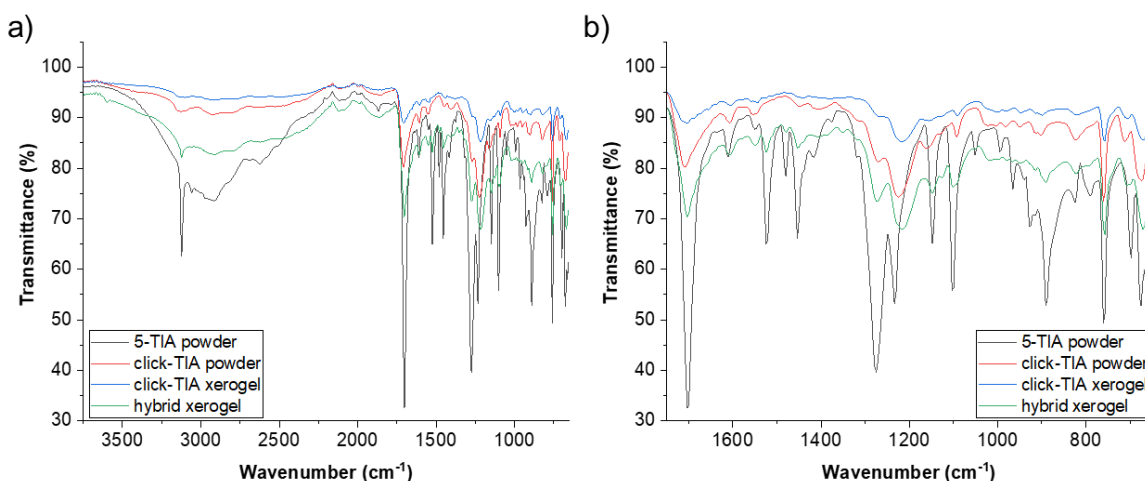


Figure 6. Comparative FT-IR spectra of **click-TIA** as synthesized (powder) and xerogel obtained from the corresponding hydrogel ($c = 19$ g L⁻¹), **5-TIA** as synthesized (powder) and hybrid xerogel derived from the hydrogel made of **click-TIA** and **5-TIA** (molar ratio 1:0.2; $c = 19$ g L⁻¹), a) complete spectrum, b) spectrum from 1750 – 750 cm⁻¹.

The solid **click-TIA** and the corresponding xerogel showed no major differences in the characteristic infrared absorption bands, suggesting that the gelator could also be aggregated, at least to some extent, involving intuitive hydrogen bonding and π -stacking interactions in its solid state similarly to that in the gel phase. The following expected absorption regions were clearly identified: 3300-2500 cm⁻¹ (O-H and aromatic C-H stretching, triazole ring); 1718-1670 cm⁻¹ (C=O stretching of aromatic carboxylic acid); 1650-1530 cm⁻¹ (aromatic C=C bending); 1468-1382 cm⁻¹ (O-H bending; C-N stretching); 1170-1110 cm⁻¹ (C-O, C-N, N=N and C=C stretching); 1010-890 cm⁻¹ (C=C, C-O and C-N stretching, O-H bending); 750-680 cm⁻¹ (aromatic C-H bending). The broad region with overlapped frequencies between 3300 and 2500 cm⁻¹ is typically observed in hydrogen bond-forming aggregates. On the other hand, the hybrid xerogel made of **click-TIA** and **5-TIA** displayed evident frequencies of both compounds.

The potential similarities between the aggregation mode of **click-TIA** in the solid state and in the gel state were further confirmed by powder X-ray diffraction (PXRD, Figure S2). The spectrum of as synthesized solid **click-TIA** demonstrated a mesoscale ordering with reflexes centered at $2\theta = 21.95^\circ, 25.70^\circ, 27.35^\circ, 27.52^\circ, 27.77^\circ, 31.69^\circ, 45.44^\circ, 56.45^\circ, 66.25^\circ, 75.28^\circ$

and 83.99° , corresponding to lattice spacings d of 4.05 Å, 3.46 Å, 3.26 Å, 3.24 Å, 3.21 Å, 2.82 Å, 1.99 Å, 1.63 Å, 1.41 Å, 1.26 Å and 1.15 Å, respectively (calculated from Bragg's law) (Figure S1). An almost identical crystalline pattern was obtained for the xerogel material obtained after freeze-drying the corresponding hydrogel, suggesting the preservation of the potential crystal packing of **click-TIA** in the gel phase, even in the presence of **5-TIA** (*i.e.*, hybrid hydrogel).

The weak and brittle nature of these gels was confirmed by oscillatory rheological experiments (Figure 7). Measurements were performed with the gels that were selected for subsequent drug release studies (see below), *i.e.* **click-TIA** and hybrid **click-TIA:5-TIA** (molar ratio 1:0.2), both at $c = 19 \text{ g L}^{-1}$.

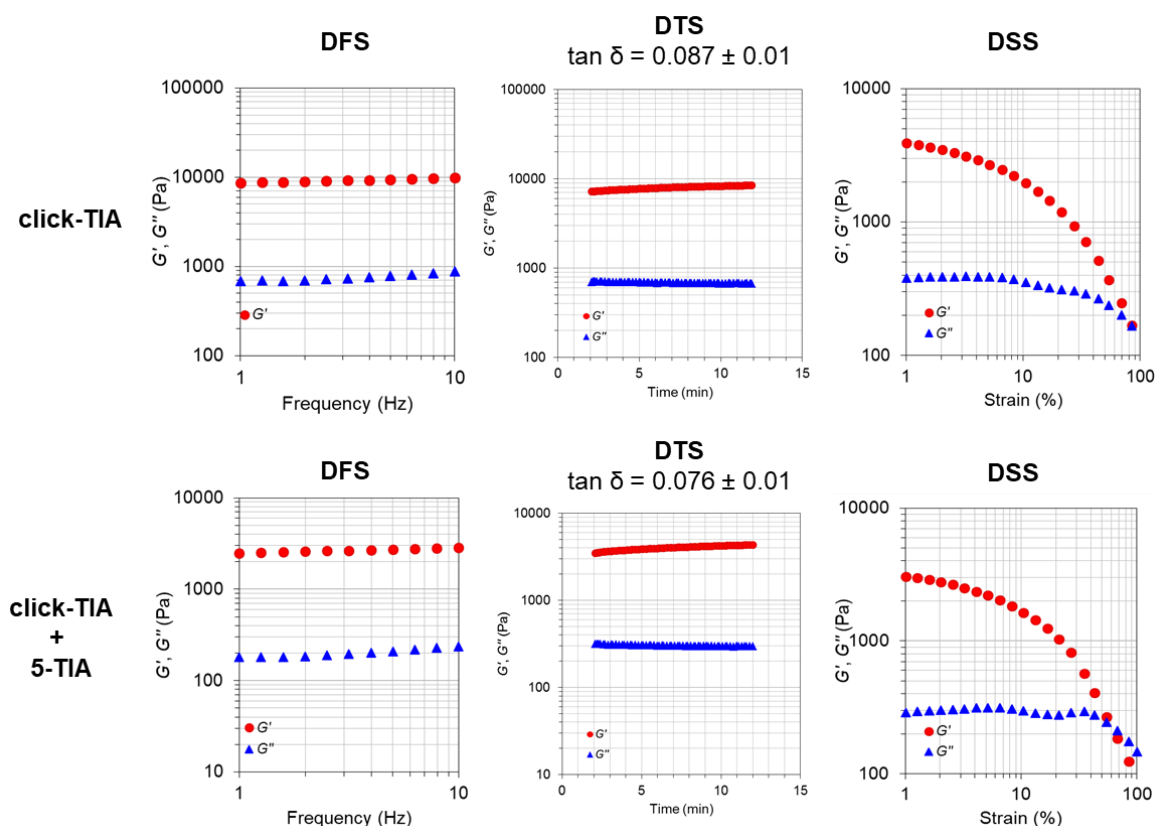


Figure 7. Oscillatory rheological experiments of hydrogel systems selected for drug delivery studies: top: gel made of **click-TIA** ($c = 19 \text{ g L}^{-1}$), bottom: hybrid hydrogel made of **click-TIA:5-TIA** (molar ratio 1:0.2, $c = 19 \text{ g L}^{-1}$).

In good agreement with viscoelastic network-like structures, the rheological data showed that the elastic component or storage modulus (G') was one order of magnitude higher than the viscous component or loss modulus (G'') for both gel systems, maintaining also a weak frequency dependence ($G' \approx \omega^{0.05}$). The incorporation of a small amount of **5-TIA** into the hydrogel formulation reduced the storage modulus to about half its value compared to the

pure **click-TIA** gel. Moreover, the $\tan \delta$ (G''/G') value was slightly lower for the hybrid gel, whereas the critical stress or yield point (γ) was significantly higher for the **click-TIA** gel. These results indicate that the **click-TIA** gel has the greater mechanical stability and damping coefficient, thus being more efficient in effectively accomplishing energy absorption and dispersal.

Field emission scanning electron microscopy (FE-SEM) of the above-mentioned model gels was recorded to gain insights about the microstructure of these materials (Figures 8, Figure S3-S6).

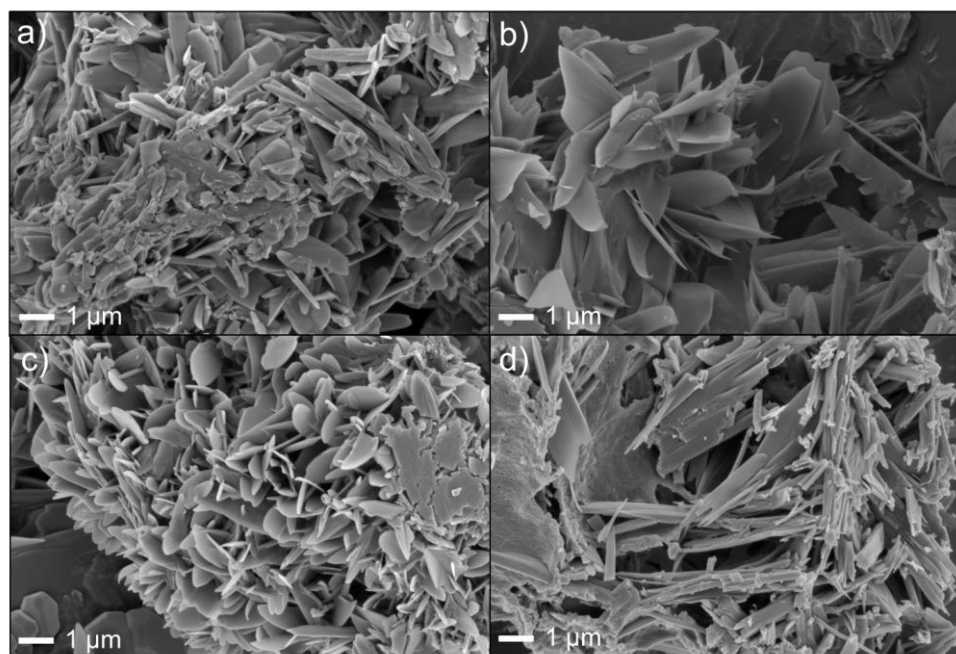


Figure 8. Representative FE-SEM images of xerogels prepared by freeze-drying the corresponding hydrogels derived from a) **click-TIA** ($c = 19 \text{ g L}^{-1}$), b) **click-TIA** + **5-TIA** (molar ratio 1:0.2, overall $c = 19 \text{ g L}^{-1}$), c) **click-TIA** ($c = 19 \text{ g L}^{-1}$) + OXT ($c = 0.8 \text{ g L}^{-1}$), d) **click-TIA** + **5-TIA** (molar ratio 1:0.2, overall $c = 19 \text{ g L}^{-1}$) + OXT ($c = 0.8 \text{ g L}^{-1}$).

Samples obtained from the hydrogel made of **click-TIA** showed clustered structures with elongated aggregates in the form of leaves of micrometer diameters, resembling some flowering plants like *Kleinia neriifolia* (i.e., endemic plant of the Canary Islands known as Verode) (Figure 8a). The incorporation of oxytetracycline hydrochloride (OXT), the drug selected for release studies, in these hydrogels did not cause significant changes in the morphology observed for the pristine gels (Figure 8c), suggesting a good robustness of the gel network for the encapsulation of therapeutic molecules. In the case of the hybrid hydrogel made of **click-TIA** and **5-TIA** (molar ratio 1:0.2), the globular and leaves-like aggregates were still observed in some areas (Figure 8b), even after incorporation of OXT, albeit fibrillar

features with high aspect ratio and extended laminar structures were mainly observed in the bulk material (Figure 8d).

3.4.3.4. *In Vitro* Cytotoxicity Evaluation of Click-TIA and 5-TIA

To determine the toxicity levels of **click-TIA** and **5-TIA**, a broad range of concentrations (*i.e.*, 2.3×10^{-4} , 9.3×10^{-4} , 1.9×10^{-3} , 2.3×10^{-3} , 9.3×10^{-3} , and 3.7×10^{-2} g L⁻¹, respectively) were screened by incubating the corresponding amount of both derivatives in the presence of HeLa cells for a period of 24 h (Figure 9).

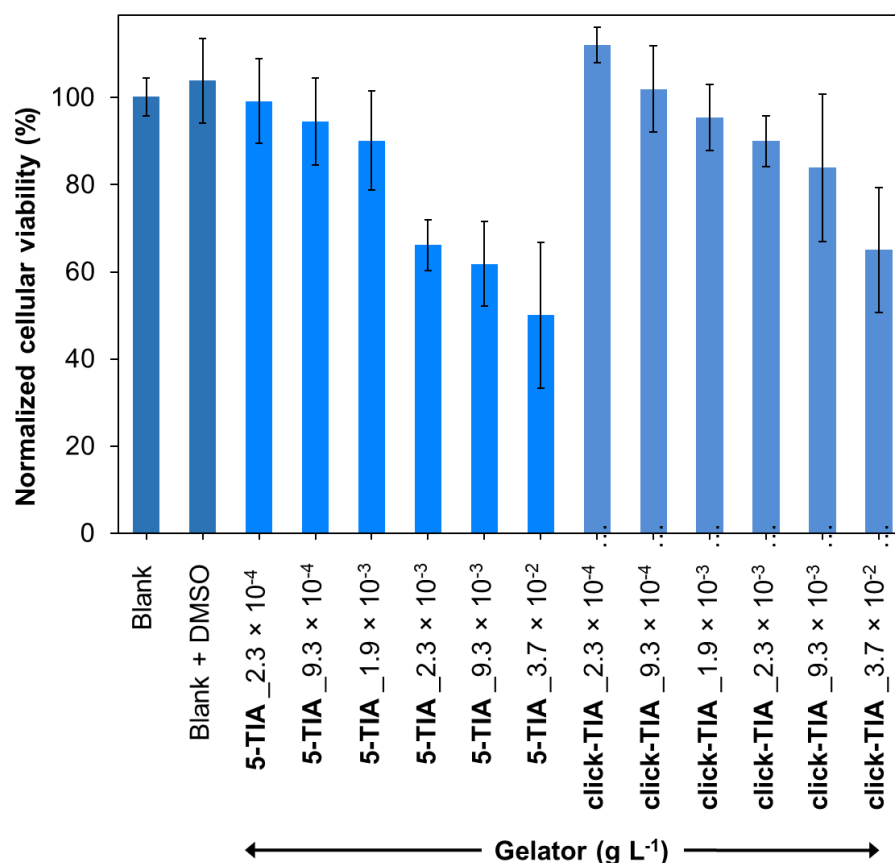


Figure 9. Cellular viabilities of HeLa cells in the presence of **click-TIA** and **5-TIA** at specified concentrations according to the MTT colorimetric assay.

Under our experimental conditions, **click-TIA** and **5-TIA** did not show any cytotoxic effect on cellular viability up to 1.9×10^{-3} g L⁻¹ (90 and 95%, respectively) when compared to untreated cells incubated with DMSO (0.5%; v/v). However, the cellular viability profile of both compounds remarkably differed at high concentrations (2.3×10^{-3} , 9.3×10^{-3} , and 3.7×10^{-2} g L⁻¹). While cell viability decreased with the increase of the **5-TIA** concentration (66%, 61%, and 50% at 2.3×10^{-3} , 9.3×10^{-3} , and 3.7×10^{-2} g L⁻¹, respectively), the cellular proliferation, in the case of **click-TIA** derivative, was less affected at the same concentrations

(89%, 83%, and 65%) and prolonging the incubation time. These results indicate the suitability of **click-TIA** to be used as part of hydrogel formulations for *in vitro* drug release applications.

3.4.3.5. OXT Encapsulation and Release *in Vitro*

The possibility of preparing hydrogels at different pH values using non-toxic **click-TIA** makes them an ideal candidate to evaluate their ability for the encapsulation and controlled release of OXT (used in the form of hydrochloride salt) as model water-soluble therapeutic cargo.²¹ OXT is a broad-spectrum antibiotic, isolated from the actinomycete *Streptomyces rimosus* and active against a wide variety of Gram-positive and Gram-negative bacteria.²² Nowadays, it is mainly used to treat acne, flare-ups of chronic bronchitis, and infections caused by *Chlamydia* (e.g., trachoma, urethritis) and *Mycoplasma* organisms (e.g., pneumonia). The release of OXT from other hydrogel systems, mainly polymer gels, has been also reported.²³ In addition, light absorption of OXT does not overlap with that of **click-TIA** (Figure S7, top), which is ideal for drug delivery studies with the tested gel formulations.

UV-vis spectra of OXT hydrochloride dissolved in PBS buffer (0.01 M) were recorded to build the calibration curve based on the maximum absorption peak of OXT at 353 nm (Figure S7, bottom). It is worth mentioning that the absorption spectrum of OXT stays nearly unchanged regardless of the pH, although tetracyclines usually show a complex acid-base behavior in aqueous solutions. In this work, for release experiments, the content of OXT embedded in each hydrogel system corresponded to 0.8 g L⁻¹ (100% loading efficiency). Moreover, no leaching of **click-TIA** was detected from the bulk gels during the equilibration period and release experiments. Figure 10 displays selected cumulative drug release profiles using the hydrogels made of **click-TIA** (Figure 10a) or the mixture **click-TIA:5-TIA** (Figure 10b) at different pH values (*i.e.*, pH 1.2 – 10, c = 19 g L⁻¹).

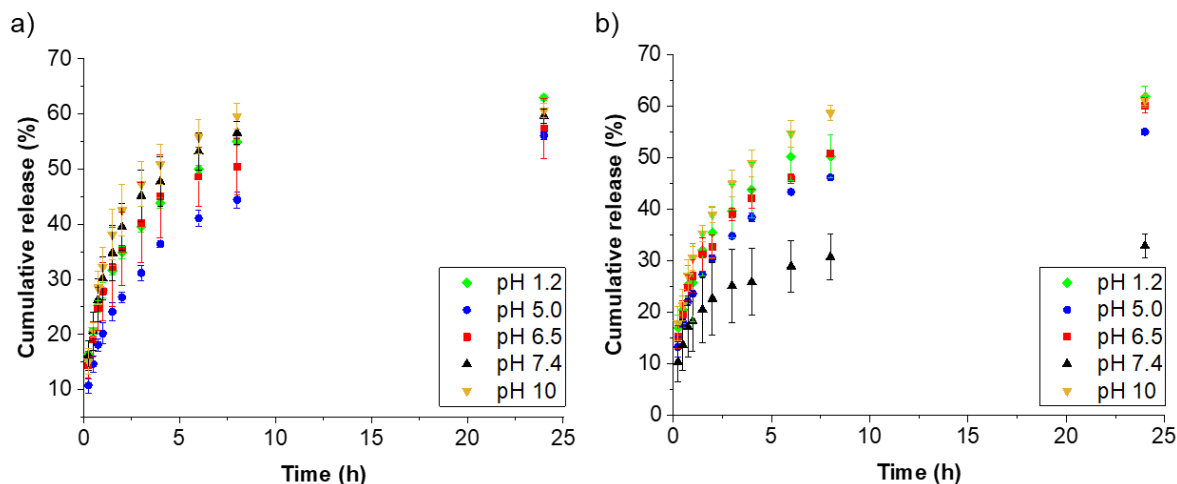


Figure 10. Representative *in vitro* release curves of OXT obtained at 37 °C at different pH values from gels made of a) **click-TIA** ($c = 19 \text{ g L}^{-1}$) and b) hybrid-2 (*i.e.* **click-TIA:5-TIA** 1:0.2; overall $c = 19 \text{ g L}^{-1}$). PBS was used as the release medium. Additional plots corresponding to other gel compositions at different pH values and fitting curves obtained from Higuchi, Korsmeyer-Peppas, and Weibull models are given in the ESI.

In the case of the hydrogel made of **click-TIA**, a plateau drug release zone (about 60%) was reached in $\sim 8 \text{ h}$ (Figure 10a). Although this is similar to the release pattern observed from some polymeric gel matrices, it should be noted that chemical and physical gels do not necessarily share the same transport mechanisms, and hence, the comparison should be made cautiously. The estimated release kinetics from **click-TIA** gels was comparable for pH values between 6.5 and 10. However, the release rate was reduced to about half of its value at pH values between 1.2 and 6.5, achieving the same maximum drug concentration (about 60%) in $\sim 17 \text{ h}$. Thus, the use of hybrid hydrogels made of **click-TIA** + **5-TIA** allowed the reduction of the release rate at $\text{pH} \leq 6.5$ (Figure 10b). Similar kinetics and plateau concentrations to those obtained with the **click-TIA** gel were also observed for the hybrid hydrogel in the range of pH studied, except for pH 7.4, where the maximum released drug was $\sim 33\%$. Nevertheless, the amount of **5-TIA** in the gel formulation (*i.e.*, within the limits that allowed the formation of stable gels) seemed to play a specific effect on the release kinetics at pH 7.4. The release rate observed in the hybrid formed by **click-TIA** + **5-TIA** at molar ratios of 1:0.1 and 1:0.4 were similar, whereas that at a molar ratio of 1:0.2 was significantly slower (Figure 11a).

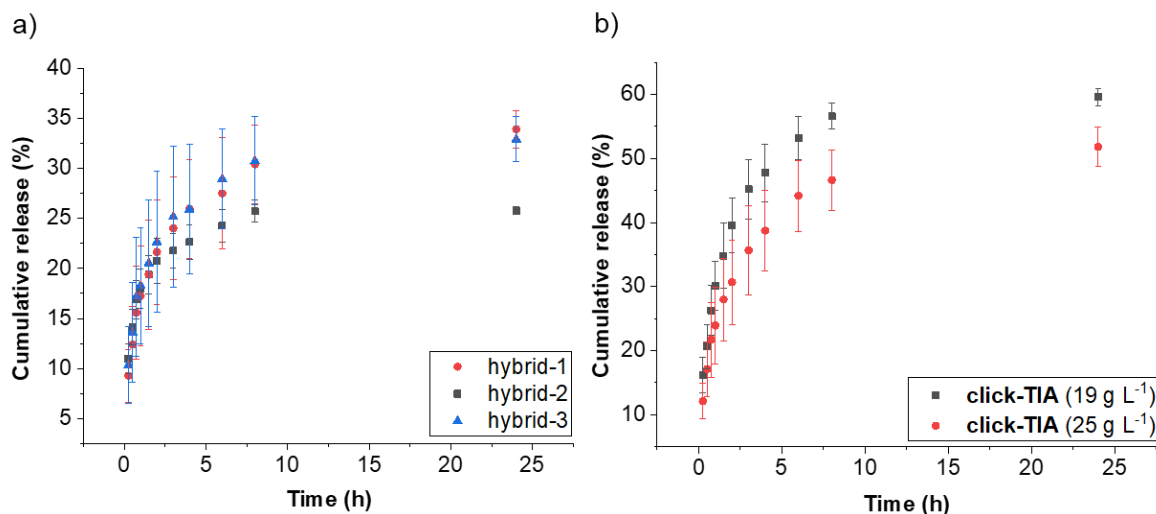


Figure 11. Representative *in vitro* release curves of OXT obtained at 37 °C at pH 7.4 with different gel compositions, a) hybrid-1 (i.e., **click-TIA:5-TIA** 1:0.1), hybrid-2 (i.e., **click-TIA:5-TIA** 1:0.2), hybrid-3 (i.e., **click-TIA:5-TIA** 1:0.4), b) **click-TIA** at $c = 19$ and 25 g L^{-1} .

Furthermore, both the release rate and final drug concentration could be reduced in $\sim 10\%$ by simply increasing 1.3-fold the gelator concentration, which increased the entanglement and stability of the gel network (Figure 11b).

The foregoing results suggest that the gel network may act as a pH-responsive drug reservoir, which undergoes expansion at alkaline pH due to deprotonation events weakening the supramolecular structure and allowing a faster drug release. Considering the pK_a values of model unsubstituted 1,2,3-triazole (~ 9.3) and isophthalic acid (~ 3.46 and ~ 4.46), it seems reasonable that protonation/deprotonation events at the carboxylic acid groups play a significant role on the release process. Thus, pH-induced conformation changes of the supramolecular gel networks due to strong electrostatic interactions constitute a plausible scenario. Moreover, the evolution of zwitterionic OXT at pH 5.0 to anionic OXT at higher pH (e.g., at pH 8.9 monoanionic OXT prevails) should also be considered to rationalize the faster release under basic conditions due to potential repulsive interactions between negatively charged drug and gelator molecules. A first-order release model fitted very well all release data regardless the gel formulation and pH value, showing almost perfect linear regression with correlation coefficients >0.99 in most cases (Figure S11), indicating a dependence of the release rate with the drug concentration. Although the first-order was identified as the best-fitting model, other kinetic models such as Korsmeyer-Peppas and Weibull were found to be also good models (correlation coefficients >0.98) for many of the examples. In contrast, the Higuchi model failed in describing the experimental data in several cases (Table S1). The release exponents obtained with the Korsmeyer-Peppas model were always <0.45 ,

suggesting a quasi Fickian transport mechanism for the release of OXT from these supramolecular hydrogel systems. Overall, the observed release rates are comparable to those obtained with some polymer gel composite matrices previously used under similar conditions.

3.4.3.6. Metal-Induced Gelation Ability of Click-TIA

Different metallogels could be obtained after mixing **click-TIA** with a stock solution of different metal acetates in organic solvents followed by sonication. **Click-TIA** alone does not form any gel in organic solvents but the presence of copper acetate and subsequent sonication resulted in the formation of blue translucent gels. The gelation behavior of **click-TIA** and $\text{Cu}(\text{OAc})_2 \cdot \text{H}_2\text{O}$ (CuA) in DMF was used as model system. The critical gelation concentration (CGC) for the equimolar mixture [CuA+ **click-TIA**] in DMF was established as 0.1 M (each component). Interestingly, different concentrations and ratios between **click-TIA** and copper acetate could also lead to gelation (Table 1).





Table 1. Gelation ability in various concentrations and ratios between **click-TIA** and copper acetate in DMF.^a

Entry	c(click-TIA)	c(CuA)	Ratio	Phase ^b
1	0.1 M	0.1 M	1:1	G
2	0.1 M	0.2 M	1:2	PG
3	0.1 M	0.3 M	1:3	P
4	0.15 M	0.15 M	1:1	G
5	0.15 M	0.2 M	1:1.3	G
6	0.15 M	0.3 M	1:2	PG
7	0.2 M	0.075 M	2.7:1	S
8	0.2 M	0.1 M	2:1	G ^c
9	0.2 M	0.2 M	1:1	G
10	0.2 M	0.3 M	2:3	G
11	0.3 M	0.1 M	3:1	P
12	0.3 M	0.2 M	3:2	G
13	0.3 M	0.3 M	1:1	G
14	0.3 M	0.4 M	3:4	G
15	0.4 M	0.1 M	4:1	P
16	0.4 M	0.2 M	2:1	G ^c
17	0.4 M	0.3 M	4:3	G
18	0.4 M	0.4 M	1:1	G

^a Upon sonication at RT for 3 min. ^b Abbreviations: G = gel; PG = partial gel; P = precipitate; S = solution. ^c gelation overnight, if not mentioned, gelation was observed immediately after sonication.

Interestingly, gels could be obtained at an equimolar ratio as well as with an excess of either **click-TIA** or CuA. Moreover, a series of studies were carried out to determine the influence of the metal counter anion on the gelation phenomenon (Table 2).

Table 2. Effect of the counter anion of gelation ability between **click-TIA** and different copper salts in DMF.^a

Entry	Metal salt	c(click-TIA)	c(metal salt)	Pictures	Phase ^b
1	Cu(ClO ₄) ₂ ·6H ₂ O	0.2 M	0.2 M		S
2	Cu(ClO ₄) ₂ ·6H ₂ O	0.3 M	0.3 M		S
3	Cu(SO ₄) ₂ ·5H ₂ O	0.2 M	0.2 M		S
4	Cu(SO ₄) ₂ ·5H ₂ O	0.3 M	0.3 M		S
5	CuCl ₂	0.2 M	0.2 M		S
6	CuCl ₂	0.3 M	0.3 M		S
7	Cu(NO ₃) ₂ ·3H ₂ O	0.2 M	0.2 M		S
8	Cu(NO ₃) ₂ ·3H ₂ O	0.3 M	0.3 M		S

^a Upon sonication at RT for 3-5 min. ^b Abbreviations: S = solution.

Interestingly, it was found that the acetate anions are solely able to form gels. Other anions (such as nitrate, chlorate, chloride and sulfate) led to the formation of clear solutions upon sonication at room temperature. These results indicate that the counter anion plays an important role in the supramolecular assembly of copper-**click-TIA** complexes as has been observed for other metallogels.^{13,24}

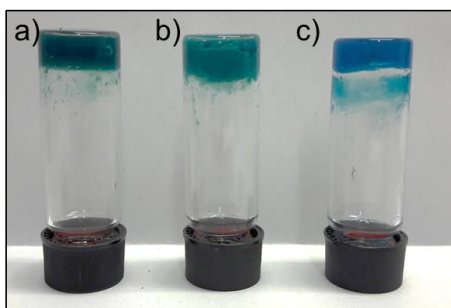
Furthermore, the gelation ability of the gelator system [CuA + **click-TIA**] was evaluated for various solvents upon sonication at RT for 3-5 min (Table 3).

Table 3. Gelation ability in various solvents for the system [CuA (0.2 M) + **click-TIA** (0.2 M)].^a

Entry	Solvent	Phase ^b
1	acetone	P
2	acetic anhydride	P
3	acetonitrile	I
4	chloroform	I
5	DCM	I
6	DMSO	PG
7	DMA	G
8	DMF	G
9	Et ₂ O	I
10	EtOH	P
11	ethyl acetate	P
12	glycerin	P
13	<i>n</i> -hexane	I
14	MeOH	P
15	pyridine	G
16	THF	P
17	toluene	I

^a Upon sonication at RT for 3-5 min. ^b Abbreviations: G = gel; PG = partial gel; P = precipitate; I = insoluble.

We found that stable gels could be prepared in at least three solvents: DMA, DMF and pyridine, partial gelation was observed in DMSO (Figure 13). Interestingly, the color of the metallogels is greenish-blue when prepared with DMA or DMF, whereas it is blue when prepared with pyridine. In the rest of the tested solvents, the gelator system was only forming precipitates. Although **click-TIA** is able to form hydrogels (as discussed in chapter 3.4.3.2.) but in the absence of any metal salt, it is unable to form a gel in organic solvents.

**Figure 13.** Metallogels prepared with **click-TIA**:CuA (0.2 M:0.2 M) in a) DMA, b) DMF, and c) pyridine.

The effect of water to form either MOFs or metallogels was previously reported with **5-TIA**.¹³ Therefore, we checked the role of water in our model system [CuA (0.2 M) + **click-TIA** (0.2 M)] and varied the volume of water (Table S2). Although no MOF formation could be observed metallogels consisting of H₂O:DMF with up to a ratio of 2:3 (v/v) could be prepared. At higher concentrations of water, no gelation occurred.

3.4.3.7. Characterization of Metallogels

To gain additional insight into the complexation process, metallogels (**1-3**) with 0.2 M **click-TIA** and varying amounts of copper acetate (0.5-1.5 equiv.) were prepared and further investigated (Figure 14a).

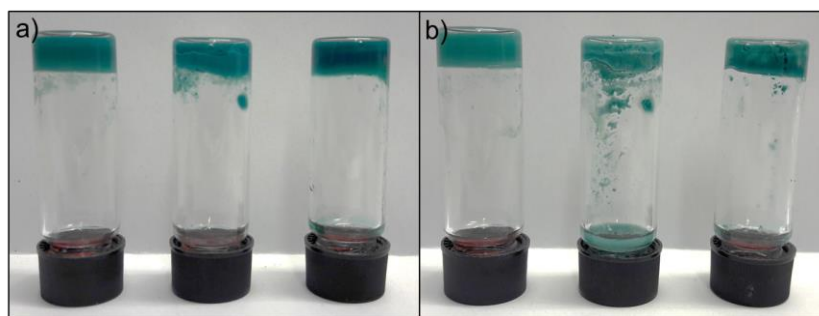


Figure 14. Metallogel prepared with different **click-TIA**:CuA ratios, left: metallogel-1, middle: metallogel-2, right: metallogel-3, a) before heating, b) after heating to 150 °C.

Interestingly, the metallogels display different thermostability at temperatures ranging from room temperature to 150 °C which is accompanied in all cases by a color change from greenish-blue to green (Figure 14b). The best thermostability could be observed with metallogel-1, whereas metallogel-2 lost about the half of the liquid. In addition, metallogel-2 and -3 seem to get inhomogeneous after heating to 150 °C which needs to be further investigated.

Oscillatory rheological experiments were performed in order to confirm the viscoelastic gel state and to examine the qualitative difference between metallogel-1, -2, and -3 (Figure 15).

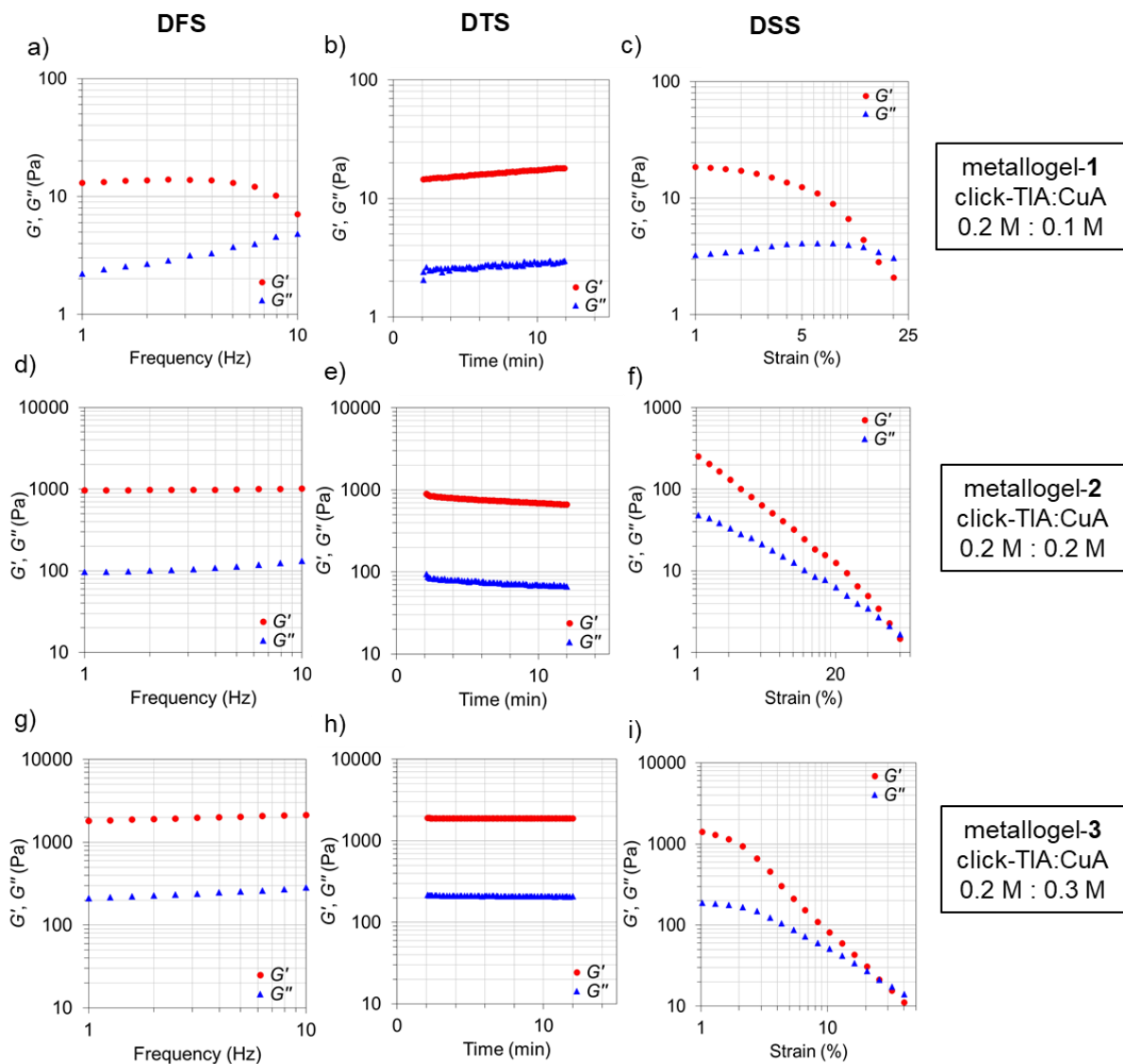


Figure 15. Oscillatory rheological measurements of metallogel-1, -2, and -3.

First, the storage modulus G' and the loss modulus G'' were measured as a function of shear strain (dynamic strain sweep experiment, DSS) and angular frequency ω (dynamic frequency sweep experiment, DFS) to determine the linear viscoelastic regime. Within the linearity limits of deformation, G' was in all three cases one order of magnitude higher than the loss modulus G'' . Only for metallogel-1 was frequency dependence observable. With increasing CuA content, the storage modulus was 13 Pa, 960 Pa and 1810 Pa for **1**, **2** and **3**, respectively (Table S3). Interestingly, the $\tan \delta$ (G''/G') value was the highest for metallogel-1 ($\tan \delta = 0.166$) and the lowest for **2** ($\tan \delta = 0.100$). Moreover, the obtained critical stress or yield point (γ) was significantly high for metallogel-2 with 80%, whereas only 16% and 32%

were achieved for **1** and **2**, respectively. These results indicate that metallogel-**2** has the greatest mechanical stability and damping coefficient in comparison to **1** and **3**.

Fourier transform infrared (FT-IR) spectra of the xerogels obtained from the corresponding metallogels **1-3** (Figure 16) showed a strong absorption band of the carboxylic acid at 1640 cm^{-1} which is between the frequencies of the free ligand (1707 cm^{-1}) and copper acetate (1595 cm^{-1}) due to metal-coordinated carboxylates. Furthermore, free copper acetate has two absorption bands at 1438 and 1420 cm^{-1} whereas the xerogels display only one peak which is shifted to lower frequencies (1394 cm^{-1}). The intensities of the peaks of the xerogels depend on the **click-TIA**:CuA ratio. Interestingly, the intensities decrease following the order: metallogel-**2** > metallogel-**1** > metallogel-**3**, *i.e.* the xerogel prepared with the highest CuA content displays the lowest intensities. This can be explained that more Cu^{2+} ions are present which can interact more with the carboxylic acids, leading to less free vibration of the $\text{C}=\text{O}$ stretching. Furthermore, this observation confirms that the orientation between **click-TIA** and CuA is different depending on the ratio.

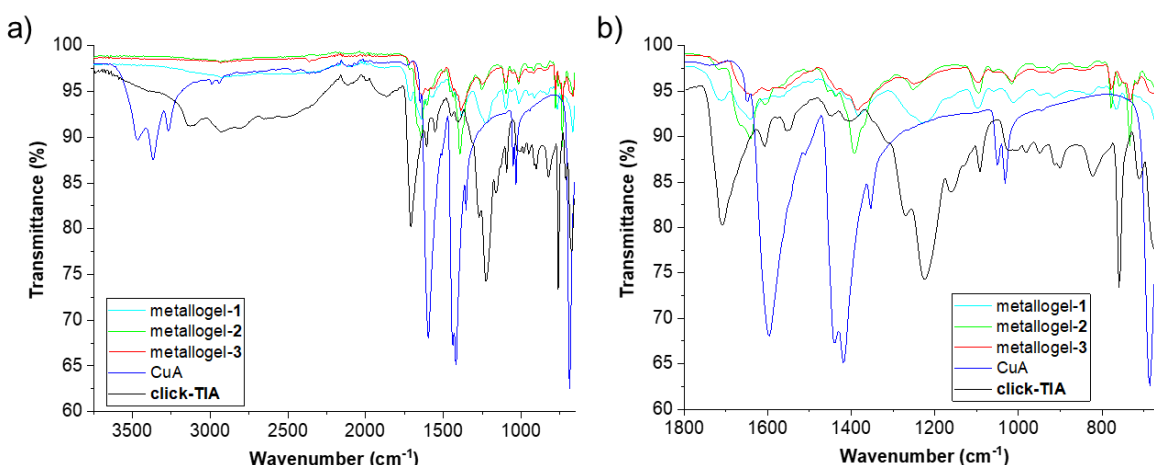


Figure 16. FT-IR spectra of xerogels prepared from the metallogels **1-3**, CuA and solid **click-TIA**, a) complete spectrum, b) fingerprint area.

The PXRD pattern of the xerogels of the corresponding metallogels **1-3** was compared with pure **click-TIA** powder. The data (Figure S12) shows a transformation undergone by the ligand-Cu aggregates with increasing copper acetate concentrations. At 0.5 equivalents, the pattern still resembles that of the pure ligand, although the reflexes at $2\theta = 21.9^\circ$, 25.7° and 27.4° disappeared. At the equimolar ratio between **click-TIA** and CuA, additional reflexes appear at $2\theta = 2.2^\circ - 19.9^\circ$ which could belong to aggregation. With further increase in CuA concentration to 1.5 equivalents, only two reflexes at small 2θ (8.7° and 10.4°) could be observed. The PXRD patterns show that there are different types of assemblies between

click-TIA and CuA which are ratio-dependent and further confirmed by scanning electron microscopy (SEM).

Scanning electron microscope (SEM) images of the xerogels obtained from the metallogels **1-3** were recorded in order to gain insights into the microstructure of the materials (Figure 17, Figure S13-15).

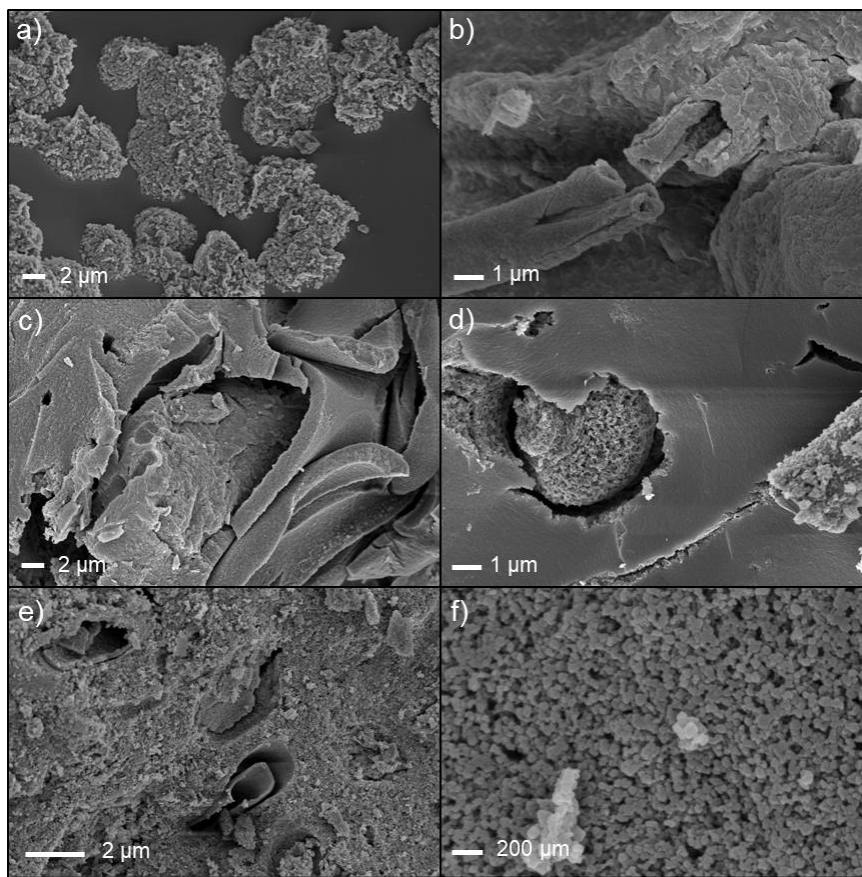


Figure 17. SEM images of the xerogels of a) metallogel-1, b)-d), metallogel-2, and e)-f) metallogel-3.

Here, the xerogels show a remarkable influence on the CuA content. The xerogel obtained from metallogel-1 composes spherical structures with the size around 5 μm (Figure 17a) which consist of entangled fibers resembling hard corals with diameters below 0.5 μm (Figure S13). Spherical structures can also be observed with xerogels obtained from metallogel-2, *i.e.* the equimolar ratio between **click-TIA** and CuA, although they seem to be covered under a layer of about 2 μm (Figure 17c-d). Besides the spheres and layer formation, also twined fibers are visible with a diameter of ~ 1-2 μm and an inner cavity of about 200 nm which seems to consist of recoiled layers (Figure 17b). A porous material consisting of densed aggregates below 100 nm (Figure 17f), can be observed with xerogels obtained from metallogel-3 which is interspersed with holes/tubes of about 4 μm (Figure 17e).

3.4.4. Conclusion and Outlook

In conclusion, the replacement of 1,2,4-triazole moiety in 5-(4H-1,2,4-triazol-4-yl)isophthalic acid (**5-TIA**) by 1,2,3-triazole enabled the preparation of a new LMW hydro- and metallogelator (*i.e.*, 5-(1H-1,2,3-triazol-5-yl)isophthalic acid; **click-TIA**).

In sharp contrast to **5-TIA**, its isostere **click-TIA** undergoes self-assembly in water upon sonication, leading to the formation of stable supramolecular hydrogels with a critical gelation concentration of 6 g L⁻¹. The viscoelastic and brittle nature of the materials was demonstrated by oscillatory rheological measurements. Gels made of **click-TIA** as well as hybrid gels made of **click-TIA** + **5-TIA** (molar ratio 1:0.2) were used to compare different properties of the materials. Although no thermoreversibility was achieved with these materials upon a classical heating-cooling cycle, reversible transitions were achieved by heating hydrogels made of **click-TIA** at concentrations below 12 g L⁻¹ (*i.e.*, *gel*-to-*sol* phase transition) and subsequent sonication of the corresponding isotropic solutions for ~ 2-3 min (*i.e.*, *sol*-to-*gel* phase transition). The thermal stability of the hydrogels increased with the gelator concentration allowing gels that remained stable up to 104 °C when the concentration of **click-TIA** was adjusted to 25 g L⁻¹. In general, the incorporation of **5-TIA** into the gel formulation (*i.e.*, **click-TIA**:**5-TIA** = 1:0.2) caused a decrease of the thermal stability, which can be overcome by increasing the gelator concentration. Gels made of only **click-TIA** showed greater mechanical stability than the hybrid gels, and morphologies consisting in clustered structures were observed by SEM of the corresponding xerogels. Finally, neither **click-TIA** nor **5-TIA** showed cytotoxic effects on cellular viability up to ~ 86% when compared to untreated cells incubated with DMSO (1%). Furthermore, the hydrogels allowed the encapsulation and *in vitro* controlled release of oxytetracycline that followed first-order kinetics. In the case of the hydrogel made of **click-TIA**, a maximum drug release of ~ 60% was reached after ~ 8 h within a pH range between 6.5 and 10. Interestingly, the release rate was reduced to about half of its value at pH values between 1.2 and 5.0, whereas the use of hybrid hydrogels made of **click-TIA** + **5-TIA** allowed to reduce the rate at pH ≤ 6.5. Complementary research to fully understand the underlying mechanism of the pH-induced release with these hydrogels, as well as additional studies in the presence of release modifiers (*e.g.*, ions), are currently underway.

Besides the hydrogelation ability, **click-TIA** is also able to form metallogels in the presence of CuA in different solvents (*i.e.* DMA, DMF, pyridine). Gelation could only be observed with acetate as counter anion, suggesting that the counter anion plays a key role in the self-

assembly. Stable metallogels could be obtained at different ratios of **click-TIA**:CuA. Three metallogel formulations in DMF were used for further characterizations. Oscillatory rheological measurements confirm the viscoelastic and brittle nature of the gels. Metallogel-2 (*i.e.*, **click-TIA**:CuA 0.2 M: 0.2 M) displayed the highest mechanical stability in comparison to metallogel-1 (*i.e.* **click-TIA**:CuA 0.2 M: 0.1 M) and metallogel-3 (*i.e.* **click-TIA**:CuA 0.2 M: 0.3 M), whereas metallogel-1 show the highest thermal stability. All metallogels underlie a color change from greenish-blue to green at high temperatures. Interestingly, the metallogel with the highest CuA content displays the less intensive bands in the FT-IR spectra corresponding to the bands of CuA. This observation can be explained by different assembly mechanism depending on the concentration of CuA which is further confirmed by SEM.

3.4.5. Experimental Part

3.4.5.1. Materials and Methods

All reagents were used as received without further purification. All solvents for synthesis were dried by distillation. Phosphate-buffered saline (PBS) solutions were prepared with Na₂PO₄, KH₂PO₄, NaCl, and KCl, and the pH values were adjusted by using diluted HCl or NaOH solutions. Deionized water was used to prepare the buffer solutions and to prepare the hydrogels. Oxytetracycline hydrochloride (OXT) was purchased from Sigma Aldrich (≥95%).

Nuclear magnetic resonance (NMR) spectra, ¹H NMR (400 or 500 MHz) and ¹³C NMR (75 or 125 MHz), were recorded as δ, parts per million (ppm), relative to the signal of the residual solvent (for ¹H NMR: CHCl₃ = 7.26 ppm, DMSO = 2.50 ppm; for ¹³C NMR: CHCl₃ = 77 ppm, DMSO = 39.5 ppm). Coupling constants (J) are given in Hertz (Hz). The following notations indicate the multiplicity of the signals: s = singlet, br s = broad singlet, d = doublet, t = triplet, q = quartet, dd = doublet of doublets, m = multiplet. Multiplicity in ¹³C NMR spectra was assigned from DEPT135 and DEPT90 experiments and was expressed by the abbreviations s (C), d (CH), t (CH₂), and q (CH₃). Estimated error or reported values: 0.01 ppm (δ, ¹H NMR), 0.1 ppm (δ, ¹³C NMR), 0.1 Hz (J, coupling constant). Melting points were determined on a Büchi B-540 model. Mass spectra were recorded with a Waters LCT Premier XE Micromass spectrometer using electrospray ionization (ESI+-TOF). Flash chromatography was performed with silica gel (230-400 mesh) as the stationary phase. The solvent system used as the mobile phase is indicated in each case. Thin-layer chromatography (TLC) analysis were carried out on silica gel 60 F254 aluminum sheets and visualized using UV light (365 nm), a phosphomolybdic acid solution 10 wt% in MeOH or a vanillin solution (6 g of vanillin, 450 mL of ethanol, 40 mL of AcOH and 30 mL of H₂SO₄). Sonication treatments were done using a sonication bath USC200th VWR, 45 kHz, 60 W. UV-Vis spectroscopy was performed with an Ocean Optics DH2000-BAL UV-vis/NIR spectrophotometer. FT-IR spectra were recorded with an Agilent Technologies Cary 630 FTIR spectrometer equipped with a Golden Gate Diamond ATR (attenuated total reflection).

3.4.5.2. Synthesis of 5-(1*H*-1,2,3-triazol-5-yl)isophthalic acid (click-TIA)

Dimethyl 5-((trimethylsilyl)ethynyl)isophthalate (2)

Pyridine (7.64 mL, 94.5 mmol) was added to a solution of dimethyl 5-hydroxyisophthalate (**1**) (13.5 g, 63.9 mmol) in dry DCM (420 mL) under argon atmosphere. Then, the mixture was cooled to 0 °C and trifluoromethanesulfonic anhydride (11.78 mL, 69.3 mmol) was added

dropwise over a period of 30 min. The reaction mixture was stirred for 1 h at 0 °C, after which time an aqueous HCl solution (1 M, 150 mL) was added. The organic layer was washed with deionized water (200 mL) and brine (100 mL), dried over anhydrous MgSO₄, filtered and concentrated under reduced pressure to yield a crude, which was used in the next step without further purification.

To a solution of the above crude in benzene (150 mL) under argon at RT were added, subsequently, 1,4-diazabicyclo[2.2.2]-octane (DABCO) (7.78 g, 69.3 mmol), trimethylsilylacetylene (10.0 mL, 69.3 mmol), PdCl₂(Ph₃)₂ (880 mg, 1.26 mmol), and CuI (120 mg, 0.63 mmol). The reaction mixture was stirred overnight at RT, after which time the solvent was removed under vacuum. The resulting solid was redissolved in DCM (200 mL) and washed with aqueous HCl solution (1 M, 100 mL) and brine (100 mL). The combined organic layers were dried over anhydrous MgSO₄, filtered and concentrated under reduced pressure. The obtained residue was purified by column chromatography in silica gel using 5% EtOAc/hexane as eluent, affording compound **2** as a white solid (17.38 g, 59.85 mmol, 95% overall yield): ¹H NMR (500 MHz, CDCl₃) δ (ppm) = 0.25 (s, 9H), 3.93 (s, 6H), 8.27 (d, J = 1.7 Hz, 2H), 8.58 (dd, J = 1.7 Hz, 1H); ¹³C NMR (125 MHz, CDCl₃) δ (ppm) = -0.1 (q), 55.6 (q), 96.8 (s), 102.9 (s), 124.4 (s), 130.4 (d), 131.0 (s), 137.0 (d), 165.7 (s); mp 103–104 °C; HRMS (ESI): m/z calcd for C₁₅H₁₈O₄NaSi [M+Na⁺]: 313.0872, found: 313.0873.

Dimethyl 5-ethynylisophthalate (4)

To a solution of compound **3** (17.0 g, 58.5 mmol) in THF (300 mL) at 0 °C was added water (10.5 mL, 585 mmol) and TBAF (64.35 mL of 1 M solution in THF, 64.35 mmol). The mixture was stirred for 5 min and then, the reaction was quenched with saturated aqueous NH₄Cl (40 mL) and extracted with DCM (2 × 100 mL). The combined organic layers were dried over anhydrous MgSO₄, filtered and concentrated under reduced pressure. The resulting crude was purified by column chromatography with silica gel using 10% EtOAc/hexane as eluent, affording compound **4** (12.1 g, 55.45 mmol, 95% yield) as a white solid: ¹H NMR (500 MHz, CDCl₃) δ (ppm) = 3.17 (s, 1H), 3.95 (s, 6H), 8.31 (d, J = 1.7 Hz, 2H), 8.63 (dd, J = 1.6 Hz, 1H); ¹³C NMR (125 MHz, CDCl₃) δ (ppm) = 52.7 (q), 79.3 (d), 81.7 (s), 123.4 (s), 130.8 (d), 131.2 (s), 137.2 (d), 165.6 (s); mp 127–128 °C; HRMS (ESI): m/z: calcd for C₁₂H₁₀O₄Na [M+Na⁺]: 241.0477, found: 241.0472.

Dimethyl 5-(1H-1,2,3-triazol-5-yl)isophthalate (5)

CuI (525 mg, 2.75 mmol) and azidotrimethylsilane (10.0 g, 11.5 mL, 82.5 mmol) were added to a solution of compound **4** (12.0 g, 55.0 mmol) in a mixture DMF/MeOH 9:1 (99 mL:11 mL).

The reaction mixture was heated to 100 °C overnight. After this time, the solution was filtered through a pad of Celite, and the solvent removed under reduced pressure. The resulting residue was dissolved in DCM (200 mL), washed with deionized water (100 mL), dried over anhydrous MgSO_4 , filtered, and concentrated under reduced pressure to yield **5** (14.3 g, 54.74 mmol, > 99% yield) as a brown solid, which was used in the next step without further purification: ^1H NMR (500 MHz, DMSO-d_6) δ (ppm) = 3.90 (s, 6H), 8.34 (dd, J = 1,6 Hz, 1.5 Hz, 1H), 8.58 (d, J = 1.6 Hz, 2H), 8.61 (br s, 1H); ^{13}C NMR (125 MHz, DMSO-d_6) δ (ppm) = 52.5 (q), 128.6 (d), 129.9 (d), 130.9 (q), 165.1 (s); mp 213-215 °C; HRMS (ESI): m/z : calcd for $\text{C}_{12}\text{H}_{10}\text{N}_3\text{O}_4$ [M-H]: 260.0671, found: 260.0661.

5-(1H-1,2,3-triazol-5-yl)isophthalic acid (click-TIA)

Compound **5** (14.0 g, 53.5 mmol) was dissolved in 200 mL of NaOH aqueous solution at 15% w/w. The mixture was stirred at RT for 2 h and then the reaction was acidified with concentrated HCl. So-formed white precipitate was filtered and washed with cold water and acetone to afford compound **click-TIA** (12.4 g, 53.18 mmol, > 99% yield) as a pale white solid: ^1H NMR (500 MHz, DMSO-d_6) δ (ppm) = 8.43 (s, 1H), 8.63 (s, 3H), 13.44 (br s, 2H), 15.26 (br s, 1H); ^{13}C NMR (125 MHz, DMSO-d_6) δ (ppm) = 129.3 (d), 130.0 (d), 132.2 (s), 166.5 (s); mp 271–272 °C; HRMS (ESI): m/z : calcd for $\text{C}_{10}\text{H}_6\text{N}_3\text{O}_4$ [MH]: 232.0358, found: 232.0357.

3.4.5.3. Synthesis of 5-TIA

Compound **5-TIA** was synthesized following the previously reported with slight modifications.^{13,25}

(E)-N'-((E)-(Dimethylamino)methylene)-N,N-dimethylformohydrazonamide dihydrochloride (6)

SOCl_2 (11.9 g, 7.26 mL, 100 mmol) was added dropwise to DMF (50 mL) at 0 °C and stirred at RT. Then hydrazine monohydrate (**7**) (2.50 g, 2.58 mL, 50.0 mmol) was added slowly at 0 °C leading to a white suspension. The mixture was allowed to warm to RT and stirred overnight. After filtration, the obtained solid was washed with DMF (2 × 10 mL) and Et_2O (2 × 10 mL). The residue was dried under reduced pressure affording compound **9** (5.80 g, 27.0 mmol, 54% yield) as a white solid: ^1H NMR (300 MHz, D_2O) δ (ppm) = 8.24 (s, 2H), 3.18–2.99 (m, 12H); ^{13}C NMR (75 MHz, D_2O) δ (ppm) = 158.5, 43.9; FT-IR (solid, cm^{-1}) ν = 3473, 2945, 2571, 2079, 1945, 1703, 1609, 1479, 1398, 1297, 1092, 753; mp >200 °C; MS (ESI): m/z = 143 [$\text{M} + \text{H}$]⁺ (−2HCl) (100%), 144 (6.4%).

5-(4*H*-1,2,4-Triazol-4-yl)isophthalic acid (**5-TIA**)

Compound **9** (1.20 g, 5.58 mmol) was added to a solution of 5-aminoisophthalic acid (**10**) (842.3 mg, 4.65 mmol) in xylene (mixture of isomers, 15 mL) and the mixture was stirred at 135 °C for 7 h. After this time, the solvent was decanted and the precipitate was washed with EtOAc (20 mL) and EtOH (20 mL). The residue was dried under reduced pressure and recrystallized from propan-2-ol, affording compound **5-TIA** (236 mg, 1.01 mmol, 22% yield) as a white solid. ¹H NMR (400 MHz, DMSO-*d*₆) δ (ppm) 9.32 (s, 2H), 8.48 (m, 1H), 8.42 (m, 2H). ¹³C NMR (75 MHz, DMSO-*d*₆) δ (ppm) 165.6, 141.4, 134.6, 128.8, 125.7. FT-IR (solid, cm⁻¹) ν = 3123, 2948, 1703, 1561, 1446, 1286, 1259, 1144, 1080, 890, 764, 697; MS (ESI): *m/z* = 234.0 [M + H]⁺, 467.1 [2M + H]⁺.

3.4.5.4. Preparation of Hydrogels

Typically, a weighted amount of the corresponding gelator (*i.e.*, **click-TIA** or a hybrid made of **click-TIA** + **5-TIA**) and an appropriate amount of water were placed into a screw-capped glass vial (4 cm length × 1 cm diameter). The mixture was quickly stirred with a spatula and then sonicated for ~ 2–3 min until everything was homogeneous. The resulting solution was rest at RT until the gel was formed. The material was preliminary classified as a gel if it did not exhibit gravitational flow upon turning the vial upside-down at RT. The gel state was further confirmed by oscillatory rheological measurements.

3.4.5.5. Cell Viability Studies

The metabolic activity of the cells was measured after 18 h using the MTT test (MTT = 3-(4,5dimethylthiazol-2-yl)-2,5-diphenyltetrazolium bromide). HeLa cells (8000 cell/well) were incubated in Dulbecco's modified Eagle's medium (DMEM) supplemented with 10% FBS at 37 °C for 24 h. Several working concentrations of **click-TIA** or **5-TIA** were previously prepared in DMSO to get a final **click-TIA** or **5-TIA** concentration of 2.3×10^{-4} , 9.3×10^{-4} , 1.9×10^{-3} , 2.3×10^{-3} , 9.3×10^{-3} , and 3.7×10^{-2} g L⁻¹, respectively. Cell viability studies were performed using 0.5% DMSO (v/v) at all sample concentrations. HeLa cells were incubated with the corresponding concentration of **click-TIA** or **5-TIA** for 24 h at 37°C (5% CO₂). Subsequently, DMEM was removed, and cells were washed with PBS (200 μL). Fresh DMEM (200 μL) was added, and cells were incubated for 12 h at 37 °C. Finally, 25 μL of MTT (3-(4,5-dimethylthiazol-2-yl)-2,5-diphenyltetrazolium bromide) at a concentration of 5 g L⁻¹ in PBS was added directly in each well, and cells were incubated for four additional hours at 37 °C. The liquid was removed, and formazan crystals were dissolved in DMSO (200 μL).

After 15 min incubation, absorbance was measured at 560 nm wavelength on Promega Glomax Multidetector System instrument. Results were expressed as a relative percentage of untreated cells (control).

3.4.5.6. Procedure for Preparation of Drug-Loaded Hydrogels and *in Vitro* Drug Release Experiments

A weighted amount of the corresponding gelator and 1 mL of an aqueous stock solution of oxytetracycline hydrochloride (OXT) (0.8 g L^{-1}) were placed in a screw-capped glass vial and sonicated until the gel was formed (ca. 3–5 min). Obtained hydrogel materials equilibrated at RT for 16 h. After this time, the gels were overlaid with PBS buffer (1 mL, pH 1–10)²⁶ corresponding to time = 0 of the release studies. At selected points of time, aliquots (100 μL) were removed from the supernatant and diluted with PBS to reach 1 mL of total volume. Then fresh PBS buffer (100 μL) was added over the gel to maintain infinite sink conditions. Drug concentrations were determined by UV–vis spectroscopy after proper calibration using the maximum absorbance of OXT at $\lambda = 353 \text{ nm}$. Each experiment was performed at least in triplicate. Experiments with different gelator concentrations and compositions, as described in the text, were carried out in a similar manner. The data obtained from the *in vitro* release experiments were fitted according to four drug release mathematical models, namely first-order release,²⁷ Higuchi,²⁸ Korsmeyer-Peppas,²⁹ and Weibull.³⁰ Note: it is known that OXT undergoes degradation at high temperatures (*i.e.*, $\geq 43 \text{ }^{\circ}\text{C}$), which is also accelerated by light.³¹ However, we have previously observed that OXT starts degrading in PBS gel media even at $37 \text{ }^{\circ}\text{C}$ after 48 h of incubation.³² Therefore, we limited the *in vitro* release studies in this work to 24 h, and the OXT-loaded gels were maintained in dark to avoid photodecomposition.

3.4.5.7. Preparation of Metallogels

Typically, a weighted amount of **click-TIA** and an appropriate amount of a metal acetate stock solution were placed into a screw-capped glass vial (4 cm length \times 1 cm in diameter). The mixture was quickly stirred with a spatula and then sonicated for 3–5 min until everything was homogeneous. The resulting solution was rest at RT until the gel was formed. The material was preliminary classified as a gel if it did not exhibit gravitational flow upon turning the vial upside-down at RT. The gel state was further confirmed by oscillatory rheological measurements. Three model formulations with different **click-TIA**:CuA ratios were used for

further characterization: metallogel-1 (**click-TIA**:CuA 0.2 M:0.1 M), metallogel-2 (**click-TIA**:CuA 0.2 M:0.2 M), metallogel-3 (**click-TIA**:CuA 0.2 M:0.2 M).

→ Additional information on gel characterization and drug release kinetics can be found in the ESI on the enclosed CD or in the ESI of the paper.

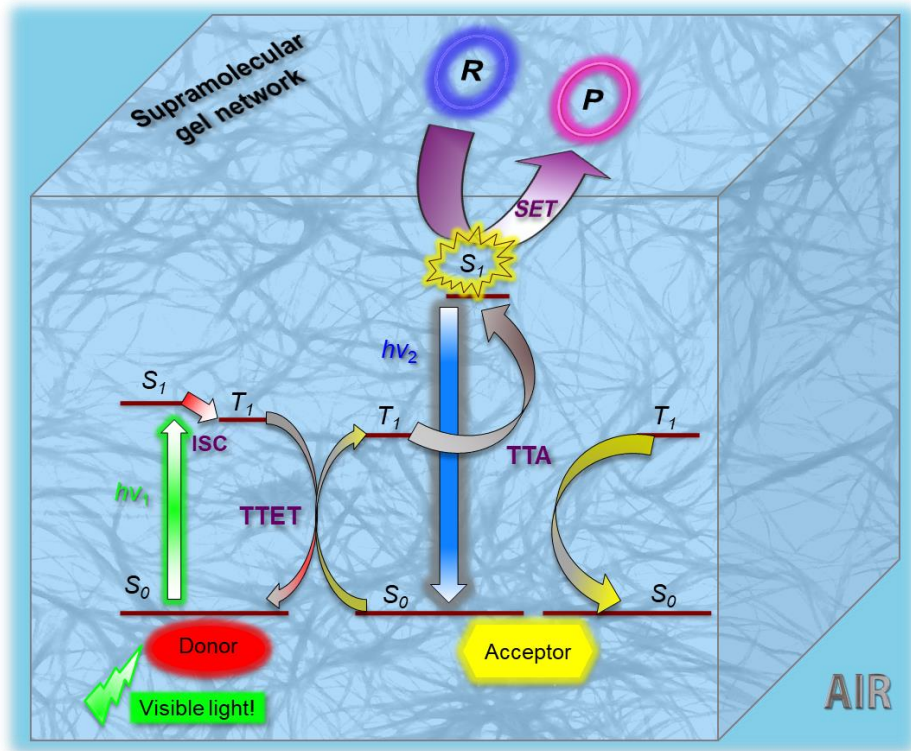
3.4.6. References

- [1] a) Y. Huang, Y. Ding, T. Li, M. Yang, *Anal. Methods* **2015**, *7*, 411–415; b) J. L. Drury, D. J. Mooney, *Biomaterials* **2003**, *24*, 4337–4351; c) R. G. Ellis-Behnke, Y. X. Liang, S. W. You, D. K. Tay, S. Zhang, K. F. So, G. E. Schneider, *Proc. Natl. Acad. Sci. U.S.A.* **2006**, *103*, 5054–5059; d) M. W. Tibbitt, K. S. Anseth, *Biotechnol. Bioeng.* **2009**, *103*, 655–663.
- [2] a) F. Qu, Y. Zhang, A. Rasooly, M. Yang, *Anal. Chem.* **2014**, *86*, 973–976; b) S. J. Jhaveri, J. D. McMullen, R. Sijbesma, L.-S. Tan, W. Zipfel, C. K. Ober, *Chem. Mater.* **2009**, *21*, 2003–2006.
- [3] D. Kühbeck, R. J. Koopmans, D. D. Díaz, *Chem. Soc. Rev.* **2011**, *40*, 427–448.
- [4] a) S. Kiyonaka, K. Sugiyasu, S. Shinkai, I. Hamachi, *J. Am. Chem. Soc.* **2002**, *124*, 10954–10955; b) B. Adhikari, G. Palui, A. Banerjee, *Soft Matter* **2009**, *5*, 3452–3460; c) P. Chakraborty, B. Roy, P. Bairi, A. K. Nandi, *J. Mater. Chem.* **2012**, *22*, 20291–20298.
- [5] a) S. Bera, D. Haldar, *J. Mater. Chem. A* **2016**, *4*, 6933–6939; b) S. Kiyonaka, K. Sada, I. Yoshimura, S. Shinkai, N. Kato, I. Hamachi, *Nat. Mater.* **2004**, *3*, 58–64; c) P. K. Vemula, G. John, *Chem. Commun.* **2006**, 2218–2220.
- [6] a) L.A. Estroff, A. D. Hamilton, *Chem. Rev.* **2004**, *104*, 1201–1218; b) D. K. Smith, *Nat. Chem.* **2010**, *2*, 162–163; c) N. M. Sangeetha, U. Maitra, *Chem. Soc. Rev.* **2005**, *34*, 821–836; d) A. Ajayaghosh, V. K. Praveen, C. Vijayakumar, *Chem. Soc. Rev.* **2008**, *37*, 109–122; e) M. George, R. G. Weiss, *Acc. Chem. Res.* **2006**, *39*, 489–497; f) S. Samai, J. Dey, K. Biradha, *Soft Matter* **2011**, *7*, 2121–2126.
- [7] a) C. D. Jones, J. C. Tan, G. O. Lloyd, *Chem. Commun.* **2012**, *48*, 2110–2112; b) J. Le Bideau, L. Viau, A. Vioux, *Chem. Soc. Rev.* **2011**, *40*, 907–925; c) X. Yu, L. Chen, M. Zhang, T. Yi, *Chem. Soc. Rev.* **2014**, *43*, 5346–5371; d) P. Dastidar, *Chem. Soc. Rev.* **2008**, *37*, 2699–2715; e) S. Ray, A. K. Das, A. Banerjee, *Chem. Mater.* **2007**, *19*, 1633–1639; f) A. Pal, H. Basit, S. Sen, V. K. Aswal, S. Bhattacharya, *J. Mater. Chem.* **2009**, *19*, 4325–4334.
- [8] P. Dastidar, R. Roy, R. Parveen, S. Ganguly, J. Majumder, M. Paul, in *Functional Supramolecular Materials: From Surfaces to MOFs*, ed. R. Banerjee, RSC, **2017**, chapter 2.
- [9] a) N. Brown, *Bioisosteres in Medicinal Chemistry*; Wiley-VCH: Weinheim, **2012**; Vol. 54; b) Y. Hamada, Y. Kiso, *Expert Opin. Drug Discovery* **2012**, *7*, 903–922.

-
- [10] J. Bachl, J. Mayr, F. J. Sayago, C Cativiela, D. D. Díaz, *Chem. Commun.* **2015**, 51, 5294–5297.
- [11] C. W. Thornber, *Chem. Soc. Rev.* **1979**, 8, 563–580.
- [12] A. Burger, *Prog. Drug Res.* **1991**, 37, 287–371.
- [13] A. Mallick, E.-M. Schön, T. Panda, K. Sreenivas, D. D. Díaz, R. Banerjee, *J. Mater. Chem.*, **2012**, 22, 14951–14963.
- [14] J. J. Marrero-Tellado, D. D. Díaz, *CrystEngComm*, **2015**, 17, 7978–7985.
- [15] W.-Y. Gao, R. Cai, T. Pham, K. A. Forrest, A. Hogan, P. Nugent, K. Williams, L. Wojtas, R. Luebke, L. J. Weselinski, M. J. Zaworotko, B. Space, Y.-S. Chen, M. Eddaoudi, X. Shi, S. Ma, *Chem. Mater.* **2015**, 27, 2144–2151.
- [16] H. Bouas-Laurant, J.-P. Desvergne, *Molecular Gels: Materials with Self-Assembled Fibrilla Networks*; Eds.: G. R. Weiss, P. Terech, Springer: The Netherlands, **2006**.
- [17] J. Schiller, J. V. Alegre-Requena, E. Marqués-López, R. P. Herrera, J. Casanovas, C. Alemán, D. D. Díaz, *Soft Matter* **2016**, 12, 4361–4374.
- [18] a) L. A. Estroff, A. D. Hamilton, *Chem. Rev.* **2004**, 104, 1201–1218; b) D. K. Smith, *Nat. Chem.* **2010**, 2, 162–163; c) N. M. Sangeetha, U. Maitra, *Chem. Soc. Rev.* **2005**, 34, 821–836; d) A. Ajayaghosh, V. K. Praveen, C. Vijayakumar, *Chem. Soc. Rev.* **2008**, 37, 109–122; e) M. George, R. G. Weiss, *Acc. Chem. Res.* **2006**, 39, 489–497; f) S. Samai, J. Dey, K. Biradha, *Soft Matter* **2011**, 7, 2121–2126.
- [19] a) C. D. Jones, J. C. Tan, G. O. Lloyd, *Chem. Commun.* **2012**, 48, 2110–2112; b) J. Le Bideau, L. Viau, A. Vioux, *Chem. Soc. Rev.* **2011**, 40, 907–925; c) X. Yu, L. Chen, M. Zhang, T. Yi, *Chem. Soc. Rev.* **2014**, 43, 5346–5371; d) P. Dastidar, *Chem. Soc. Rev.* **2008**, 37, 2699–2715; e) S. Ray, A. K. Das, A. Banerjee, *Chem. Mater.* **2007**, 19, 1633–1639; f) A. Pal, H. Basit, S. Sen, V. K. Aswal, S. Bhattacharya, *J. Mater. Chem.* **2009**, 19, 4325–4334.
- [20] E. Morin, E.-M. Schön, G. Budin, A. Wagner, J.-S. Remy, D. D. Díaz, *J. Mater. Chem.* **2011**, 21, 641–644.
- [21] T. Mosmann, *J. Immunol. Methods* **1983**, 65, 55–63.
- [22] J. Fischer, C. R. Ganellin, *Analogue-Based Drug Delivery*; John Wiley & Sons, **2006**.
- [23] a) A. Moretto, L. Tesolin, F. Marsilio, M. Schiavon, M. Berna, F. M. Veronese, *Farmaco* **2004**, 59, 1–5; b) A. Cesaretti, B. Carlotti, P. L. Gentili, C. Clementi, R. Germani, F. Elisei, *Phys. Chem. Chem. Phys.* **2014**, 16, 23096–23107; c) P. Chetoni, G. Di Colo, M. Grandi, M. Morelli, M. F. Saettone, S. Darougar, *Eur. J. Pharm. Biopharm.* **1998**, 46, 125–132.
-

- [24] a) A. Y.-Y. Tam, K. M.-C. Wong, V. W.-W. Yam, *Chem. Eur. J.* **2009**, *15*, 4775-4778;
b) M.-O. M. Piepenbrock, N. Clarke, J. W. Steed, *Langmuir*, **2009**, *25*, 8451-8456.
- [25] R. K. Bartlett, I. R. Humphrey, *J. Chem. Soc. C.* **1967**, 1664-1666.
- [26] H. Zhang, Y. Dong, L. Wang, G. Wang, J. Wu, Y. Zheng, H. Yang, S. Zhu, *J. Mater. Chem.* **2011**, *21*, 13530-13537.
- [27] E. Mathiowitz, *Encyclopedia of Controlled Drug Delivery*, 1st ed., Wiley, **1999**, *2*, 698-729.
- [28] T. Higuchi, *J. Pharm. Sci.* **1963**, *52*, 1145-1149.
- [29] P. L. Ritger, N. A. Peppas, *J. Controlled Release* **1987**, *5*, 37-42.
- [30] W. Weibull, *J. Appl. Mech.* **1951**, *18*, 293-297.
- [31] A. M. Doi, M. K. Stoskopf, *J. Aquat. Anim. Health* **2000**, *12*, 246-253.
- [32] J. Mayr, *Synthesis, Characterization and Application of Smart Materials Based on Low-Molecular-Weight Compounds and Polymers*, PhD Dissertation, University of Regensburg, Regensburg, Germany, **2017**.

3.5. Photoreduction of Aryl Halides by TTA-UC Under Aerobic Conditions in Gel Medium



This chapter has been published in:

M. Häring, R. Pérez-Ruiz, A. J. v. Wangelin, D. D. Díaz, 'Intragel photoreduction of aryl halides by green-to-blue upconversion under aerobic conditions', *Chem. Commun.* **2015**, 51, 16848-16851. – Reproduced with permission from *Chem. Commun.* **2015**, 51, 16848-16851.

Author contribution:

MH performed the experiments. RPR measured GC-FID and did the spectroscopic investigations. All authors contributed to the scientific discussion of the results.

3.5.1. Abstract

Gel materials have been recognized as promising confined media to enhance photoinduced reactions of reactants that are physically embedded in the gel network. In particular, stimuli-responsive supramolecular self-assembled gels that are unreactive to light irradiation constitute versatile materials to enhance both unimolecular and bimolecular photoinduced processes (in comparison to those carried out in solution) such as dimerization, isomerization and redox reactions, including multistep mechanism.

The first proof-of-concept for the application of intragel green-to-blue photon up-conversion to a chemical reaction is reported. The developed method allows the photoreduction of aryl halides at room temperature under aerobic conditions via single electron transfer (SET) that are not possible in solutions under mild conditions.

3.5.2. Introduction

Through millions of years of evolution, nature has used confinement and compartmentalization to access otherwise slow or forbidden pathways and achieve high selectivity under mild conditions.¹ This has inspired scientists all over the world to study the effects of reactant confinement in non-conventional media on their chemical properties and reactivity.² The fields of photochemistry and photocatalysis, among others, have also capitalized on the benefits of spatial confinement,^{3,4} which are related to changes in key properties such as light absorption, formation of redox intermediates, lifetime of excited species, thermodynamics of reacting mixtures, kinetics of competitive steps and adsorption/desorption of chemical species.^{3,5} Literature precedents of confined photo-induced reactions involve the use of mesoporous inorganic materials,⁶ microemulsions,⁷ micelles,⁸ vesicles,⁹ polyelectrolyte multilayered capsules,¹⁰ proteins¹¹ and photocatalyst-loaded liquid foams,¹² among others.¹³ Furthermore, the emerging research field focused on the use of viscoelastic gels¹⁴ as tunable and processable reaction vessels for photochemical and photophysical transformations of embedded reactants, providing similar or superior results than those obtained in solution¹⁵ has been reviewed recently. Among these photo-induced processes, photon up-conversion (UC)¹⁶ based on triplet-triplet annihilation (TTA) between organic compounds is one of the most powerful wavelength conversion technologies that can be performed with low-intensity and non-coherent light.¹⁷ TTA-UC involves the generation of the triplet excited state (T_1) of a donor (sensitizer) by intersystem crossing (ISC) from the singlet excited state (S_1) which is formed by low energy absorption ($h\nu_1$). Subsequently, triplets of the acceptor (emitter) are populated by triplet-triplet energy transfer (TTET) from the triplets of the donor (Dexter mechanism). A higher singlet energy level is accessed upon collision of two acceptor molecules in their triplet states (TTA) causing delayed upconverted fluorescence ($h\nu_2$) (Figure 1). Such photochemical cascade of events have found high-tech applications in several fields including photovoltaics, photocatalysis, bioimaging and phototherapy.¹⁸⁻²¹ The first examples of TTA-UC within gel networks using different chromophore pairs have been reported very recently by the groups of Simon,²² Schmidt²³ and Kimizuka.²⁴⁻²⁶ These studies demonstrated the highly efficient photochemical UC in organogel media and, in some cases, even under air-saturated conditions.²⁴ A major aspect of this approach is the adaptable nature of supramolecular fibrillar gel networks, which allows efficient and cooperative incorporation of donor/acceptor pairs while preserving the structural integrity of the bulk material. Such promising results lead to the motivation to investigate

applications of intragel TTA-UC to accomplish chemical transformations via single electron transfer (SET) that are unaffordable in solution under mild conditions (Figure 1).

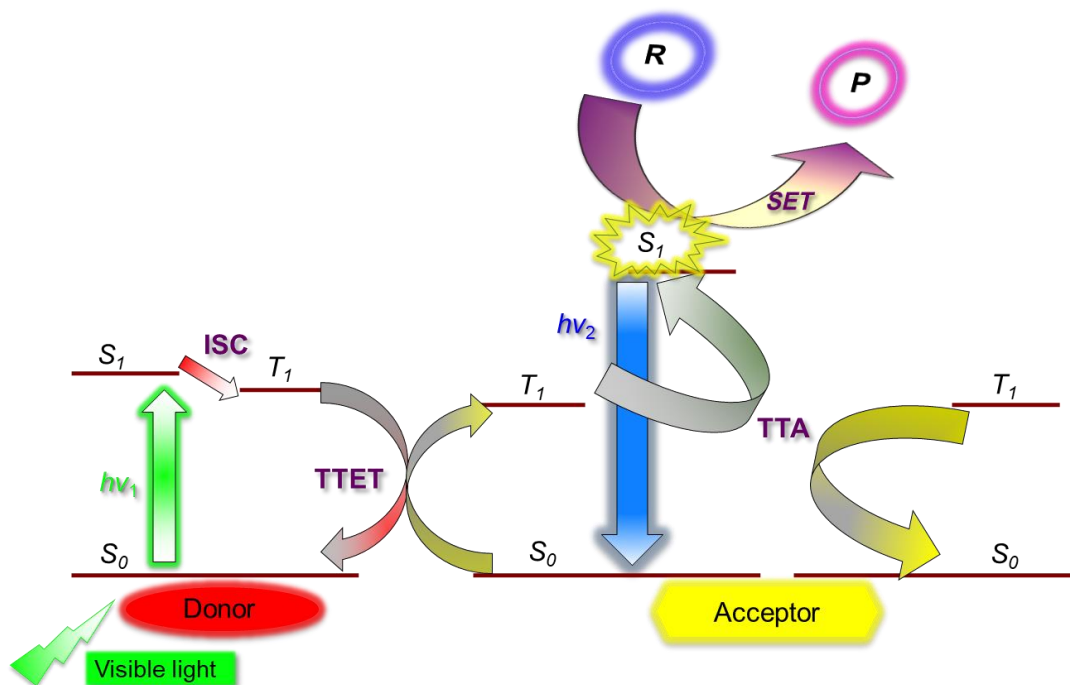
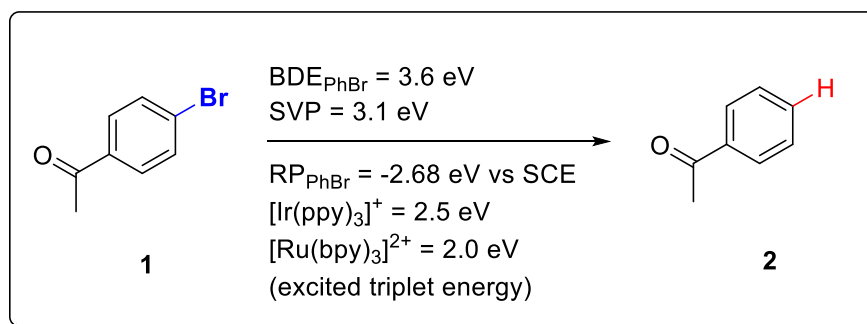


Figure 1. The general concept of this study: Two photon process based on TTA-UC produces one photon of higher energy that can be used in chemical reactions. This event can be achieved using visible light at RT and in air when confined into a gel doped with a donor/acceptor pair, R = reactant, P = product.

Aligned to the growing research field of visible light-mediated reactions,²⁷ the photoreduction of aryl halides was chosen as a model reaction (Scheme 1) because it constitutes a major scientific challenge at visible wavelengths due to their high bond dissociation energies (BDE).

Scheme 1. Scientific challenge of the photocatalyzed reduction of aryl halides at visible wavelength.



BDE = bond dissociation energy, SVP = single visible photon, RP = reduction potential.

This is especially critical in the case of non-activated aryl bromides whose BDE (e.g., $\text{BDE}_{\text{PhBr}} = 3.6 \text{ eV}$) significantly exceeds the maximum of a single visible photon (3.1 eV).^{28,29} Their reduction potentials (e.g., $\text{PhBr} = -2.68 \text{ eV vs SCE}$)³⁰ are also beyond the excited triplet

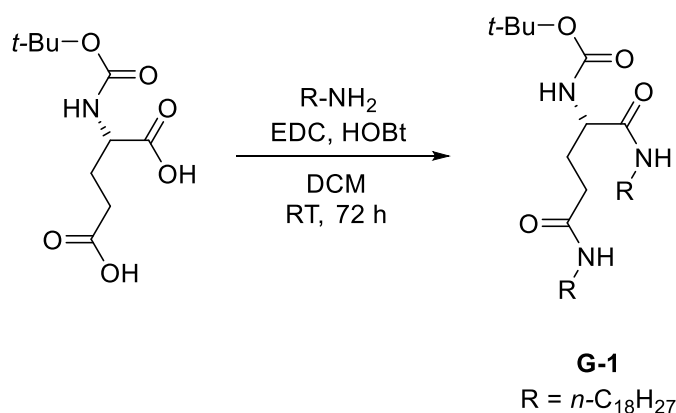
energies of common photoactive 1e-reductants (e.g., $[\text{Ir}(\text{ppy})_3]^+ = 2.5 \text{ eV}$; $[\text{Ru}(\text{bpy})_3]^{2+} = 2.0 \text{ eV}$)³¹. Indeed, only a few examples based on photoinduced electron transfer (PET) have been reported to achieve such bond activation.³² However, the application of TTA-UC confined in a supramolecular microenvironment for this purpose has remained unexplored.

3.5.3. Results and Discussion

3.5.3.1. Synthesis of LMW gelators

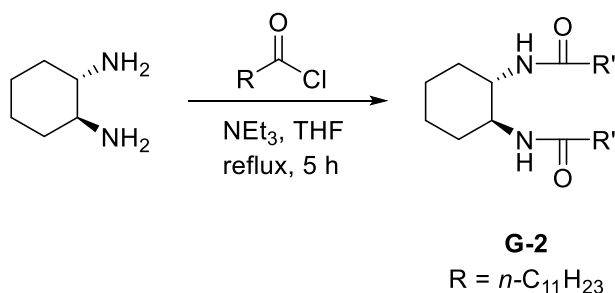
Two well-known low-molecular-weight (LMW) gelators, *N,N'*-bis(octadecyl)-*L*-*boc*-glutamic diamide (**G-1**) and *N,N'*-((1*S*,2*S*)-cyclohexane-1,2-diyl)didodecanamide (**G-2**) were previously synthesized according to the literature.^{24,33,34} **G-1** and **G-2** are able to form physical gels which will be used as confined reaction media.³⁵

Scheme 2. Synthesis of the LMW gelator **G-1**.³³



G-1 is obtained through amidation of the corresponding *L*-*Boc*-glutamic acid with octadecylamine by using EDC as coupling reagent in DCM (Scheme 2). In a wide range of solvents, physical gels could be obtained by dissolving **G-1** in a solvent under heating. The solvent-dependent CGC for **G-1** is ranging from 2-21 g L⁻¹.

Scheme 3. Synthesis of the LMW gelator **G-2**.³⁴



G-2 was prepared by the reaction of (1*S*,2*S*)-1,2-diaminocyclohexane and lauroyl chloride in THF in the presence of trimethylamine (Scheme 3). Like **G-1**, **G-2** is also able to form physical gels in various solvents after heating. The solvent-dependent CGC for **G-2** is between 2-44 g L⁻¹.

3.5.3.2. TTA-UC System

The photoreduction of aryl halides with platinum(II) octaethylporphyrin (PtOEP) as sensitizer and 9,10-diphenylanthracene (DPA) as emitter embedded in supramolecular (physical) gel networks were used to study this proof-of-concept (Figure 2). The PtOEP/DPA system has been previously characterized and employed as a benchmark donor/acceptor pair in TTA-UC studies^{21,36} including intragel processes,²⁴ which made it the ideal choice for this study.

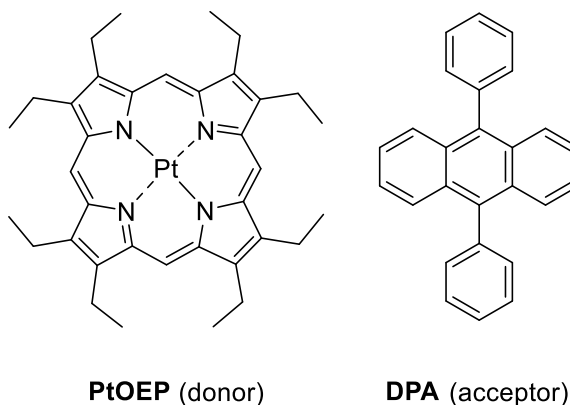
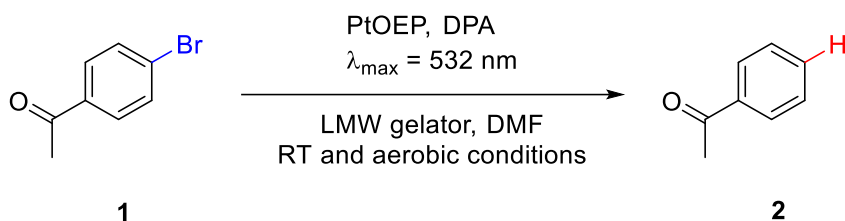


Figure 2. Structures of the used donor/acceptor system PtOEP/DPA.

3.5.3.3. Intragel Photoreduction

For initial optimizations, an aerated DMF solution of **1** (10 mM), PtOEP (33 μ M) and DPA (6.7 mM) was photolyzed with a pulsed laser at 532 nm for 2 h leading to very low conversion of **1** (Table 1, entry 1).

Table 1. Optimization reaction of intragel photoreduction of **1** in air.^a



Entry	Gelator	[G] ^k (g L ⁻¹)	Conversion ^l (%)	Mass balance (%)	Yield ^m (%)
1 ^b	-	-	6	96	2
2	G-1	10	65	98	58
3 ^c	G-1	10	0	-	0
4	G-1	6	55	93	42

continued next page

Continuation of Table 1

Entry	Gelator	[G] ^k (g L ⁻¹)	Conversion ^l (%)	Mass balance (%)	Yield ^m (%)
5	G-1	7	53	98	47
6	G-1	8	48	99	43
7	G-1	13	59	84	40
8	G-1	20	60	88	44
9 ^d	G-1	10	13	100	14
10 ^e	G-1	10	54	99	48
11 ^f	G-1	10	32	93	24
12 ^g	G-1	10	68	93	56
13 ^h	G-1	10	10	98	9
14 ⁱ	G-1	10	24	97	19
15 ^j	G-1	20	0	-	0
16	G-2	10	60	90	47
17	G-2	15	62	89	48

^a Conditions: [1] = 10 mM, [PtOEP] = 33 μM, [DPA] = 6.7 mM, in air, room temperature, 2 h irradiation with a pulsed laser at λ_{exc} = 532 nm. Gels were prepared using the indicated gelator in DMF. ^b 2 h irradiation in aerated DMF solution. ^c Control experiment in the absence of PtOEP. ^d [1] = 50 mM. ^e 3 h irradiation. ^f [DPA] = 1.0 mM. ^g Experiment under N₂. ^h 2 h irradiation using green LED (λ_{max} = 525 nm, 3.8 W). ⁱ 24 h irradiation using green LED (λ_{max} = 525 nm, 3.8 W). ^j Control experiment using benzene as solvent. ^k Concentration of LMW gelator. ^l Conversion calculated by GC-FID. ^m Total yield calculated by GC-FID. *n*-Pentadecane was used as internal standard for quantitative GC-FID analyses. Estimated error from randomly duplicated experiments ± 2%.

This was supported by nearly complete decolorization of the solution after irradiation (Figure 3a). In sharp contrast, a remarkable increase of conversion, excellent mass balance and good overall yield were observed when the gel made of **G-1** in aerated DMF was used as confined medium (Table 1, entry 2).

No decolorization of the mixture was observed after light exposure in this case (Figure 3b), indicating that the TTA system (PtOEP/DPA) was stable under these conditions affording the photoreduction product **2** without formation of byproducts. Irradiation experiments were carried out at room temperature in an acclimatized room; potential thermal effects were ruled out by measuring the temperature of the gel samples after 2 h irradiation, which showed an increment of only 2 °C.

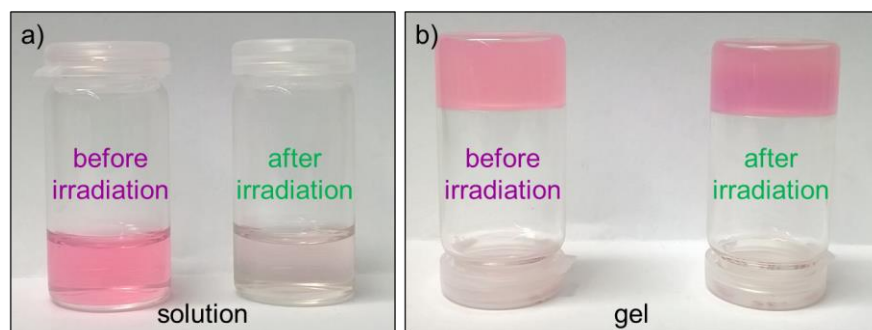


Figure 3. a) Photographs of doped solutions before/ after irradiation (Table 1, entry 1) showing decolorization caused by degradation of PtOEP, b) Photographs of doped gel before/ after irradiation (Table 1, entry 2). T_{gel} (48 ± 2 °C) remained constant after irradiation.

As expected, the control experiment in the absence of the donor PtOEP showed no conversion (Table 1, entry 3). At this point, mixtures of **1**, PtOEP and DPA in the presence of different **G-1** concentrations were submitted to steady-state irradiations. Similar conversions, as well as mass balances and total yields, were obtained for all cases (Table 1, entries 4-8) suggesting that **G-1** was not involved in the photoreaction but playing a crucial role as nanoreactor. In comparison to the result obtained under optimized conditions (Table 1, entry 2), the use of either higher substrate concentration, longer irradiation times or lower acceptor concentration resulted in lower conversions and yields (Table 1, entries 9-11). Very interestingly, comparable results were obtained when the model reaction was carried out under nitrogen atmosphere instead of aerobic conditions (Table 1, entry 12 vs 2), which is indicative of the efficient confinement effect of the gel network for photoinduced radical reactions in air. On the other hand, green LED irradiation ($\lambda_{max} = 525$ nm, 3.8 W) resulted in very low conversion regardless the irradiation time, presumably due to the formation of insufficient concentration of DPA triplet states for the TTA process, favoring other deactivation pathways such as phosphorescence or self-quenching (Table 1, entries 13-14). It is also noteworthy that photoreduction of **1** by means of intragel TTA-UC was not specific of gelator **G-1**. In this respect, another model gelator (**G-2**) lacking the carbamate unit and involving a different assembly pattern³⁴ also provided a suitable supramolecular network for the photolysis of **1** in the presence of PtOEP and DPA (Table 1, entries 16-17). Considering the great structural versatility of LMW gelators and, therefore, the tunable properties of their gels, this result bears special relevance to future optimization of intragel photo processes.

Furthermore, oscillatory rheological measurements (*i.e.*, DFS, DSS and DTS) confirmed the preservation of the gel nature of the samples after irradiation (Figure 4). Destruction of the gels at low frequency and below 5% strain indicated the brittle nature of the materials. DTS

measurements at 0.01% strain and 1 Hz frequency confirmed the stability of the gel materials as a function of the ageing time at room temperature. The storage modulus G' was approximately one order of magnitude higher than the loss modulus G'' within the linear viscoelastic regime. The undoped gel was made of **G-1** ($c = 10 \text{ g L}^{-1}$) and the doped gel as described in Table 1 (entry 2) before and after 2 h irradiation with a pulsed laser at $\lambda_{\text{exc}} = 532 \text{ nm}$.

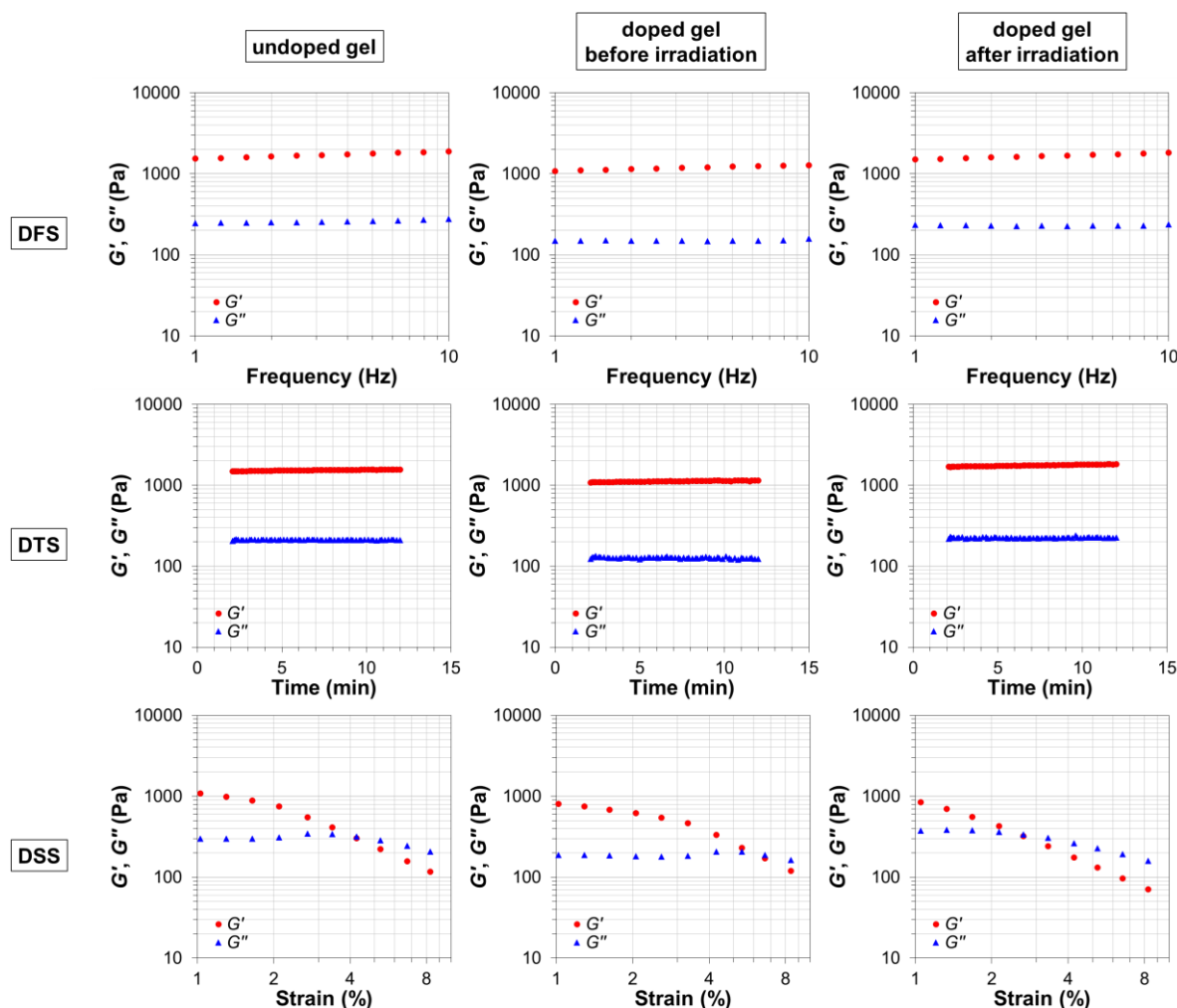


Figure 4. Oscillatory rheological experiments of model undoped and doped gels. Conditions for preparing the doped gel: $[\mathbf{G-1}] = 10 \text{ g L}^{-1}$, $[1] = 10 \text{ mM}$, $[\text{PtOEP}] = 33 \text{ }\mu\text{M}$, $[\text{DPA}] = 6.7 \text{ mM}$.

$G_{\text{el-to-sol}}$ transition temperatures (T_{gel}), absolute moduli and mean values of $\tan \delta$ were found almost invariable within the experimental error both after initial gel doping and after irradiation, suggesting the maintenance of the mechanical damping properties of the parent (undoped) supramolecular gel network during the experiments.

Figure 5 shows a few more examples of intragel photoreductions in air that strongly support the proof of concept.

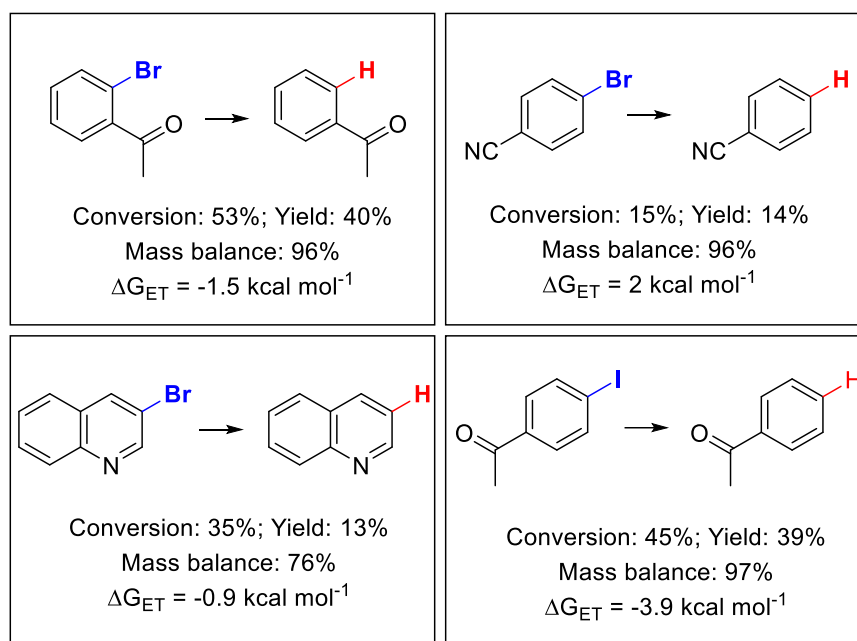


Figure 5. Additional examples of intragel photocatalyzed reduction at RT in air.

The observed differences in reactivity can be correlated with the activation barriers, for instance, SET vs back-electron transfer (BET). It is important to emphasize that, as expected, substituted aryl bromides with very high reduction potentials (e.g., alkyl-, MeO-, CF₃-, NO₂-substituted compounds) showed no photoreduction activity under the conditions. Hence, the reduction potentials of the aryl halides, as well as the oxidation potential of DPA, were obtained in DMF solution by cyclic voltammetry. Taking into account the singlet energy of DPA, which was found to be 71.5 kcal mol⁻¹ in aerated DMF, and the relative permittivity of the DMF ($\epsilon = 36.7$), the free energy changes ΔG_{ET} associated with the electron transfer from the DPA singlet were obtained using the Weller equation (Eq. 1).³⁷ Accordingly, SET from ¹(DPA)* appeared to be thermodynamically feasible for the aryl halides used in this proof of concept study.

$$\Delta G_{ET} \text{ (kcal mol}^{-1}\text{)} = 23.06 \times [E_{ox} - E_{red} + (2.6/\epsilon) - 0.13] - E^*(S^1) \quad (\text{Eq. 1})$$

3.5.3.4. Mechanistic Investigation

A possible reaction mechanism for the intragel photocatalytic reduction of aryl halides by sequential TTA, SET and H-atom transfer (HAT) is outlined in Figure 6.

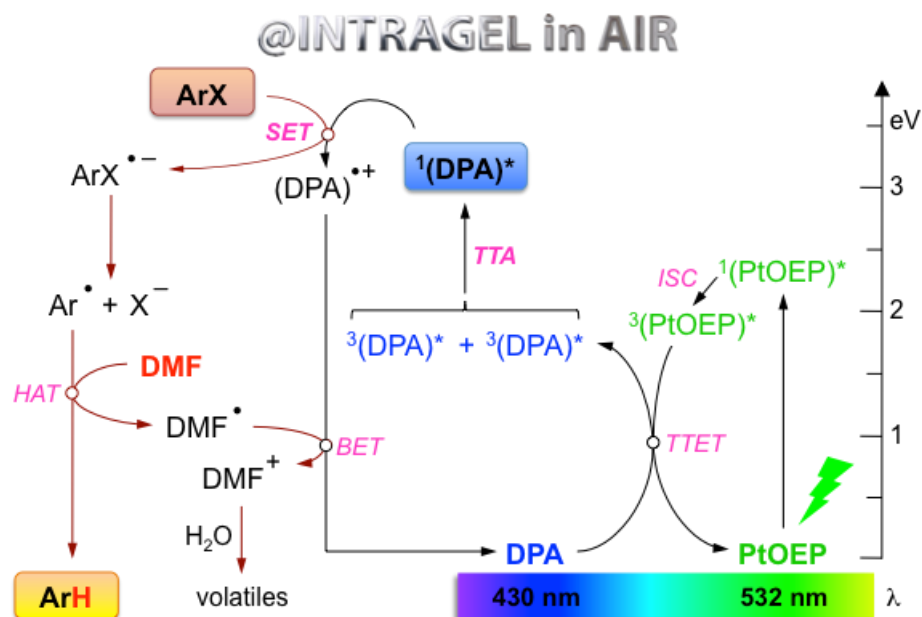


Figure 6. A plausible mechanism for visible light photocatalytic reduction of aryl halides at RT in air based on the combination of TTA-UC and SET processes within a gel network.

The process is initiated by the selective excitation of PtOEP at 532 nm to generate the $^3(\text{PtOEP})^*$ state after efficient ISC. Subsequently, PtOEP could be restored upon TTET with DPA, giving rise to long-lived $^3(\text{DPA})^*$. After migration through the stabilizing gel network, a collision between two $^3(\text{DPA})^*$ molecules effects population of the $^1(\text{DPA})^*$ state. These species can induce SET to the electrophilic aryl halides, leading to the formation of the unstable radical anions $\text{ArX}^{\bullet-}$, which undergo fragmentation affording the corresponding aryl radicals Ar^\bullet and anions X^- . Finally, rapid HAT from solvent (DMF) molecules yields the formal reduction product ArH (this was confirmed by using DMF-d_7). The formed radical DMF^\bullet may regenerate DPA by BET giving highly electrophilic DMF^+ species, which are known to be hydrolyzed into volatile products upon workup.³⁸ To rule out the possibility of gelator molecules being involved in the trapping Ar^\bullet by N-H abstraction, control experiments were performed with benzene and toluene as solvents. In agreement with the proposed mechanism, no conversion of the starting material was observed in these cases (Table 1, entry 15).

3.5.4. Conclusion and Outlook

For the first time, it was demonstrated the possibility of photocatalytic reduction of aryl halides through cleavage of the C-halogen bond by means of low-energy visible light irradiation of a proper donor/acceptor system embedded in a physical gel. The strategy is based on the unprecedented combination of a cascade of photophysical and photochemical events involving green-to-blue TTA-UC, SET and HAT as key steps. The gel network provides a suitable stabilizing microenvironment to achieve the challenging multistep process under aerobic conditions, at RT and without additional additives such as bases or acids. Good conversions and excellent mass balances were observed with several aryl halides. In general, large active reaction areas, good diffusion properties, reversibility, reduced overheating effects, multistimuli responsiveness, reusability and tunable structural/ functional properties are some of the major features of physical gels as confined reaction media or micro/nanoreactors. Considering the great versatility of supramolecular gel networks, high functional group tolerance of low-energy visible light irradiation and other possible combinations of sensitizers and annihilators, there is plenty of room for optimization of such intragel photoinduced processes. Studies toward this direction are currently underway in our laboratories. This proof of concept goes well beyond the classical studies of delayed fluorescence involving TTA and opens the door for future work involving bond activation pathways that are inaccessible in solution under very mild conditions.

3.5.5. Experimental Part

3.5.5.1. Materials and Methods

All reagents and solvents were used as received unless otherwise indicated. Platinum(II) octaethylporphyrin (PtOEP), 9,10-diphenylanthracene (DPA), 4-bromoacetophenone, 2-bromoacetophenone, 4-bromobenzonitrile, 3-bromoquinoline, 4-iodoacetophenone, and acetophenone were commercially available. *N,N*-Dimethylformamide (DMF, p.a. grade) was used as solvent without further purification. Anhydrous DMF (Aldrich) was used for experiments under nitrogen atmosphere.

Gel-to-sol transition temperatures (T_{gel}) were determined using a custom-made set-up where a sealed vial was placed into a mold of an alumina block and heated up at 1 °C/5 min using an electric heating plate equipped with a temperature control couple. The values obtained by this method have been previously verified with different supramolecular gels by means of DSC measurements as well as the inverse flow method (IFM).³⁹ It should be noted that the values determined by IFM strongly depend on factors such as cooling rate, aging time, thermal history, and degree of hysteresis among others. Moreover, verification of the independence of the position inside the custom-made apparatus has also been carried out.⁴⁰ Herein, the temperature at which the gel started to break was defined as T_{gel} with an estimated error of ± 2 °C after several heating-cooling cycles. Oscillatory rheology was performed with a AR 2000 Advanced rheometer (TA Instruments) equipped with a Julabo C cooling system. A 500 μm gap setting and a torque setting of 40,000 dynes/cm² at 25 °C were used for the measurements in a plain-plate (40 mm, stainless steel). The following experiments were performed using 2 mL total gel volume: a) Dynamic strain sweep (DSS): variation of G' and G'' with strain (from 0.01 to 100%); b) dynamic frequency sweep (DFS): variation of G' and G'' with frequency (from 0.1 to 10 Hz at 0.1% strain); c) dynamic time sweep (DTS): variation of G' and G'' with time keeping the strain and frequency values constant and within the linear viscoelastic regime as determined by DSS and DFS measurements (strain = 0.1% strain; frequency = 1 Hz). GC-FID was performed on a 7820A Agilent GC which was calibrated using a four-point calibration vs. 10 mM of the internal standard *n*-pentadecane. The GC oven temperature program was adjusted as follows: The initial temperature (50 °C) was kept for 0.5 min, and subsequently increased at a rate of 25 °C min⁻¹ over a period of 8 min until the final temperature (280 °C) was reached and maintained for 10 min. UV-vis analyses were performed on a Varian Cary 50 UV-vis spectrophotometer. Steady-state fluorescence measurements were performed with Horiba FluoroMax4 fluorimeter. Excitation and emission

slit widths were 1 nm. Screw-cap Hellma quartz SUPRASIL® cuvettes (117.100F-QS, 10 ×10 mm) with a screw-cap with PTFE-coated silicon septum were used. DPA concentration was 0.01 mM in DMF. Laser flash photolysis system: The pump source is an optical parametric oscillator (OPO) pumped by the third Harmonic of an Nd:YAG-laser (Surelite II and Surelite OPO PLUS, Continuum). The wavelength can be set from 400 nm to ca. 700 nm, with a pulse width of ca. 5 nm. The typical pulse duration is 8 ns. LED photolysis system: The vial containing the corresponding doped gel was placed vertically above the aperture of the LED during the experiments using a custom made cooling apparatus. The redox potentials were measured by cyclic voltammetry with an Autolab PGSTAT302N Metrohm apparatus. All measurements were made in deaerated DMF containing tetrabutylammonium tetrafluoroborate (0.1 M) as supporting electrolyte, a glassy carbon as working electrode, a platinum wire as counter electrode, a silver wire as pseudo reference and ferrocene as internal standard. The scan rate was 0.05 V s⁻¹. Potentials are reported with respect to the saturated calomel electrode (SCE) as reference.⁴¹

3.5.5.2. Synthesis of LMW Gelator

LMW gelators **G-1** and **G-2** were synthesized according to literature procedures and showed spectroscopic data in agreement to those published.^{33,34}

N,N'-bis(octadecyl)-L-boc-glutamic diamide (**G-1**)

Boc-L-glutamic acid (2.47 g, 0.01 mol) and octadecylamine (5.39 g, 0.02 mol) were mixed in a 250 mL flask and dry DCM (200 mL) was added. Then 1-ethyl-3-(3-dimethylaminopropyl)carbodiimide hydrochloride (EDC) (4.02 g, 0.022 mol) and 1-hydroxybenzotriazole (HOBt, 2.97 g, 0.022 mol) were added to the mixture and stirred at RT for 72 h. The obtained white solid was isolated by filtration and washed three times with DCM. The crude product was dissolved in THF and precipitated by water. A fine white solid obtained (6.5 g, 87% yield). ¹H NMR (300 MHz, CDCl₃), δ (ppm) = 0.86-0.89 (t, 6H, J = 6.8 Hz); 1.25 (br s, 60H), 1.43 (s, 9H); 1.47-1.50 (m, 4H); 1.85-2.05 (m, 2H); 2.25-2.40 (m, 2H); 3.20-3.25 (m, 2H), 4.10 (br s, 1H); 5.63 (br s, 1H); 6.11 (br s, 1H); 6.57 (br s, 1H).

N,N'-((1*S*,2*S*)-cyclohexane-1,2-diyl)didodecanamide (**G-2**)

To a stirred solution of (1*S*,2*S*)-(+)-*N,N'*-dimethyl-1,2-cyclohexanediamine (114 mg, 1.00 mmol) in THF (18 ml) lauroyl chloride (438 mg, 475 µl, 2.00 mmol) and NEt₃ (337 mg, 787 µl, 3.33 mmol) were added dropwise. The mixture was refluxed for 5 h and allowed to cool to RT. The precipitated triethylammonium chloride was filtered off and the solvent of the

remaining filtrate removed under reduced pressure. The obtained residue was washed with aqueous 1 M HCl (4x5 ml) and water (4x5 ml), dried and recrystallized from acetone affording **G-2** as a white solid in 39% yield (187 mg, 0.391 mmol). ¹H-NMR (400 MHz, CDCl₃) δ (ppm) = 5.88 (s, 2H), 3.65 (m, 2H), 2.11 (m, 4H), 2.02 (m, 2H), 1.75 (m, 2H), 1.57 (m, 4H), 1.25 (s, 36H), 0.88 (t, J = 6.44 Hz, 6H).

3.5.5.3. General Procedure for Photocatalytic Dehalogenation Reaction

A suspension of **G-1** (10 g L⁻¹), **1** (10 mM), PtOEP (33 μ M), DPA (6.7 mM) and *n*-pentadecane (10 mM, internal standard) in DMF (2 mL) was gently heated with a heat gun at 80 °C during 1 min until an isotropic solution was obtained. The corresponding gel was obtained upon cooling the mixture to RT. The corresponding gel was irradiated under aerobic conditions during 120 min in a pulsed Nd:YAG-laser instrument using 532 nm as selective wavelength. Afterwards, dichloromethane (5 mL) was added and washed with brine (5 mL). The organic phase was separated, dried (Na₂SO₄) and filtered for further analysis. GC-FID was used to follow the course of the reaction and determining conversions and total yields.

→ Additional information can be found in the ESI on the enclosed CD or in the ESI of the paper.

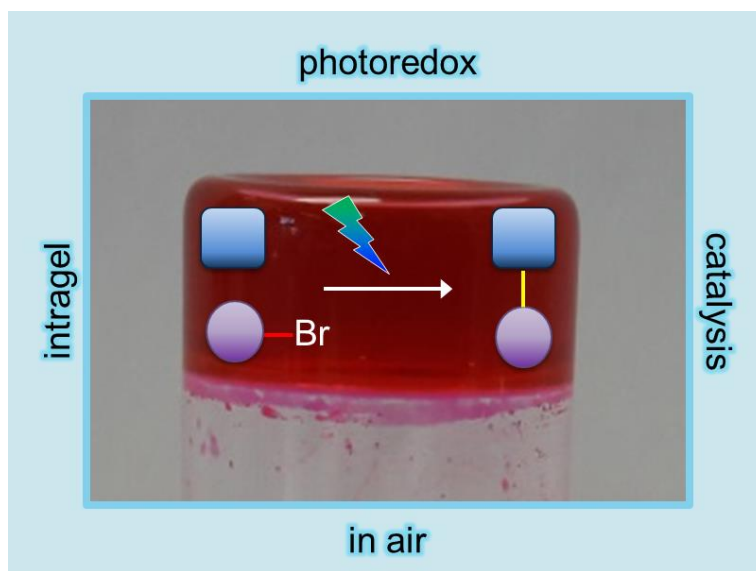
3.5.6. References

- [1] J. A. Prescher, C. R. Bertozzi, *Nat. Chem. Biol.*, **2005**, 1, 13-21.
- [2] Z. V. Todres in *Organic Chemistry in Confined Media*. Springer, Switzerland, **2013**.
- [3] G. Palmisano, V. Augugliaro, M. Pagliaro, L. Palmisano, *Chem. Commun.*, **2007**, 3425-3437.
- [4] a) D. G. Shchukin, D. V. Sviridov, *J. Photochem. Photobiol. C*, **2006**, 7, 23-39; b) M. D. Ward, *Chem. Soc. Rev.*, **1997**, 26, 365-375; c) A. Maldotti, A. Molinari, R. Amadelli, *Chem. Rev.*, **2002**, 102, 3811-3836.
- [5] a) M. Pagliaro, R. Ciriminna, G. Palmisano, *Chem. Soc. Rev.*, **2007**, 36, 932-940; b) E. E. Santiso, A. M. George, C. H. Turner, M. K. Kostov, K. E. Gubbins, M. Buongiorno-Nardelli, M. Sliwinska-Bartkowiak, *Appl. Surf. Sci.*, **2005**, 252, 766-777.
- [6] M. Antonietti, G. A. Ozin, *Chem. Eur. J.*, **2004**, 10, 28-41.
- [7] J. G. Riess, *Chem. Rev.*, **2001**, 101, 2797-2920.
- [8] C. Harris, P. V. Kamat, *ACS Nano*, **2009**, 3, 682-690.
- [9] O. V. Vasil'tsova, V. N. Parmon, *Kinet. Catal.*, **1999**, 40, 62-70.
- [10] K. Uekama, F. Hirayama, T. Irie, *Chem. Rev.*, **1998**, 98, 2045-2076.
- [11] D. Limones-Herrero, R. Pérez-Ruiz, M. C. Jiménez, M. A. Miranda, *Photochem. Photobiol.*, **2014**, 90, 1012-1016.
- [12] D. G. Shchukin, E. A. Ustinovich, A. I. Kulak, D. V. Sviridov, *Photochem. Photobiol. Sci.*, **2004**, 3, 157-159.
- [13] J. H. Fendler, *Chem. Rev.*, **1987**, 87, 877-899.
- [14] D. K. Smith in *Supramolecular Chemistry: From Molecules to Nanomaterials*, eds. J. W. Steed, A. P. Gale, Wiley, Chichester, UK, 1 st ed., **2012**, 7, 3355-3376.
- [15] R. Pérez-Ruiz, D. D. Díaz, *Soft Matter*, **2015**, 11, 5180-5187.
- [16] a) J. Zhou, Q. Liu, W. Feng, Y. Sun, F. Li, *Chem. Rev.*, **2015**, 115, 395-465; b) G. Chen, H. Qiu, P. N. Prasad, X. Chen, *Chem. Rev.*, **2014**, 114, 5161-5214.
- [17] a) J. I. Bardagí, V. A. Vaillard, R. A. Rossi in *Encyclopedia of Radicals in Chemistry, Biology and Materials*, eds. C. Chatgililoglu and A. Studer, Wiley, **2012**, 333; b) J. Zhao, S. Ji and H. Guo, *RSC Adv.*, **2011**, 1, 937-950; c) T. N. Singh-Rachford, F. N. Castellano, *Coord. Chem. Rev.*, **2010**, 254, 2560-2573.
- [18] J. Z. Zhao, S. M. Ji, H. M. Guo, *RSC Adv.*, **2011**, 1, 937-950.
- [19] J. H. Kim, J. H. Kim, *J. Am. Chem. Soc.*, **2012**, 134, 17478-17481.
- [20] A. Monguzzi, R. Tubino, S. Hoseinkhani, M. Campione, F. Meinardi, *Phys. Chem. Chem. Phys.*, **2012**, 14, 4322-4332.

- [21] V. Gray, D. Dzebo, M. Abrahamsson, B. Albinsson K. Moth-Poulsen, *Phys. Chem. Chem. Phys.*, **2014**, 16, 10345-10352.
- [22] R. Vadrucchi, C. Weder, Y. C. Simon, *Mater. Horiz.*, **2015**, 2, 120-124.
- [23] K. Sripathy, R. W. MacQueen, J. R. Peterson, Y. Y. Cheng, M. Dvorak, D. R. McCamey, N. D. Treat, N. Stingelind, T. W. Schmidt, *J. Mater. Chem. C*, **2015**, 3, 616-622.
- [24] P. Duan, N. Yanai, H. Nagatomi, N. Kimizuka, *J. Am. Chem. Soc.*, **2015**, 137, 1887-1894.
- [25] P. Duan, N. Yanai, Y. Kurashige, N. Kimizuka, *Angew. Chem., Int. Ed.*, **2015**, 54, 7544-7549.
- [26] T. Ogawa, N. Yanai, A. Monguzzi, N. Kimizuka, *Sci. Rep.*, **2015**, 5, 10882.
- [27] (a) V. Balzani, P. Ceroni, A. Juris, *Photochemistry and Photophysics: Concepts, Research, Applications*, Wiley-VCH, Weinheim, **2014**; (b) A. G. Griesbeck, M. Oelgemöller, F. Ghetti, *CRC Handbook of Organic Photochemistry and Photobiology*, 3rd edn, CRC Press, Boca Raton, **2012**.
- [28] (a) D. M. Schultz, T. P. Yoon, *Science*, **2014**, 343, 1239176; (b) D. Ravelli, S. Protti, M. Fagnoni, A. Albini, *Curr. Org. Chem.*, **2013**, 17, 2366-2373; (c) C. K. Prier, D. A. Rankic, D. W. C. MacMillan, *Chem. Rev.*, **2013**, 113, 5322-5363; (d) M. Reckenthäler, A. G. Griesbeck, *Adv. Synth. Catal.*, **2013**, 355, 2727-2744.
- [29] Procedures for visible light-mediated aromatic functionalization require the use of highly electrophilic arenediazonium salts or aryl iodides. For selected examples, see (a) M. Majek, A. Jacobi von Wangelin, *Angew. Chem., Int. Ed.*, **2015**, 54, 2270-2274; (b) D. P. Hari, P. Schroll, B. König, *J. Am. Chem. Soc.*, **2012**, 134, 2958-2961; (c) J. D. Nguyen, E. M. D'Amato, J. M. R. Narayanam and C. R. J. Stephenson, *Nat. Chem.*, **2012**, 4, 854-859.
- [30] C. P. Andrieux, C. Blocman, J.-M. Dumas-Bouchiat, J.-M. Saveant, *J. Am. Chem. Soc.*, **1979**, 101, 3431-3441.
- [31] For a compilation of dyes and their redox potentials, see: <http://brsmblog.com/diroccos-electrochemical-series-photocatalysts/>.
- [32] (a) I. Ghosh, T. Ghosh, J. I. Bardagi, B. König, *Science*, **2014**, 346, 725; (b) E. H. Discekici, N. J. Treat, S. O. Poelma, K. M. Mattson, Z. M. Hudson, Y. Luo, C. J. Hawker, J. R. de Alaniz, *Chem. Commun.*, **2015**, 11705-11708.
- [33] Y. Li, T. Wang, M. Liu, *Soft Matter*, **2007**, 3, 1312-1317.

-
- [34] K. Hanabusa, M. Yamada, M. Kimura, H. Shirai, *Angew. Chem., Int. Ed. Engl.*, **1996**, 35, 1949-1951.
- [35] a) M. Vriezema, M. C. Aragonès, J. A. A. W. Elemans, J. J. L. M. Cornelissen, A. E. Rowan and R. J. M. Nolte, *Chem. Rev.*, **2005**, 105, 1445-1489; b) D. Kühbeck, R. J. Koppmans, D. D. Díaz, *Chem. Soc. Rev.*, **2011**, 40, 427-448.
- [36] (a) J.-H. Kim, J.-H. Kim, *J. Am. Chem. Soc.*, **2012**, 134, 17478-17481; (b) Y. C. Simon, C. Weder, *J. Mater. Chem.*, **2012**, 22, 20817-20830.
- [37] A. Weller, *Z. Phys. Chem.*, **1982**, 133, 93-98.
- [38] M. Majek, F. Filace, A. Jacobi von Wangelin, *Chem.-Eur. J.*, **2015**, 21, 4518-4522.
- [39] J. E. Eldrige, J. D. Ferry, *J. Phys. Chem.*, **1954**, 58, 992-995.
- [40] J. Bachl, A. Hohenleutner, B. B. Dhar, C. Cativiela, U. Maitra, B. König, D. D. Díaz, *J. Mater. Chem. A*, **2013**, 1, 4577-4588.
- [41] V. V. Pavlishchuk, A. W. Addison, *Inorg. Chim. Acta*, **2000**, 298, 97-102.

3.6. Air-Sensitive Photoredox Catalysis Performed under Aerobic Conditions in Gel Networks



This chapter has been published in:

M. Häring, A. Abramov, K. Okumura, I. Ghosh, B. König, N. Yanai, N. Kimizuka, D. D. Díaz, 'Air-sensitive photoredox catalysis performed under aerobic conditions in gel networks', *J. Org. Chem.*, **2018**, doi: 10.1021/acs.joc.8b00797 – Reproduced with permission from J. Org. Chem., 2018, doi: 10.1021/acs.joc.8b00797. Copyright 2018 American Chemical Society.

Author contribution:

MH performed the experiments for the photocatalytic arylation reaction, rheology and UV-vis-spectroscopy. AA performed the experiments for the trifluoromethylation reaction. NY did the photophysical characterization of $\text{Ru}(\text{phen})_3\text{Cl}_2$. All authors contributed to the scientific discussion of the results.

3.6.1. Abstract

In this chapter, it was demonstrated that useful C-C bond forming photoredox catalysis, here the arylation reaction of aryl halides, can be performed in air using easily-prepared gel networks as reaction media to give similar results as are obtained under inert-atmosphere conditions. These reactions are completely inhibited in homogeneous solution in air. However, the supramolecular fibrillar gel networks confine the reactants and block oxygen diffusion allowing air-sensitive catalytic activity under ambient conditions. The mechanism of this remarkable protection was investigated, focusing on boundary effect in the self-assembled supramolecular gels that enhance the rates of productive reactions over diffusion-controlled quenching of excited states. The observations suggest the occurrence of triplet sensitized chemical reactions in the gel networks within the compartmentalized solvent pools held in between the nanofibers. The combination of enhanced viscosity and added interfaces in supramolecular gel media seems to be a key factor to facilitate the reactions under aerobic conditions.

3.6.2. Introduction

Nature uses confined and compartmentalized environments such as organelles to carry out chemical reactions under mild conditions with precise control of kinetics and selectivity. Over the last few decades, this has served as an inspiration to develop artificial nanoreactors based on directed self-assembly of small molecules through non-covalent interactions.¹⁻³ Within this context, photochemistry can benefit from confined spaces,^{4,5} for example when performed in mesoporous inorganic materials,⁶ microemulsions,⁷ micelles,^{8,9} vesicles,¹⁰ polyelectrolyte nanoparticles,¹¹ foams,¹² and gels.^{13,14} The confinement may improve photochemical processes by influencing key aspects such as light absorption and the lifetime of redox intermediates.^{15,16} Among the above-mentioned confined media, physical or supramolecular gels¹⁷ are typically made of low-molecular-weight (LMW) compounds, self-assembled through non-covalent interactions (e.g., hydrogen-bonding, van der Waals, charge-transfer, dipolar, π - π stacking), which usually provides reversible *gel-to-sol* phase transitions as a response to external stimuli. The solid-like appearance and rheological behavior of these materials result from the immobilization of the liquid (major component) into the interstices of a self-assembled matrix (minor component) through high surface tension and capillary forces, making the liquid pools different from homogeneous solutions.¹⁷ The formation of the 3D-network interconnected through numerous junction zones results from the entanglement of 1D-strands of gelator molecules, typically of nm diameters and mm lengths, and can increase the viscosity of the medium by factors up to 10^{10} . Along these lines, our group recently reported¹⁸ the first photoreduction of aryl halides in air by low energy light irradiation of a proper donor/acceptor pair embedded in a physical gel,¹⁷ which protected triplet excited states from oxygen deactivation (see chapter 3.5.). In this study, it is hypothesized that compartmentalized low viscosity media provided by self-assembled gels could facilitate even more challenging air-sensitive photoinduced C-C cross-coupling reactions under aerobic conditions.¹⁹ Boundary effects may enhance the rates of the productive reactions over diffusion-controlled quenching of excited states. In order to demonstrate this, it was focused on two important processes involving (1) functionalization of aryl halides and (2) trifluoromethylation of arenes (only a short summary will be given of the trifluoromethylation).

3.6.3. Results and Discussion

3.6.3.1. Synthesis of LMW Gelator

The LMW gelators *N,N'*-bis(octadecyl)-L-Boc-glutamic diamide (**G-1**), (1*S*,2*S*)-dodecyl-3-[2(3-dodecyl-ureido)cyclohexyl]urea (**G-2**), *N,N'*-((1*R*,2*R*)-cyclohexane-1,2-diyl)didodecanamide (**G-3**) were synthesized according to the literature.²⁰⁻²² 1,3:2,4-bis(3,4-dimethylbenzylidene)-sorbitol (**G-4**) was commercially available. Figure 1 provides an overview of the four LMW gelators that were used in this study.

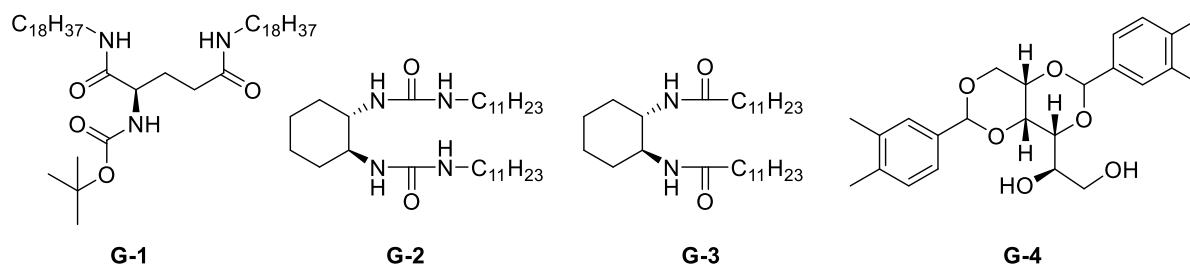


Figure 1. Overview of the four LMW gelators used in this study.

3.6.3.2. Photocatalytic Arylation Reaction

The selective functionalization of aryl-halides was obtained with rhodamine-6G (Rh-6G) as photocatalyst.²³ As previously described, this process is based on the possibility of tuning the redox potential of Rh-6G over a range of 2.4 V using different colors of visible light (Figure 2).^{23,24}

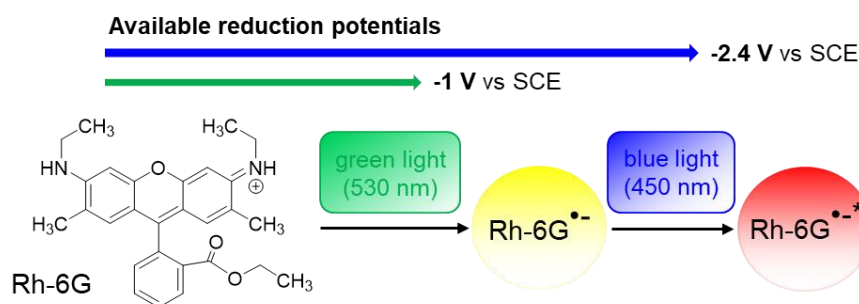


Figure 2. Light-color-selective generation of the redox active species Rh-6G^{•-} and Rh-6G^{•-•-} which provide drastically different reduction potentials for photocatalysis. Adapted from ref. 23 with permission from John Wiley and Sons.

The strategy involves the generation of the ground-state Rh-6G^{•-} radical anion in the presence of an electron donor under green-light irradiation, and the excited Rh-6G^{•-•-} radical anion upon blue light irradiation. However, due to the instability of Rh-6G radical anions in the presence of oxygen, so far, an oxygen-free environment has been required to carry out these reactions. This limitation is overcome by simply including a small amount of a low-molecular-weight (LMW) gelator in the reaction mixture, which transforms the solution into a viscoelastic gel medium.

For the initial proof-of-concept, 2-bromobenzonitrile (**1**) was used as test substrate, *N*-methylpyrrole (**2**) as trapping agent, Rh-6G as photocatalyst, *N,N*-diisopropylethylamine (DIPEA) as electron donor, *N,N'*-bis(octadecyl)-*L*-Boc-glutamic diamide (**G-1**) as gelator, and DMSO as solvent.

Table 1. Control experiments for intragel C-H arylation between **1** and **2** as model reaction.^a

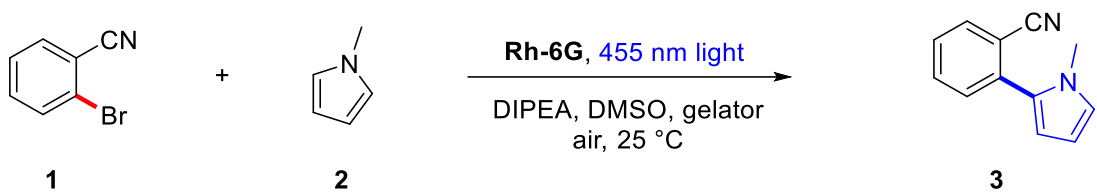
Entry	Rh-6G (10 mol%)	DIPEA (1.5 equiv.)	Modifications	Yield of 3 (%) ^b
1	✓	✓	-	53 ^c
2	✗	✓	No photocatalyst	9
3	✓	✗	No donor	3
4	✗	✗	No catalyst, no donor	3
5	✓	✓	530 nm light	12
6	✓	✓	No gelator	5

^a Reactants and conditions: **1** (0.1 mmol), **2** (1.8 mmol), DIPEA (0.15 mmol, 1.5 equiv.), Rh-6G (10 mol%), **G-1** (10 g L⁻¹), DMSO (1.5 mL), 24 h, 25 °C, reaction flask was equipped with two needles to ensure air flow.

^b Determined by GC-FID with biphenyl as internal standard. ^c Not optimized reaction conditions for reaction inside gel medium.

In agreement with previous observations,²³ the dehalogenative arylation reaction between **1** and **2** was ineffective in aerated DMSO solution at room temperature leading to very low yield (5% yield estimated by GC) of the desired coupling product (Table 1, entry 6) upon irradiation with blue LED light ($\lambda_{\text{Ex}} = 455 \pm 15$ nm). In contrast, when the same reaction was performed under aerobic conditions within the gel made of **G-1** (10 g L⁻¹), the GC yield improved drastically to 53% (Table 1, entry 1). Control experiments confirmed that the arylation reaction is a photochemically mediated process, when the photocatalyst (Table 1, entry 2), the electron donor or both (Table 1, entry 3 and 4, respectively) were omitted, only low yields were obtained. In addition, the wavelength of the light plays a crucial role, applying 530 nm (Table 1, entry 5) instead of 455 nm significantly decreased the yield. The control reactions additionally prove that the gelator has no catalytic effect on the arylation reaction, it only provides an inert reaction medium. Further optimization experiments were performed with different gelators and variations of the gelator concentration (Table 2).

Table 2. Gelator screening of intragel C-H arylation between **1** and **2** as model reaction.^a

			
Entry	Gelator	Gelator concentration [g L ⁻¹]	Yield of 3 [%] ^c
1	G-1	2	54
2	G-1	5	53
3	G-1	10	57
4	G-1	15	69
5	G-2	15	62
6	G-3	15	49
7 ^b	G-4	120	60

^a Reactants and conditions: **1** (0.1 mmol), **2** (1.8 mmol), DIPEA (0.15 mmol, 1.5 equiv.), Rh-6G (10 mol%), **G-1** (10 g L⁻¹), DMSO (1.5 mL), 24 h, 25 °C, reaction flask was equipped with two needles to ensure air flow.^b As solvent DMSO/toluene 4:6 was used instead of only DMSO, otherwise no gel state was achieved. ^c Yield was determined by GC-FID with biphenyl as internal standard.

The yield could be improved by increasing the gelator concentration of **G-1** (Table 2, entry 4) to 15 g L⁻¹. The use of other LMW gelators like **G-2** (entry 5) or **G-3** (entry 6) instead of **G-1** provided comparable results in the photoredox reductive arylation with slight differences in the yields. Remarkably, the use of **G-4** (entry 7) suppressed the formation of the reduction byproduct. These results suggest a possible effect of the gel network on different reaction pathways by interactions with the reactants.

Optimization of the amount of DIPEA (Table 3), lead to the best result (73%, GC yield) using 15 g L⁻¹ of **G-1** and 2.2 equiv. of DIPEA with respect to **1** (Table 3, entry 3).

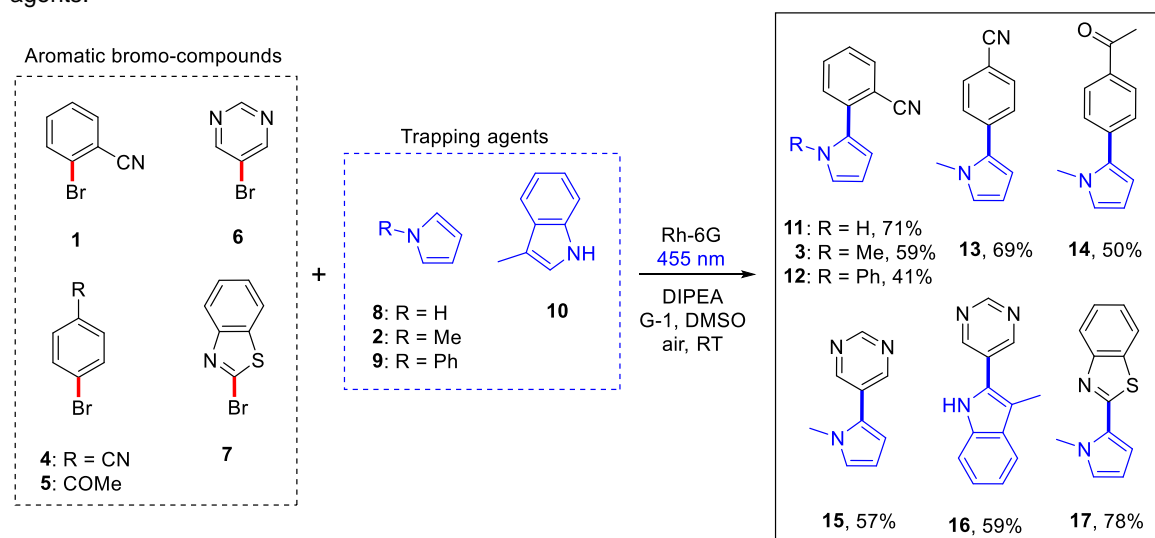
Table 3. Optimization of the reaction conditions for intragel C-H arylation between **1** and **2** as model reaction.^a

Entry	Rh-6G [mol%]	DIPEA [equiv.]	G-1 [g L ⁻¹]	Yield of 3 [%] ^b
1	10	1.5	15	69
2	15	1.5	15	65
3	15	2.2	15	73

^a Reactants and conditions: **1** (0.1 mmol), **2** (1.8 mmol), DIPEA (0.15 mmol, 1.5 equiv.), Rh-6G (10 mol%), **G-1** (10 g L⁻¹), DMSO (1.5 mL), 24 h, 25 °C, reaction flask was equipped with two needles to ensure air flow.

^b Yield was determined by GC-FID with biphenyl as internal standard.

The scope of the intragel photoredox catalytic arylation in air was established using differently substituted aryl or hetero aryl halides and trapping agents (Scheme 1).

Scheme 1. Substrate scope of intragel cross-coupling reactions between bromo-compounds and trapping agents.^a

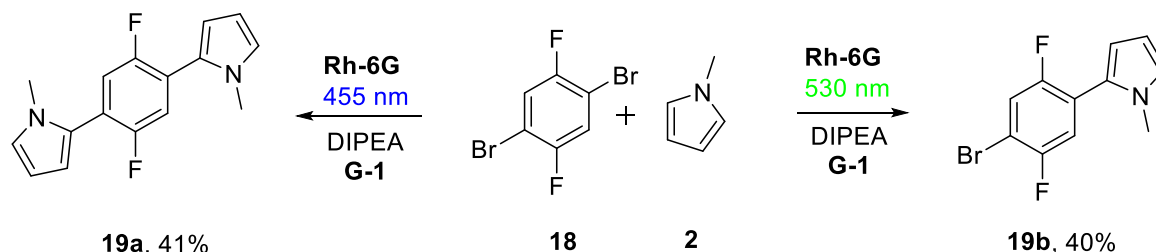
^a Reaction conditions: Bromo-compound **1**, **4-7** (0.1 mmol), trapping agent **2**, **8-10** (5-18 equiv.), Rh-6G (15 mol%), DIPEA (2.2 equiv.), **G-1** (15 g L⁻¹), DMSO, air, RT, λ_{ex} = 455 nm, reaction time: 24-96 h. Yield of isolated products.

Aromatic bromo compounds bearing electron-withdrawing substituents (*i.e.*, -CN, -COMe) (**1**, **4**, **5**) reacted with pyrrole derivatives (**2**, **8**, **9**) at RT affording the desired cross-coupling products (**3**, **11-14**) with modest to good isolated yields and mass balances (> 90%) that were comparable to those obtained in solution under strict inert conditions and identical reaction times (Figure S10).

Indeed, UV-vis spectroscopy confirmed that the photocatalyst inside the gel shows similar stability than in solution maintained under nitrogen atmosphere (Figure S9). Interestingly,

the use of pyrrole (**8**) as trapping agent gave slightly better results than *N*-methylpyrrole (**2**) or *N*-phenylpyrrole (**9**), being the opposite in solution. Different heterocycles such as 5-bromopyrimidine (**6**) and 2-bromobenzo[*d*]thiazole (**7**) were also coupled with *N*-methylpyrrole (**2**) and 3-methylindole (**10**) providing the expected cross-coupling products in good yields (**15-17**). The selective activation of Rh-6G depending on the irradiation wavelength, previously shown in solution under inert atmosphere,²³ was also achieved in gel medium under aerobic conditions (Scheme 2).

Scheme 2. Chromoselective one- or two-fold substitution reactions.^a



^a Reaction conditions: Bromo-compound **18** (0.1 mmol), trapping agent **2** (5-18 equiv.), Rh-6G (15 mol%), DIPEA (2.2 equiv.), **G-1** (15 g L⁻¹), DMSO, air, RT, λ_{Ex} = 455 nm or 530 nm, reaction time: 96 h. Yield of isolated products.

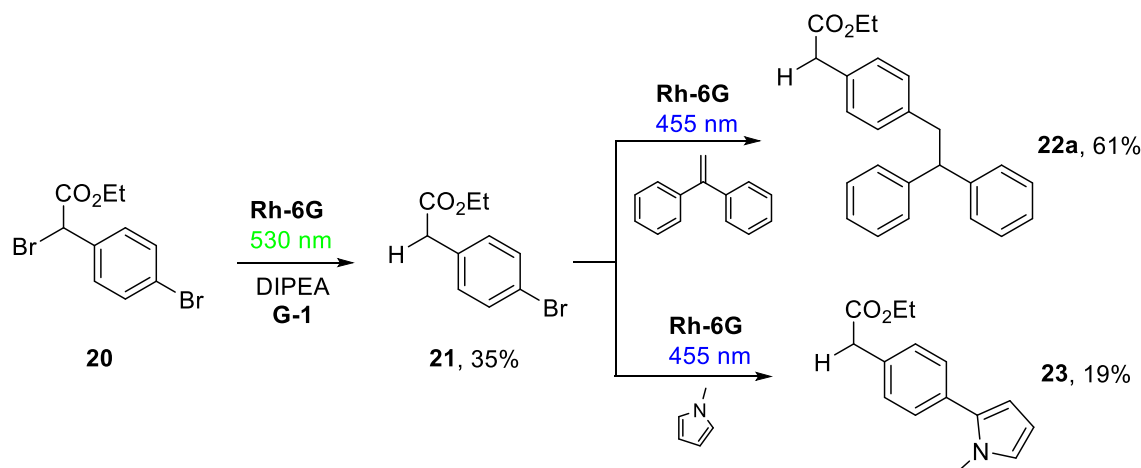
Thus, the coupling between 1,4-dibromo-2,5-difluorobenzene (**18**) and *N*-methylpyrrole (**2**) lead to the corresponding monosubstituted product **19b** upon irradiation with green LED light (λ_{Ex} = 530 ± 15 nm), which generates the photocatalytic ground state Rh-6G^{•-} radical anion. The bifunctionalized product **19a** was obtained when the same reaction mixture was irradiated with blue light (λ_{Ex} = 455 ± 15 nm) due to the enhanced reduction power of Rh-6G through the formation of the excited Rh-6G^{•-*} radical anion.

These results indicate that the supramolecular gel network enables the generation of air-sensitive radical species and highly reducing photoredox conditions under aerobic conditions. It should be emphasized that the photocatalytic reaction selected for this study also presents some limitations such as aryl bromide substrates with several electron-donating groups due to their very high reduction potential.²³ Such substrate limitations occur regardless of the reaction media when using the same photocatalytic system and,

therefore, they are not related to the gel medium, which is responsible for the oxygen-blocking effect.

This chromoselective photocatalytic arylation can also be used to perform sequential reactions in aerated gel (Scheme 3).

Scheme 3. Sequential substitution reactions.^a



^a Reaction conditions: First step: Bromo-compound **20** (0.1 mmol), Rh-6G (15 mol%), DIPEA (2.2 equiv.), **G-1** (15 g L⁻¹), DMSO, air, RT, λ_{Ex} = 530 nm, reaction time: 24 h. Yield of **21** was determined by GC-FID with internal standard. Second step: Bromo-compound **21** (0.1 mmol), trapping agent (1.8 mmol), Rh-6G (15 mol%), DIPEA (2.2 equiv.), **G-1** (15 g L⁻¹), DMSO, air, RT, λ_{Ex} = 455 nm, reaction time: 96 h. Yield of **22a** and **23** are determined after isolation.

Thus, irradiation with green light of ethyl 2-bromo-(4-bromophenyl)acetate (**20**), which possess two different carbon–halogen bonds (*i.e.*, benzylic and aryl), lead to dehalogenation at the benzylic position affording the corresponding product **21** in modest yield. Isolation of **21** and a new intragel reaction in the presence of a trapping agent such as 1,1-diphenylethylene, which possess extremely low reactivity towards nucleophiles and electrophiles,²⁵ and irradiation with blue light enabled the activation of the remaining carbon–bromide bond affording the desired product **22a** in 61% yield. Only traces (< 1%) of the unsaturated product (*i.e.*, [Ph]₂C=CH-Aryl, see **22b** in Experimental Part) were detected in the NMR of the crude reaction mixture. In contrast, the saturated:unsaturated ratio was 2.8:1 when the reaction was carried out in solution under nitrogen. Other trapping agents such as *N*-methylpyrrole (**2**) also afforded the expected coupling product with **23** albeit in this case with a lower yield. It is important to note that the non-covalent nature of the supramolecular network allows easy separation of the desired products and reutilization of the gelator without any detriment on its gelation ability.

Oscillatory rheological measurements (*i.e.*, dynamic frequency, strain and time sweeps (DFS, DSS and DTS, respectively)) and determination of the *gel-to-sol* transition

temperature (T_{gel}) before and after irradiation confirmed that the gel state (*i.e.*, storage modulus $G' >$ loss modulus G'') during the reactions was preserved (Figures 6).

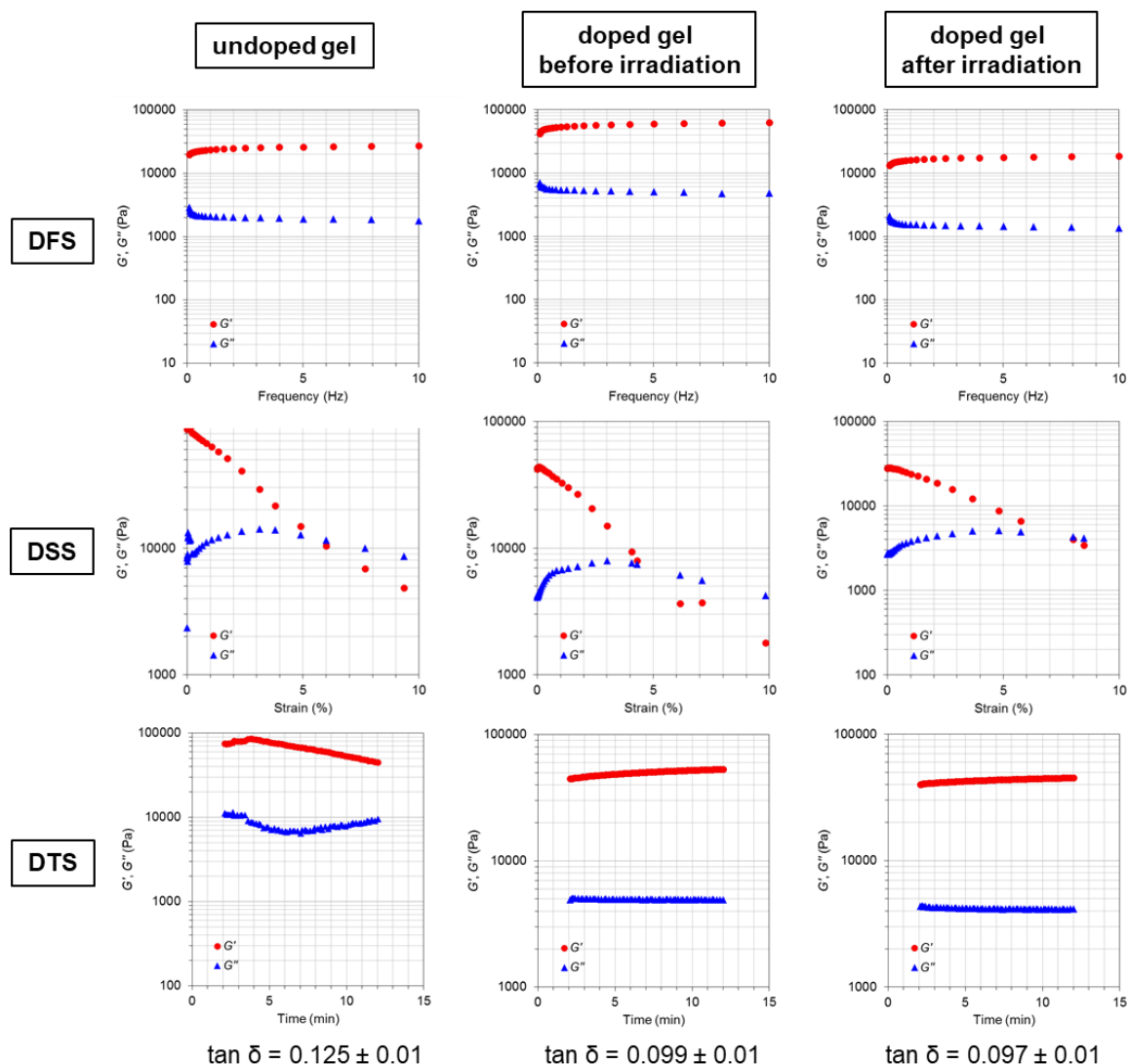


Figure 6. Oscillatory rheological experiments of model undoped and doped brittle gels before and after irradiation. Conditions for preparing the doped gel: **1** (0.1 mmol), **2** (1.8 mmol), Rh-6G (10 mol%), DIPEA (2.2 mmol), **G-1** (15 g L⁻¹), DMSO (1.5 mL). Irradiation conditions: $\lambda_{\text{ex}} = 455$ nm, 24 h. Note: T_{gel} of undoped gel made of **G-1** (61 ± 2 °C) remained practically constant, within the experimental error, upon doping and irradiation, *i.e.* T_{gel} of doped gel before irradiation = 57 ± 2 °C, T_{gel} of doped gel after irradiation = 59 ± 2 °C.

In all cases, G' was approximately one order of magnitude higher than G'' within the linear viscoelastic regime (*i.e.*, 0.1% strain and 1 Hz frequency). These values were also stable over time as determined by DTS experiments. Additionally, DFS and DSS measurements showed a reduction of the elastic response (G') of the materials by one order of magnitude after the reactions. However, both the dissipation factor ($\tan \delta = G''/G'$) and the *sol*-to-*gel* transition temperature (T_{gel}) of the gels remained practically constant before and after irradiation within the experimental error and did not show significant differences with the

corresponding undoped gels. These results suggest some morphological changes of the gels, but without a major detriment of their damping properties and thermal stability. Interestingly, comparative field-emission scanning electron microscopy (FE-SEM) images of undoped gels (Figure 7a), gels loaded with the photocatalyst Rh-6G (Figure 7b), and gels loaded with the photocatalyst, substrates and reagents, before (Figure 7c) and after irradiation (Figure 7d), indicated that the incorporation of the substrates caused apparently a higher impact on the fibrillar morphology of the xerogel network than the photocatalysts alone. Visible fragmentation of some fibers was observed after the reaction, albeit the gel phase was retained.

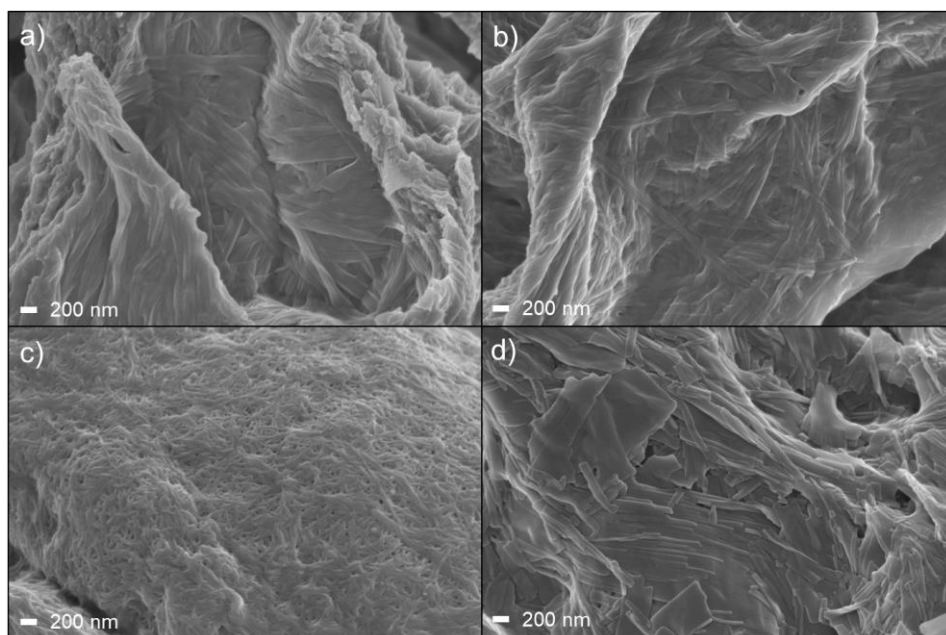


Figure 7. Representative scanning electron microscopy images of xerogels prepared by freeze drying of the corresponding gels. Composition of doped gel: **1** (0.1 mmol), **2** (1.8 mmol), Rh-6G (10 mol%), DIPEA (2.2 mmol), **G-1** = 15 g L⁻¹, DMSO (1.5 mL); a) undoped gel, b) doped with photocatalyst, c) doped with reactants before irradiation, and d) after irradiation.

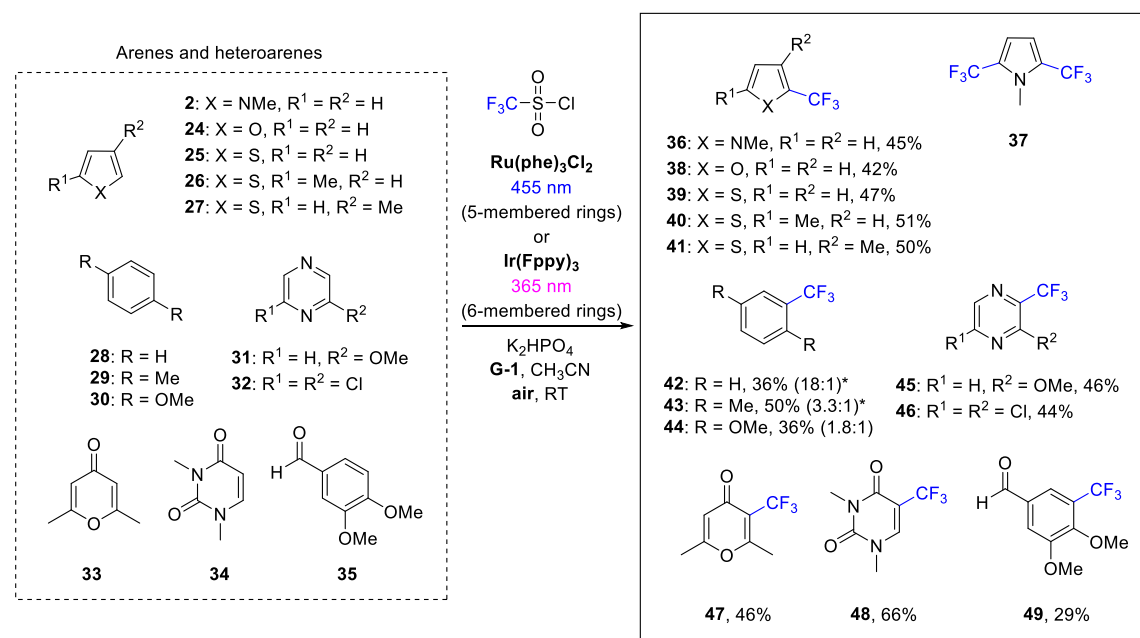
3.6.3.3. Photocatalytic Trifluoromethylation Reaction

Trifluoromethylated aromatic products constitute important structures for medicinal chemistry.²⁶⁻²⁹ As previously reported,³⁰ the trifluoromethylation of arenes and heteroarenes can be performed using Ru(phen)₃Cl₂ as photocatalyst to generate trifluoromethyl radicals ($\cdot\text{CF}_3$) via reduction of triflyl chloride (TfCl) upon irradiation at suitable wavelengths. The mechanism involves the formation of a cyclohexadienyl radical from the corresponding arene, which is further oxidized to form a cyclohexadienyl cation that affords the desired CF₃ arene upon facile deprotonation in the presence of K₂HPO₄.³⁰ In general, this reaction requires a strict inert gas atmosphere. However, when the reaction was performed in gel medium under aerobic conditions within identical reaction times, it provided comparable yields to solution reactions under inert conditions (Figure S10).

Initially, a series of control experiments (Table S1) in both aerated solution and gel media were performed using **G-1** as LMW gelator, MeCN as solvent, *N*-methylpyrrole (**2**) as substrate, as well as Ru(phen)₃Cl₂, TfCl, and K₂HPO₄ as mentioned above. The samples were irradiated with blue LED light ($\lambda_{\text{Ex}} = 455$ nm), and the gelator concentration was fixed at 10 g L⁻¹, although this variable was found to have a minor influence in this case (Table S4). The results showed that no reaction occurred in either aerated solution or aerated gel in the dark (Table S1). In addition, no or negligible background reaction occurred with different substrates in aerated gel in the absence of the photocatalyst (Table S1 and S3).

Several electron-rich 5-membered heteroarenes (**2**, **24-27**) were converted to the desired products in moderate yields (Scheme 4).

Scheme 4. Substrate scope of intragel trifluoromethylation of 5- and 6-membered (hetero)arenes with TfCl.^a



^a Reaction conditions: (hetero)arene **2**, **24-35** (0.25 mmol, TfCl (2-4 equiv.), photocatalyst: Ru(phen)₃Cl₂ (for 5-membered rings) or Ir(Fppy)₃ (for 6-membered rings) (catalyst loading: 1 mol% for 5-membered heteroarenes and 6-membered arenes; 2 mol% for 6-membered heteroarenes), K₂HPO₄ (3 equiv.), **G-1** (10 g L⁻¹), MeCN (2.5 mL), air, RT, $\lambda_{\text{Ex}} = 455$ nm (for Ru(phen)₃Cl₂) or 365 nm (for Ir(Fppy)₃), reaction time: 24-48 h. Yields were determined in this case by ¹⁹F-NMR using hexafluorobenzene (1 equiv.) as internal standard. Isolation of representative products showed ~ 10% decreased yields with respect to NMR yields. *The minor disubstituted position is labeled with the respective carbon atom number.

In general, obtained yields and mass balances (>90%) were comparable to those obtained in solution under rigorous inert conditions. Unless otherwise stated, the reported yields correspond in this case to values obtained directly from NMR analyses of the corresponding reaction crudes in the presence of a proper internal standard. Other substrates such as 6-membered unactivated arenes (**28-35**) yielded, regardless of the reaction media, mainly the monosubstituted product (**42-44**) mixed sometimes with a disubstituted derivative as minor product. The amount of disubstituted product increased

with the electronic density of the aromatic system in the starting material (**30** > **29** > **28**) and the amount of TfCl. Various electron-deficient 6-membered heteroarenes (**31-33**), as well as some natural compounds (34, 35), were also tested affording the desired products (**45-47**, **48**, and **49**, respectively) with modest to good yields, which were in general comparable to those obtained in solution under an inert atmosphere. The reactions proceed equally well using LED irradiation or a household light bulb (Table S6- S8). Interestingly, although **G-1** and **G-3** gave similar results, the use of Fmoc-Lys(Fmoc)-OH as LMW gelator resulted in much lower selectivity (Table S9), suggesting again the possibility of further optimization based on the nature of the gel network. In addition, a stable gel integrity before and after irradiation could be confirmed by rheology (Figure S6) and investigation of the morphology by FE-SEM (Figure S7).

3.6.3.4. Mechanistic Investigation

At this point, additional experiments were carried out in order to get insights into the mechanism by which the gel network facilitate the photocatalytic processes in air. Remarkably, both Rh-6G and Ru-catalyzed reactions were also achieved in aerated solution and in the presence of gelator **G-1** at a concentration slightly below the critical gelation concentration (CGC). In this situation, the gel network is not yet fully developed despite the formation of molecular aggregates, which also increase the viscosity of the medium.¹⁷ Although the product yields were about 10-15% lower than those obtained in the gel phase, the results suggest potential intermolecular interactions within some domains of the gel network and/or a beneficial effect of the enhanced viscosity reducing the oxygen diffusion. The latter was also supported by the formation of the reaction product in aerated frozen solution, albeit in about half yield compared to that observed in the gel at RT (Figure S11).

Furthermore, spectroscopic studies under different conditions were performed. Kimizuka and co-workers have previously demonstrated that platinum(II) octaethylporphyrin (PtOEP, sensitizer) and 9,10-diphenylanthracene (DPA, emitter) were solvophobically incorporated inside the gel nanofibers formed from **G-1** in DMF.³¹ In that example, the supramolecular gel showed efficient triplet-triplet annihilation (TTA)-based photon upconversion (UC) even under aerated conditions, because the triplet excited states of PtOEP and DPA were protected from the quenching by dissolved molecular oxygen. Importantly, the solvophobic accumulation of sensitizers and emitters in gel nanofibers is essential, since these excited triplets were quenched in the **G-1** gel formed in less polar carbon tetrachloride.

This observation leads to the idea to perform intragel photoreduction of aryl halides in air.¹⁸ It was initially expected that a similar oxygen blocking effect might also occur during C–C bond-forming photoredox catalysis, assuming that the photocatalysts are accumulated in the gel nanofibers. However, such oxygen barrier effect was not observed in phosphorescence lifetime measurements conducted for Ru(phen)₃Cl₂ (1 mM) in acetonitrile with/ without **G-1** (10 g L⁻¹). These specimens were prepared in air or Ar-filled glovebox ([O₂] < 0.1 ppm). The deaerated solution and deaerated gel samples prepared under Ar atmosphere showed phosphorescence lifetimes of 377 ns and 325 ns, respectively (Figure 8). On the other hand, both aerated solution and aerated gel samples showed much shorter lifetimes (*i.e.*, 105 ns and 139 ns, respectively) than those observed for the corresponding deaerated samples. This result indicates that the Ru complex is not effectively shielded inside gel nanofibers from dissolved oxygen.

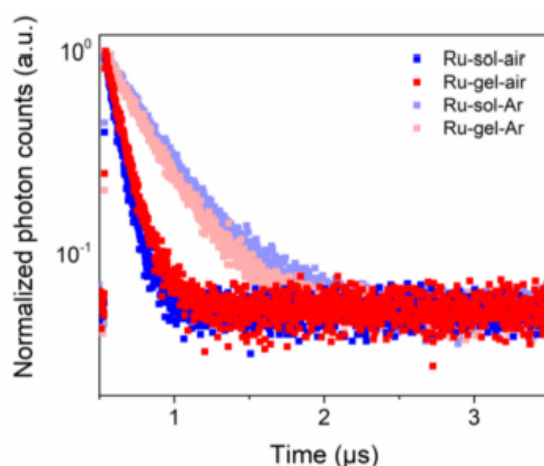


Figure 8. Photoluminescence decay at 605 nm of Ru(phen)₃Cl₂ in aerated/deaerated acetonitrile in the absence/presence of **G-1** under pulsed excitation at 405 nm.

For investigating the possibility of local oxygen consumption under continuous light exposure, phosphorescence lifetime of aerated gel samples was measured after a prolonged photoirradiation. The samples were irradiated by a xenon lamp through a 450 nm band-pass filter, which are conditions similar to those of the photocatalytic reaction using LED irradiation at 445 nm. Oxygen quenches the excited metal-to-ligand charge-transfer (³MLCT) state. Transfer of triplet energy to oxygen converts it into the excited singlet state. The singlet oxygen has a long lifetime and is a highly reactive species, which serves as a powerful oxidant in photosensitized oxidation processes. We expected that such singlet oxygen formed in the system (*i.e.*, gel prepared in air) would show some deteriorative actions to the gelator molecules, and therefore, the quenching of the ³MLCT states by oxygen would result in the consumption of local molecular oxygen concentration in the gel. If this is the case, the photoillumination over long periods may lead to the recovery of phosphorescence lifetime of the Ru complex. However, no significant

difference was observed in the phosphorescence decays after photoirradiation for 8, 15, and 24 h (Figure S14). The local consumption of oxygen during photoirradiation may take place, but its effect is too small to be detected by the change in phosphorescence decay curves. Furthermore, kinetic studies did not show an induction period for the reaction in aerated gel vs solution under nitrogen (Figure S15). We further investigated the effect of other additives and reactants in the reaction such as K_2HPO_4 , $TfCl$, and **2** at the same concentrations as those in the reaction. Elongation of phosphorescence decay was not observed for these specimens (Figure S15). These results indicate that the Ru complex undergoes oxygen quenching as it is dissolved in the MeCN solution phase trapped between the gel nanofibers.

Taking together all the experimental evidences and considering that photoinduced electron transfer (ET) is unlikely to be faster than the quenching of the 3MLCT states by dissolved molecular oxygen, the occurrence of triplet-sensitized chemical reactions in the organogel could take place within the confined solvent pools held in between the nanofibers. There, the volume/surface ratio and viscosity change dramatically compared to the homogeneous solution. This is in agreement with earlier kinetics studies of some photoinduced ET-based reactions in gel media compared to homogeneous and micellar solutions.¹⁴ In contrast to our previous observations based on TTA-UC,^{18,31} the photocatalytic species here are not incorporated into the gel fibers. Moreover, the gel significantly slows down the diffusion of external oxygen through the gel-air interface (Figure S11), thus preventing a fast deactivation of excited species generated after the initial photoexcitation of the catalysts (e.g., $Rh-6G^{*-}$, Figure S12). In contrast to free diffusion in solution, the oxygen initially trapped in the gel which was proven to be still reactive (Figure S11), should go through numerous entangled fibers to quench active species compartmentalized in other solvent pools. Thus, even a non-fully meshed network may offer some interfaces to protect against oxygen deactivation compared to the homogeneous solution. This was supported by the observation of product in aerated solution in the presence of the gelator slightly below its CGC. Although the combination of high viscosity and liquid interfaces in supramolecular gel media seems to be a key factor to facilitate the reactions, other effects such as increased local substrate concentration or affinity of substrates and active catalytic species to the surface of the fibers cannot be excluded at this point.^{32,33}

3.6.4. Conclusion and Outlook

In conclusion, air-sensitive C–C bond-forming photoredox catalysis can be performed under aerobic conditions using supramolecular gels, which are very easy to prepare and remove, as confined reaction media. The desired products are obtained in similar yields compared to reactions in homogeneous solutions under strict inert conditions. A judicious hydrophobic hydrophilic balance of the photocatalysts, the nature of the solvent and type of gel network are parameters that can be used to optimize intragel reactivity. Due to its facile operation, this method may expedite high-throughput screening of photocatalysts, automatization of photoinduced processes, and facilitate the way photochemistry and photocatalysis are traditionally carried out in research laboratories.

3.6.5. Experimental Part

3.6.5.1. Materials and Methods

Unless otherwise stated, all chemicals were used as received without further purification and were purchased from ABCR, Acros, Sigma-Aldrich, TCI Europe or Merk. Photochemical reactions were performed using a custom-made set-up with suitable LEDs (3.5 V, 700 mA), *i.e.* $\lambda_{\text{ex}} = 455 \pm 15$ nm, $\lambda_{\text{ex}} = 530 \pm 15$ nm. The yields reported are referred to the isolated compounds unless otherwise stated. Oxygen- and moisture-free reactions were carried out with dry and degassed solvents, as well as glassware subjected to several evacuations (vacuum)/refill (nitrogen) cycles. Column chromatography was performed using flash silica gel (40 – 63 μm). Thin-layer chromatography was performed using Merck pre-coated TLC aluminum sheets silica gel ALUGRAM® Xtra SIL G/UV254. Visualization was accomplished with short wavelength (254 nm) and near UV (366 nm) lights. NMR spectra were recorded on Bruker Avance 400 (^1H : 400 MHz, ^{13}C : 101 MHz) and Bruker Avance 300 (^1H : 300 MHz, ^{13}C : 75 MHz) spectrometers. Chemical shifts for ^1H NMR were reported as δ , parts per million (ppm), relative to the signal of CHCl_3 at 7.26 ppm or of DMSO at 2.50 ppm. Chemical shifts for ^{13}C NMR were reported as δ , ppm, relative to the signal of CDCl_3 at 77 ppm or of DMSO at 39.5 ppm. Coupling constants J are given in Hertz (Hz). The following notations indicate the multiplicity of the signals: s = singlet, br s = broad singlet, d = doublet, t = triplet, q = quartet, dd = doublet of doublets, td = triplet of doublets, m = multiplet. Gas chromatography (GC) analyses were performed using a capillary column (length: 30 m; diam. 0.25 mm; film: 0.25 μm) using He gas as carrier and FID detector. UV-Vis measurements were performed on an Ocean Optics DH-2000-BAL UV-VIS-NIR spectrophotometer. Measurements under different conditions were carried out as follows: (1) Solution under nitrogen: A screw-capped cuvette with septum was equipped with a small stirring bar and charged with 3 mL of a 16.7 μM rhodamine-6G solution in DMSO and subsequently evacuated and backfilled with N_2 (3x). DIPEA (50 μL) was added and another vacuum- N_2 cycle was applied. The stirred reaction mixture was irradiated at 455 nm LED and UV-Vis spectra were recorded every 10 min. (2) Solution in air: A cuvette was equipped with a small stirring bar and charged with 3 mL of a 16.7 μM rhodamine-6G solution in DMSO and DIPEA (50 μL). The stirred reaction mixture was irradiated in air (without cap) with 455 nm LED and UV-Vis spectra were recorded every 10 min. (3) Gel under nitrogen: A screw-capped vial septum was charged with 10 mg L^{-1} gelator, 3 mL of a 16.7 μM rhodamine-6G solution in DMSO and subsequently evacuated and backfilled with N_2 (3x). DIPEA (50 μL) was added and another vacuum- N_2 cycle was applied. The reaction mixture was heated until everything was dissolved and the hot solution was transferred into a screw-capped cuvette, which was previously evacuated

and backfilled with N₂ (3x). The mixture was subsequently allowed to cool to RT leading to gelation. The gel was then irradiated with 455 nm LED and UV-Vis spectra were recorded every 10 min. (4) Gel in air: A 5 mL vial was charged with 10 mg L⁻¹ gelator, 3 mL of a 16.7 μ M rhodamine-6G solution in DMSO and DIPEA (50 μ L). The reaction mixture was heated until everything was dissolved and the hot solution was transferred into a cuvette. The mixture was allowed to cool to RT leading to gelation. The gel was then irradiated in air (without cap) with 455 nm LED and UV-Vis spectra were recorded every 10 min. High-resolution mass spectra (HRMS) were obtained from the central analytic mass spectrometry facilities of the Faculty of Chemistry and Pharmacy (University of Regensburg) and are reported according to the IUPAC recommendations 2013. Oscillatory rheology was performed with a AR 2000 Advanced rheometer (TA Instruments) equipped with a Julabo C cooling system. A 500 or 1000 μ m gap setting and a torque setting of 40,000 dynes cm⁻² at 25 °C were used for the measurements in a plain-plate (40 mm, stainless steel). The following experiments were performed using 1.5 – 2.5 mL total gel volume: (1) Dynamic frequency sweep (DFS): variation of G' and G'' with frequency (from 0.1 to 10 Hz at 0.1% strain); (2) dynamic strain sweep (DSS): variation of G' and G'' with strain (from 0.01 to 100%); (3) dynamic time sweep (DTS): variation of G' and G'' with time, keeping the strain and frequency constant and within the linear viscoelastic regime as determined by DSS and DFS measurements (strain = 0.1%; frequency = 1 Hz). Gel-to-sol transition temperatures (T_{gel}) were determined using a custom-made set-up where a sealed vial was placed into a mold of an alumina block and heated up at 2 °C/5 min using an electric heating plate equipped with a temperature control couple. The temperature at which the gel started to collapse was defined as T_{gel} . The values obtained by this method have been previously verified with different supramolecular gels by means of DSC measurements as well as the inverse flow method. Moreover, verification of the independence of the position inside the custom-made apparatus has also been carried out.¹⁴ Herein, the temperature at which the gel started to break was defined as T_{gel} with an estimated error of ± 2 °C after several heating-cooling cycles. Field Emission Scanning Electron Microscopy (FE-SEM) images of the bulk xerogels were obtained with a Zeiss Merlin, Field Emission Scanning Electron Microscope operated at an accelerating voltage of 10 kV. For visualization, samples were prepared by the freeze-drying (FD) method as follows: A 4 mL glass vial containing the corresponding gel (total volume = 1 mL) was frozen in liquid nitrogen and the solvent was immediately evaporated under reduced pressure (0.6 mmHg) overnight at RT. The obtained fibrous solid was placed on top of a tin plate and shielded with Pt (40 mA during 30-60 s; film thickness = 5-10 nm). Images were taken at the University of Zaragoza (Servicio General de Apoyo a la Investigación-SAI).

3.6.5.2. Synthesis of LMW Gelators

LMW gelators **G-1**,²⁰ **G-2**²¹ and **G-3**²² were synthesized according to literature procedures with slight modifications. **G-4** was purchased from CHEMOS GmbH & Co. KG (catalog number 187667).

N,N'-Bis(octadecyl)-L-Boc-glutamic diamide (**G-1**)

Boc-glutamic acid (0.01 mol, 1.0 equiv) and octadecylamine (0.02 mol, 2.0 equiv) in dichloromethane (200 mL) were mixed. Then 1-ethyl-3-(3-dimethylaminopropyl)carbodiimide hydrochloride (EDC) (0.022 mol, 2.2 equiv) was added to the mixture and stirred at RT for 72 h. The obtained white solid was isolated by filtration and washed three times with DCM. The crude product was dissolved in THF and precipitated by water. A fine white solid was obtained (80%). ¹H NMR (300 MHz CDCl₃) δ (ppm) = 6.69 (brs, 1H), 6.32 (brs, 1H), 5.77 (brs, 1H), 4.08 (brs, 1H), 3.26 – 3.22 (m, 4H), 2.41 – 2.27 (m, 2H), 2.06 – 1.93 (m, 2H), 1.58 – 1.46 (m, 4H), 1.43 (s, 9H), 1.25 (s, 60H), 0.87 (t, 6H).

(S,S)-Dodecyl-3-[2(3-dodecyl-ureido)cyclohexyl]urea (**G-2**)

A solution of dodecylisocyanate (15 mmol, 2.0 equiv) in toluene (20 mL) was slowly added to a solution of (S,S)-1,2-cyclohexyldiamine (7 mmol, 1.0 equiv) in toluene (100 mL). The reaction mixture was stirred for 16 h at RT and 2 h at 100 °C. After cooling to RT, the gel-like reaction mixture was filtered to give a white waxy solid. The waxy solid was further stirred for 16 h with DCM (50 mL) and collected by filtration. This procedure was repeated with diethyl ether. After drying, a white solid was obtained (70%). ¹H NMR (300 MHz, CDCl₃) δ (ppm) = 5.18 (brs, 2H), 4.67 (brs, 2H), 3.42 (m, 2H), 3.08 (m, 4H), 2.03 (d, 2H), 1.72 (m, 6H), 1.45 (m, 4H), 1.25 (s, 36H), 0.87 (t, 6H).

N,N'-((1*R*,2*R*)-Cyclohexane-1,2-diyl)didodecanamide (**G-3**)

The compound was prepared following the general procedure with modifications. To a stirred solution of (1*R*,2*R*)-(+)-*N,N'*-dimethyl-1,2-cyclohexanediamine (1.00 mmol, 1.0 equiv) in THF (18 mL), lauroyl chloride (2.00 mmol, 2.0 equiv) and triethylamine (3.33 mmol, 3.3 equiv) were added dropwise. The mixture was refluxed for 5 h and allowed to cool to RT. The precipitated triethylammonium chloride was filtered off and the solvent of the remaining filtrate removed under reduced pressure. The obtained residue was washed with aqueous 1 M HCl (4 × 5 mL) and water (4 × 5 mL), dried and recrystallized from acetone affording **G-3** as a white solid in 39% yield. ¹H NMR (300 MHz, CDCl₃)

δ (ppm) = 5.86 (d, 2H), 3.65 (m, 2H), 2.15 – 1.96 (m, 6H), 1.79 – 1.67 (m, 2H), 1.57 (s, 8H), 1.25 (s, 33H), 0.88 (s, 6H).

1,3:2,4-Bis(3,4-dimethylbenzylidene)-sorbitol (G-4)

The compound was commercially available and was used without further purification.

3.6.5.3. General Procedure for Photocatalytic Arylation Reaction

General procedure for the arylation in gel medium and air: A 5-mL snap vial was charged with the respective aryl halide (0.1 mmol, 1.0 equiv.), trapping reagent (1.8 mmol, 18 equiv.), DIPEA (0.22 mmol, 2.2 equiv.), Rh-6G (15 mol%), **G-1** (15 g L⁻¹), DMSO (1.5 mL) and sealed with a cap. The reaction mixture was gently heated with a heat gun at 80 °C during 1 min until an isotropic solution was obtained. The corresponding gel was obtained upon cooling the mixture to RT. The snap vial was then equipped with two needles to ensure a constant air atmosphere. The reaction was irradiated through the plane bottom side of the snap vial using a 455 (\pm 15) nm LED at 25 °C. The reaction progress was monitored by GC-FID. After completion of the reaction as judged by GC-FID, the reaction mixture of three reactions (performed in parallel) was combined and transferred into a separating funnel and adequate amount of distilled water and brine were added. The mixture was extracted with ethyl acetate (3 \times 15 mL). The combined organic layers were dried over MgSO₄, filtered, and concentrated under reduced pressure. Purification of the crude product was achieved by flash silica gel column chromatography using hexanes/ethyl acetate as eluents. Note: The gelator can be easily separated and reused in subsequent experiments without any detriment of its gelation properties.

*2-(1H-Pyrrol-2-yl)benzonitrile (11)*²³

The compound was prepared according to the general procedure. A 5-mL snap vial was charged with 2-bromobenzonitrile (**1**) (0.1 mmol, 1.0 equiv), Rh-6G (0.015 mmol, 0.15 equiv), pyrrole (**8**) (1.8 mmol, 18 equiv), DIPEA (0.22 mmol, 2.2 equiv), **G-1** (15 g L⁻¹), DMSO (1.5 mL) and sealed with a cap. The reaction mixture was gently heated with a heat gun at 80 °C during 1 min until an isotropic solution was obtained. The corresponding gel was obtained upon cooling the mixture to RT. The snap vial, equipped with two needles to ensure a constant air atmosphere was irradiated through the plane bottom side of the snap vial using a 455 (\pm 15) nm LED at 25 °C for 48 h. Three reactions were run in parallel, and the combined reaction mixture was subjected to the work-up procedure outlined in the general procedure. The crude product was purified by flash column chromatography on silica gel using a mixture of ethyl acetate (20%) and hexanes as an eluent (R_f = 0.3) to provide the title compound (36 mg from the combined mixture of three

reactions, 71% yield). ^1H NMR (300 MHz, $\text{DMSO-}d_6$) δ (ppm) = 11.52 (brs, 1H), 7.87 – 7.78 (m, 1H), 7.76 – 7.65 (m, 2H), 7.41 – 7.30 (m, 1H), 7.05 – 6.98 (m, 1H), 6.88 – 6.80 (m, 1H), 6.27 – 6.18 (m, 1H); ^{13}C NMR (75 MHz, $\text{DMSO-}d_6$) δ (ppm) = 135.5, 134.3, 133.3, 127.2, 126.3, 126.0, 121.2, 119.4, 109.5, 109.4, 106.3.

*2-(1-Methyl-1H-pyrrol-2-yl)benzonitrile (3)*²³

The compound was prepared according to the general procedure. A 5-mL snap vial was charged with 2-bromobenzonitrile (**1**) (0.1 mmol, 1.0 equiv), Rh-6G (0.015 mmol, 0.15 equiv), *N*-methylpyrrole (**2**) (1.8 mmol, 18 equiv), DIPEA (0.22 mmol, 2.2 equiv), **G-1** (15 g L⁻¹), DMSO (1.5 mL) and sealed with a cap. The reaction mixture was gently heated with a heat gun at 80 °C during 1 min until an isotropic solution was obtained. The corresponding gel was obtained upon cooling the mixture to RT. The snap vial, equipped with two needles to ensure a constant air atmosphere was irradiated through the plane bottom side of the snap vial using a 455 (\pm 15) nm LED at 25 °C for 24 h. Three reactions were run in parallel, and the combined reaction mixture was subjected to the work-up procedure outlined in the general procedure. The crude product was purified by flash column chromatography on silica gel using a mixture of ethyl acetate (15%) and hexanes as an eluent (R_f = 0.4) to provide the title compound (32 mg from the combined mixture of three reactions, 59% yield). ^1H NMR (300 MHz, CDCl_3) δ (ppm) = 7.89 (dd, 1H), 7.73 (dt, 1H), 7.59 – 7.48 (m, 2H), 6.94 (t, 1H), 6.29 (dd, 1H), 6.13 (dd, 1H), 3.55 (s, 3H); ^{13}C NMR (75 MHz, $\text{DMSO-}d_6$) δ (ppm) = 136.1, 133.8, 133.0, 130.7, 129.2, 127.9, 125.3, 118.7, 111.4, 111.0, 107.7, 34.5.

*2-(1-Phenyl-1H-pyrrol-2-yl)benzonitrile (12)*²³

The compound was prepared according to the general procedure. A 5-mL snap vial was charged with 2-bromobenzonitrile (**1**) (0.1 mmol, 1.0 equiv), Rh-6G (0.015 mmol, 0.15 equiv), *N*-phenylpyrrole (**9**) (1.8 mmol, 18 equiv), DIPEA (0.22 mmol, 2.2 equiv), **G-1** (15 g L⁻¹), DMSO (1.5 mL) and sealed with a cap. The reaction mixture was gently heated with a heat gun at 80 °C during 1 min until an isotropic solution was obtained. The corresponding gel was obtained upon cooling the mixture to RT. The snap vial, equipped with two needles to ensure a constant air atmosphere was irradiated through the plane bottom side of the snap vial using a 455 (\pm 15) nm LED at 25 °C for 48 h. Three reactions were run in parallel, and the combined reaction mixture was subjected to the work-up procedure outlined in the general procedure. The crude product was purified by flash column chromatography on silica gel using a mixture of ethyl acetate (5%) and hexanes as an eluent (R_f = 0.3) to provide the title compound (30 mg from the combined mixture of three reactions, 41% yield). ^1H NMR (300 MHz, $\text{DMSO-}d_6$) δ (ppm) 7.81 – 7.72 (m, 1H),

7.56 – 7.45 (m, 1H), 7.45 – 7.17 (m, 6H), 7.16 – 7.00 (m, 3H), 6.56 (dd, 1H), 6.39 (t, 1H); ^{13}C NMR (75 MHz, DMSO- d_6) δ (ppm) = 139.1, 135.8, 133.4, 132.6, 130.7, 129.2, 128.4, 127.6, 126.7, 125.4, 125.0, 118.2, 113.3, 111.1, 109.5.

*4-(1-Methyl-1H-pyrrol-2-yl)benzonitrile (13)*²³

The compound was prepared according to the general procedure. A 5-mL snap vial was charged with 4-bromobenzonitrile (**4**) (0.1 mmol, 1.0 equiv), Rh-6G (0.015 mmol, 0.15 equiv), *N*-methylpyrrole (**2**) (1.8 mmol, 18 equiv), DIPEA (0.22 mmol, 2.2 equiv), **G-1** (15 g L⁻¹), DMSO (1.5 mL) and sealed with a cap. The reaction mixture was gently heated with a heat gun at 80 °C during 1 min until an isotropic solution was obtained. The corresponding gel was obtained upon cooling the mixture to RT. The snap vial, equipped with two needles to ensure a constant air atmosphere was irradiated through the plane bottom side of the snap vial using a 455 (\pm 15) nm LED at 25 °C for 24 h. Three reactions were run in parallel, and the combined reaction mixture was subjected to the work-up procedure outlined in the general procedure. The crude product was purified by flash column chromatography on silica gel using a mixture of ethyl acetate (15%) and hexanes as an eluent (R_f = 0.2) to provide the title compound (37 mg from the combined mixture of three reactions, 69% yield). ^1H NMR (300 MHz, CDCl₃) δ (ppm) = 7.66 – 7.60 (m, 2H), 7.49 – 7.42 (m, 2H), 6.77 – 6.71 (m, 1H), 6.30 (dd, 1H), 6.19 (dd, 1H), 3.67 (s, 3H); ^{13}C NMR (75 MHz, DMSO- d_6) δ (ppm) = 137.3, 132.3, 131.5, 127.7, 126.5, 119.0, 110.6, 108.1, 107.9, 35.2.

*1-(4-(1-Methyl-1H-pyrrol-2-yl)phenyl)ethan-1-one (14)*²³

The compound was prepared according to the general procedure. A 5-mL snap vial was charged with 4'-bromoacetophenone (**5**) (0.1 mmol, 1.0 equiv), Rh-6G (0.015 mmol, 0.15 equiv), *N*-methylpyrrole (**2**) (1.8 mmol, 18 equiv), DIPEA (0.22 mmol, 2.2 equiv), **G-1** (15 g L⁻¹), DMSO (1.5 mL) and sealed with a cap. The reaction mixture was gently heated with a heat gun at 80 °C during 1 min until an isotropic solution was obtained. The corresponding gel was obtained upon cooling the mixture to RT. The snap vial, equipped with two needles to ensure a constant air atmosphere was irradiated through the plane bottom side of the snap vial using a 455 (\pm 15) nm LED at 25 °C for 70 h. Three reactions were run in parallel, and the combined reaction mixture was subjected to the work-up procedure outlined in the general procedure. The crude product was purified by flash column chromatography on silica gel using a mixture of ethyl acetate (15%) and hexanes as an eluent (R_f = 0.3) to provide the title compound (30 mg from the combined mixture of three reactions, 50% yield). ^1H NMR (300 MHz, CDCl₃) δ (ppm) = 8.03 – 7.95 (m, 2H), 7.54 – 7.46 (m, 2H), 6.81 – 6.74 (m, 1H), 6.35 (dd, 1H), 6.23 (dd, 1H), 3.72 (s, 3H); ^{13}C

NMR (75 MHz, DMSO- d_6) δ (ppm) = 197.2, 137.3, 134.2, 132.2, 128.5, 127.2, 126.0, 110.0, 107.8, 35.2, 26.5.

*5-(1-Methyl-1H-pyrrol-2-yl)pyrimidine (15)*³⁴

The compound was prepared according to the general procedure. A 5-mL snap vial was charged with 5-bromopyrimidine (**6**) (0.1 mmol, 1.0 equiv), Rh-6G (0.015 mmol, 0.15 equiv), *N*-methylpyrrole (**2**) (1.8 mmol, 18 equiv), DIPEA (0.22 mmol, 2.2 equiv), **G-1** (15 g L⁻¹), DMSO (1.5 mL) and sealed with a cap. The reaction mixture was gently heated with a heat gun at 80 °C during 1 min until an isotropic solution was obtained. The corresponding gel was obtained upon cooling the mixture to RT. The snap vial, equipped with two needles to ensure a constant air atmosphere was irradiated through the plane bottom side of the snap vial using a 455 (\pm 15) nm LED at 25 °C for 72 h. Three reactions were run in parallel, and the combined reaction mixture was subjected to the work-up procedure outlined in the general procedure. The crude product was purified by flash column chromatography on silica gel using a mixture of ethyl acetate (50%) and hexanes as an eluent (R_f = 0.3) to provide the title compound (38 mg from the combined mixture of three reactions, 79% yield). ¹H NMR (300 MHz, CDCl₃) δ (ppm) = 9.12 (s, 1H), 8.8 (s, 2H), 6.86 – 6.79 (m, 1H), 6.37 (dd, 1H), 6.25 (dd, 1H), 3.71 (s, 3H); ¹³C NMR (75 MHz, CDCl₃) δ (ppm) = 156.5, 155.4, 127.6, 127.0, 126.0, 110.9, 108.8, 35.2.

*3-Methyl-2-(pyrimidin-5-yl)-1H-indole (16)*³⁴

The compound was prepared according to the general procedure. A 5-mL snap vial was charged with 5-bromopyrimidine (**6**) (0.1 mmol, 1.0 equiv), Rh-6G (0.015 mmol, 0.15 equiv), 3-methylindole (**10**) (1.8 mmol, 18 equiv), DIPEA (0.22 mmol, 2.2 equiv), **G-1** (15 g L⁻¹), DMSO (1.5 mL) and sealed with a cap. The reaction mixture was gently heated with a heat gun at 80 °C during 1 min until an isotropic solution was obtained. The corresponding gel was obtained upon cooling the mixture to RT. The snap vial, equipped with two needles to ensure a constant air atmosphere was irradiated through the plane bottom side of the snap vial using a 455 (\pm 15) nm LED at 25 °C for 48 h. Three reactions were run in parallel, and the combined reaction mixture was subjected to the work-up procedure outlined in the general procedure. The crude product was purified by flash column chromatography on silica gel using a mixture of ethyl acetate (15 – 40%) and hexanes as an eluent (R_f = 0.1 at 30% ethyl acetate in hexanes) to provide the title compound (37 mg from the combined mixture of three reactions, 59% yield). ¹H NMR (300 MHz, CDCl₃) δ (ppm) = 9.12 (s, 1H), 9.01 (s, 2H), 7.66 – 7.51 (m, 1H), 7.45 – 7.36 (m, 1H), 7.31 – 7.09 (m, 3H), 2.49 (s, 3H); ¹³C (75 MHz, CDCl₃) δ (ppm) = 156.8, 155.0, 136.7, 129.5, 127.8, 126.9, 123.7, 120.2, 119.5, 112.0, 111.1, 9.6.

*2-(1-Methyl-1H-pyrrol-2-yl)benzo[d]thiazole (17)*³⁴

The compound was prepared according to the general procedure. A 5-mL snap vial was charged with 2-bromobenzo[d]thiazole (**7**) (0.1 mmol, 1.0 equiv), Rh-6G (0.015 mmol, 0.15 equiv), *N*-methylpyrrole (**2**) (1.8 mmol, 18 equiv), DIPEA (0.22 mmol, 2.2 equiv), **G-1** (15 g L⁻¹), DMSO (1.5 mL) and sealed with a cap. The reaction mixture was gently heated with a heat gun at 80 °C during 1 min until an isotropic solution was obtained. The corresponding gel was obtained upon cooling the mixture to RT. The snap vial, equipped with two needles to ensure a constant air atmosphere was irradiated through the plane bottom side of the snap vial using a 455 (± 15) nm LED at 25 °C for 72 h. Three reactions were run in parallel, and the combined reaction mixture was subjected to the work-up procedure outlined in the general procedure. The crude product was purified by flash column chromatography on silica gel using a mixture of ethyl acetate (5 – 40%) and hexanes as an eluent (*R*_f = 0.2 at 15% ethyl acetate in hexanes) to provide the title compound (50 mg from the combined mixture of three reactions, 78% yield). ¹H NMR (300 MHz, CDCl₃) δ (ppm) = 7.99 – 7.91 (m, 1H), 7.85 – 7.79 (m, 1H), 7.43 (dt, 1H), 7.31 (dt, 1H), 6.87 – 6.79 (m, 2H), 6.21 (q, 1H), 4.15 (s, 3H); ¹³C NMR (75 MHz, DMSO-*d*₆) δ (ppm) = 159.8, 153.6, 132.9, 128.9, 126.2, 125.3, 124.6, 121.9, 121.6, 114.9, 108.7, 36.6.

*2,2'-(2,5-Difluoro-1,4-phenylene)bis(1-methyl-1H-pyrrole) (19a)*²³

The compound was prepared according to the general procedure but with double amount of *N*-methylpyrrole (**2**). A 5-mL snap vial was charged with 1,4-dibromo-2,5-difluorobenzene (**18**) (0.1 mmol, 1.0 equiv), Rh-6G (0.015 mmol, 0.15 equiv), *N*-methylpyrrole (**2**) (2.6 mmol, 26 equiv), DIPEA (0.22 mmol, 2.2 equiv), **G-1** (15 g L⁻¹), DMSO (1.5 mL) and sealed with a cap. The reaction mixture was gently heated with a heat gun at 80 °C during 1 min until an isotropic solution was obtained. The corresponding gel was obtained upon cooling the mixture to RT. The snap vial, equipped with two needles to ensure a constant air atmosphere was irradiated through the plane bottom side of the snap vial using a 455 (± 15) nm LED at 25 °C for 96 h. Three reactions were run in parallel, and the combined reaction mixture was subjected to the work-up procedure outlined in the general procedure. The crude product was purified by flash column chromatography on silica gel using a mixture of ethyl acetate (5%) and hexanes as an eluent (*R*_f = 0.4) to provide the title compound (33 mg from the combined mixture of three reactions, 41% yield). ¹H NMR (300 MHz, DMSO-*d*₆) δ (ppm) = 7.38 (t, 2H), 7.00 – 7.25 (m, 2H), 6.31 – 6.21 (m, 2H), 6.18 – 6.09 (m, 2H), 3.60 (s, 6H); ¹³C NMR (75 MHz, DMSO-

d_6) δ (ppm) = 156.3 (dd), 153.1 (dd), 125.4, 124.7, 120.9, 120.7 (dd), 120.5, 118.0, 117.8 (dd), 117.6, 110.8, 107.6, 34.4.

2-(4-Bromo-2,5-difluorophenyl)-1-methyl-1H-pyrrole (**19b**)²³

The compound was prepared according to the general procedure. A 5-mL snap vial was charged with 1,4-dibromo-2,5-difluorobenzene (**18**) (0.1 mmol, 1.0 equiv), Rh-6G (0.015 mmol, 0.15 equiv), *N*-methylpyrrole (**2**) (1.8 mmol, 18 equiv), DIPEA (0.22 mmol, 2.2 equiv), **G-1** (15 g L⁻¹), DMSO (1.5 mL) and sealed with a cap. The reaction mixture was gently heated with a heat gun at 80 °C during 1 min until an isotropic solution was obtained. The corresponding gel was obtained upon cooling the mixture to RT. The snap vial, equipped with two needles to ensure a constant air atmosphere was irradiated through the plane bottom side of the snap vial using a 530 (\pm 15) nm LED at 25 °C for 96 h. Three reactions were run in parallel, and the combined reaction mixture was subjected to the work-up procedure. The crude product was purified by flash column chromatography on silica gel using a mixture of ethyl acetate (5%) and hexanes as an eluent (R_f = 0.5) to provide the title compound (33 mg from the combined mixture of three reactions, 40% yield). ¹H NMR (300 MHz, DMSO- d_6) δ (ppm) = 7.81 (q, 1H), 7.49 (q, 1H), 6.97 – 6.91 (m, 1H), 6.26 – 6.20 (m, 1H), 6.12 (q, 1H), 3.56 (s, 3H); ¹³C NMR (75 MHz, DMSO- d_6) δ (ppm) = 125.0, 124.7, 121.9 – 121.3 (m), 120.7, 120.3, 118.3 (dd), 117.9 (dd), 111.0, 107.6 (dd), 34.4 (dd).

Ethyl 2-(4-bromophenyl)acetate (**21**)²³

A 5-mL snap vial was charged with ethyl 2-bromo-2-(4-bromophenyl)acetate (**20**) (0.1 mmol, 1.0 equiv), Rh-6G (0.015 mmol, 0.15 equiv), DIPEA (0.22 mmol, 2.2 equiv), **G-1** (15 g L⁻¹), DMSO (1.5 mL) and sealed with a cap. The reaction mixture was gently heated with a heat gun at 80 °C during 1 min until an isotropic solution was obtained. The corresponding gel was obtained upon cooling the mixture to RT. The snap vial, equipped with two needles to ensure a constant air atmosphere was irradiated through the plane bottom side of the snap vial using a 530 (\pm 15) nm LED at 25 °C for 24 h. The yield was determined by GC-FID with biphenyl as internal standard (35% yield).

Ethyl 2-(4-(2,2-diphenylethyl)phenyl)acetate (**22a**)²³

The compound was prepared according to the general procedure. A 5-mL snap vial was charged with ethyl 2-(4-bromophenyl)acetate (**21**) (0.1 mmol, 1.0 equiv), Rh-6G (0.015 mmol, 0.15 equiv), 1,1-diphenylethylene (1.8 mmol, 18 equiv), DIPEA (0.22 mmol, 2.2 equiv), **G-1** (15 g L⁻¹), DMSO (1.5 mL) and sealed with a cap. The reaction mixture was gently heated with a heat gun at 80 °C during 1 min until an isotropic solution was

obtained. The corresponding gel was obtained upon cooling the mixture to RT. The snap vial, equipped with two needles to ensure a constant air atmosphere was irradiated through the plane bottom side of the snap vial using a 455 (\pm 15) nm LED at 25 °C for 96 h. Three reactions were run in parallel, and the combined reaction mixture was subjected to the work-up procedure outlined in the general procedure. The crude product was purified by flash column chromatography on silica gel using a mixture of ethyl acetate (5%) and hexanes as an eluent (R_f = 0.4) to provide the title compound (63 mg from the combined mixture of three reactions, 61% yield). ^1H NMR (300 MHz, $\text{DMSO}-d_6$) δ (ppm) = 7.39 – 7.30 (m, 4H), 7.28 – 7.18 (m, 4H), 7.17 – 7.00 (m, 6H), 4.34 (t, 1H), 4.03 (q, 2H), 3.53 (s, 2H), 3.34 (d, 2H), 1.14 (t, 3H); ^{13}C NMR (75 MHz, $\text{DMSO}-d_6$) δ (ppm) = 171.1, 144.6, 138.6, 131.6, 128.8, 128.2, 127.7, 125.9, 60.1, 51.8, 13.9.

*Ethyl 2-(4-(2,2-diphenylvinyl)phenyl)acetate (22b)*²³

22b was formed along with the **22a** in the same reaction mixture (11.6 mg from the combined mixture of two reactions, yield 17%). ^1H NMR (300 MHz, $\text{DMSO}-d_6$) δ (ppm) = 7.47 – 7.19 (m, 8H), 7.19 – 7.10 (m, 2H), 7.10 – 6.98 (m, 3H), 6.98 – 6.88 (m, 2H), 4.04 (q, J = 7.2 Hz, 2H), 3.56 (s, 2H), 1.15 (t, J = 7.1 Hz, 3H); ^{13}C NMR (75 MHz, $\text{DMSO}-d_6$) δ (ppm) = 171.0, 142.5, 141.5, 140.0, 135.4, 133.1, 129.7, 129.3, 129.0, 128.4, 127.8, 127.7, 127.6, 127.4, 127.0, 60.3, 39.9, 14.1. HRMS: calculated m/z for $\text{C}_{24}\text{H}_{26}\text{NO}_2$ [($\text{M}+\text{NH}_4$)⁺] 360.1958; found 360.1964.

*Ethyl 2-(4-(1-methyl-1H-pyrrol-2-yl)phenyl)acetate (23)*²³

The compound was prepared according to the general procedure. A 5-mL snap vial was charged with ethyl 2-(4-bromophenyl)acetate (0.1 mmol, 1.0 equiv.), **Rh-6G** (0.015 mmol, 0.15 equiv.), *N*-methylpyrrole (1.8 mmol, 18 equiv.), DIPEA (0.22 mmol, 2.2 equiv.), **G-1** (15 g L⁻¹), DMSO (1.5 mL) and sealed with a cap. The reaction mixture was gently heated with a heat gun at 80 °C during 1 min until an isotropic solution was obtained. The corresponding gel was obtained upon cooling the mixture to RT. The snap vial, equipped with two needles to ensure a constant air atmosphere was irradiated through the plane bottom side of the snap vial using a 455 (\pm 15) nm LED at 25 °C for 96 h. Three reactions were run in parallel, and the combined reaction mixture was subjected to the work-up procedure outlined in the general procedure and purified using chromatography on silica gel using a hexanes/EtOAc mixture to provide the title compound (14 mg from the combined mixture of three reactions, 19% yield). ^1H NMR (300 MHz, $\text{DMSO}-d_6$) δ (ppm) = 7.43 – 7.34 (m, 2H), 7.34 – 7.25 (m, 2H), 6.86 – 6.79 (m, 1H), 6.15 (dd, 1H), 6.05 (dd, 1H),

4.09 (q, 2H), 3.68 (s, 2H), 3.63 (s, 3H), 1.19 (t, 3H); ^{13}C NMR (75 MHz, DMSO- d_6) δ (ppm) = 171.1, 133.0, 132.5, 131.4, 129.3, 127.7, 124.2, 108.3, 107.2, 60.2, 34.8, 14.0.

3.6.5.4. General Procedure for Photocatalytic Trifluoromethylation Reaction

All experiments in solution were performed following the general procedures previously described in the literature²⁷ but using LEDs as irradiation source instead of fluorescent light bulbs. Different general procedures used in this work are described as followed:

General procedure A

An oven-dried 5 mL vial was loaded with Ru(phen) $_3$ Cl $_2$ (1.8 mg, 0.0025 mmol), K $_2$ HPO $_4$ (131 mg, 0.75 mmol) and **G-1** (10 g L $^{-1}$). MeCN (2.5 mL) and the desired heteroarene (0.25 mmol) were added and the vial was capped with a septum. The resulting solution was treated with ultrasound for 1 min and heated with a heat gun (heating level 3 of 10) until the gelator was completely dissolved. Before the gel was formed, triflyl chloride (53 μ L, 0.5 mmol) was added using a syringe. After the gel formation, the vials were placed under the corresponding LED irradiation for 24 h. After this time, the gels were dissolved by gently heating with the heat gun, and EtOAc (2.5 mL) and hexafluorobenzene (1 equiv.) were added for subsequent analysis.

General procedure B

Similar to procedure A but using Ir(dFppy) $_3$ (1.9 mg, 0.0025 mmol) as photocatalyst.

General procedure C

Similar to procedure A but using double the amount of TfCl (106 μ L, 1 mmol) and Ir(dFppy) $_3$ (3.8 mg, 0.005 mmol) as photocatalyst.

General procedure D

Similar to procedure A but using 1 equiv of TfCl.

*1-Methyl-2-(trifluoromethyl)-1H-pyrrole (36)*²⁷

The title compound was prepared by general procedure D using *N*-methylpyrrole (**2**) (22 μ L, 0.25 mmol). ^1H NMR (300 MHz, CDCl $_3$) δ (ppm) = 3.64 (s, 3H, CH $_3$); 6.01 (m, 1H, CR $_2$ H), 6.44 (m, 1H, CR $_2$ H), 6.65 (t, 1H; CR $_2$ H); ^{19}F NMR (282 MHz, CDCl $_3$) δ (ppm) = -59.3.

*1-Methyl-2,5-bis(trifluoromethyl)-1H-pyrrole (37)*²⁷

The title compound was prepared by general procedure A using *N*-methylpyrrole (**2**) (22 μ L, 0.25 mmol). ^1H NMR (300 MHz, CDCl $_3$) δ (ppm) = 3.70 (s, 3H, CH $_3$); 6.47 (s, 2H, CR $_2$ H); ^{19}F NMR (282 MHz, CDCl $_3$) δ (ppm) = -60.2.

*2-(Trifluoromethyl)furan (38)*²⁷

The title compound was prepared by general procedure D using furan (**24**) (18 μ L, 0.25 mmol). ¹H NMR (300 MHz, CDCl₃) δ (ppm) = 6.33 – 6.36 (s, 1H, CR₂H); 6.66 – 6.69 (m, 1H, CR₂H); 7.42 (s, 1H, CR₂H); ¹⁹F NMR (282 MHz, CDCl₃) δ (ppm) = -64.80.

*2-(Trifluoromethyl)thiophene (39)*²⁷

The title compound was prepared by general procedure D using thiophene (**25**) (20 μ L, 0.25 mmol). ¹H NMR (300 MHz, CDCl₃) δ (ppm) = 7.01 (m, 1H, CR₂H); 7.37 (m, 1H, CR₂H), 7.43 (dd, J = 5.0 Hz, 1.3 Hz, 1H, CR₂H); ¹⁹F NMR (282 MHz, CDCl₃) δ (ppm) = -55.5.

*2-Methyl-5-(trifluoromethyl)thiophene (40)*²⁷

The title compound was prepared by general procedure A using 2-methyl thiophene (**26**) (24 μ L, 0.25 mmol). ¹H NMR (300 MHz, CDCl₃) δ (ppm) = 2.40 (d, J = 1.0 Hz, 3H, CH₃); 6.79 (dd, J = 5.2, 3.4 Hz, 1H, CR₂H), 6.98 (dd, J = 5.2, 1.2 Hz, 1H, CR₂H); ¹⁹F NMR (282 MHz, CDCl₃) δ (ppm) = -55.7.

*3-Methyl-2-(trifluoromethyl)thiophene (41)*²⁷

The title compound was prepared by general procedure A using 3-methyl thiophene (**27**) (24 μ L, 0.25 mmol). ¹H NMR (300 MHz, CDCl₃) δ (ppm) = 2.28 (d, J = 1.7 Hz, 3H, CH₃); 7.14 (d, J = 4.7 Hz, 1H, CR₂H), 7.28 (d, J = 5.1 Hz, 1H, CR₂H); ¹⁹F NMR (282 MHz, CDCl₃) δ (ppm) = -54.8.

*Trifluoromethyl benzene (42)*²⁷

The title compound was prepared by general procedure B using benzene (**28**) (23 μ L, 0.25 mmol). ¹H NMR (300 MHz, CDCl₃) δ (ppm) = 7.34 - 7.42 (m, 2H, ArH); 7.45 (d, J = 7.1 Hz, 1H, ArH), 7.51 (d, J = 8.1 Hz, 2H, ArH); ¹⁹F NMR (282 MHz, CDCl₃) δ (ppm) = -63.4.

*1,4-Dimethyl-2-(trifluoromethyl)benzene (43)*²⁷

The title compound was prepared by general procedure B using *p*-xylene (**29**) (31 μ L, 0.25 mmol). ¹H NMR (300 MHz, CDCl₃) δ (ppm) = 2.26 (s, 3H, CH₃); 2.33 (s, 3H, CH₃); 7.05 (d, J = 7.7 Hz, 1H, ArH); 7.11 (d, J = 8.2 Hz, 1H, ArH), 7.28 (s, 1H); ¹⁹F-NMR (282 MHz, CDCl₃) δ (ppm) = -62.3. Note: Ratio monosubstituted:disubstituted (in gel) = 3.3:1. Ratio (in solution) = 2.5:1.

*1,4-Dimethoxy-2-(trifluoromethyl)benzene (44)*²⁷

The title compound was prepared by general procedure B using 1,4-dimethoxybenzene (**30**) (35.6 mg, 0.25 mmol). ¹H NMR (300 MHz, CDCl₃) δ (ppm) = 3.68 (s, 1H, CH₃); 3.75 (s, 1H, CH₃); 6.86 (d, *J* = 9.2 Hz, 1H, ArH); 6.92 (dd, *J* = 9.2, 3.2 Hz, 1H, ArH), 6.98 (d, *J* = 3.0 Hz, 1H, ArH); ¹⁹F NMR (282 MHz, CDCl₃) δ (ppm) = -63.0. Note: Ratio monosubstituted:disubstituted (in gel) = 1.8:1. Ratio (in solution) = 1.5:1.

*2-Methoxy-3-(trifluoromethyl)pyrazine (45)*²⁷

The title compound was prepared by general procedure C using 2-methoxypyrazine (**31**) (24.2 μL, 0.25 mmol). ¹H NMR (300 MHz, CDCl₃) δ (ppm) = 4.06 (s, 3H, CH₃); 8.11 (d, *J* = 2.6 Hz, 1H, ArH), 8.24 (d, *J* = 2.5 Hz, 1H, ArH); ¹⁹F NMR (282 MHz, CDCl₃) δ (ppm) = -68.43.

*3,5-Dichloro-2-(trifluoromethyl)pyrazine (46)*²⁷

The title compound was prepared by general procedure C using 2,6-dichloropyrazine (**32**) (37.3 mg, 0.25 mmol). ¹H NMR (300 MHz, CDCl₃) δ (ppm) = 8.48 (s, 1H); ¹⁹F NMR (282 MHz, CDCl₃) δ (ppm) = -67.03.

*2,6-Dimethyl-3-trifluoromethyl-γ-pyrone (47)*²⁷

The title compound was prepared following the general procedure C run in quadruplicate with 2,6-dimethyl-γ-pyrone (**33**) (124.4 mg, 1 mmol). After 24 h, 10 mL of brine was added to the reaction mixture, which was then extracted using EtAc (3×) and DCM (1×). The combined organic mixtures were dried over Na₂SO₄ and purified by chromatography using 10-50% (200 mL in 5 % steps till 25 %, 1.0 L solvent; 600 mL with 50 %) ethyl acetate in petroleum ether and after that a second flash chromatography (4:4:1 of hexanes:EtOAc:MeOH) affording the desired compound (89.0 mg, 46 % yield) as a white solid powder. ¹H NMR (300 MHz, CDCl₃) δ (ppm) = 2.26 (d, *J* = 0.5 Hz, 3H, CH₃); 2.48 (q, *J* = 2.8 Hz, 3H, CH₃), 6.15 (s, 1H); ¹⁹F NMR (282 MHz, CDCl₃) δ (ppm) = -58.8.

*1,3-Dimethyl-5-trifluoromethyluracil (48)*²⁷

The title compound was prepared following the general procedure C run in quadruplicate with 1,3-dimethyluracil (**34**) (140 mg, 1 mmol). After 24 h, 10 mL of brine was added to the reaction mixture, which was then extracted using EtOAc (3×) and DCM (1×). The combined organic mixtures were dried over Na₂SO₄ and purified by chromatography using 10 – 60% (200 mL in 10 % steps; 1.2 L solvent) ethyl acetate in petroleum ether affording the desired compound (139.1 mg, 67 % yield) as a white solid powder. ¹H NMR (300 MHz,

CDCl_3) δ (ppm) = 3.36 (s, 3H, CH_3); 3.49 (s, 3H, CH_3), 7.67 (d, J = 1.0 Hz, 1H); ^{19}F NMR (282 MHz, CDCl_3) δ (ppm) = -64.3 (s).

*3,4-Dimethoxy-5-(trifluoromethyl)benzaldehyde (49)*²⁷

The title compound was prepared by general procedure C using 3,4-dimethoxybenzaldehyde (**35**) (41.6 mg, 0.25 mmol). After 48 h the reaction mixture was analyzed by NMR. ^1H NMR (300 MHz, CDCl_3) δ (ppm) = 3.85 (s, 3H, CH_3); 3.87 (s, 3H, CH_3); 7.08 (s, 1H, ArH); 7.48 (s, 1H, ArH), 10.12 (q, J = 2.1 Hz, 1H, CHO); ^{19}F NMR (282 MHz, CDCl_3) δ (ppm) = -54.23.

→ Additional information can be found in the ESI on the enclosed CD or in the ESI of the paper.

3.6.6. References

- [1] M. Otte, *ACS Catal.* **2016**, *6*, 6491-6510.
- [2] M. Vriezema, M. C. Aragonès, J. A. A. W. Elemans, *Chem. Rev.* **2005**, *105*, 1445-1489.
- [3] S. B. P. E. Timmermans, J. C. M. van Hest, *Curr. Opin. Colloid Interface Sci.* **2018**, *35*, 26-35.
- [4] D. G. Shchukin, D. V. Sviridov, *J. Photochem. Photobiol.*, **2006**, *7*, 23- 39.
- [5] A. Maldotti, A. Molinari, R. Amadelli, *Chem. Rev.* **2002**, *102*, 3811-3836.
- [6] T. Nakamura, A. Son, Y. Umehara, T. Ito, R. Kurihara, Y. Ikemura, K. Tanabe, *Bioconjugate Chem.* **2016**, *27*, 1058-1066.
- [7] H. N. Kagalwala, D. N. Chirdon, I. N. Mills, N. Budwal, S. Bernhard, *Inorg. Chem.* **2017**, *56*, 10162-10171.
- [8] D. Limones-Herrero, R. Pérez-Ruiz, M. C. Jiménez, M. A. Miranda, *Photochem. Photobiol.* **2014**, *90*, 1012-1016.
- [9] C. Harris, P. V. Kamat, *ACS Nano* **2009**, *3*, 682-690.
- [10] J. Wen, C. Ma, P. Huo, X. Liu, M. Wei, Y. Liu, X. Yao, Z. Ma, Y. Yan, *J. Environ. Sci.* **2017**, *60*, 98-107.
- [11] S. Ghasimi, S. Prescher, Z. J. Wang, K. Landfester, J. Yuan, K. A. I. Zhang, *Angew. Chem., Int. Ed.* **2015**, *54*, 14549-14553.
- [12] K. Zhang, W. Zhou, X. Zhang, B. Sun, L. Wang, K. Pan, B. Jiang, G. Tian, H. Fu, *Appl. Catal., B* **2017**, *206*, 336-343.
- [13] R. Pérez-Ruiz, D. D. Díaz, *Soft Matter* **2015**, *11*, 5180-5187.
- [14] J. Bachl, A. Hohenleutner, B. B. Dhar, C. Cativiela, U. Maitra, B. König, D. D. Díaz, *J. Mater. Chem. A* **2013**, *1*, 4577-4588.
- [15] V. Ramamurthy, S. Gupta, *Chem. Soc. Rev.* **2015**, *44*, 119-135.
- [16] M. Pagliaro, R. Ciriminna, G. Palmisano, *Chem. Soc. Rev.* **2007**, *36*, 932-940.
- [17] D. D. Díaz, D. Kühbeck, R. J. Koopmans, *Chem. Soc. Rev.* **2011**, *40*, 427-448 and references therein.
- [18] M. Häring, R. Pérez-Ruiz, A. J. von Wangelin, D. D. Díaz, *Chem. Commun.* **2015**, *51*, 16848-16851.
- [19] D. Ravelli, S. Protti, M. Fagnoni, *Chem. Rev.* **2016**, *116*, 1152 9850-9913.
- [20] Y. Li, T. Wang, M. Liu, *Soft Matter* **2007**, *3*, 1312-1317.
- [21] J. van Esch, F. Schoonbeek, M. de Loos, H. Kooijman, A. L. Spek, R. M. Kellogg, B. L. Feringa, *Chem.-Eur. J.* **1999**, *5*, 937-950.
- [22] K. Hanabusa, M. Yamada, M. Kimura, H. Shirai, *Angew. Chem., Int. Ed. Engl.* **1996**, *35*, 1949-1951.

-
- [23] I. Gosh, B. König, *Angew. Chem., Int. Ed.*, **2016**, *55*, 7676-7679.
- [24] L. Marzo, I. Gosh, F. Esteban, B. König, *ACS Catal.* **2016**, *6*, 6780-6784.
- [25] W. Liu, H. Cao, H. Zhang, H. Zhang, K. H. Chung, C. He, H. Wang, F. Y. Kwong, A. Lei, *J. Am. Chem. Soc.* **2010**, *132*, 16737-16740.
- [26] Y. Zhou, J. Wang, Z. Gu, S. Wang, W. Zhu, J. L. Acena, V. A. Soloshonok, K. Izawa, H. Liu, *Chem. Rev.* **2016**, *116*, 422-518.
- [27] J. Wang, M. Sánchez-Roselló, J. L. Acena, C. Del Pozo, A. E. Sorochinsky, S. Fustero, V. A. Soloshonok, H. Liu, *Chem. Rev.* **2014**, *114*, 2432-2506.
- [28] N. A. Meanwell, *J. Med. Chem.* **2011**, *54*, 2529-2591.
- [29] K. Müller, C. Faeh, F. Diederich, *Science* **2007**, *317*, 1881-1886.
- [30] D. A. Nagib, D. W. C. MacMillan, *Nature* **2011**, *480*, 224-228.
- [31] P. Duan, N. Yanai, H. Nagatomi, N. Kimizuka, *J. Am. Chem. Soc.* **2015**, *137*, 1887-1894.
- [32] M. Hansen, F. Li, L. Sun, B. König, *Chem. Sci.* **2014**, *5*, 2683-2687.
- [33] R. Roa, W. K. Kim, M. Kanduc, J. Dzubiella, *ACS Catal.* **2017**, *7*, 5604-5611.
- [34] I. Gosh, R. S. Shaikh, B. König, *Angew. Chem., Int. Ed.* **2017**, *56*, 8544-8549.

4. List of Abbreviations

1D	one-dimensional
3D	three-dimensional
5-TIA	5-(<i>4H</i> -1,2,4-triazol-4-yl)isophthalic acid
Alg-PBA	alginate-phenylboronic acid
atm	atmosphere
ATR	attenuated total reflection
BDE	bond dissociation energy
BET	back-electron transfer
BMIM-PF ₆	1-butyl-3-methylimidazolium hexafluorophosphate
brs	broad singlet
BSA	bovine serum albumin
CDCl ₃	deuterated chloroform
CGC	critical gelation concentration
CHCl ₃	chloroform
CH ₃ CN	acetonitrile
click-TIA	5-(<i>1H</i> -1,2,3-triazol-5-yl)isophthalic acid
c	concentration
CO ₂	carbon dioxide
CuA	copper acetate
d	doublet
D ₂ O	deuterated water
DABCO	1,4,-diazabicyclo[2.2.2]octane
dd	doublet of doublet
DCM	dichloromethane
DEF	Diesel exhaust fluid
DFS	dynamic frequency sweep
DIPEA	<i>N,N</i> -diisopropylethylamine
DMA	dimethylacetamide
DMEM	Dulbecco's modified Eagle's medium
DMF	dimethylformamide
DMSO	dimethylsulfoxide
DPA	9,10-diphenylanthracene

DS	degree of substitution
DSC	differential scanning calorimetry
DSS	dynamic strain sweep
DTA	differential thermal analysis
DTS	dynamic time sweep
EA	elemental analysis
EDC	1-(3-dimethylaminopropyl)-2-ethylcarbodiimide hydrochloride
EDTA	ethylenediaminetetraacetic acid
ESI	electrospray ionization
ET	electron transfer
Et ₃ N	trimethylamine
Et ₂ O	diethyl ether
EtOAc	ethyl acetate
EtOH	ethanol
<i>etc.</i>	<i>et cetera</i> , engl.: and so on
FBS	fetal bovine serum
FD	freeze-drying
FE-SEM	field emission scanning electron microscopy
FID	flame ionization detector
FT-IR	Fourier-transform infrared spectroscopy
g	gram
G'	storage modulus
G''	loss modulus
ε_t	true strain
<i>e.g.</i>	<i>exempli gratia</i> , engl.: for example
γ	yield point
GC	gas chromatography
HAT	H-atom transfer
HCl	hydrochloric acid
HOBt	1-hydroxybenzotriazole
HPLC	high performance liquid chromatography
h	hour/ hours
H ₂ O	water
<i>i.e.</i>	<i>id est</i> , engl.: that is

IFM	inverse-flow method
<i>i</i> -PrOH	isopropanol
Ir(Fppy) ₃	tris[2-(2,4-difluorophenyl)pyridine]iridium(III)
ISC	intersystem crossing
λ	wavelength, stretch ratio
L	liter
LED	light-emitting diode
LMW	low-molecular-weight
LVE	linear viscoelastic
μ	micro
m	milli, multiplet
M	molar
MeOH	methanol
min	minute, minutes
MOF	metal organic framework
MTT	3-(4,5-dimethylthiazol-2-yl)-2,5-diphenyltetrazolium bromide
MWCO	molecular weight cut off
NaOH	sodium hydroxide
N	normal
n.d.	not detectable
NMR	nuclear magnetic resonance spectroscopy
ω	frequency
OXT	oxytetracycline hydrochloride
PBA	phenylboronic acid
PBS	phosphate buffered saline
PET	photoinduced electron transfer
POM	polarized optical microscopy
ppm	parts per million
PTC	phase-transfer catalyst
PtOEP	platinum(II) octaethylporphyrin
PVA	poly(vinyl alcohol)
q	quartet
Rh-6G	rhodamine-6G
RP	reduction potential

Ru(phen) ₃ Cl ₂	tris(1,10-phenanthroline)ruthenium(II) chloride
RT	room temperature
σ_t	true stress
s	singlet, second
SCE	saturated calomel electrode
SD	standard deviation
SEC	size-exclusion chromatography
SEM	scanning electron microscopy
SET	single electron transfer
SVP	single visible photon
t	triplet
TBAB	tetra- <i>n</i> -butylammonium bromide
TBAF	<i>n</i> -butylammonium fluoride
T _d	destruction temperature
TEM	transmission electron microscopy
TfCl	triflyl chloride
TGA	thermal gravimetric analysis
T _{gel}	<i>gel-to-sol</i> transition temperature
THF	tetrahydrofuran
TLC	thin-layer chromatography
TMEDA	tetramethylethylenediamine
TMS	trimethylsilyl
TOF	time-of-flight
TTA	triplet-triplet annihilation
TTET	triplet-triplet energy transfer
UC	upconversion
UV	ultraviolet
Vis	visible
w/v	mass concentration

5. Curriculum Vitae

Marleen Häring

(Master of Science)

Persönliche Daten

Geburtsdatum:	25.03.1989
Geburtsort:	Ebersberg
Staatsangehörigkeit:	Deutsch

Ausbildung

01/2015 – 05/2018	Wissenschaftlicher Mitarbeiter/ Doktorand Institut für Organische Chemie, Universität Regensburg Promotion bei Prof. Dr. David Díaz Díaz Dissertation: <i>‘Synthesis, Characterization and Application of New Functional Gels’</i>
10/2017	Forschungsaufenthalt am IMDEA Energy Institute in Móstoles/Madrid (Spanien), Betreuung durch Dr. Raul Pérez-Ruiz
03/2016 – 05/2016	Forschungsaufenthalt am Institut Charles Gerhard Montpellier (ICGM) in Montpellier (Frankreich), Betreuung durch Prof. Dr. Françoise Quignard
02/2013 – 11/2014	Masterstudium (M. Sc.) in Chemie, Universität Regensburg, Schwerpunkte: Organische Chemie, Bioanalytik, Biochemie Masterarbeit: <i>‘Biopolymer-based Catalysis’</i> , Betreuung durch Prof. Dr. David Díaz Díaz

10/2009 – 02/2013	Bachelorstudium (B. Sc.) in Chemie, Universität Regensburg Bachelorarbeit: ' <i>C-O Activation as Trifluoromethyl Substituted Benzoates towards Reductive Fragmentation Reactions under Visible Light Photocatalysis</i> ', Betreuung durch Prof. Dr. Oliver Reiser
05/2009	Abitur am Asam-Gymnasium in Munich

Publikationsliste

- [1] M. Häring, A. Abramov, K. Okumura, I. Ghosh, B. König, N. Yanai, N. Kimizuka, D. D. Díaz, '*Air-sensitive photoredox catalysis performed under aerobic conditions in gel networks*', *J. Org. Chem.*, **2018**, doi:10.1021/acs.joc.8b00797.
- [2] M. Häring, D. D. Díaz, '*Ferritin-basierte makroporöse Gelnanoreaktionen*', *Nach. Chem.* **2018**, akzeptiertes Manuskript.
- [3] M. Häring, J. Rodríguez-López, S. Grijalvo, M. Tautz, R. Eritja, V. S. Martín, D. D. Díaz, '*Isosteric substitution of 4H-1,2,4-triazole by 1H-1,2,3-triazole in isophthalic derivative enabled hydrogel formation of controlled drug release*', *Mol. Pharm.* **2018**, doi: 10.1021/acs.molpharmaceut.7b01049.
- [4] T. Das, M. Häring, D. Haldar, D. D. Díaz, '*Phenylalanine and derivatives as versatile low-molecular-weight gelators: design, structure and tailored function*', *Biomater. Sci.* **2018**, **6**, 38-59.
- [5] A. Pettignano, S. Grijalvo, M. Häring, R. Eritja, N. Tanchoux, F. Quignard, D. D. Díaz, '*Boronic-acid-modified alginate enables direct formation of injectable, self-healing and multistimuli-responsive hydrogel*', *Chem. Commun.* **2017**, **53**, 3350-3353.
- [6] M. Häring, A. Abramov, D. D. Díaz, '*Unreactive gel networks as versatile confined spaces for enhanced photoinduced processes*', *Macromol. Symp.* **2017**, **372**, 87-101.
- [7] A. Abramov, M. Häring, D. D. Díaz, '*Anregen und tauschen*', *Nach. Chem.* **2017**, **65**, 1100-1105.
- [8] S. Kumari, M. Häring, S. S. Gupta, D. D. Díaz, '*Catalytic microporous biohydrogels made of ferritin-encapsulated gold nanoparticles*', *ChemPlusChem* **2017**, **82**, 225-232.

-
- [9] M. Häring, D. D. Díaz, ‚*Supramolecular metallogels with bulk self-healing properties prepared by in situ metal complexation*‘, *Chem. Commun.* **2016**, 52, 13068-13081.
- [10] M. Häring, A. Pettignano, F. Quignard, N. Tanchoux, D. D. Díaz, ‚*Keratin protein-catalyzed nitroaldol (Henry) reaction and comparison with other biopolymers*‘, *Molecules* **2016**, 21, 1122.
- [11] M. Häring, D. D. Díaz, ‚*Protonenleitende und selbstheilende weiche Gelmaterialien*‘, *Praxis der Naturwissenschaften* **2016**, 6/65, 5-9.
- [12] T. Feldner, M. Häring, J. Esquena, S. Subhadeep, R. Banerjee, D. D. Díaz, ‚*Supramolecular metallogel that impart self-healing properties to other gel networks*‘, *Chem. Mater.* **2016**, 28, 3210-3217.
- [13] M. Häring, R. Pérez-Ruiz, A. J. v. Wangelin, D. D. Díaz, ‚*Intragel photoreduction of aryl halides by green-to-blue upconversion under aerobic conditions*‘, *Chem. Commun.* **2015**, 51, 16848-16851.
- [14] M. Häring, J. Schiller, J. Mayr, S. Grijalvo, R. Eritja, D. D. Díaz, ‚*Magnetic gel composites for hyperthermia cancer therapy*‘, *Gels* **2015**, 1, 135-161.
- [15] J. Mayr, M. Häring, J. Schiller, D. D. Díaz, ‚*Supramolekulare Gele: einfach und funktionell*‘, *Nachr. Chem.* **2015**, 63, 899-903.
- [16] M. Häring, M. M. P. Madrigal, D. Kühbeck, A. Pettignano, F. Quignard, D. D. Díaz, ‚*DNA-catalyzed Henry reaction in pure water and the striking influence of organic buffer systems*‘, *Molecules* **2015**, 20, 4136-4147.
- [17] D. Kühbeck, J. Mayr, M. Häring, M. Hofmann, F. Quignard, D. D. Díaz, ‚*Evaluation of the nitroaldol reaction in the presence of metal ion-crosslinked alginates*‘, *New J. Chem.* **2015**, 39, 2306-2315.

Publikationsliste (in Kollaboration)

- [1] M. Tiffner, M. Häring, D. D. Díaz, M. Waser, ‚*Cationic polymers bearing quaternary ammonium groups-catalyzed CO₂ fixation with epoxides*‘, *Top. Catal.*, **2018**, doi:10.1007/s11244-018-0996-0.

-
- [2] S. Pérez-Rentero, R. Eritja, M. Häring, C. Saldías, D. D. Díaz, 'Synthesis, characterization and self-assembly of a tetrathiafulvalene (TFF) – triglycyl derivative', *Appl. Sci.* **2018**, 8, 671.
- [3] M. C. Saborio, O. Bertran, S. Lanzalaco, M. Häring, D. D. Díaz, F. Estrany, C. Aleman, 'Cationic ionene as n-dopant agent of poly(3,4-ethylenedioxythiophene)', *Phys. Chem. Chem. Phys.* **2018**, 20, 9855-9864.
- [4] M. Pérez-Madrigal, J. Torras, J. Casanovas, M. Häring, C. Aleman, D. D. Díaz, 'A paradigm shift for prepring versatile M2+-free gels from unmodified sodium alginate', *Biomacromolecules* **2017**, 18, 2967-2979.
- [5] A. Pettignano, M. Häring, L. Bernardi, N. Tanchoux, F. Quignard, D. D. Díaz, 'Self-healing alginate-gelatin biohydrogels based on dynamic covalent chemistry: Elucidation of key parameters', *Mater. Chem. Front.* **2017**, 1, 73-79.
- [6] E. S. Dragan, J. Mayr, M. Häring, A. Irina, D. D. Díaz, 'Spectroscopic characterization of azo dyes aggregation induced by DABCO-based ionene polymers and dye removal efficiency as a function of ionene structure', *ACS Appl. Mater. Interfaces* **2016**, 8, 30908-30919.
- [7] M. Tiffner, K. Zielke, J. Mayr, M. Häring, D. D. Díaz, M. Waser, 'Phase-transfer catalysis with ionene polymers', *ChemistrySelect* **2016**, 1, 4030-4033.
- [8] J. V. Alegre-Requena, M. Häring, R. P. Herrera, D. D. Díaz, 'Regulatory parameters of self-healing alginate hydrogel networks prepared via mussel-inspired dynamic chemistry', *New J. Chem.* **2016**, 40, 8493-8501.

Präsentationen

- [1] 'Uncovering the nature of superheroes', Weihnachtsskolloquium **2017**, Regensburg (Vortrag)
- [2] 'Tuning the properties of soft gel materials', IMDEA Energy Institute **2017**, Mostóles/Spain (Vortrag mit Einladung).
- [3] 'Synthesis and application of soft functional materials', Tag der Chemie **2017**, Regensburg (Poster)

-
- [4] *'Uncovering the catalytic activity of biopolymers towards C-C bond formation and beyond'*, EuCheMS (Konferenz) **2016**, Sevilla/Spain (Poster)
 - [5] *'Intragel photoreduction of aryl halides by green-to-blue upconversion under aerobic conditions'*, Orchem (Konferenz) **2016**, Weimar (Poster)
 - [6] *'Supramolecular metallogels with self-healing ability'*, Institut Charles Gerhardt Montpellier (ICGM) **2016**, Montpellier/France (Vortrag mit Einladung)
 - [7] *'Green-to-blue Christmas'*, Weihnachtskolloquium **2015**, Regensburg (Vortrag)
 - [8] *'Self-healing and adhesive properties of oxalic acid-based metallogels'* Wissenschaftsforum (Wifo) (Konferenz) **2015**, Dresden (Vortrag)

6. Acknowledgements

Zu allererst möchte ich mich herzlich bei Prof. Dr. David Díaz Díaz bedanken. Vielen Dank für die Aufnahme in die Arbeitsgruppe, die Bereitstellung der interessanten Projekte und die Unterstützung während der Master- und Doktorarbeit. Er hat mich nicht nur unterstützt, sondern stets gefördert und motiviert und mir zwei Auslandsaufenthalte ermöglicht. Vielen Dank!

Ich bin auch meinen Zweitgutachter, Prof. Dr. Mario Waser, dankbar, dass er sich die Zeit nimmt und den weiten Weg auf sich nimmt um bei meinem Kolloquium da zu sein. Ich bin auch Prof. Dr. Jens Schlossmann und Prof. Dr. Rainer Müller dankbar, dass sie bei meinem Kolloquium Drittprüfer und Vorsitz sind.

Ich danke Dr. Raul Pérez-Ruiz für die Aufnahme und Unterstützung während meines Forschungsaufenthaltes am IMDEA Energy Institut in Móstoles/Madrid. Die Zeit war unbeschreiblich gut. Ich möchte ihm aber auch für die Zusammenarbeit während seiner Zeit an der Uni Regensburg danken. Ich habe viel gelernt und viel gelacht.

Ich möchte mich hier auch bei Prof. Dr. Françoise Quignard und Dr. Nathalie Tanchoux bedanken, die mir die Möglichkeit gegeben haben, einen Forschungsaufenthalt in Montpellier in ihren Laboren zu machen. Sie haben mich in dieser Zeit unterstützt und angeleitet. Auch meinen Kollegen, insbesondere Asja, möchte ich danken, für die Unterstützung im Labor und und auch außerhalb davon. Sie ist mir eine gute Freundin geworden. Es war eine wunderbare Zeit in Frankreich.

Ich danke Prof. Dr. Oliver Reiser für die zeitweise finanzielle Unterstützung und die Möglichkeit am Mag(net)icFun Projekt mitzuarbeiten, sowie die Erlaubnis verschiedene instrumentelle analytische Geräte mitzubenutzen.

Ich danke meinen Laborkollegen für die entspannte und oft auch lustige Arbeitsatmosphäre. Danke Dr. Judith Mayr, Tobias Feldner, Sushma Kumari, Mar Pérez-Madrigal, Jana Schiller, Rory Whelan, Dr. Elaine Armelin, Dr. Santiago Grijalvo, Dr. Asja Pettignano, Dr. Juan Vincente Alegre-Requena, Markus Tautz, Dr. César Saldías, Daniela Guzmán-Angel, Ting Li, Alex Abramov, Dr. Debasish Haldar, Dr. Binoy Maiti, Dr. Enock Dare, Isaac Sonsona and Noelia Machado.

Desweiteren dank ich meinen Forschungspraktikanten für ihre Unterstützung. Danke Milena Schenk, Michaela Raab, Alex Abramov, Wanda Putri-Sacharissa, Dounia Slim, Eva Dorskocil und Henrik Vernickel.

Besonderer Dank gilt auch Roxane Harteis, Helena Konkel, Brigitte Eichenseher, Klaus Döring, Dr. Peter Kreitmeier und dem analytischen Department für ihre technische Unterstützung.

Ich möchte auch Prof. Dr. Archim und Prof. Dr. Rainer Müller danken für die Erlaubnis ihre Geräte mitbenutzen zu dürfen. Ich danke dabei auch Dr. Manuel Gregoritz, Moritz Graf und Katharina Häckl für die Hilfe bei Rheologie und DSC.

Ich danke den Leuten aus dem zweiten Stockwerk für die gegenseitige Hilfe und Unterstützung bei Problemen jeglicher Art und die gemeinsame Zeit in der Küche.

Ich möchte auch besonders meinen Chemikerfreunden danken, die das Studium und die Doktorarbeit zu etwas Besonderem gemacht haben. Besonderem Dank gilt natürlich Marina Kaas, mit der ich mich ab dem ersten Semester durch alle Prüfungen und Praktika gekämpft hab oder wir uns davon abgelenkt haben. Ich danke aber auch Sabine Möhle, Sabine Kerres, Benjamin Kastl, Matze Gnahn, Andreas Seegerer, Felix Riedlberger, Philipp Büschlmeier, Marco Peteranderl für die gute Zeit während dem Studium und darüber hinaus. Es war mir ein Fest und auch in Zukunft denke ich, werden wir weiter gemeinsam Feste feiern.

Vielen Dank gilt auch Jana Schiller und Dirk Herrmann. Aus Kollegen werden Freunde und Nachbarn, die die Liebe zu verschiedenen Hobbies teilen, insbesondere gutem Essen. Ich danke euch und eurer Freundschaft.

Ich danke auch alle anderen, die ich nicht namentlich nenne, da die Liste sonst unendlich lang werden würde, aber auch ihr ward ein wichtiger Teil in meinem Leben.

Natürlich danke ich auch meinen „Nicht-Chemikerfreunden“, insbesondere Michaela Prell, Katharina Einfeld und Sabrina Schertel. Danke für eure jahrelange Freundschaft, die keine Grenzen kennt und keine Entfernung scheut. Ich bin mir sicher, dass ihr immer ein Teil meines Lebens sein werdet. Mein Herz tanzt.

Ich danke auch Nadja Tedesco, Sarah und Florian Hiemer für die, zwar noch nicht ganz so lange, aber deswegen nicht unwichtigere Freundschaft. Ihr alle bereichert mein Leben.

Ganz besonderem Dank gilt meiner Familie! Sie hat mich zu jeder Zeit in meinem Leben unterstützt, mir den Weg, den ich gegangen bin, ermöglicht und mein Leben bereichert. Ich bin so stolz ein Teil dieser Familie sein zu dürfen. Ich danke und liebe euch!

Obwohl ich ihn auch als Teil meiner Familie ansehe, möchte ich ihm hier noch einmal extra danken. Danke Marco Peteranderl! Danke für deine jahrelange Freundschaft, für dein Verständnis, deine Unterstützung und deine Liebe. Mein Leben wäre nur halb so schön, wärest du nicht ein Teil davon. Du bist stets an meiner Seite, auch wenn es mal schlechtere Zeiten gibt. Und du schaffst es, dass gute Zeiten zu noch besseren Zeiten werden. Danke! Danke! Danke!

7. Declaration

Herewith I declare that this present dissertation is a presentation of my original work prepared single-handed. Wherever contributions from others are involved, all of them are marked clearly, with reference to the literature and licenses.

Regensburg, 06. July 2018

Marleen Häring